Final Report

Project Title:

Catalytic upgrading of methane into high-value hydrocarbons via oxidative coupling of methane

By

Asst. Prof. Dr. Anusorn Seubsai

May / 2020

Contract No. MRG6180232

Final Report

Project Title:

Catalytic upgrading of methane into high-value hydrocarbons via oxidative coupling of methane

Researcher	Institute
1. Asst. Prof. Dr. Anusorn Seubsai	Chemical Engineering Department, Kasetsart University
2. Prof. Dr. Metta Chareonpanich	Chemical Engineering Department, Kasetsart University
3. Asst. Prof. Dr. Chalida Niamnuy	Chemical Engineering Department, Kasetsart University

This project granted by the Thailand Research Fund

Project Code: MRG6180232

Project Title: Catalytic upgrading of methane into high-value hydrocarbons via oxidative coupling of methane

Investigator: Asst. Prof. Dr. Anusorn Seubsai

E-mail Address: fengasn@ku.ac.th

Project Period: May 2nd, 2018 - May 1st, 2020

Abstract: A combinatorial approach was applied to explore active binary catalysts for oxidative coupling of methane (OCM) to value-added hydrocarbons (C_{2+}). A screening of 25 selected single components on SiO_2 for OCM reaction identified the top-14 single active components as follows: La > Ce > Ga > Al > Ca > Cr > Ba > Na_2WO_4 > Mn > Cu > Ti > Zn > Rb > Ni. Binary catalyst screening was then performed and resulted in a combination of Na_2WO_4 and Mn producing the most active binary catalyst. X-ray powder diffraction measurement of the Na_2WO_4-Mn/SiO_2 catalyst revealed that the presence of alpha-cristobalite phase was essential for the activation of methane. Moreover, the X-ray photoelectron spectroscopy spectrum of the Na_2WO_4-Mn/SiO_2 catalyst showed that the binding energy of W4f and Mn 2p shifted toward a lower binding energy, thereby enhancing the catalytic activity. Optimization of C_{2+} production of the catalyst by varying Na_2WO_4:Mn weight ratios, total metal loadings, catalyst weights, and feeding gas compositions, achieved maximum C_{2+} yield of 23.54% with 60.5% selectivity and 39.67% methane conversion. Furthermore, the activity of the Na_2WO_4-Mn/SiO_2 catalyst was monitored with time-on-steam for 50 h, revealing good catalyst stability. For the study of the effects of metal oxide additives into the Na_2WO_4/SiO_2 catalyst on the performance of the OCM reaction, first, Na_2WO_4-TiO_2/SiO_2 catalyst, along with the single catalysts of its components (Na_2WO_4/SiO_2 and TiO_2/SiO_2), was investigated. We found that 5 wt% Na_2WO_4+ 5 wt% TiO_2 on the SiO_2 support was a superior catalyst for OCM reaction compared to the single catalysts. The maximum C_{2+} formation of the Na_2WO_4-TiO_2/SiO_2 catalyst was found under test conditions of a N_2/($4CH_4$:$1O_2$) feed gas ratio of 1:1, a reactor temperature of 700 ºC, and gas hourly space velocity of 9,500 h^{-1}, exhibiting 71.7% C_{2+} selectivity, 6.8% CH_4 conversion, and 4.9% C_{2+} yield. Moreover, the activity of the catalyst had good stability over 24 h of on-stream testing. The characterizations of the Na_2WO_4-TiO_2/SiO_2 catalyst using various advanced instruments revealed that a crystalline structure of alpha-cristobalite of SiO_2 was present along with TiO_2 crystals, substantially enhancing the activity of the catalyst for OCM reaction to C_{2+}. Second, several metal oxide additives—including oxides of Co, Mn, Cu, Fe, Ce, Zn, La, Ni, Zr, Cr, and V—were investigated with the Na_2WO_4-Ti/SiO_2 catalyst. All of the catalysts were prepared using co-impregnation and the catalyst activity test was performed in a fixed-bed reactor at a reaction temperature range of 600–800 ºC and atmospheric pressure. The physicochemical properties of the prepared catalysts relating to their catalytic activity were discussed by using advance instrument. Na_2WO_4-Ti/SiO_2 added Mn was found to be the most active catalyst, involving shifts of binding energies of W 4f and Ti 2p toward lower binding energies. Moreover, a variety

of operating conditions—including reactant- to-nitrogen gas ratio, catalyst mass, reaction temperature, and total feed flow rate—were intensively examined for the OCM reaction using the Na_2WO_4-Ti-Mn/SiO_2 catalyst. The maximum C_{2+} yield was subsequently discovered at 22.09% with 62.3% C_{2+} selectivity and 35.43% CH_4 conversion. Additionally, the stability of the Na_2WO_4-Ti-Mn/SiO_2 catalyst was also monitored with time on stream for 24 h and it was found that the activity of the catalyst sligltly decreased over time.

Keywords : Catalyst screening, Light hydrocarbons, Metal oxide catalyst, Oxidative coupling of methane, Silica support

บทคัดย่อ: การศึกษาประสิทธิภาพของตัวเร่งปฏิกิริยาคู่ควบของมีเทน หรือปฏิกิริยาออกซิเดทีฟคัปปลิ้งของมีเทน เริ่มจากการคัดเลือกโลหะออกไซด์มาทั้งหมด 25 ชนิด เติมลงบนตัวรองรับซิลิกา โดยผลจากการศึกษานี้พบว่าตัวเร่งปฏิกิริยาที่มีประสิทธิภาพสูงสุด 14 ชนิดแรก ได้แก่ La > Ce > Ga > Al > Ca > Cr > Ba > Na_2WO_4 > Mn > Cu > Ti > Zn > Rb > Ni จากนั้นทำการศึกษาผลของการเติมโลหะออหไซด์ผสม 2 ชนิดบนตัวรองรับซิลิกา พบว่าการผสมกันระหว่าง Na_2WO_4-Mn/SiO_2 ให้ความว่องไวของตัวเร่งปฏิกิริยาสูงที่สุด การศึกษาการเลี้ยวเบนของรังสีเอ็กซ์พบว่าตัวเร่งปฏิกิริยา Na_2WO_4-Mn/SiO_2 มีเฟสของ alpha-cristobalite ซึ่งมีความสำคัญมากสำหรับการกระตุ้นมีเทนให้เกิดปฏิกิกิริยา นอกจากนี้ การศึกษาทางด้านรังสีโฟโต้อิเล็กตรอนของตัวเร่งปฏิกิริยานี้พบว่า พลังงานพันธะของ W4f และ Mn 2p เกิดการชิฟไปทางด้านพลังงานต่ำลง ซึ่งส่งผลทำให้ตัวเร่งปฏิกิริยามีประสิทธิภาพมากขึ้น การศึกษาการเพิ่มค่าร้อยละผลได้ของตัวเร่งปฏิกิริยานี้โดยการปรับเปลี่ยนค่าอัตราส่วนโดยน้ำหนักของโลหะน้ำหนักรวมของโลหะต่อตัวรองรับ ปริมาณตัวเร่งปฏิกิริยาที่ใช้ และค่าอัตราส่วนของแก๊สขาเข้า พบว่าค่าร้อยละผลได้สูงสุดที่ได้คือ 23.54 ที่ค่าร้อยละการเลือกเกิดของผลิตภัณฑ์ที่ 60.5 และค่าร้อยละการแปลงผันของมีเทนที่ 39.67 นอกจากนี้การทดสอบตัวเร่งปฏิกิริยานี้เป็นเวลา 50 ชั่วโมง พบว่าตัวเร่งปฏิกิริยานี้ให้ผลความเถียรภาพที่ดี สำหรับการศึกษาผลกระทบของการเติมสารประกอบโลหะออกไซด์ในตัวเร่งปฏิกิริยา Na_2WO_4/SiO_2 โดยในส่วนแรกได้ทำการศึกษาการเติม TiO_2 เทียบกับตัวเร่งปฏิกิริยาเดี่ยวของ Na_2WO_4 และตัวเร่งปฏิกิริยาคู่ผสมของทั้งคู่ พบว่าตัวเร่งปฏิกิริยา 5 wt% Na_2WO_4+ 5 wt% TiO_2 บนตัวรองรับซิลิกาเป็นตัวเร่งปฏิกิริยาที่ดีกว่าตัวเร่งปฏิกิริยาเดี่ยว ค่าร้อยละผลได้ C_{2+} ของตัวเร่งปฏิกิริยาคู่นี้ได้สูงสุดที่สภาวะการทดสอบที่อัตราส่วนของ N_2/(4CH_4:1O_2) ที่ 1/1 อุณหภูมิ 700 องศาเซลเซียส ค่าความเร็วแก๊สที่ 9500 h^{-1} โดยได้ค่าร้อยละผลได้ที่ 71.7 ค่าร้อยละการเลือกเกิดของ C_{2+} ที่ 71.7 และค่าร้อยละการแปลงผันของมีเทนที่ 4.9 นอกจากนี้ยังพบว่าตัวเร่งปฏิกิริยานี้มีเสถียรภาพที่ดีสำหรับการทดสอบ 24 ชั่วโมง การวิเคราะห์ด้วยเครื่องมือขั้นสูงต่างๆ พบว่า โครงสร้างของ alpha-cristobalite ที่อยู่กับ TiO_2 จะช่วยส่งเสริมทำให้ความว่องไวของตัวเร่งปฏิกิริยานี้ดีขึ้น ในส่วนที่สอง การศึกษาสารประกอบโลหะออกไซด์ที่เลือกเติมในตัวเร่งปฏิกิริยา Na_2WO_4-Ti/SiO_2 ได้แก่ Co, Mn, Cu, Fe, Ce, Zn, La, Ni, Zr, Cr และ V โดยเตรียมตัวเร่งปฏิกิริยาจากวิธีการจุ่มชุ่มและทดสอบความว่องไวของตัวเร่งปฏิกิริยาในเครื่องปฏิกรณ์แบบแบดคงที่ ช่วงอุณหภูมิสำหรับทำปฏิกิริยา 600-800 องศาเซลเซียส ความดันบรรยากาศ การศึกษาคุณสมบัติทางเคมีกายภาพของตัวเร่งปฏิกิริยาที่จัดเตรียมขึ้นเพื่อศึกษาความว่องไวของตัวเร่งปฏิกิริยาด้วยเครื่องมือขั้นสูงต่างๆ พบว่าตัวเร่งปฏิกิริยา Na_2WO_4-Ti/SiO_2 ที่มีการเติม Mn พบว่ามีความว่องไวของตัวเร่งปฏิกิริยาในการเกิดปฏิกิริยามากที่สุด เป็นผลมาจากการเปลี่ยนแปลงพลังงานพันธะของ W 4f และ Ti 2p มีค่าต่ำกว่าตัวเร่งปฏิกิริยาอื่น รวมไปถึงสภาวะการดำเนินการของปฏิกิริยาที่สภาวะต่าง ๆ ได้แก่ อัตราส่วนของสารตั้งต้นและก๊าซไนโตรเจน ปริมาณตัวเร่งปฏิกิริยา อุณหภูมิของปฏิกิริยาและอัตราการไหลของก๊าซขาเข้าถูกทดสอบในการเกิดปฏิกิริยาคู่ควบมีเทนโดยใช้ตัวเร่งปฏิกิริยา Na_2WO_4-Ti-Mn/SiO_2 จากผลการทดลองพบว่าค่าร้อยละของผลผลิต C_{2+} สูงสุดคือ 22.09 ค่าร้อยละ

ของการเลือกเกิดของผลิตภัณฑ์ C_{2+} สูงสุดคือ 62.3 และค่าร้อยละของการเปลี่ยนแปลงมีเทนสูงสุดคือ 35.43 นอกจากนี้ได้มีการทดสอบความเสถียรของตัวเร่งปฏิกิริยา Na_2WO_4-Ti-Mn/SiO_2 เป็นเวลา 24 ชั่วโมง พบว่ามีค่าความว่องไวลดลงเล็กน้อย

คำสำคัญ : การคัดกรองตัวเร่งปฏิกิริยา, สารประกอบไฮโดรคาร์บอนชนิดเบา, ตัวเร่งปฏิกิริยาที่เป็นออกไซด์, ปฏิกิริยาคู่ควบของมีเทน, ตัวรองรับซิลิกา

Final report

Executive summary

This project, the PI investigated several active metal oxides supported on Si-based compounds for oxidative coupling of methane (OCM). The report is divided into three parts as follows.

Part I: A combinatorial approach was applied to explore active binary catalysts for OCM to value-added hydrocarbons (C_{2+}). A screening of 25 selected single components on SiO_2 for OCM reaction identified the top-14 single active components as follows: La > Ce > Ga > Al > Ca > Cr > Ba > Na_2WO_4 > Mn > Cu > Ti > Zn > Rb > Ni. Binary catalyst screening was then performed and resulted in a combination of Na_2WO_4 and Mn producing the most active binary catalyst. X-ray powder diffraction measurement of the Na_2WO_4-Mn/SiO_2 catalyst revealed that the presence of α-cristobalite phase was essential for the activation of methane. Moreover, the X-ray photoelectron spectroscopy spectrum of the Na_2WO_4-Mn/SiO_2 catalyst showed that the binding energy of W4f and Mn 2p shifted toward a lower binding energy, thereby enhancing the catalytic activity. Optimization of C_{2+} production of the catalyst by varying Na_2WO_4:Mn weight ratios, total metal loadings, catalyst weights, and feeding gas compositions, achieved maximum C_{2+} yield of 23.54% with 60.5% selectivity and 39.67% methane conversion. Furthermore, the activity of the Na_2WO_4-Mn/SiO_2 catalyst was monitored with time-on-steam for 50 h, revealing good catalyst stability.

Part II: Na_2WO_4-TiO_2/SiO_2 catalyst, along with the single catalysts of its components (Na_2WO_4/SiO_2 and TiO_2/SiO_2), was investigated for OCM reaction to C_{2+}. We found that 5 wt% Na_2WO_4+ 5 wt% TiO_2 on the SiO_2 support was a superior catalyst for OCM reaction compared to the single catalysts. The maximum C_{2+} formation of the Na_2WO_4-TiO_2/SiO_2 catalyst was found under test conditions of a N_2/($4CH_4$:$1O_2$) feed gas ratio of 1:1, a reactor temperature of 700 ºC, and gas hourly space velocity of 9,500 h^{-1}, exhibiting 71.7% C_{2+} selectivity, 6.8% CH_4 conversion, and 4.9% C_{2+} yield. Moreover, the activity of the catalyst had good stability over 24 h of on-stream testing. The characterizations of the Na_2WO_4-TiO_2/SiO_2 catalyst using XRD, FT-IR, XPS, FE-SEM, and TEM revealed that a crystalline structure of α-cristobalite of SiO_2 was present along with TiO_2 crystals, substantially enhancing the activity of the catalyst for OCM reaction to C_{2+}.

Part III: The effects of metal oxide additives into the Na_2WO_4-Ti/SiO_2 catalyst on the performance of the OCM reaction were investigated. Several metal oxide additives—including oxides of Co, Mn, Cu, Fe, Ce, Zn, La, Ni, Zr, Cr, and V—were investigated with the Na_2WO_4-Ti/SiO_2 catalyst. All of the catalysts were prepared using co-impregnation and the catalyst activity test was performed in a fixed-bed reactor at a reaction temperature range of 600–800 °C and atmospheric pressure. The physicochemical properties of the prepared catalysts relating to their catalytic activity were discussed by using the information of X-ray diffraction (XRD), X-ray photoelectron spectroscopy (XPS), and scanning electron microscopy (SEM) measurements. Na_2WO_4-Ti/SiO_2 added Mn was found to be the most active catalyst, involving shifts of binding energies of W 4f and Ti 2p toward lower binding energies. Moreover, a variety of operating conditions—including reactant- to-nitrogen gas ratio, catalyst mass, reaction temperature, and total feed flow rate—were intensively examined for the OCM reaction using the Na_2WO_4-Ti-Mn/SiO_2 catalyst. The maximum C_{2+} yield was subsequently discovered at 22.09% with 62.3% C_{2+} selectivity and 35.43% CH_4 conversion. Additionally, the stability of the Na_2WO_4-Ti-Mn/SiO_2 catalyst was also monitored with time on stream for 24 h and it was found that the activity of the catalyst sligltly decreased over time.

Introduction

The direct utilization of methane, the main component in natural gas and biogas, as an alternate chemical feedstock to petroleum is a highly desirable but difficult goal in industrial catalysis. Many direct and indirect methods have been proposed and studied to convert CH_4 into more-useful products, including olefins (e.g. C_2H_4, C_3H_6) and higher-molecular-weight hydrocarbons and liquids (e.g. benzene and gasoline). The production of ethylene (C_2H_4) from NG represents a particularly desirable process because of its massive worldwide use as an intermediate in the production of plastics, such as polyethylene and polyvinylchloride (PVC). All indirect methane-conversion routes utilize a high temperature, endothermic, and costly steam-reforming process as the first step, from which synthetic gas (H_2/CO mixtures) is produced. This step is followed by the synthesis of useful products through various catalytic processes. Although direct methods avoid the use of costly syngas, they remain uneconomical, owing, in part, to low yields of hydrocarbon compounds (C_{2+}), high temperatures, and low throughputs. High temperatures are particularly detrimental because they result in catalyst deactivation and create problems for reactors. In the oxidative coupling of methane (OCM), CH_4 is directly converted into C_2H_6, C_2H_4, C_3H_6, and water in the presence of O_2 and a suitable catalyst. The OCM has received immense global attention, as evidenced by the large number of catalysts that have been investigated for this transformation. However, the best catalysts reported to date have not met the industrial requirements (i.e. C_{2+} selectivity + C_{2+} yield > 110).

Many previous results reported in the literature suggest that a suitable catalyst that could be used in industrial processes for OCM to produce C_{2+} chemicals requires the properties as follows; i) metal oxides because they can tolerate the operating conditions (i.e. under oxygen and heat), ii) stable and inert support, iii) high surface area, and iv) high basicity of catalyst's surface. This project, the PI therefore investigated several active metal oxides supported on Si-based compounds for the OCM reaction. The details of this projects are follows.

Objectives

To synthesize metal oxides on silica-based supports as catalysts

To synthesize hydrocarbons (C_{2+}) via oxidative coupling of methane by using the prepared catalysts

To characterize the synthesized catalysts using advanced instruments

This report is divided into three parts;

Part I : Screening of single and binary catalysts for oxidative coupling of methane to value-added chemicals

Part II : Synthesis of Light Hydrocarbons via Oxidative Coupling of Methane over Silica-supported Na_2WO_4-TiO_2 Catalyst

Part III : Investigation of metal oxide additives onto Na_2WO_4-Ti/SiO_2 catalysts for oxidative coupling of methane to value-added chemicals

Part I : Screening of single and binary catalysts for oxidative coupling of methane to value-added chemicals

I-1. Introduction

Methane (CH_4) is the primary constituent of natural gas and biogas. Since it is abundant in natural resources, it is of great interest for conversion of CH_4 into value-added chemicals (C_{2+}) such as ethylene and ethane. Oxidative coupling of methane (OCM) using solid catalysts is one of the most attractive chemical reactions to directly convert CH_4 into value-added hydrocarbons. This catalytic reaction has been of interest to industrial and academic researchers since the 1980s. In a condition where O_2 is present without a catalyst being used, CH_4 can be directly oxidized at high temperatures (>700 ºC), known as direct gas-phase oxidation of CH_4. The input energy can break the C—H bonds of CH_4 into a methyl radical, which can further react with another methyl radical to form ethane. Additionally, ethylene, other C_{2+}, and CO_x can form under such uncontrollable pathways [1-3]. Therefore, selective solid catalysts have been researched for use in the OCM reaction.

In the past several years, many solid catalysts have been investigated for this transformation. Potential catalysts have been reported including Mn modified with various types of supports and co-catalysts [4-9], such as oxides of Mg [10, 11], Na [12, 13], Li [14, 15], and Na_2WO_4 [16, 17]. The C_{2+} yields and C_{2+}selectivities were approximately <16.0% and 25.3–60.5%, respectively. Binary catalysts of Na_2WO_4-Mn have been widely investigated because this metal combination is highly active for OCM [18-24], providing 2.1–26.4% C_{2+} yields and 42.8–80.0% C_{2+} selectivities. Other metal oxide catalysts and mixed metal oxides have also been found active for OCM including $LaXO_3$ [25-27], Ag/$SrFeO_3$ [28], Metal or PtSn/SiO_2 [29-32], Metal–Mg [33-36], and La_2O_3/CaO [37-39]. However, a viable catalyst that meets the industrial requirements (i.e. C_{2+} selectivity plus C_{2+} yield > 110) has yet to be found. Therefore, the search for new catalysts for OCM reaction is still continuing.

For the rapid search of new active catalysts from large numbers of experiments to test via reactions, combinatorial synthesis and screening can be applied effectively [40]. Here, we present a successful attempt to rapidly search for binary catalysts for OCM by applying the combinatorial approach. First, a number of elements/components were selected from active ones that have been reported in the literature as well as taking onto account their availability. A screening test was then quickly made to attain active single components. Subsequently, a binary screening was carried out, which delivered a highly active binary catalyst. The catalyst discovered was then carefully investigated to achieve the optimal C_{2+} yield at a certain reactor temperature, and also intensively characterized to understand why it was highly active in the OCM reaction.

I-2. Experimental

I-2.1 Catalyst preparation

All catalysts were prepared using impregnation. In total, 25 single component catalysts and 91 binary catalysts were prepared on SiO_2 (amorphous fumed silica powder, surface area of 85-115 m^2/g, Alfa Aesar) at 5 and 10 wt%, respectively. The binary catalysts used a metal weight ratio of 1:1. Briefly, each metal precursor (see Table I-S1) was dissolved in DI water. Then, each metal ion solution was determined and pipetted into the SiO_2

support to achieve the desired weight percentages and metal weight ratio. The mixture was stirred at room temperature for 2 h, then heated to 115 °C and stirred until dried. The obtained powder was calcined at 800 °C for 4 h in an air furnace at a heating rate of 5 °C/min. After the calcination, a fine powder was obtained.

I-2.2 Catalyst activity test

Catalytic activity for OCM reaction of each catalyst was examined in a traditional packed bed reactor at atmospheric pressure and in a reactor temperature of 700 ºC. Each prepared catalyst (2–200 mg) was packed in a quartz tube (0.5 cm in inner diameter) and sandwiched between two quartz wools. The feed gases were CH_4 (Praxair, 99.995 %), O_2 (Praxair, 99.95 %), and N_2 (Praxair, 99.999 %) at a volume ratio of CH_4:O_2:N_2= 3:1:0 or 3:1:4 at a total flow rate of 35 mL/min (GHSV = 210,000–2,000 h^{-1}) controlled by mass flow controllers (Aalborg GFC17). The effluent gas was analyzed by gas chromatography (SHIMADZU, GC-14A) equipped with a thermal conductivity detector (TCD, for detecting CO, CO_2, and CH_4) and a flame ionization detector (FID, for detecting C_{2+} products, i.e. C_2H_4, C_2H_6, C_3H_6, C_3H_8, C_4H_8, and C_4H_{10}). The activity of the catalyst was evaluated after the system had reached the set point for 2h. The %CH_4 conversion, %C_{2+} selectivity, %CO_x selectivity, and %C_{2+} yield were calculated using equations (1)–(4).

$$\%\ CH_4\ \text{conversion} = \frac{\text{moles of } CH_4 \text{ input} - \text{moles of } CH_4 \text{ output}}{\text{moles of } CH_4 \text{ input}} \times 100 \quad (1)$$

$$\%\ C_{2+}\ \text{selectivity} = \frac{\text{moles of } C_{2+}}{\text{Total moles of products}} \times 100 \quad (2)$$

$$\%\ CO_x\ \text{selectivity} = \frac{\text{moles of } CO_x}{\text{Total moles of products}} \times 100 \quad (3)$$

$$\%\ C_{2+}\ \text{yield} = \frac{\%\ CH_4 \text{conversion} \times \%\ C_{2+} \text{selectivity}}{100} \quad (4)$$

I-2.3 Catalyst characterization

The XRD patterns of the samples were conducted using X-ray powder diffraction (X-Ray Diffractometer, XRD: Philips: X'Pert, using Cu-Kα radiation, 40 kV and 30 mA, 0.02° step size, 0.5 s step time). The surface morphology of the catalysts was imaged using a scanning electron microscope with an energy dispersive X-ray spectrometer (FE-SEM/EDS, FE-SEM: JEOL JSM7600F). The surface area, pore volume, and pore size of the catalysts were analyzed using N_2-physisorption (BET: 3Flex Physisorption Micromeritics). The electronic states of silicon (Si 2p), tungsten (W 4f), manganese (Mn 2p), and sodium (Na 1s) for the catalysts were characterized using X-ray photoelectron spectrometry (XPS, Kratos Axis Ultra DLD, using Al K_α for the X-ray source). Coke formation of fresh used catalysts was also analyzed using thermogravimetric analysis-derivative thermogravimetry (TGA-DTG, Perkin Elmer Pyris 1 TGA). A sample of 10 mg was loaded into an alumina crucible. Each sample was initialized by introducing air (zero gas, Lab grade purity, Thai Standard Gas Co., Ltd (TSG)) gas at a feed flow rate of 100 mL/min. The system was then heated from room temperature to 1000 °C with a heating rate of 10 ºC/min.

I-3. Results and discussion

The catalytic activity for OCM reaction of each single component catalyst compared with a blank test (without a catalyst used) is presented in Fig. I-1 (also see Table I-S2 & Fig. I-S1–S3). It should be noted that some elements/components were not chosen for the screening test because they are expensive (Ru, Rh, Pd, Ir, Pt, and Au), unstable at high temperatures (Ag), toxic, or unavailable. In addition, the elements that generally yielded a high CH_4 combustion to CO_x (Ru, Rh, Pd, Ir, and Pt [41]) were not of interest. Moreover, it is important to note that the C_{2+} yield was the criterion used to identify a superior catalyst when comparing the activities of catalysts.

From Fig. I-1, La/SiO_2 had the highest C_{2+} yield at 5.56% with 52.8% C_{2+} selectivity and 10.53% CH_4 conversion under the test conditions. Surprisingly, the catalytic performance of the blank test conducted under the same test conditions was relatively high compared to these catalysts, giving 3.72% yield, 38.6% C_{2+} selectivity and 9.64% CH_4 conversion. This indicated that the gas phase reaction for the OCM reaction could take place at this reactor temperature (700 ºC) [1, 8, 42]. The top-14 active catalysts that with a C_{2+} yield higher than that of the blank test were (in order), giving 5.56–3.83 % C_{2+} yields. The other single component catalysts had a C_{2+} yield lower than that of the blank test, suggesting that those single components are inactive for the OCM reaction.

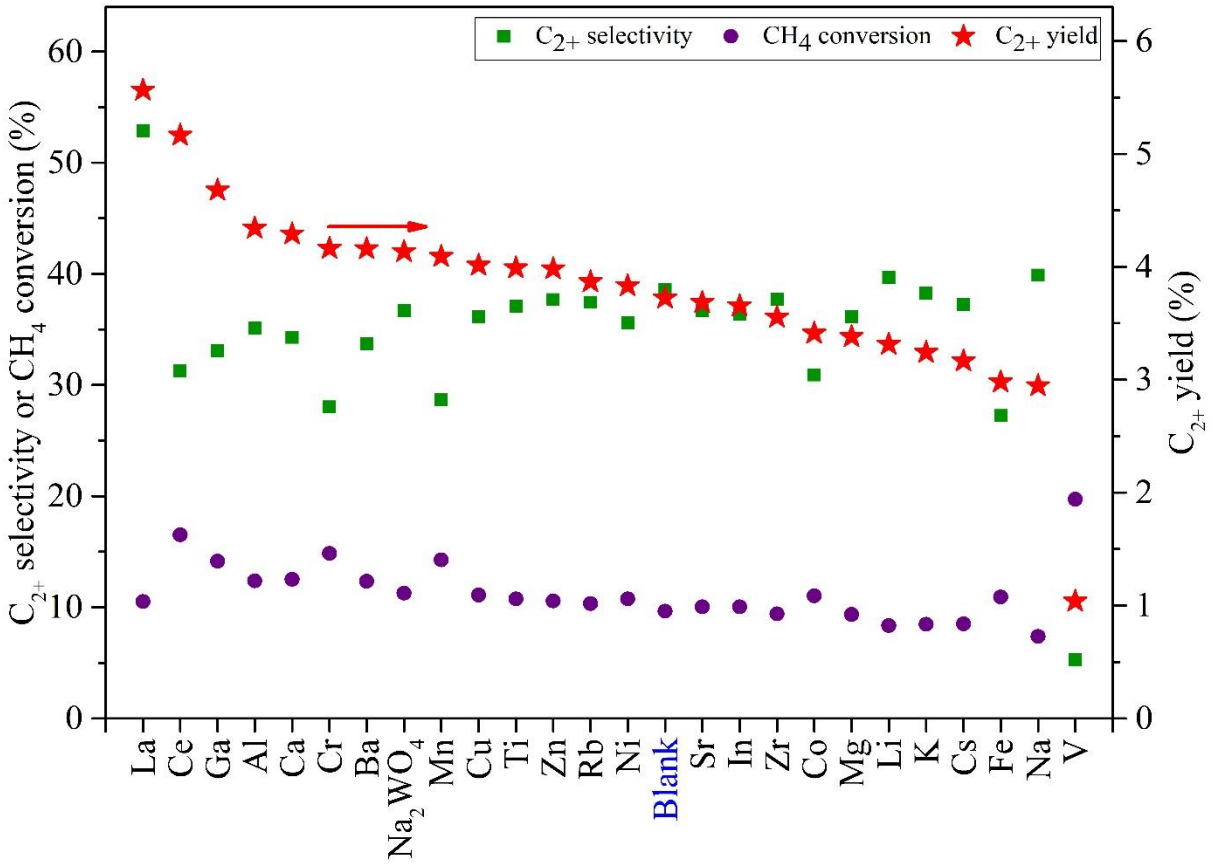

Fig. I-1. C_{2+} selectivity, CH_4 conversion, and C_{2+} yield of single component catalysts (10 wt%) compared with a blank test. Testing conditions: reactor temperature = 700 °C at atmospheric pressure, CH_4:O_2:N_2 = 3:1:0, total flow rate = 35 mL/min (GHSV = 50,000 h^{-1}), catalyst amount = 8.0 mg.

The search of binary catalysts (combinations of two main active components that exhibit a synergistic catalyst effect for the OCM reaction) was the primary purpose of this work. A number of active components must be chosen for binary screening. Practically, all of the components could be chosen for the binary catalyst screening test. However, it is believed that a combination of a relatively high active component mixed with another high active component is more likely to exhibit a synergistic catalyst effect as evidenced in previous works [41, 43] .

In order to narrow the choices of active components and shorten the time of the screening test, the top-14 single components achieving a C_{2+} yield higher than that of the blank test shown in Fig. I-1 were chosen for further binary catalyst screening. These 14 components were made into binary catalysts, which were prepared by combining each one with the other 13 in turn, providing 91 binary catalysts in total. Each catalyst was prepared using a co-impregnation method that involved an active component ratio of 1:1 and a total weight loading of the active component on SiO_2 of 10 wt%. The results of the screening test are presented in Figs. 2 a)–d) and the values of the products and the byproducts are presented in Table I-S3. It was found that the outstanding catalyst was the combination of Na_2WO_2 and Mn on the SiO_2 support (Na_2WO_4-Mn/SiO_2), giving the highest C_{2+} yield of 9.18% with 36.2% C_{2+} selectivity and 25.36% CH_4 conversion. Several other catalysts also provided a C_{2+} yield higher than that of the blank test. It is interesting to see that many of the binary catalysts made from Ga (including Ga-Za, Ga-Rb, Ga-Cr, Ga-Al, and Ga-Na_2WO_4) were in the top-23 active binary catalysts (Fig. I-2a). Moreover, the binary catalyst that offered the highest selectivity was Ca-La, yielding 44.7% C_{2+} selectivity with 4.96% C_{2+} yield and 11.10% CH_4 conversion. These catalysts are of great interest for future study.

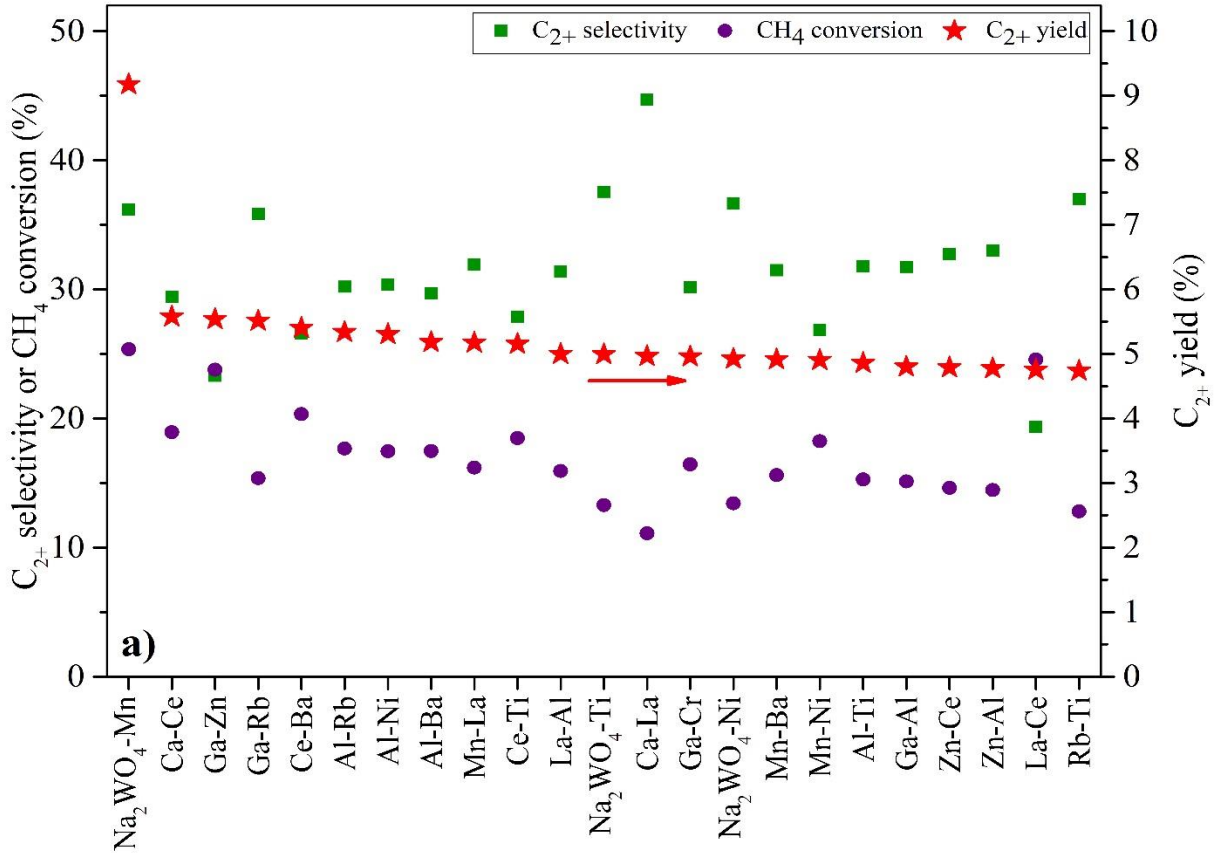

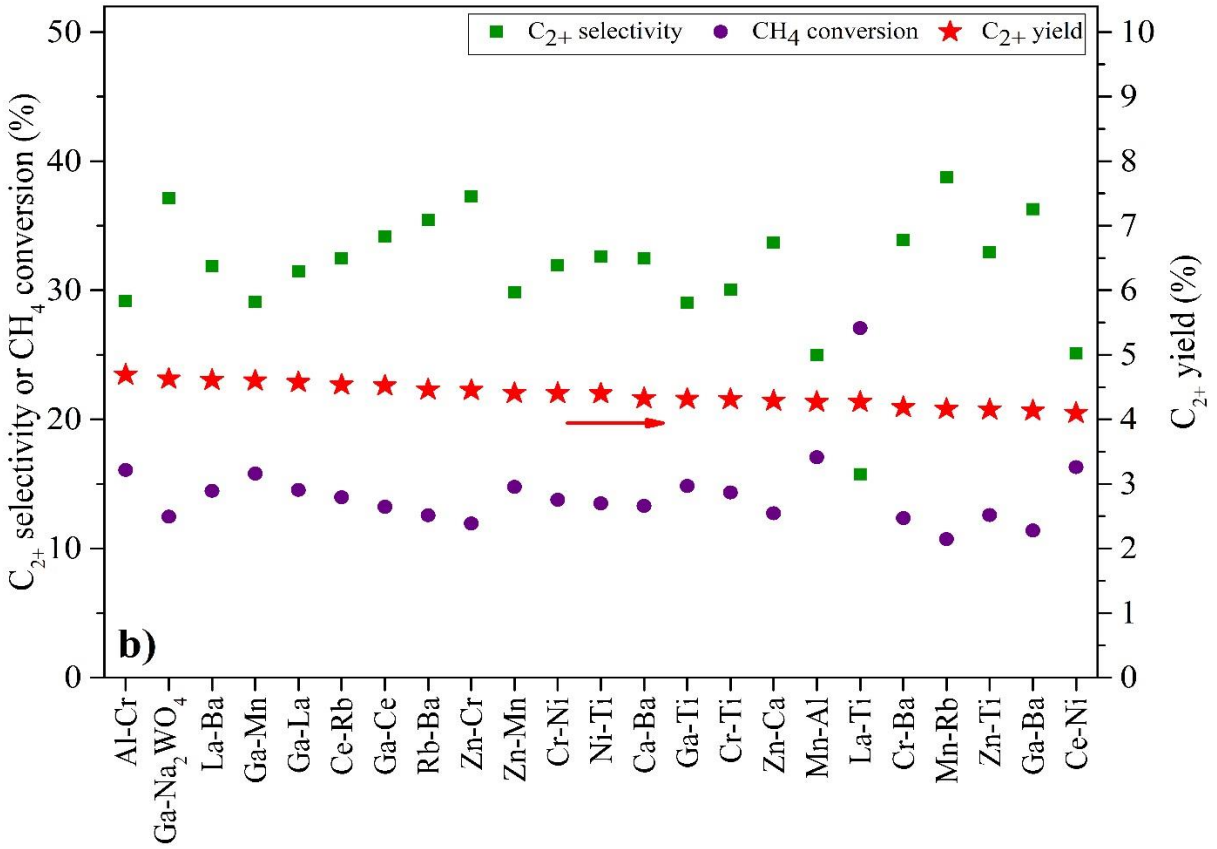
C2+ selectivity
CH4 conversion
C2+ yield
C2+ selectivity or CH4 conversion (%)
C2+ yield (%)
b)
Al-Cr
Ga-Na2WO4
La-Ba
Ga-Mn
Ga-La
Ce-Rb
Ga-Ce
Rb-Ba
Zn-Cr
Zn-Mn
Cr-Ni
Ni-Ti
Ca-Ba
Ga-Ti
Cr-Ti
Zn-Ca
Mn-Al
La-Ti
Cr-Ba
Mn-Rb
Zn-Ti
Ga-Ba
Ce-Ni

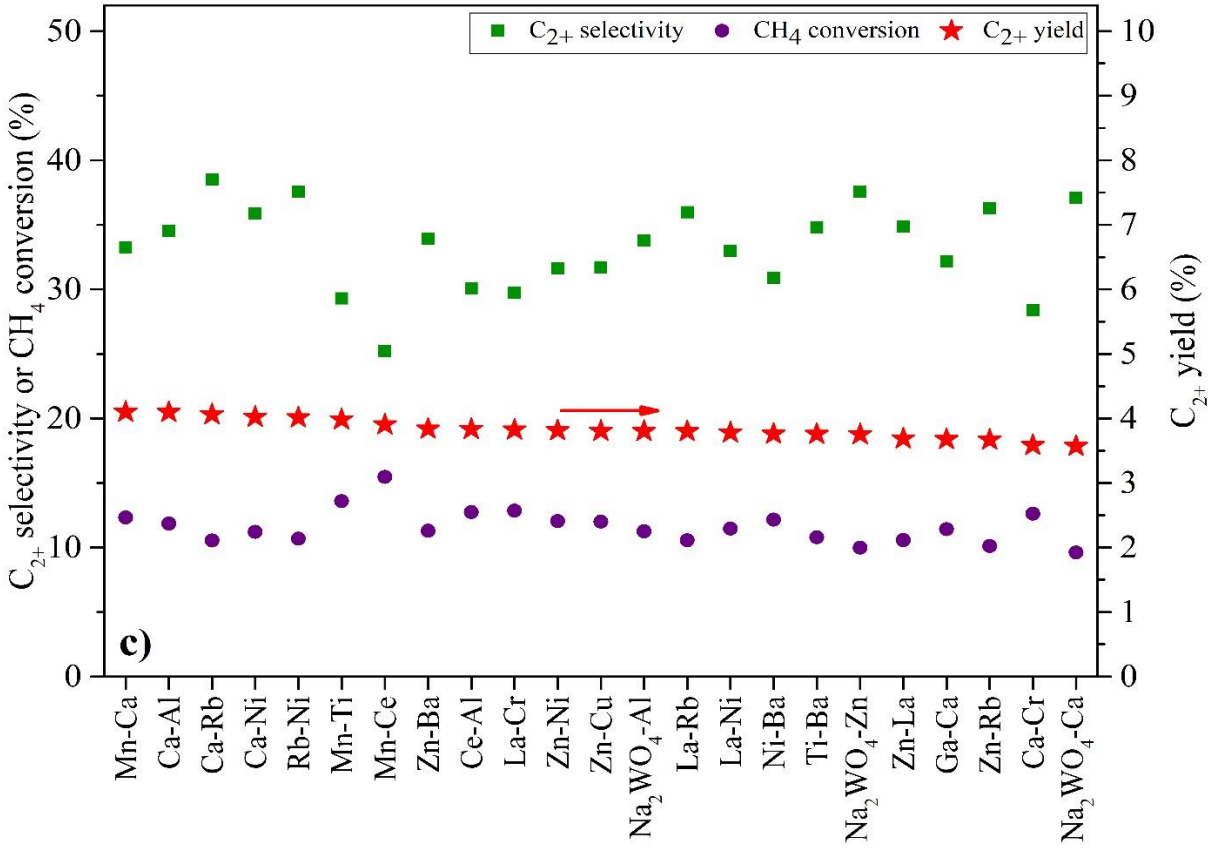
C2+ selectivity
CH4 conversion
C2+ yield
C2+ selectivity or CH4 conversion (%)
C2+ yield (%)
c)
Mn-Ca
Ca-Al
Ca-Rb
Ca-Ni
Rb-Ni
Mn-Ti
Mn-Ce
Zn-Ba
Ce-Al
La-Cr
Zn-Ni
Zn-Cu
Na2WO4-Al
La-Rb
La-Ni
Ni-Ba
Ti-Ba
Na2WO4-Zn
Zn-La
Ga-Ca
Zn-Rb
Ca-Cr
Na2WO4-Ca

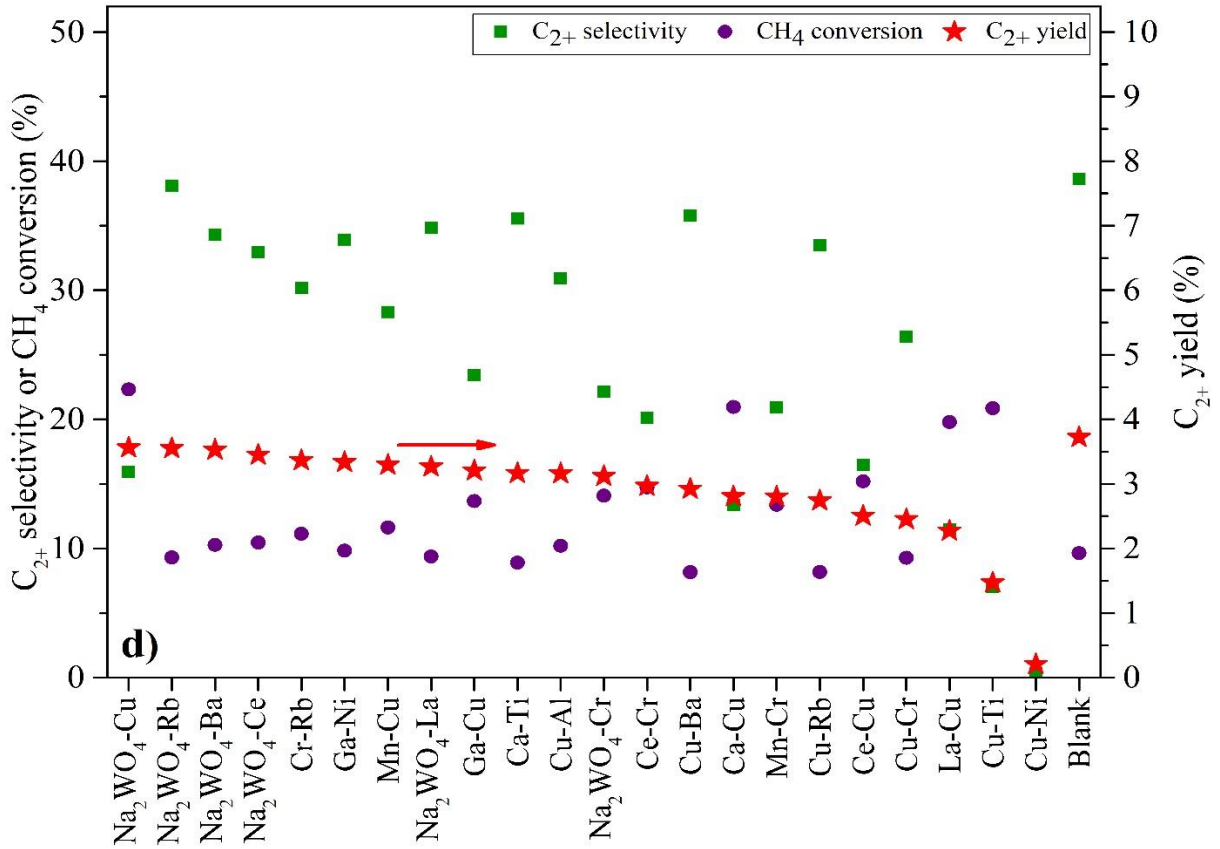

Fig. I-2. a)–d) C_{2+} selectivity, CH_4 conversion, and C_{2+} yield of binary catalysts (weight ratio of 1:1 and total weight loading of 10 wt% on SiO_2) compared with a blank test. Testing conditions: reactor temperature = 700 °C at atmospheric pressure, CH_4:O_2:N_2 = 3:1:0, total flow rate = 35 mL/min (GHSV = 50,000 h^{-1}), catalyst amount = 8.0 mg.

The Na_2WO_4-Mn/SiO_2 catalyst was further studied by varying the weight ratio of Na_2WO_4:Mn, while the total weight loading was maintained at 10 wt%. The results are plotted in Fig. I-3 and the distributions of the products and the byproducts are listed in Table I-S4. Promisingly, when the Na_2WO_4:Mn was 6:4, the values of all of the activities—C_{2+} selectivity, CH_4 conversion, and C_{2+} yield—were the highest at 49.6%, 29.14%, and 14.44%, respectively. As seen in the XRD patterns is presented in Fig. I-4 (also see Table I-S9), the characteristic peaks of α-cristobalite appeared for catalysts containing Na_2WO_4, while for catalysts containing Mn, the characteristic peaks of Mn_2O_3 were dominant compared to those of Mn_3O_4. Furthermore, as seen in the SEM images Fig 5, the particle size and shape of the catalyst at the Na_2WO_4:Mn ratio of 6:4 were uniform throughout the sample. At low Na_2WO_4:Mn ratios, amorphous SiO_2 could still be observed and at high Na_2WO_4:Mn ratios, very large particles (α-cristobalite) formed. These indicated that the formation of α-cristobalite and crystalline manganese oxides and the particle size are essential for catalytic activity.

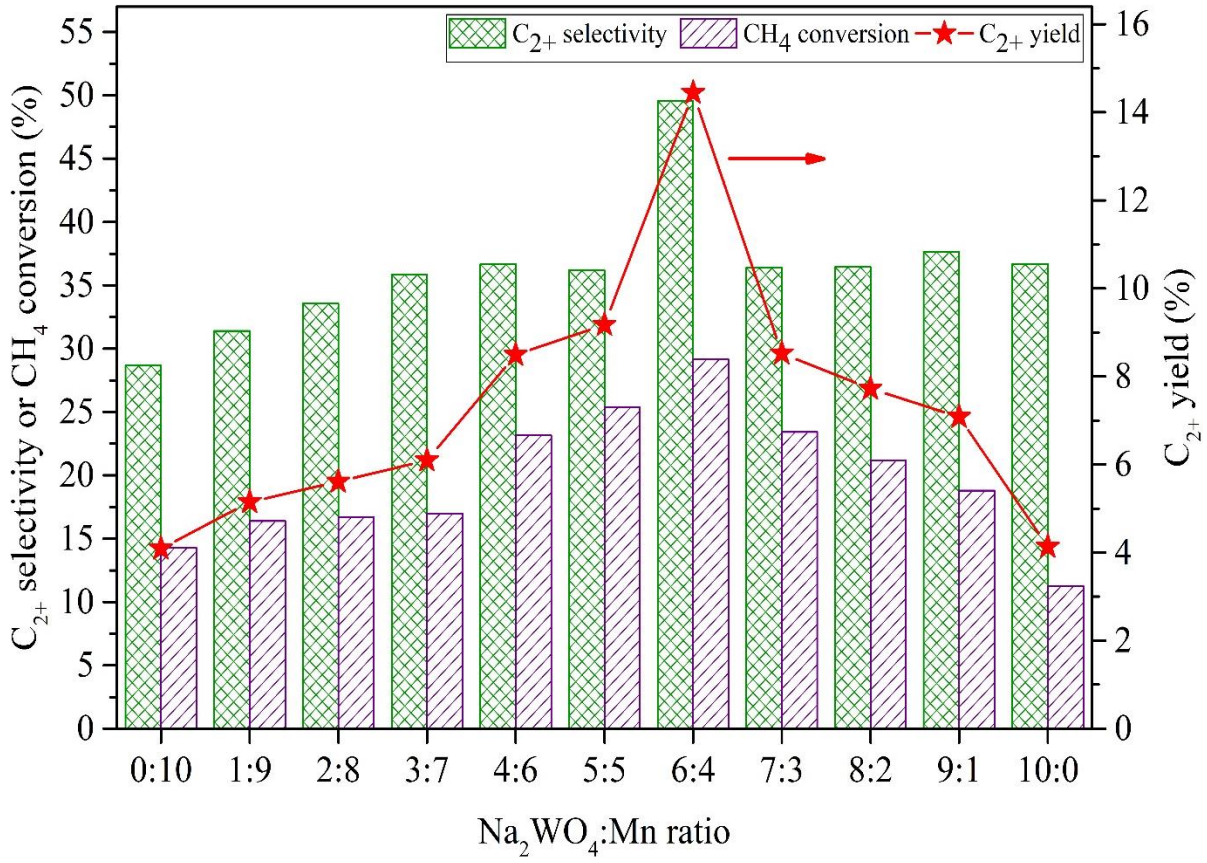

Fig. I-3. C_{2+} selectivity, CH_4 conversion, and C_{2+} yield of Na_2WO_4-Mn/SiO_2 catalysts at different weight ratios of Na_2WO_4:Mn with a total weight loading of 10 wt% on SiO_2. Testing conditions: reactor temperature = 700 °C at atmospheric pressure, CH_4:O_2:N_2 = 3:1:0, total flow rate = 35 mL/min (GHSV = 50,000 h^{-1}), catalyst amount = 8.0 mg.

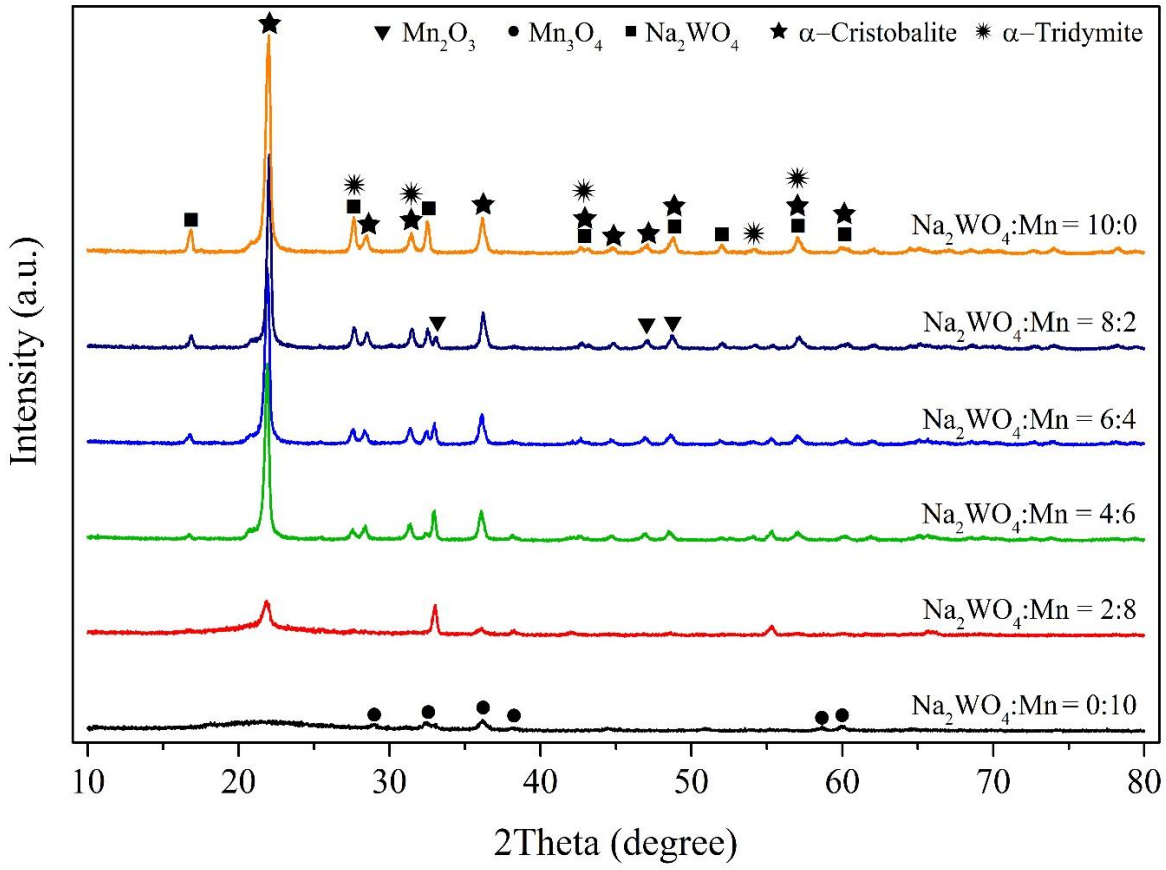

Fig. I-4. XRD patterns of Na_2WO_4-Mn/SiO_2 catalysts at different weight ratios, fixing the total metal loading on SiO_2 at 10 wt%.

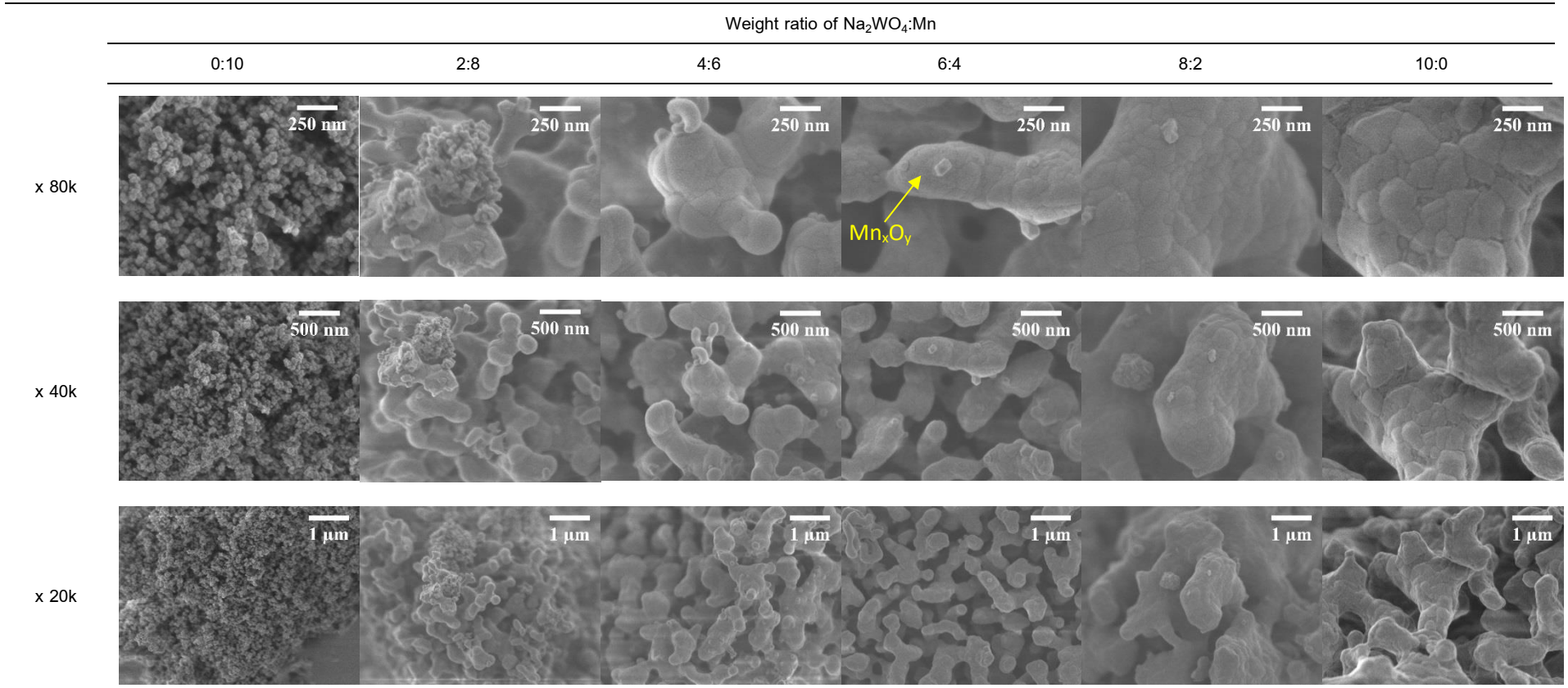

Fig. I-5. FE-SEM images of Na_2WO_4:Mn catalysts at different weight ratios, fixing the total metal loading on SiO_2 at 10 wt%.

Moreover, N_2-physisorption was used to determine the surface area of the catalysts presented in Fig. I-4, as shown in Table I-1. The catalyst impregnated with only Mn (Na_2WO_4:Mn ratio = 0:10) had the largest BET surface area (80.01 m^2/g) among the catalysts. The BET surface area of the catalysts containing Na_2WO_4 was relatively much smaller (<5 m^2/g) than that of the catalyst impregnated with only Mn because the combinations of Na_2WO_4 and silica result in the occurrence of the α-cristobalite phase, which has large particle sizes and very small pore volumes, in good agreement with the observations in Figs. 4 and 5. In addition, the basicity of each catalyst in Fig. I-4 was determined using CO_2-TPD, as shown in Figs. S7. It was found that only the catalyst impregnated with only Mn had one clear peak at 213 °C—assigned to be a weak basic site—while no clear peaks could be observed for the other catalysts. It was possible that the catalysts containing Na_2WO_4 had such a small BET surface area that a trace amount of CO_2 could be adsorbed and desorbed and/or the catalytic materials themselves possessed a low CO_2 adsorption capacity. This implies that the basicity of the catalysts containing Na_2WO_4 and Mn on SiO_2 did not play a significant role in OCM reaction due to the fact that the active site or the active component is the key to the reaction.

Table I-1. BET surface area, pore volume, and pore size of Na_2WO_4-Mn/SiO_2 catalysts at different Na_2WO_4:Mn weight ratios. The total metal loading on SiO_2 of each catalyst was fixed at 10 wt%.

Weight ratio of Na_2WO_4:Mn	BET surface area (m^2/g)	Pore volume (cm^3/g)	Pore size (Å)
0:10	80.01	0.6728	336.36
2:8	4.97	0.0166	134.43
4:6	2.65	0.0082	124.41
6:4	2.06	0.0077	150.25
8:2	0.95	0.0032	132.72
10:0	2.12	0.0071	135.20

Furthermore, the effect of the total weight loading of Na_2WO_4 and Mn on SiO_2 was investigated, as presented in Fig. I-6. The products and byproducts are also presented in Table I-S5. Clearly, the total weight loading of the active components strongly influenced the catalytic activity. Increasing the total weight loading from 2.5 to 10 wt% resulted in sharp increases in the C_{2+} selectivity, CH_4 conversion, and C_{2+} yield. The optimal C_{2+} yield occurred at a total weight loading of 10 wt%, yielding 14.44% C_{2+} yield with 49.6% C_{2+} selectivity and 29.14% CH_4 conversion. Above 10 wt%, the C_{2+} yield and the CH_4 conversion steadily decreased; while the C_{2+} selectivity slowly decreased until 20 wt%, and then slightly increased from 36.0% to 48.3% at 30 wt%. As observed from the XRD patterns is presented in Fig. I-7 (also see Table I-S9) and the SEM images Fig. I-8, the particle size and shape of the catalyst at 10 wt% loading were noticeably more uniform and smaller than those of the catalysts at > 10 wt%. When comparing the catalysts between 5 wt% and 10 wt%, it was more likely that there were fewer small particles (ca. 50 μm, being manganese oxides particles) of the catalyst at 5 wt% than at 10 wt%, which indicated that the catalyst at 10 wt% had the highest activity.

Furthermore, the BET surface areas, pore sizes, and pore volumes of the catalysts in Fig. I-7 were determined using N_2-physisorption, as presented in Table I-2. Increasing the total metal loadings from 5 to 25 wt% resulted in reductions in the BET surface areas and pore volumes, in good agreement with the observation based on the SEM images in Fig. I-8. However, the BET surface area of the catalyst at 30 wt% loading increased slightly, perhaps because the amount of α-cristobalite structure was the smallest relative to the other catalysts, due to the smallest amount of SiO_2 being used, resulting in more Na_2WO_4 and MnO_x particles being present on the surface, which caused the creation of rough surfaces and thereby increased the surface area of the 30 wt% catalyst. CO_2-TPD measurements of the catalysts in Fig. I-7 were also investigated, as presented in Fig. I-S8. Similar to Fig. I-S7, all the catalysts had very low basicity as described earlier.

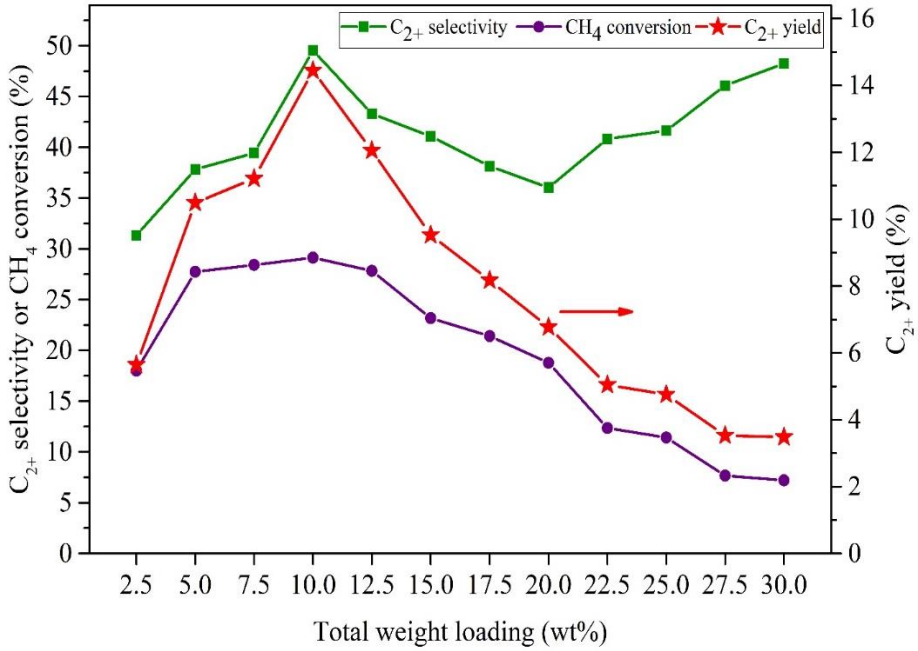

Fig. I-6. C_{2+} selectivity, CH_4 conversion, and C_{2+} yield of Na_2WO_4-Mn/SiO_2 catalysts at different total weight loadings from 2.5 to 30.0 wt% on SiO_2, with the Na_2WO_4:Mn weight ratio of 6:4. Testing conditions: reactor temperature = 700 °C at atmospheric pressure, CH_4:O_2:N_2 = 3:1:0, total flow rate = 35 mL/min (GHSV = 50,000 h^{-1}), catalyst amount = 8.0 mg.

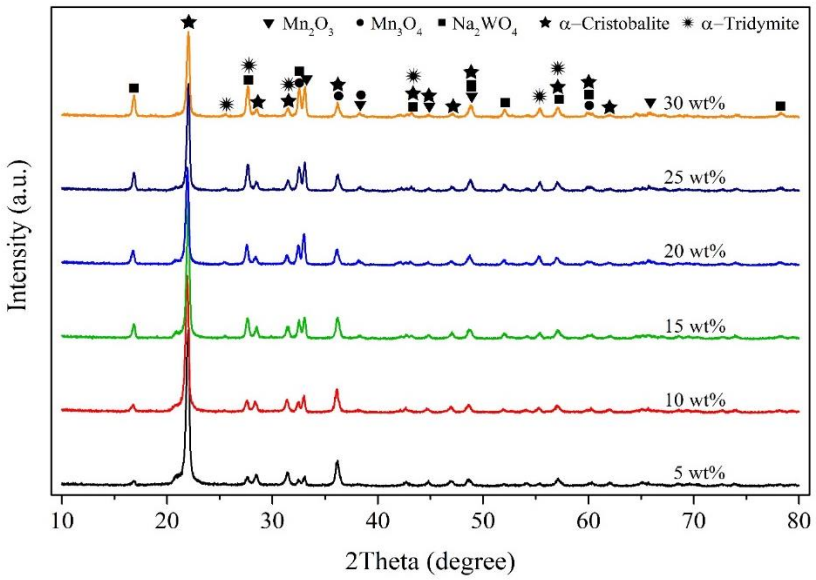

Fig. I-7. XRD patterns of Na_2WO_4-Mn/SiO_2 catalysts at different total metal loadings on SiO_2, fixing the Na_2WO_4:Mn ratio at 6:4.

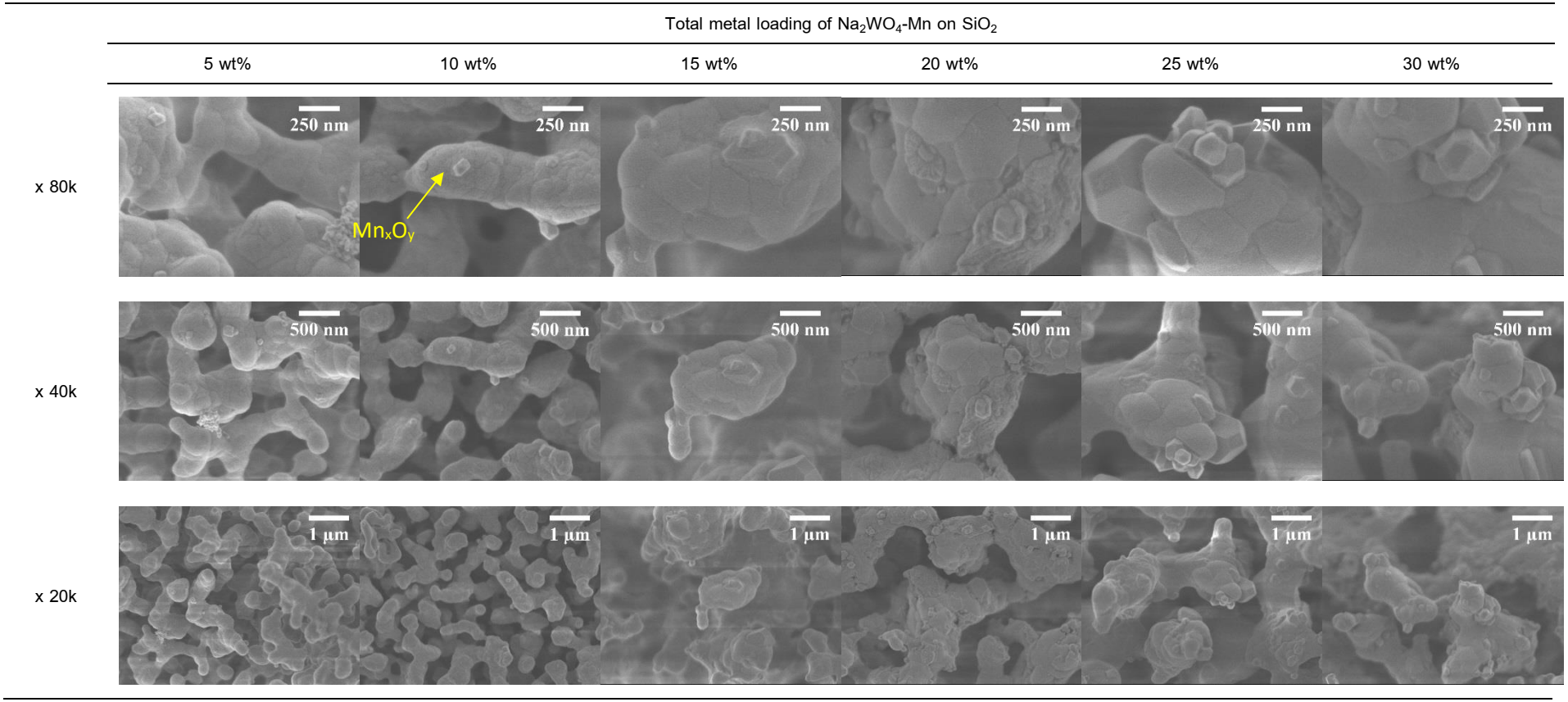

Fig. I-8. FE-SEM images of Na_2WO_4-Mn/SiO_2 catalysts at different total metal loadings on SiO_2, fixing the Na_2WO_4:Mn ratio at 6:4.

Table I-2. BET surface area, pore volume, and pore size of Na_2WO_4-Mn/SiO_2 catalysts at different total metal loadings. The metal ratio of Na_2WO_4:Mn was fixed at 6:4.

Total metal loading of Na_2WO_4-Mn on SiO_2	BET surface area (m^2/g)	Pore volume (cm^3/g)	Pore size (Å)
5 wt%	2.38	0.0086	144.87
10 wt%	2.06	0.0077	150.25
15 wt%	0.84	0.0035	170.07
20 wt%	0.46	0.0035	303.74
25 wt%	0.35	0.0019	222.20
30 wt%	1.20	0.0046	154.32

The surface chemistries of the MnO_x/SiO_2, Na_2WO_4/SiO_2 and optimal Na_2WO_4-Mn/SiO_2 catalysts were analyzed using XPS, as presented in Fig. I-9. Multiple scan spectra were conducted in the Si, Mn, Na and W regions. These spectra confirmed that the Na_2WO_4-Mn/SiO_2 catalyst comprised SiO_2 (2p = 103.5 eV), Mn_2O_3 ($2p_{3/2}$ = 641.3 eV, $2p_{1/2}$ = 653.6 eV), Na_2O (1s = 1071.5 eV) and WO_3 ($4f_{7/2}$ = 33.2 eV, $4f_{5/2}$ = 35.3 eV) [44]. Of note was that the characteristic XPS peaks of Si (Fig.9a) of the Na_2WO_4/SiO_2 and Na_2WO_4-Mn/SiO_2 catalysts relative to the Mn/SiO_2 catalyst shifted from 103.5 to 103.2 eV because the SiO_2 phase in the Mn/SiO_2 catalyst is amorphous, but the SiO_2 phases in the Na_2WO_4/SiO_2 and Na_2WO_4-Mn/SiO_2 catalysts are α-cristobalite. For Na 1s (see Fig. I-9c), no substantial shift of the peaks was found. Interestingly, significant changes in binding energies were observed in Figs. 9b and 9d, as the binding energies of Mn 2p and W 4f of the Na_2WO_4-Mn/SiO_2 catalyst shifted toward lower binding energies compared to the binding energies of Mn and W of the single Mn/SiO_2 and Na_2WO_4/SiO_2 catalysts, respectively. This suggested that the bond strengths of W—O and Mn—O became weaker, resulting in an improvement in the oxygen mobility over the surface of the Na_2WO_4-Mn/SiO_2 catalyst, thereby enhancing the activation of CH_4 [22].

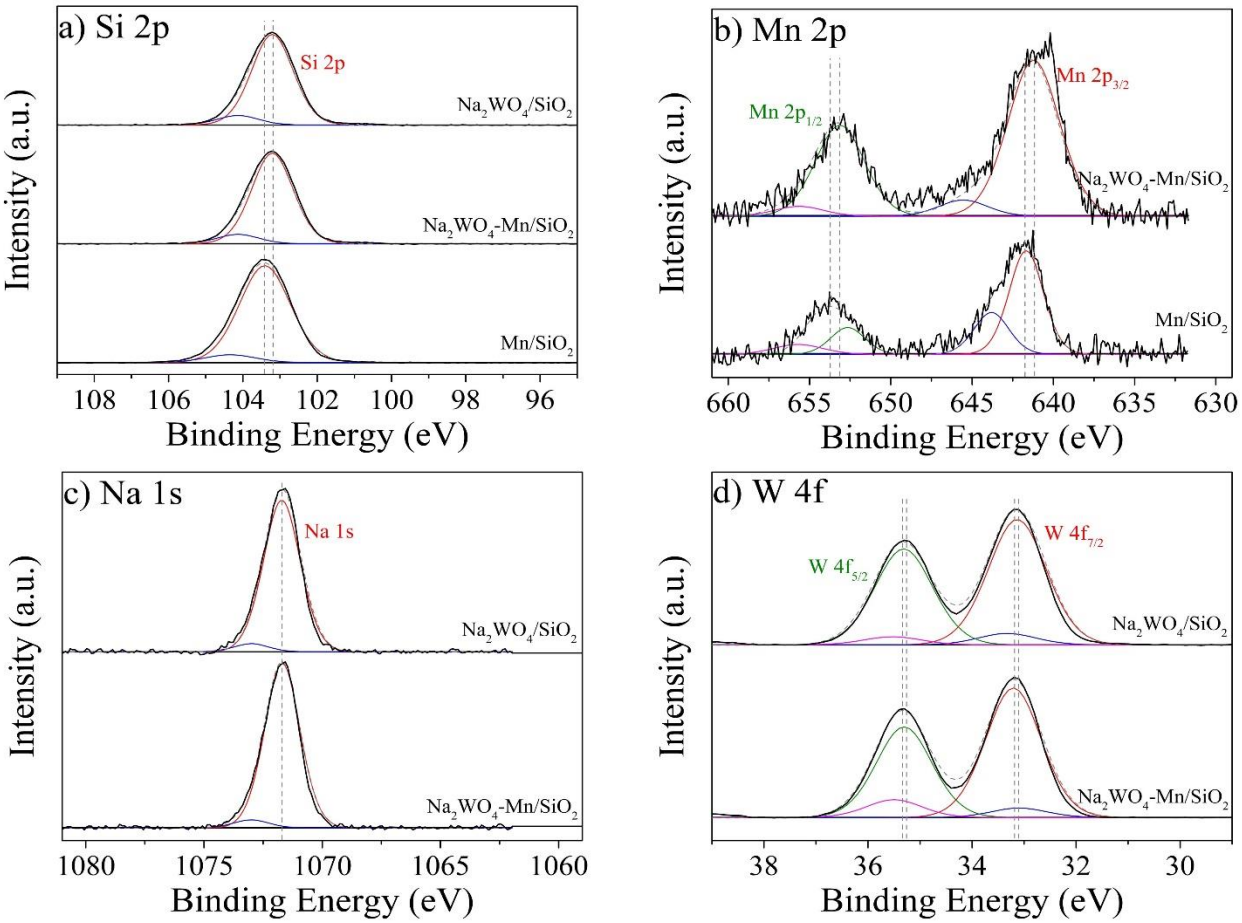

Fig. I-9. XPS spectra of a) Si 2p, b) Mn 2p, c) Na 1s and d) W 4f regions obtained from Mn/SiO_2, Na_2WO_4/SiO_2 and Na_2WO_4-Mn/SiO_2 catalysts.

The optimal catalyst was further investigated for two feeding gas conditions—with and without N_2 gas feedings—and at different catalyst amounts in the reactor by fixing the total feed gas flow rate at 35 mL/min. The results and the details of the two conditions are shown in Fig. I-10 and the values of the products and the byproducts are presented in Table I-S6 and S7. For the condition without N_2 feeding, the C_{2+} productivity increased rapidly with increasing catalyst amounts from 2 to 30 mg. Note that the GHSV values were lowered with increased catalyst amounts due to the increased catalyst volume. The C_{2+} yield reached an optimal point of 16.77% with 53.9% C_{2+} selectivity and 31.15% CH_4 conversion. After the optimal point, the activity of the catalyst slowly decreased. For the condition with N_2 feeding at a ratio of CH_4:O_2:N_2 = 3:1:4, the catalyst amount was in a range from 20 to 200 mg. Similarly, the C_{2+} productivity increased sharply when the catalyst amount increased from 20 to 50 mg, achieving the optimal C_{2+} yield of 18.59% with 55.0% C_{2+} selectivity and 33.82% CH_4 conversion. Above 50 mg, the C_{2+} productivity gradually decreased.

It can be noticed that when adding the inert gas to the feeding system, the optimal C_{2+} yield shifted toward a higher catalyst amount. This can be explained by considering that at the same catalyst amount (such as 20 mg), the chance for the reactant gases to interact with the active sites of the condition without N_2 feeding is lower than that of the condition with N_2 feeding, and thus more catalyst is required; consequently all of the reactant gases can interact with the active sites before leaving the catalyst bed.In addition, the optimal C_{2+} yield

of the condition with N_2 feed was slightly higher than that of the condition without N_2, suggesting that lowering the concentration of the reactant gases using an inert gas favored the conversion of methane. This could occur because the diffusion of the reactants and other species over the catalyst's surface in the diluted condition of the reactants is unlimited. It is also interesting to see that after the optimum catalyst amounts, the CH_4 conversion and the C_{2+} selectivity minimally reduced, resulting in a gradual decrease of the C_{2+} yield. It is possible that the C_{2+} products further reacted with other active sites of the catalyst to produce CO_x and/or a partial amount of the detected CH_4 had been generated from the C_{2+} products [2, 45-47]. Thus, the C_{2+} productivity decreased with increasing CH_4 conversion.

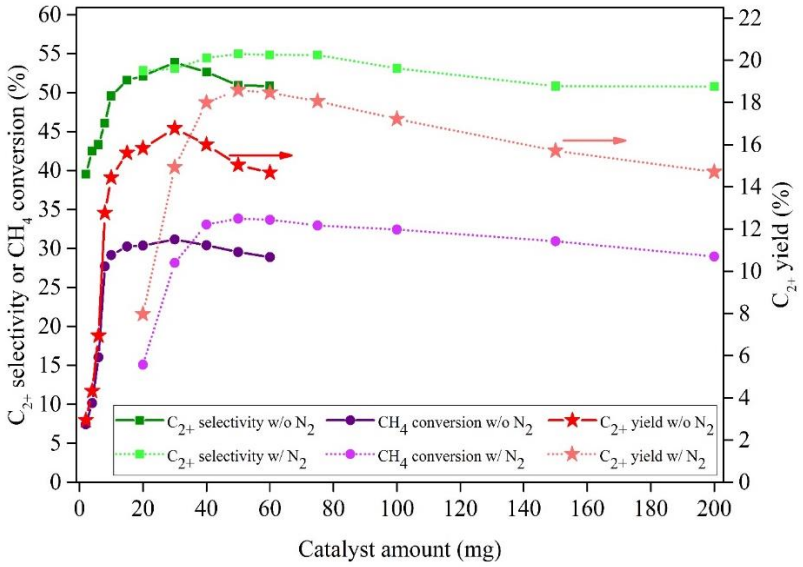

Fig. I-10. C_{2+} selectivity, CH_4 conversion, and C_{2+} yield of Na_2WO_4-Mn/SiO_2 catalysts at different catalyst weights, with Na_2WO_4:Mn weight ratio of 6:4, total weight loading of 10 wt% on SiO_2. Testing conditions: reactor temperature = 700 °C at atmospheric pressure, total flow rate = 35 mL/min. For the condition w/o N_2 feeding; CH_4:O_2:N_2 = 3:1:0, catalyst weight = 2–75 mg (GHSV =210,000–5,500 h^{-1}). For the condition w/ N_2 feeding; CH_4:O_2:N_2 = 3:1:4, catalyst amount = 20–200 mg (GHSV =17,000–2,000 h^{-1}).

The stability test of the Na_2WO_4-Mn/SiO_2 catalyst using the optimal conditions for 50 h is shown in Fig. I-11 (see also Table I-S8. for the values of each product and byproduct). The performance of the catalyst constantly increased from the beginning to the maximum C_{2+} yield in the sixth hour of testing. The maximum C_{2+} yield was achieved at 23.54% with 60.5% C_{2+} selectivity and 39.67% CH_4 conversion. After that, the performance of the catalyst slightly decreased until the end of testing, resulting in a 18.44% C_{2+} yield with 55.4% C_{2+} selectivity and 33.30% CH_4 conversion, which was a C_{2+} yield reduction of approximately 21.7% from the maximum point. Hence, the catalyst was quite good during the 50 h period. The used catalyst was then taken to further analyze using SEM, XRD, and TGA-DTG, and these results were compared with those of the fresh catalyst in order to identify any causes of the slow deactivation of the catalyst, as presented in Fig. I-12. The SEM images of the fresh and used catalysts (see Figs. 12a and 12b, respectively) revealed that the particle size of the used catalyst increased to approximately four times the fresh catalyst. The difference in the XRD patterns of the fresh and used catalysts (see Fig. I-12c) was the appearance of the α-tridymite phase in

the used catalyst. This implied that a phase transformation of α-cristobalite to α-tridymite slowly occurred during the reaction, considerably slowing the deactivation of the catalyst. The TGA-DTG profiles (see Fig. I-12d) had no peak for coke decomposition. Generally, the peak for coke decomposition can be seen at about 500–600 °C [48]. Therefore, it was concluded that the slow deactivation of the catalyst resulted from the catalyst sintering and the phase transformation of α-cristobalite to α-tridymite without coke deposition on the catalyst's surface.

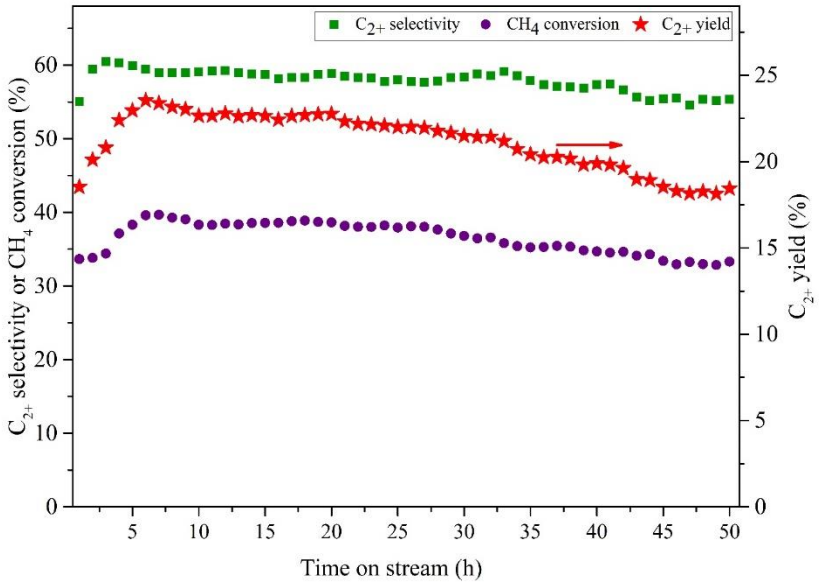

Fig. I-11. Catalyst stability test of Na_2WO_4-Mn/SiO_2 catalysts, with a Na_2WO_4:Mn weight ratio of 6:4. Testing conditions: reactor temperature = 700 °C at atmospheric pressure, CH_4:O_2:N_2 = 3:1:4, total flow rate = 35 mL/min (GHSV = 14,500 h^{-1}), catalyst amount = 50.0 mg.

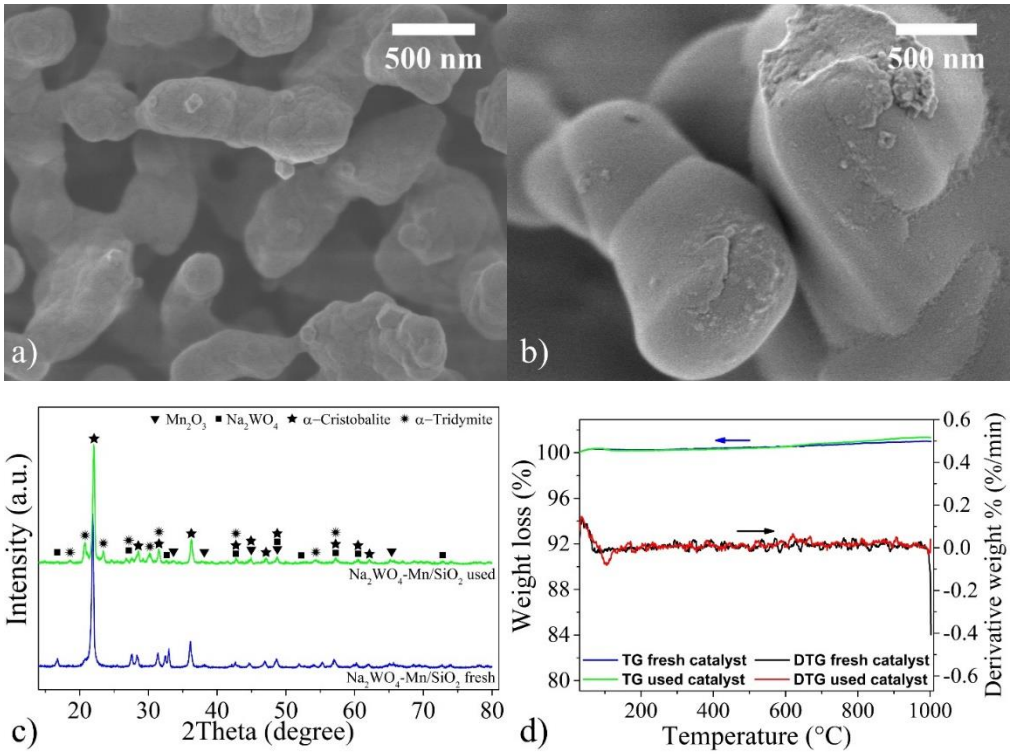

Fig. I-12. The used Na_2WO_4-Mn/SiO_2 catalyst was taken to further analyze, a) FE-SEM images of fresh catalysts, b) FE-SEM images of used catalysts, c) XRD patterns of fresh and used catalyst, and d) TGA-DTG profiles of fresh and used catalyst. With Na_2WO_4:Mn weight ratio of 6:4, total weight loading of 10 wt% on SiO_2.

I-4. Conclusion

In the pursuit of binary catalysts for the OCM reaction, 25 single components were first charily selected and prepared on amorphous SiO_2. The screening of these single catalysts provided 14 single catalysts that achieved a $\%C_{2+}$ yield higher than that of the blank test. The 14 components were then chosen to prepare binary catalysts by combining each one with the other 13 in turn, giving 91 binary catalysts in total. Subsequently, binary catalyst screening was carried out, revealing several active binary catalysts. The most active binary catalyst was the combination of Na_2WO_4 and Mn. Optimization of this catalyst was further investigated carefully by varying the Na_2WO_4:Mn ratio, the total metal loading on SiO_2, the catalyst amount, and the stability test, resulting in the highest C_{2+} yield of 23.54%, with 60.5% C_{2+} selectivity and 39.67% CH_4 conversion. The measurements of the binding energies of W and Mn using XPS revealed that the bond strengths of W—O and Mn—O became weaker, thereby enhancing the catalytic activity of the Na_2WO_4-Mn/SiO_2 catalyst. Moreover, the stability of the catalyst was monitored during 50 h of testing, disclosing that the catalyst very slowly deactivated due to the catalyst sintering and the phase transformation of α-cristobalite to α-tridymite.

Acknowledgements

This work was financially supported by the Department of Chemical Engineering and the Faculty of Engineering at Kasetsart University, Bangkok, Thailand; the Kasetsart University Research and Development Institute (KURDI); the Center of Excellence on Petrochemical and Materials Technology, the National Nanotechnology Center (NANOTEC), NSTDA, Ministry of Science and Technology, Thailand, through its program of Research Network NANOTEC (RNN); the Thailand Research Fund and the Commission on Higher Education (grant # MRG6180232).

References for Part I.

[1] P. Schwach, X. Pan, X. Bao, Direct conversion of methane to value-added chemicals over heterogeneous catalysts: challenges and prospects, Chem. Rev. 117 (2017) 8497-8520.

[2] J. Sun, J.W. Thybaut, G.B. Marin, Microkinetics of methane oxidative coupling, Catal. Today 137 (2008) 90-102.

[3] V.S. Arutyunov, L.N. Strekova, The interplay of catalytic and gas-phase stages at oxidative conversion of methane: A review, J. Mol. Catal. A: Chem. 426 (2017) 326-342.

[4] G.E. Keller, M.M. Bhasin, Synthesis of ethylene via oxidative coupling of methane: I. Determination of active catalysts, J. Catal. 73 (1982) 9-19.

[5] D.J. Wang, M.P. Rosynek, J.H. Lunsford, Oxidative coupling of methane over oxide-supported sodium-manganese catalysts, J. Catal. 155 (1995) 390-402.

[6] S.A. Driscoll, D.K. Gardner, U.S. Ozkan, Characterization, activity, and adsorption/desorption behavior of alkali-promoted molybdate catalysts for the oxidative coupling of methane, J. Catal. 147 (1994) 379-392.

[7] M.G. Colmenares, U. Simon, M. Yildiz, S. Arndt, R. Schomaecker, A. Thomas, F. Rosowski, A. Gurlo, O. Goerke, Oxidative coupling of methane on the Na_2WO_4-Mn_xO_y catalyst: COK-12 as an inexpensive alternative to SBA-15, Catal. Commun. 85 (2016) 75-78.

[8] V.I. Vedeneev, O.V. Krylov, V.S. Arutyunov, V.Y. Basevich, M.Y. Goldenberg, M.A. Teitel boim, The role of initiation in oxidative coupling of methane, Appl. Catal., A 127 (1995) 51-63.

[9] U. Zavyalova, M. Holena, R. Schlögl, M. Baerns, Statistical analysis of past catalytic data on oxidative methane coupling for new insights into the composition of hgh-performance catalysts, ChemCatChem 3 (2011) 1935-1947.

[10] T.K. Chan, K.J. Smith, Oxidative coupling of methane over cobalt—magnesium and manganese—magnesium mixed oxide catalysts, Appl. Catal. 60 (1990) 13-31.

[11] F.P. Larkins, M.R. Nordin, The effects of transition metal oxides on the methane oxidative coupling activity of doped MgO catalysts I. Zinc and manganese, J. Catal. 130 (1991) 147-160.

[12] K. Otsuka, T. Komatsu, Active catalysts in oxidative coupling of methane, J. Chem. Soc., Chem. Commun. (1987) 388-389.

[13] S. Hou, Y. Cao, W. Xiong, H. Liu, Y. Kou, Site requirements for the oxidative coupling of methane on SiO_2-supported Mn catalysts, Ind. Eng. Chem. Res. 45 (2006) 7077-7083.

[14] Y. Amenomiya, V.I. Birss, M. Goledzinowski, J. Galuszka, A.R. Sanger, Conversion of methane by oxidative coupling, Cat. Rev. 32 (1990) 163-227.

[15] R. Burch, G.D. Squire, S.C. Tsang, Comparative study of catalysts for the oxidative coupling of methane, Appl. Catal. 43 (1988) 105-116.

[16] J.A. Sofranko, J.J. Leonard, C.A. Jones, The oxidative conversion of methane to higher hydrocarbons, J. Catal. 103 (1987) 302-310.

[17] Z.C. Jiang, C.J. Yu, X.P. Fang, S.B. Li, H.L. Wang, Oxide/support interaction and surface reconstruction in the sodium tungstate(Na_2WO_4)/silica system, J. Phys. Chem. 97 (1993) 12870-12875.

[18] A. Palermo, J.P. Holgado Vazquez, A.F. Lee, M.S. Tikhov, R.M. Lambert, Critical influence of the amorphous silica-to-cristobalite phase transition on the performance of $Mn/Na_2WO_4/SiO_2$ catalysts for the oxidative coupling of methane, J. Catal. 177 (1998) 259-266.

[19] S. Pak, P. Qiu, J.H. Lunsford, Elementary reactions in the oxidative coupling of methane over $Mn/Na_2WO_4/SiO_2$ and $Mn/Na_2WO_4/MgO$ catalysts, J. Catal. 179 (1998) 222-230.

[20] J. Wang, L. Chou, B. Zhang, H. Song, J. Zhao, J. Yang, S. Li, Comparative study on oxidation of methane to ethane and ethylene over Na_2WO_4–Mn/SiO_2 catalysts prepared by different methods, J. Mol. Catal. A: Chem. 245 (2006) 272-277.

[21] S. Gu, H.S. Oh, J.W. Choi, D.J. Suh, J. Jae, J. Choi, J.M. Ha, Effects of metal or metal oxide additives on oxidative coupling of methane using Na_2WO_4/SiO_2 catalysts: reducibility of metal additives to manipulate the catalytic activity, Appl. Catal., A 562 (2018) 114-119.

[22] T.W. Elkins, H.E. Hagelin-Weaver, Characterization of $Mn–Na_2WO_4/SiO_2$ and $Mn–Na_2WO_4/MgO$ catalysts for the oxidative coupling of methane, Appl. Catal., A 497 (2015) 96-106.

[23] S. Ji, T. Xiao, S. Li, L. Chou, B. Zhang, C. Xu, R. Hou, A.P.E. York, M.L.H. Green, Surface WO_4 tetrahedron: the essence of the oxidative coupling of methane over M-W-Mn/SiO_2 catalysts, J. Catal. 220 (2003) 47-56.

[24] S. Arndt, T. Otremba, U. Simon, M. Yildiz, H. Schubert, R. Schomäcker, $Mn–Na_2WO_4/SiO_2$ as catalyst for the oxidative coupling of methane. What is really known?, Appl. Catal., A. 425–426 (2012) 53–61.

[25] N. Yamagata, Y. Abe, K. Igarashi, T. Ishikawa, M. Sahara, S. Okazaki, Importance of apparent density of $BaLa_2O_4$ catalysts in oxidative coupling of methane, Chem. Lett. 19 (1990) 1893-1896.

[26] I. Kim, G. Lee, H.B. Na, J.M. Ha, J.C. Jung, Selective oxygen species for the oxidative coupling of methane, Mol. Catal. 435 (2017) 13-23.

[27] B.M. Sollier, L.E. Gómez, A.V. Boix, E.E. Miró, Oxidative coupling of methane on Sr/La_2O_3 catalysts: Improving the catalytic performance using cordierite monoliths and ceramic foams as structured substrates, Appl. Catal., A 532 (2017) 65-76.

[28] M.S.C. Chan, E. Marek, S.A. Scott, J.S. Dennis, Chemical looping epoxidation, J. Catal. 359 (2018) 1-7.

[29] R. Voyatzis, J.B. Moffat, Cation effects in the oxidative coupling of methane on slica-supported binary alkali and alkaline earths, J. Catal. 142 (1993) 45-58.

[30] R.T. Yunarti, S. Gu, J.-W. Choi, J. Jae, D.J. Suh, J.-M. Ha, Oxidative coupling of methane using Mg/Ti-doped SiO_2-supported Na_2WO_4/Mn catalysts, ACS Sustain. Chem. Eng. 5 (2017) 3667-3674.

[31] D. Gerceker, A.H. Motagamwala, K.R. Rivera-Dones, J.B. Miller, G.W. Huber, M. Mavrikakis, J.A. Dumesic, Methane conversion to ethylene and aromatics on PtSn catalysts, ACS Catal. 7 (2017) 2088-2100.

[32] X. Guo, G. Fang, G. Li, H. Ma, H. Fan, L. Yu, C. Ma, X. Wu, D. Deng, M. Wei, D. Tan, R. Si, S. Zhang, J. Li, L. Sun, Z. Tang, X. Pan, X. Bao, Direct, nonoxidative cnversion of methane to ethylene, aromatics, and hydrogen, Science 344 (2014) 616-619.

[33] A.M. Maitra, Solid-state basicity as a guide to formulation of improved catalysts for oxidative coupling of methane: I. Performance evaluation, Appl. Catal., A 114 (1994) 65-81.

[34] T.W. Elkins, S.J. Roberts, H.E. Hagelin-Weaver, Effects of alkali and alkaline-earth metal dopants on magnesium oxide supported rare-earth oxide catalysts in the oxidative coupling of methane, Appl. Catal., A 528 (2016) 175-190.

[35] K. Omata, A. Aoki, K. Fujimoto, Oxidative coupling of methane over CaO-MgO mixed oxide, Catal. Lett. 4 (1990) 241-244.

[36] L. Luo, Y. Jin, H. Pan, X. Zheng, L. Wu, R. You, W. Huang, Distribution and role of Li in Li-doped MgO catalysts for oxidative coupling of methane, J. Catal. 346 (2017) 57-61.

[37] V.R. Choudhary, S.T. Chaudhari, A.M. Rajput, V.H. Rane, Oxidative coupling of methane to C_2-hydrocarbons over La-promoted CaO catalysts, Catal. Lett. 3 (1989) 85-87.

[38] V.H. Rane, S.T. Chaudhari, V.R. Choudhary, Oxidative coupling of methane over La-promoted CaO catalysts: Influence of precursors and catalyst preparation method, J. Nat. Gas Chem. 19 (2010) 25-30.

[39] L. Pirro, A. Obradović, B.D. Vandegehuchte, G.B. Marin, J.W. Thybaut, Model-based catalyst selection for the oxidative coupling of methane in an adiabatic fixed-bed reactor, Ind. Eng. Chem. Res. 57 (2018) 16295-16307.

[40] E. Danielson, J.H. Golden, E.W. McFarland, C.M. Reaves, W.H. Weinberg, X.D. Wu, A combinatorial approach to the discovery and optimization of luminescent materials, Nature 389 (1997) 944.

[41] W. Kumsung, M. Chareonpanich, P. Kongkachuichay, S. Senkan, A. Seubsai, Single and bimetallic catalyst screenings of noble metals for methane combustion, Catal. Commun. 110 (2018) 83-87.

[42] V.I. Vedeneev, V.S. Arutyunov, V.Y. Basevich, Kinetic limit of the ethane and ethylene yield in the gas phase condensation of methane, Russ. Chem. Bull. 44 (1995) 372-373.

[43] M. Kahn, A. Seubsai, I. Onal, S. Senkan, High-throughput synthesis and screening of new catalytic materials for the direct epoxidation of propylene, Comb. Chem. High Throughput Screen. 13 (2010) 67-74.

[44] J.F. Moulder, J. Chastain, Handbook of X-ray photoelectron spectroscopy: a reference book of standard spectra for identification and interpretation of XPS Data, Physical Electronics Division, Perkin-Elmer Corporation 1992.

[45] V. Fleischer, R. Steuer, S. Parishan, R. Schomäcker, Investigation of the surface reaction network of the oxidative coupling of methane over Na_2WO_4/ Mn/ SiO_2 catalyst by temperature programmed and dynamic experiments, J. Catal. 341 (2016) 91-103.

[46] V.I. Lomfonosov, M.Y. Sinev, Oxidative coupling of methane: mechanism and kinetics, Kinet. Catal. 57 (2016) 647-676.

[47] C. Karakaya, H. Zhu, C. Loebick, J.G. Weissman, R.J. Kee, A detailed reaction mechanism for oxidative coupling of methane over $Mn/Na_2WO_4/SiO_2$ catalyst for non-isothermal conditions, Catal. Today 312 (2018) 10-22.

[48] Y. Sang, A. Xing, C. Wang, Z. Han, Y. Wu, Near-graphite coke deposit on nano-HZSM-5 aggregates for methanol to propylene and butylene reaction, Catalysts 7 (2017) 171.

Supporting Information for:

Screenings of single and binary catalysts for oxidative coupling of methane to value-added chemicals

Table I-S1. Precursors of metal/component used for catalyst preparation.

Metal/Component	Precursor
Li	$LiNO_3$ 99.99%, Sigma-Aldrich
Na	$NaNO_3$ 99.5%, Alfa Aesar
K	KNO_3 99.0%, Sigma-Aldrich
Rb	$RbNO_3$ 99%, Alfa Aesar
Cs	$CsNO_3$ 99%, Aldrich
Mg	$MgSO_4 \cdot 7H_2O$ 99%, Fisher Chemicals
Ca	$Ca(NO_3)_2 \cdot 4H_2O$ 99.0%, Sigma-Aldrich
Sr	$Sr(NO_3)_2$ 99.995%, Merck
Ba	$Ba(NO_3)_2$ 99+%, Alfa Aesar
Ti	$C_{12}H_{28}O_4Ti$ 97+%, Alfa Aesar
V	NH_4VO_3 99.0%, Sigma-Aldrich
Cr	$Cr(NO_3)_3 \cdot 9H_2O$ 99%, Fluka
Mn	$Mn(NO_3)_2 \cdot 4H_2O$ 97%, Panreac
Fe	$FeSO_4 \cdot 7H_2O$ 99%, Ajax Fincechem
Co	$Co(NO_3)_2 \cdot 6H_2O$ 99%, Fisher scientific
Ni	$Ni(NO_3)_2 \cdot 6H_2O$ 98%, Fisher Chemic
Cu	$Cu(NO_3)_2 \cdot 3H_2O$ 98%, Ajax Fincechem
Zn	$Zn(NO_3)_2 \cdot 6H_2O$ 98.5%, QReC
Zr	$ZrO(NO_3)_2 \cdot xH_2O$ 99.5%, MATERION
Na_2WO_4	$Na_2WO_4 \cdot 2H_2O$ 98.0~101.0%, Daejung
Al	$Al(NO_3)_3 \cdot 9H_2O$ 99.997%, Sigma-Aldrich
Ga	$Ga(NO_3)_3 \cdot xH_2O$ 99.9%, Alfa Aesar
In	In 29% min, Alfa Aesar
La	$La(NO_3)_3 \cdot 6H_2O$ 99%, Himedia
Ce	$Ce(NO_3)_3 \cdot 6H_2O$ 99%, Sigma-Aldrich

Table I-S2. Performance results for silica-supported single catalysts. The total metal loading was fixed at 10 wt%, Reaction conditions: *T* = 700 °C; CH_4:O_2 = 3:1; total feed rate = 35 mL/min; mass amount = 8 mg.

Catalyst	CH_4 conversion (%)	Selectivity (%)							C_{2+} yield (%)
		CO_X	C_2H_4	C_2H_6	C_3H_6	C_3H_8	C_4H_{10}	C_{2+}	
La	10.53	47.2	30.6	18.2	2.5	0.3	1.2	52.8	5.56
Ce	16.53	68.8	18.3	10.5	1.6	0.1	0.8	31.2	5.16
Ga	14.14	66.9	19.2	11.4	1.6	0.2	0.7	33.1	4.68
Al	12.37	64.9	19.5	13.0	1.5	0.2	0.9	35.1	4.34
Ca	12.51	65.7	19.8	11.8	1.6	0.2	1.0	34.3	4.29
Cr	14.85	72.0	16.6	9.5	1.3	0.1	0.5	28.0	4.16
Ba	12.34	66.3	18.9	12.0	1.6	0.2	1.0	33.7	4.16
Na_2WO_4	11.27	63.3	19.6	14.4	1.6	0.0	1.0	36.7	4.13
Mn	14.27	71.3	16.1	10.3	1.4	0.1	0.8	28.7	4.09
Cu	11.10	63.8	24.3	10.7	0.6	0.1	0.4	36.2	4.01
Ti	10.76	62.9	19.4	14.8	1.6	0.1	1.2	37.1	3.99
Zn	10.56	62.3	20.4	14.6	1.7	0.2	0.9	37.7	3.98
Rb	10.33	62.6	19.3	15.5	1.6	0.1	0.9	37.4	3.87
Ni	10.76	64.4	19.1	14.2	1.6	0.1	0.6	35.6	3.83
Blank	9.64	61.4	20.5	15.3	1.7	0.1	0.9	38.6	3.72
Sr	10.04	63.3	19.1	14.8	1.5	0.1	1.2	36.7	3.68
In	10.05	63.6	18.7	14.9	1.6	0.1	1.0	36.4	3.65
Zr	9.42	62.3	19.5	15.5	1.6	0.1	1.0	37.7	3.55
Co	11.03	69.1	16.1	12.6	1.4	0.1	0.8	30.9	3.41
Mg	9.35	63.9	18.7	14.9	1.5	0.1	0.9	36.1	3.38
Li	8.35	60.3	19.4	17.1	1.6	0.1	1.5	39.7	3.31
K	8.47	61.7	18.8	16.8	1.6	0.1	1.0	38.3	3.24
Cs	8.50	62.8	18.5	16.1	1.5	0.1	1.0	37.2	3.16
Fe	10.93	72.7	13.5	11.8	1.1	0.1	0.8	27.3	2.98
Na	7.38	60.1	19.1	17.8	1.7	0.1	1.2	39.9	2.94
V	19.73	94.7	2.3	2.6	0.1	0.0	0.2	5.3	1.04

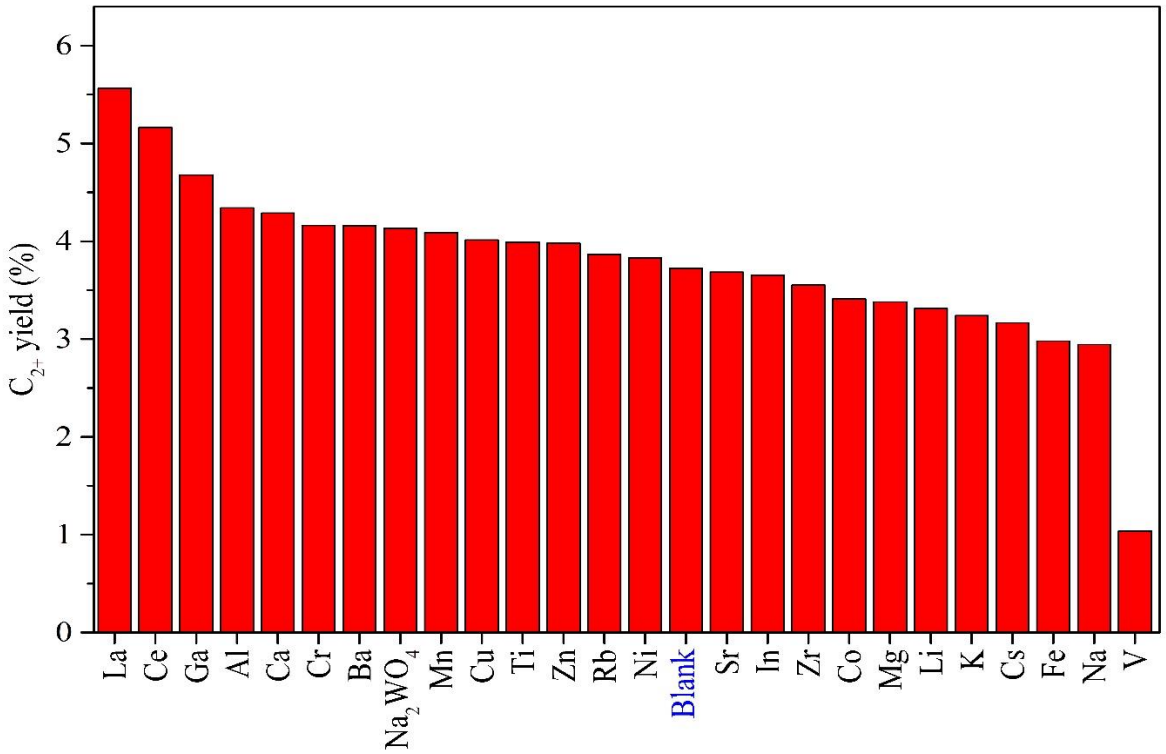

Fig. I-S1. % C_{2+} yield of silica-supported single catalysts for OCM reaction.

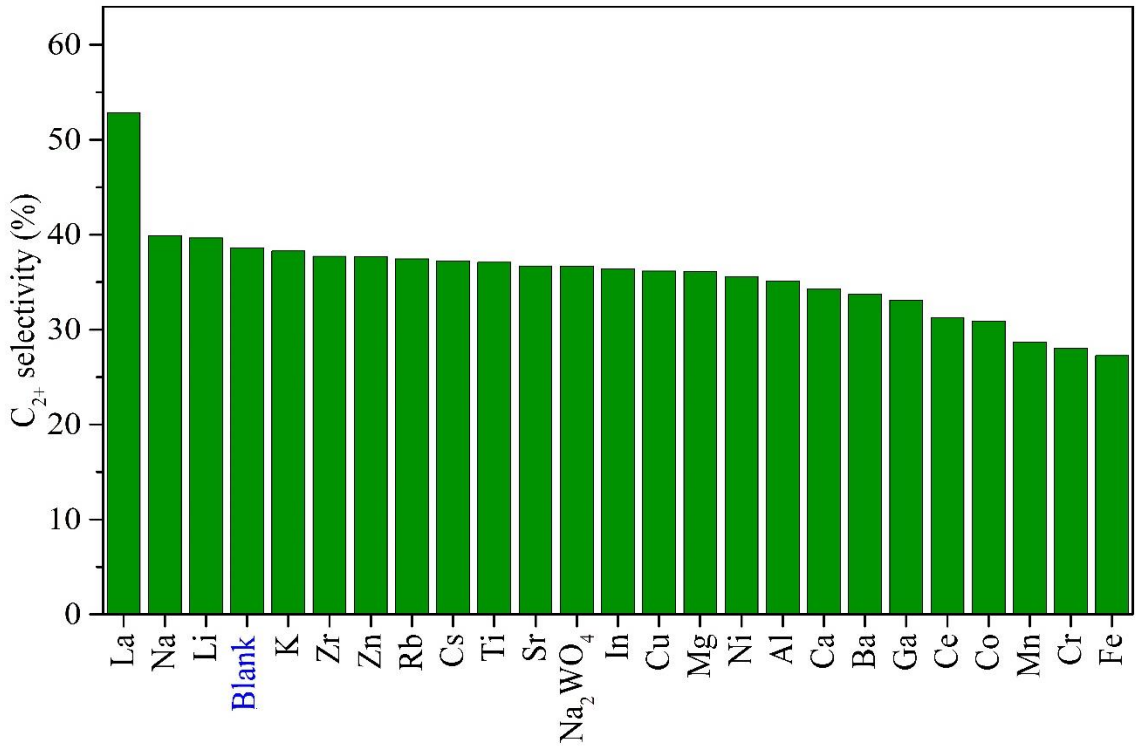

Fig. I-S2. % C_{2+} selectivity of silica-supported single catalysts for OCM reaction.

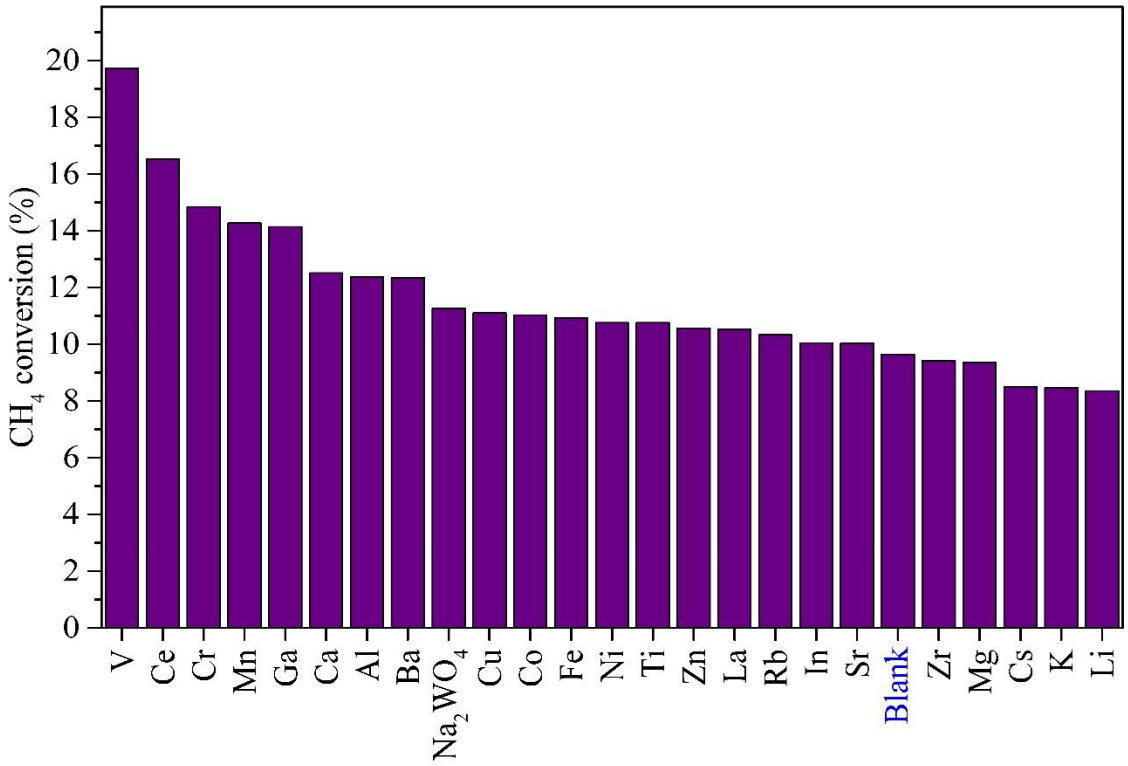

Fig. I-S3. % CH_4 conversion of silica-supported single catalysts for OCM reaction.

Table I-S3. Performance results for silica-supported binary catalysts. The total metal loading was fixed at 10 wt% at a metal ratio of 1:1, Reaction conditions: *T* = 700 °C; CH_4:O_2 = 3:1; total feed rate = 35 mL/min; mass amount = 8 mg.

Metal	CH_4 Conversion (%)	Selectivity (%)							C_{2+} Yield (%)
		CO_X	C_2H_4	C_2H_6	C_3H_6	C_3H_8	C_4H_{10}	C_{2+}	
Na_2WO_4-Mn	25.36	63.8	26.6	6.6	2.1	0.3	0.7	36.2	9.18
Ca-Ce	18.94	70.6	16.8	7.6	1.2	0.2	3.6	29.4	5.57
Ga-Zn	23.77	76.7	16.3	5.4	1.1	0.2	0.3	23.3	5.54
Ga-Rb	15.37	64.1	21.5	11.6	1.8	0.2	0.7	35.9	5.51
Ce-Ba	20.33	73.4	16.8	7.9	1.2	0.2	0.4	26.6	5.40
Al-Rb	17.67	69.8	19.3	8.7	1.5	0.2	0.5	30.2	5.34
Al-Ni	17.47	69.6	19.1	9.0	1.5	0.2	0.6	30.4	5.30
Al-Ba	17.47	70.3	19.2	8.3	1.5	0.2	0.5	29.7	5.18
Mn-La	16.19	68.1	19.4	9.9	1.6	0.2	0.8	31.9	5.17
Ce-Ti	18.48	72.1	16.9	9.0	1.3	0.2	0.5	27.9	5.15
La-Al	15.92	68.6	18.8	10.4	1.4	0.2	0.6	31.4	5.00
Na_2WO_4-Ti	13.29	62.4	22.0	12.9	1.8	0.2	0.8	37.6	4.99
Ca-La	11.10	55.3	18.5	13.4	1.9	0.1	10.8	44.7	4.96
Ga-Cr	16.44	69.8	18.9	9.4	1.5	0.1	0.2	30.2	4.96
Na_2WO_4-Ni	13.42	63.3	21.4	12.5	1.8	0.2	0.7	36.7	4.92
Mn-Ba	15.61	68.5	19.4	10.3	0.0	0.0	1.7	31.5	4.91
Mn-Ni	18.24	73.1	15.4	7.4	1.2	0.1	2.7	26.9	4.90
Al-Ti	15.27	68.2	19.6	9.9	1.6	0.2	0.6	31.8	4.86
Ga-Al	15.11	68.3	19.0	10.4	1.5	0.2	0.6	31.7	4.80
Zn-Ce	14.62	67.2	19.1	11.1	1.5	0.2	0.8	32.8	4.79
Zn-Al	14.46	67.0	19.1	11.4	1.5	0.2	0.8	33.0	4.77
La-Ce	24.57	80.7	13.6	4.4	1.0	0.1	0.2	19.3	4.75
Rb-Ti	12.80	63.0	21.2	12.5	1.9	0.2	1.3	37.0	4.74
Al-Cr	16.09	70.8	17.9	9.2	1.4	0.2	0.5	29.2	4.69
Ga-Na_2WO_4	12.47	62.9	20.6	13.8	1.8	0.1	0.8	37.1	4.63
La-Ba	14.47	68.1	18.6	10.9	1.5	0.2	0.8	31.9	4.61
Ga-Mn	15.81	70.9	17.3	9.6	1.4	0.1	0.6	29.1	4.60
Ga-La	14.54	68.5	18.5	10.6	1.5	0.2	0.7	31.5	4.57
Ce-Rb	13.97	67.5	18.6	11.3	1.7	0.1	0.7	32.5	4.53
Ga-Ce	13.23	65.8	19.6	12.1	1.6	0.1	0.8	34.2	4.52
Rb-Ba	12.57	64.5	19.9	12.5	1.7	0.2	1.2	35.5	4.46
Zn-Cr	11.94	62.7	20.4	14.1	1.7	0.1	0.9	37.3	4.45
Zn-Mn	14.77	70.2	17.8	9.8	1.5	0.1	0.6	29.8	4.41

Cr-Ni	13.78	68.0	17.9	11.3	1.5	0.2	1.1	32.0	4.40
Ni-Ti	13.49	67.4	18.5	11.0	1.6	0.2	1.3	32.6	4.40
Ca-Ba	13.31	67.5	18.8	11.3	1.5	0.2	0.7	32.5	4.32
Ga-Ti	14.85	70.9	18.2	9.0	1.4	0.1	0.3	29.1	4.32
Cr-Ti	14.34	70.0	17.1	10.2	1.4	0.1	1.1	30.0	4.31
Zn-Ca	12.73	66.3	18.8	12.3	1.5	0.1	0.8	33.7	4.29
Mn-Al	17.06	75.0	16.1	7.1	1.3	0.1	0.4	25.0	4.27
La-Ti	27.07	84.2	12.0	2.9	0.6	0.1	0.1	15.8	4.27
Cr-Ba	12.36	66.1	19.2	11.8	1.6	0.1	1.2	33.9	4.19
Mn-Rb	10.73	61.2	17.8	12.9	1.6	0.1	6.4	38.8	4.16
Zn-Ti	12.59	67.0	18.6	11.9	1.5	0.1	0.8	33.0	4.15
Ga-Ba	11.39	63.7	20.2	13.4	1.7	0.1	0.8	36.3	4.14
Ce-Ni	16.31	74.9	14.2	8.9	1.3	0.1	0.6	25.1	4.10
Mn-Ca	12.32	66.8	18.7	11.9	1.6	0.1	0.9	33.2	4.10
Ca-Al	11.86	65.5	19.2	12.6	1.6	0.2	1.0	34.5	4.10
Ca-Rb	10.54	61.5	20.8	14.8	1.8	0.1	1.0	38.5	4.06
Ca-Ni	11.21	64.1	19.3	13.8	1.6	0.1	1.0	35.9	4.02
Rb-Ni	10.68	62.4	20.5	13.7	1.8	0.1	1.4	37.6	4.01
Mn-Ti	13.59	70.7	16.1	10.1	1.3	0.1	1.6	29.3	3.98
Mn-Ce	15.48	74.8	14.3	8.9	1.2	0.1	0.8	25.2	3.90
Zn-Ba	11.30	66.1	18.5	12.8	1.5	0.1	1.0	33.9	3.84
Ce-Al	12.75	70.0	17.2	10.8	1.4	0.1	0.5	30.0	3.83
La-Cr	12.86	70.3	16.2	11.2	1.3	0.1	0.9	29.7	3.82
Zn-Ni	12.05	68.4	18.0	11.2	1.5	0.1	0.8	31.6	3.81
Zn-Cu	12.01	68.3	17.0	12.0	1.5	0.3	0.9	31.7	3.80
Na_2WO_4-Al	11.25	66.2	18.5	12.8	1.5	0.1	0.8	33.8	3.80
La-Rb	10.56	64.0	19.4	13.7	1.7	0.1	1.0	36.0	3.80
La-Ni	11.46	67.0	17.5	12.6	1.5	0.1	1.1	33.0	3.78
Ni-Ba	12.16	69.1	17.5	11.2	1.4	0.1	0.7	30.9	3.76
Ti-Ba	10.80	65.2	18.4	13.5	1.5	0.1	1.2	34.8	3.76
Na_2WO_4-Zn	9.99	62.4	20.3	14.4	1.8	0.1	0.9	37.6	3.75
Blank	9.64	61.4	20.5	15.3	1.7	0.1	0.9	38.6	3.72
Zn-La	10.57	65.1	18.8	13.3	1.6	0.1	1.0	34.9	3.69
Ga-Ca	11.42	67.8	18.6	11.7	1.6	0.0	0.3	32.2	3.68
Zn-Rb	10.11	63.7	19.3	14.2	1.7	0.1	1.0	36.3	3.67
Ca-Cr	12.61	71.6	15.2	11.2	1.2	0.1	0.7	28.4	3.58
Na_2WO_4-Ca	9.62	62.9	19.3	15.1	1.6	0.1	1.0	37.1	3.57
Na_2WO_4-Cu	22.33	84.1	7.2	7.9	0.5	0.1	0.2	15.9	3.56
Na_2WO_4-Rb	9.31	61.9	19.5	15.9	1.7	0.1	0.9	38.1	3.55

Na_2WO_4-Ba	10.27	65.7	18.5	13.3	1.6	0.1	0.9	34.3	3.53
Na_2WO_4-Ce	10.47	67.0	17.0	13.3	1.4	0.1	1.1	33.0	3.45
Cr-Rb	11.14	69.8	15.5	11.7	1.5	0.1	1.4	30.2	3.36
Ga-Ni	9.83	66.1	17.9	13.6	1.6	0.1	0.8	33.9	3.34
Mn-Cu	11.63	71.7	14.9	11.2	1.3	0.1	0.8	28.3	3.29
Na_2WO_4-La	9.38	65.2	17.5	14.8	1.5	0.1	0.9	34.8	3.27
Ga-Cu	13.68	76.6	12.2	9.4	1.1	0.1	0.7	23.4	3.21
Ca-Ti	8.90	64.4	17.9	15.0	1.5	0.1	1.0	35.6	3.17
Cu-Al	10.22	69.1	15.0	13.4	1.2	0.1	1.2	30.9	3.16
Na_2WO_4-Cr	14.09	77.9	11.8	8.7	1.0	0.1	0.5	22.1	3.12
Ce-Cr	14.73	79.9	10.8	7.9	0.9	0.1	0.5	20.1	2.97
Cu-Ba	8.16	64.2	16.8	16.6	1.4	0.1	0.8	35.8	2.92
Ca-Cu	20.97	86.6	6.5	6.1	0.4	0.1	0.3	13.4	2.81
Mn-Cr	13.38	79.1	11.0	8.5	0.9	0.1	0.5	20.9	2.80
Cu-Rb	8.18	66.5	14.1	15.3	1.1	0.1	2.8	33.5	2.74
Ce-Cu	15.21	83.5	8.4	6.8	0.7	0.0	0.5	16.5	2.50
Cu-Cr	9.27	73.6	11.4	12.7	0.9	0.1	1.3	26.4	2.45
La-Cu	19.79	88.5	6.2	4.5	0.5	0.0	0.3	11.5	2.27
Cu-Ti	20.86	93.0	3.0	3.6	0.2	0.0	0.2	7.0	1.47
Cu-Ni	57.18	99.6	0.0	0.1	0.0	0.0	0.2	0.4	0.20

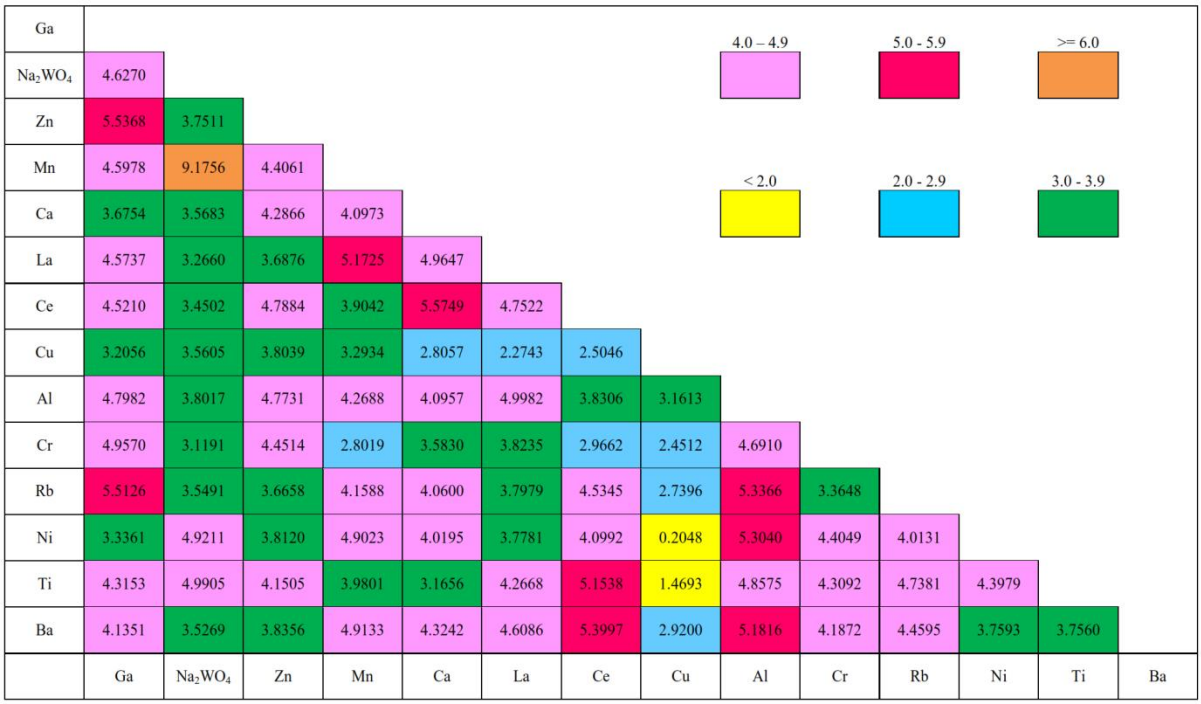

Fig. I-S4. % C_{2+} yield of silica-supported binary catalysts for OCM reaction.

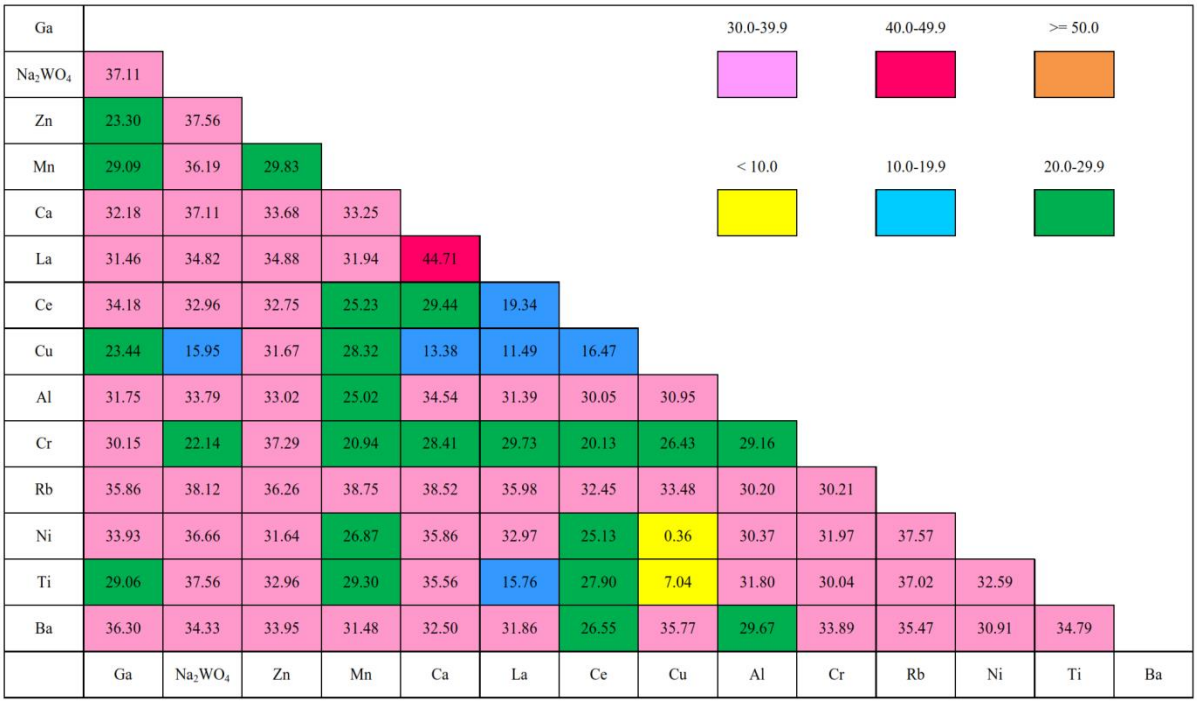

Fig. I-S5. % C_{2+} selectivity of silica-supported binary catalysts for OCM reaction.

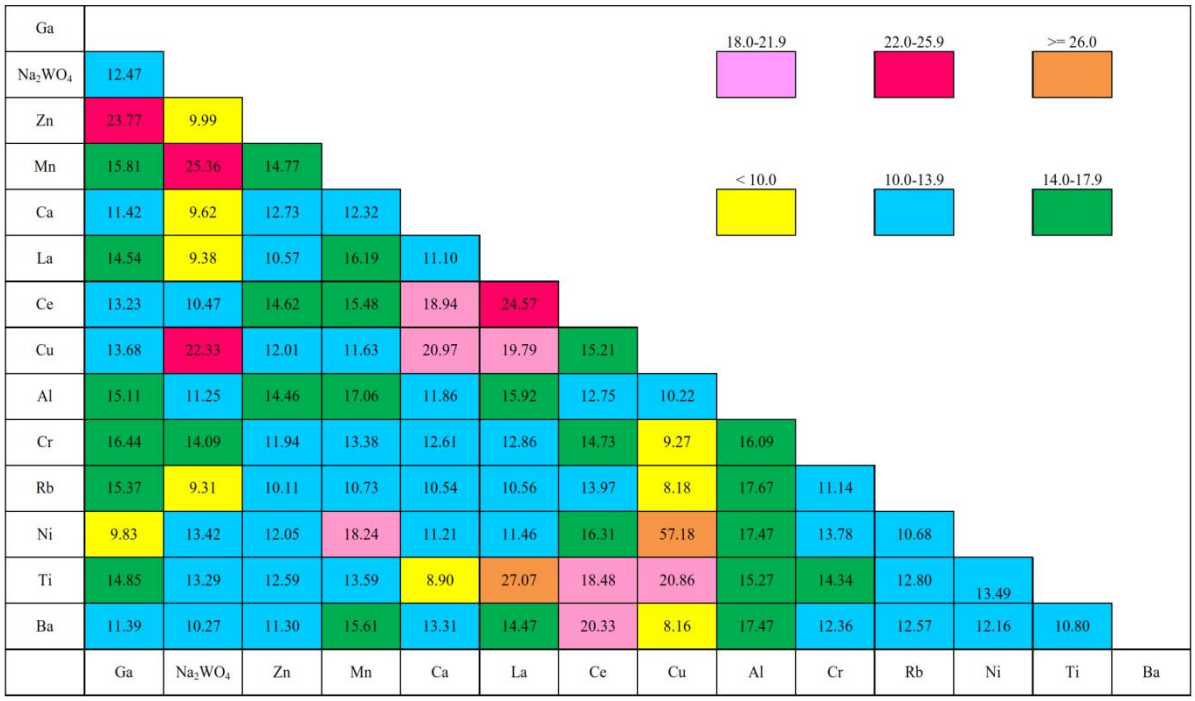

Fig. I-S6. % CH_4 conversion of silica-supported binary catalysts for OCM reaction.

Table I-S4. Performance results for Na_2WO_4-Mn/SiO_2 catalysts at different weight ratios of Na_2WO_4:Mn with a total weight loading of 10 wt% on SiO_2. Testing conditions: reactor temperature = 700 °C at atmospheric pressure, CH_4:O_2:N_2 = 3:1:0, total flow rate = 35 mL/min (GHSV = 50,000 h^{-1}), catalyst amount = 8.0 mg.

Na_2WO_4: Mn ratio	CH_4 conversion (%)	Selectivity (%)							C_{2+} yield (%)
		CO_X	C_2H_4	C_2H_6	C_3H_6	C_3H_8	C_4H_{10}	C_{2+}	
0:10	14.27	71.3	16.1	10.3	1.4	0.1	0.8	28.7	4.09
1:9	16.39	68.6	19.6	9.4	1.7	0.2	0.6	31.4	5.15
2:8	16.72	66.4	20.4	10.3	1.7	0.2	1.0	33.6	5.61
3:7	16.99	64.1	22.5	10.1	2.1	0.2	1.0	35.9	6.09
4:6	23.16	63.3	23.3	8.9	3.1	0.5	0.9	36.7	8.49
5:5	25.36	63.8	26.6	6.6	2.1	0.3	0.7	36.2	9.18
6:4	29.14	50.4	35.7	9.5	2.9	0.3	1.2	49.6	14.44
7:3	23.42	63.6	26.1	7.2	2.2	0.3	0.7	36.4	8.52
8:2	21.20	63.6	25.8	7.9	2.0	0.2	0.7	36.4	7.72
9:1	18.80	62.3	24.9	9.3	2.3	0.2	0.9	37.7	7.08
10:0	9.76	62.6	19.6	15.1	1.7	0.0	1.0	37.4	3.65

Table I-S5. Performance results for Na_2WO_4-Mn/SiO_2 catalysts at different total weight loadings from 2.5 to 30.0 wt% on SiO_2, with the Na_2WO_4:Mn weight ratio of 6:4. Testing conditions: reactor temperature = 700 °C at atmospheric pressure, CH_4:O_2:N_2 = 3:1:0, total flow rate = 35 mL/min (GHSV = 50,000 h^{-1}), catalyst amount = 8.0 mg.

Weight metal loading (wt%)	CH_4 conversion (%)	Selectivity (%)							C_{2+} yield (%)
		CO_X	C_2H_4	C_2H_6	C_3H_6	C_3H_8	C_4H_{10}	C_{2+}	
2.5	18.01	68.7	19.0	9.9	1.7	0.2	0.6	31.3	5.64
5.0	27.74	62.2	26.6	7.8	2.2	0.4	0.7	37.8	10.49
7.5	28.43	60.6	28.3	7.9	2.2	0.3	0.8	39.4	11.21
10.0	29.14	50.4	35.7	9.5	2.9	0.3	1.2	49.6	14.44
12.5	27.84	56.7	31.9	7.3	2.7	0.3	1.0	43.3	12.06
15.0	23.18	58.9	31.8	7.2	1.4	0.2	0.5	41.1	9.53
17.5	21.42	61.8	27.7	7.9	1.5	0.3	0.8	38.2	8.17
20.0	18.79	64.0	24.3	8.6	2.0	0.2	0.9	36.0	6.77
22.5	12.36	59.2	23.5	13.7	2.1	0.2	1.3	40.8	5.05
25.0	11.42	58.4	23.7	14.0	2.0	0.2	1.8	41.6	4.75
27.5	7.66	53.9	22.2	18.7	2.0	0.1	3.1	46.1	3.53
30.0	7.21	51.7	24.5	19.8	1.3	0.1	2.5	48.3	3.48

Table I-S6. Na_2WO_4-Mn/SiO_2 catalysts at different catalyst weights, with Na_2WO_4:Mn weight ratio of 6:4, total weight loading of 10 wt% on SiO_2. Testing conditions: reactor temperature = 700 °C at atmospheric pressure, total flow rate = 35 mL/min. For the condition w/o N_2 feeding; CH_4:O_2:N_2 = 3:1:0, catalyst weight = 2–75 mg (GHSV =210,000–5,500 h^{-1}).

Mass catalyst w/o N_2 feed (mg)	CH_4 conversion (%)	Selectivity (%)							C_{2+} yield (%)
		CO_X	C_2H_4	C_2H_6	C_3H_6	C_3H_8	C_4H_{10}	C_{2+}	
2.0	7.44	60.5	19.2	17.7	1.6	0.0	1.0	39.5	2.94
4.0	10.16	57.5	23.1	16.4	2.1	0.0	1.0	42.5	4.32
6.0	16.03	56.7	29.3	10.8	2.0	0.2	1.0	43.3	6.94
8.0	27.70	53.9	33.9	8.4	2.7	0.3	0.8	46.1	12.76
10.0	29.14	50.4	35.7	9.5	2.9	0.3	1.2	49.6	14.44
15.0	30.26	48.4	36.2	10.6	3.1	0.4	1.3	51.6	15.61
20.0	30.37	47.9	35.6	11.8	3.1	0.4	1.3	52.1	15.83
30.0	31.15	46.1	36.7	11.7	3.4	0.4	1.7	53.9	16.77
40.0	30.40	47.4	35.2	12.1	3.3	0.4	1.6	52.6	16.00
50.0	29.53	49.1	34.9	11.2	3.3	0.4	1.2	50.9	15.04
60.0	28.88	49.2	35.0	11.0	3.3	0.4	1.2	50.8	14.67

Table I-S7. Performance results for Na_2WO_4-Mn/SiO_2 catalysts at different catalyst weights, with Na_2WO_4:Mn weight ratio of 6:4, total weight loading of 10 wt% on SiO_2. Testing conditions: reactor temperature = 700 °C at atmospheric pressure, total flow rate = 35 mL/min. For the condition w/ N_2 feeding; CH_4:O_2:N_2 = 3:1:4, catalyst amount = 20–200 mg (GHSV =17,000–2,000 h^{-1}).

Mass catalyst w/ N_2 feed (mg)	CH_4 conversion (%)	Selectivity (%)							C_{2+} yield (%)
		CO_X	C_2H_4	C_2H_6	C_3H_6	C_3H_8	C_4H_{10}	C_{2+}	
20.0	15.09	47.2	30.7	18.7	2.4	0.3	0.7	52.8	7.97
30.0	28.14	46.9	35.8	13.4	2.6	0.5	0.8	53.1	14.93
40.0	33.05	45.6	36.0	13.9	2.9	0.6	1.1	54.4	17.99
50.0	33.82	45.0	35.4	14.4	3.2	0.6	1.4	55.0	18.59
60.0	33.67	45.2	35.1	14.6	3.1	0.6	1.5	54.8	18.47
75.0	32.94	45.2	35.0	14.6	3.2	0.6	1.4	54.8	18.06
100.0	32.43	46.9	34.5	13.5	3.2	0.5	1.3	53.1	17.22
150.0	30.92	49.2	33.2	12.6	3.1	0.5	1.4	50.8	15.71
200.0	28.96	49.2	36.2	10.1	3.3	0.2	1.0	50.8	14.71

Table I-S8. Performance results for Catalyst stability test of Na_2WO_4-Mn/SiO_2 catalysts, with the Na_2WO_4:Mn weight ratio of 6:4. Testing conditions: reactor temperature = 700 °C at atmospheric pressure, CH_4:O_2:N_2 = 3:1:4, total flow rate = 35 mL/min (GHSV = 14,500 h^{-1}), catalyst amount = 50.0 mg.

TOS	CH_4 conversion	Selectivity (%)							C_{2+} yield
(h)	(%)	CO_X	C_2H_4	C_2H_6	C_3H_6	C_3H_8	C_4H_{10}	C_{2+}	(%)
1	33.67	45.0	36.3	13.5	3.3	0.6	1.4	55.1	18.53
2	33.82	40.6	38.6	15.3	3.6	0.6	1.5	59.4	20.11
3	34.41	39.5	39.9	14.7	3.7	0.5	1.6	60.5	20.80
4	37.12	39.7	41.2	13.4	3.6	0.5	1.7	60.3	22.40
5	38.32	40.1	40.9	13.2	3.6	0.5	1.7	59.9	22.95
6	39.60	40.6	40.1	13.6	3.5	0.5	1.7	59.4	23.54
7	39.67	41.1	40.0	13.5	3.5	0.5	1.6	58.9	23.38
8	39.29	41.1	40.0	13.3	3.4	0.5	1.7	58.9	23.16
9	39.05	41.0	40.3	13.3	3.4	0.5	1.4	59.0	23.03
10	38.33	40.9	40.9	12.7	3.7	0.5	1.3	59.1	22.64
11	38.29	40.8	41.2	12.3	3.6	0.3	1.7	59.2	22.65
12	38.46	40.8	41.1	12.6	3.6	0.2	1.7	59.2	22.78
13	38.35	41.0	41.7	11.8	3.6	0.4	1.6	59.0	22.61
14	38.56	41.2	41.7	11.7	3.6	0.4	1.5	58.8	22.68
15	38.57	41.3	41.7	11.6	3.5	0.4	1.5	58.7	22.64
16	38.59	41.9	41.3	11.5	3.6	0.4	1.3	58.1	22.43
17	38.80	41.7	41.6	11.2	3.6	0.3	1.6	58.3	22.64
18	38.88	41.7	41.8	11.1	3.6	0.3	1.6	58.3	22.69
19	38.71	41.3	42.6	11.0	3.5	0.2	1.5	58.7	22.74
20	38.64	41.1	42.3	11.2	3.6	0.3	1.5	58.9	22.76
21	38.17	41.5	42.0	11.1	3.6	0.3	1.5	58.5	22.32
22	38.04	41.7	41.9	11.1	3.6	0.3	1.4	58.3	22.19
23	38.02	41.7	41.9	11.0	3.6	0.3	1.5	58.3	22.15
24	38.21	42.2	41.6	10.9	3.5	0.3	1.4	57.8	22.08
25	37.93	42.0	41.7	10.9	3.5	0.3	1.4	58.0	22.00
26	38.11	42.3	41.9	11.0	3.1	0.2	1.5	57.7	22.00
27	38.05	42.3	41.6	11.2	3.2	0.4	1.2	57.7	21.95
28	37.65	42.2	41.7	11.3	3.1	0.4	1.3	57.8	21.77
29	37.13	41.7	41.6	11.7	3.4	0.4	1.3	58.3	21.65
30	36.79	41.6	41.7	11.8	3.0	0.4	1.5	58.4	21.48
31	36.45	41.2	42.3	11.7	2.9	0.4	1.4	58.8	21.43
32	36.58	41.4	42.1	11.2	3.4	0.4	1.6	58.6	21.43
33	35.82	40.9	42.6	11.5	3.5	0.4	1.2	59.1	21.18

34	35.40	41.5	42.3	11.3	3.4	0.4	1.1	58.5	20.73
35	35.24	42.1	42.7	10.8	3.2	0.4	0.9	57.9	20.42
36	35.29	42.6	42.6	10.4	3.1	0.4	0.8	57.4	20.24
37	35.45	42.9	42.5	10.3	3.1	0.4	0.8	57.1	20.26
38	35.35	43.0	43.0	10.0	3.0	0.4	0.8	57.0	20.16
39	34.83	43.1	41.7	10.9	3.2	0.4	0.8	56.9	19.81
40	34.70	42.7	42.2	10.9	3.0	0.3	0.8	57.3	19.89
41	34.51	42.6	41.5	10.8	3.8	0.4	0.9	57.4	19.81
42	34.64	43.4	41.5	10.7	3.2	0.4	0.9	56.6	19.62
43	34.11	44.4	41.1	10.4	3.1	0.4	0.7	55.6	18.98
44	34.30	44.8	40.9	10.2	3.0	0.4	0.7	55.2	18.92
45	33.42	44.6	41.1	10.3	3.1	0.4	0.7	55.4	18.52
46	32.94	44.5	41.0	10.4	3.1	0.4	0.7	55.5	18.29
47	33.25	45.4	40.4	10.2	3.0	0.4	0.7	54.6	18.15
48	32.97	44.6	41.1	10.2	3.0	0.4	0.6	55.4	18.25
49	32.86	44.8	40.9	10.3	3.0	0.4	0.7	55.2	18.13
50	33.30	44.6	41.1	10.2	3.0	0.4	0.7	55.4	18.44

Table I-S9. The characteristic XRD values (2θ) of crystalline phases found from the samples.

Crystalline phase	ICDD No.	2θ (degree)
α-Tridymite-Silicon Oxide (α-SiO_2)	00-001-0378	25.552, 27.735, 31.500, 43.203, 55.371, 57.142
α-Cristobalite-Silicon Oxide (α-SiO_2)	00-001-0438	22.109, 28.553, 31.500, 36.148, 43.203, 44.848, 47.086, 48.829, 57.142, 58.643, 62.064
Sodium Tungsten Oxide (Na_2WO_4)	00-012-0772	16.876, 27.735, 32.392, 43.203, 48.829, 52.079, 57.142, 58.643, 78.317
Manganese Oxide (Mn_2O_3)	00-001-1061	33.140, 38.145, 44.848, 48.829, 65.796
Manganese Oxide (Mn_3O_4)	00-018-0803	28.918, 32.392, 36.148, 38.145, 58.643, 59.997

CO_2-TPD procedure:

The basicity of catalysts were determined using CO_2-temperature programmed desorption (CO_2-TPD). The measurements were carried out to achieve CO_2-TPD profiles by operating in continuous-flow Inconel tube reactor. Each sample was initialized by introducing Ar gas at a feed flow rate of 35 cc/min at 35-500 °C with a heating rate 10 ºC/min and holding at 500 °C for 2 hours to reduce and clean catalyst's surface. After that, it was cooled down to 50 °C. The CO_2/Ar mixture gas (10% CO_2) was then introduced into the catalyst bed at 50 ºC and a total flow rate of 35 cc/min for 2 hours. Next, the excess CO_2 over surface catalyst was purged by introducing Ar gas at 35 cc/min for 2 hours. The CO_2 consumption was continuously monitored using a TCD-equipped GC (Shimadzu GC-2014). The temperature was risen from 50 to 800 °C with a heating rate of 10 °C/min.

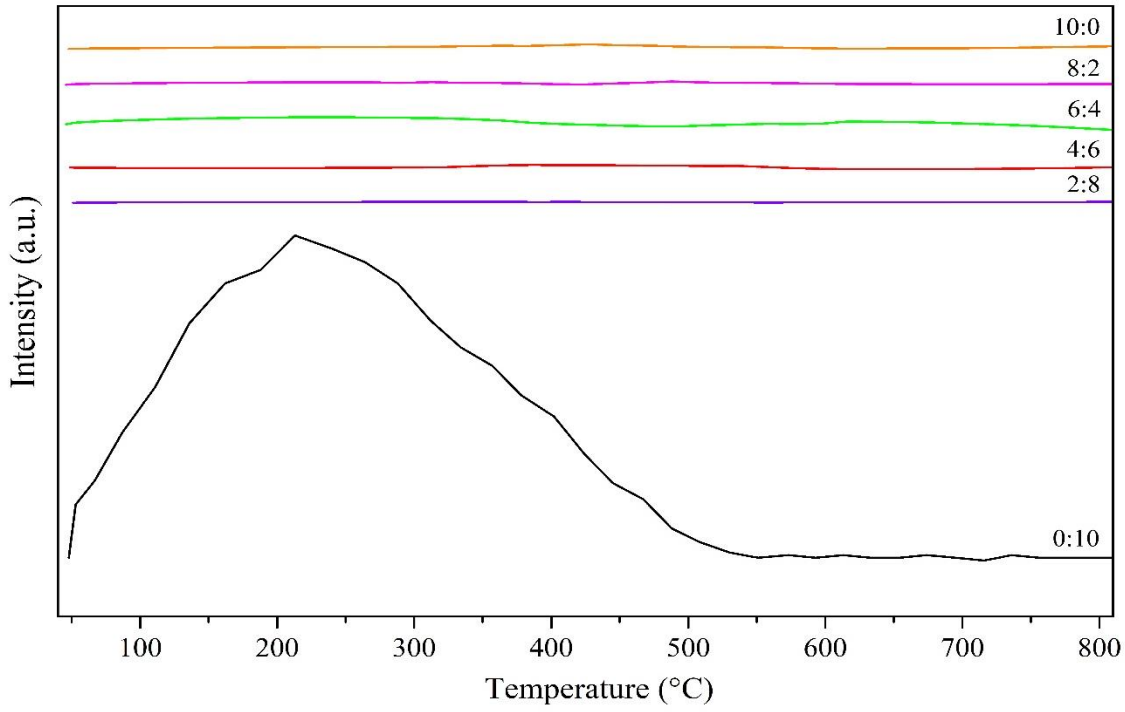

Fig. I-S7. CO_2-TPD of Na_2WO_4:Mn catalysts at different weight ratios, fixing the total metal loading on SiO_2 at 10 wt%.

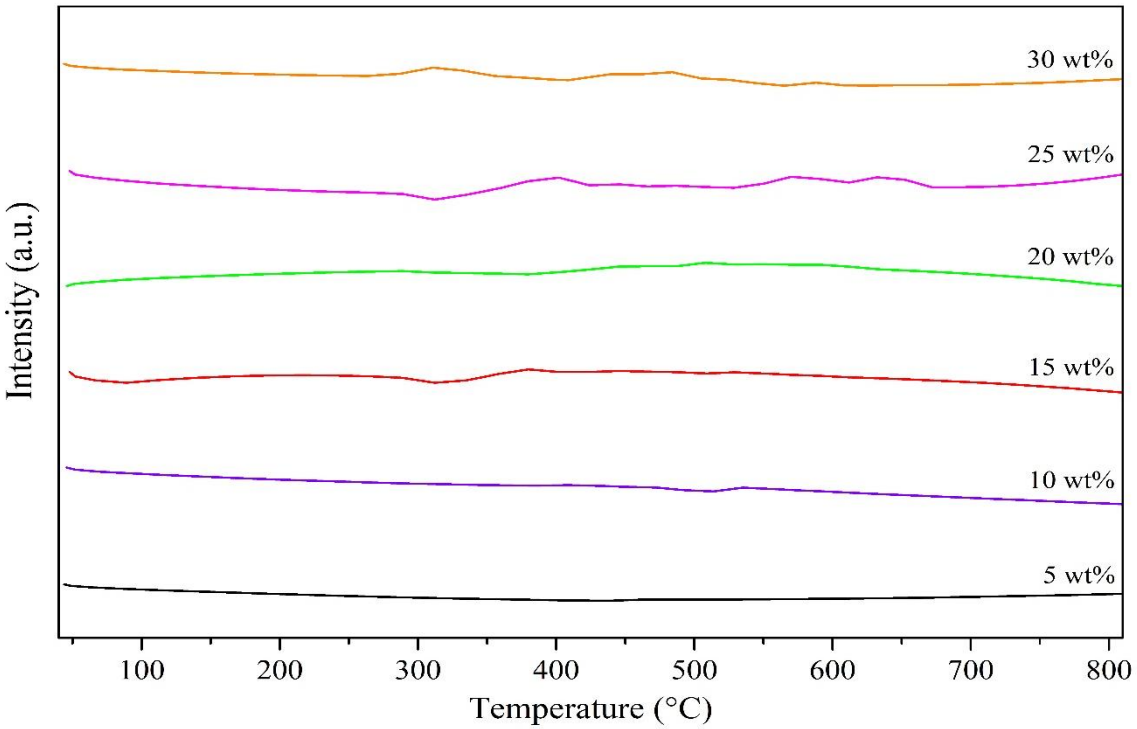

Fig. I-S8. CO_2-TPD of Na_2WO_4-Mn/SiO_2 catalysts at different total metal loadings on SiO_2, fixing the Na_2WO_4:Mn ratio at 6:4.

TGA-DTG Analyst:

Thermal gravimetrical analyzer (TGA-DTG, PerkinElmer Pyris 1 TGA) measured the thermal decomposition of the as catalysts. The catalyst 15 mg were loaded in to an alumina crucibles and heated in a flow of air zero 100 mL/min (Lab grade purity, Thai Standard Gas Co., Ltd (TSG), Thailand) from room temperature to 1000 °C with a heating rate of 10 ºC/min.

Part II : Synthesis of Light Hydrocarbons via Oxidative Coupling of Methane over Silica-supported Na_2WO_4-TiO_2 Catalyst

II-1. Introduction

Methane (CH_4) is the main compound of biogas and natural gas that are plentiful on Earth. It is considered a greenhouse gas with an environmental impact more than 25 times greater than CO_2 if equal amounts of these two gases are released into the atmosphere. Since methane is an abundant compound on Earth, a process that can convert methane to high value-added chemicals is a highly attractive topic for many researchers. One of the challenging topics to be considered in catalysis is oxidative coupling of methane (OCM)—a gas-phase reaction that uses O_2 or air to directly react with CH_4 to produce useful hydrocarbons (C_{2+}) such as ethylene, ethane, propane, and propylene [1, 2]. The OCM reaction is an exothermic reaction in nature and normally takes place at reaction temperatures of 600–1,000 ºC [3]. OCM can produce CO and CO_2 as byproducts. However, if a suitable catalyst is present, the reaction produces a selective product and extreme reaction temperatures can be reduced.

In the past several years, some potential catalysts have been reported, including MnO_x modified with different types of co-catalysts, supports and promotors, such as oxides of Mg, Na, and Ce. However, the C_{2+} yields and C_{2+} selectivities were quite low at approximately <16% and 25-78%, respectively [4-8]. Additionally, coke formation was found during the reaction, resulting in catalyst deactivation. Later, the coking formation was, however, prevented by introducing of chlorinated compounds with the reactant gases. Alternatively, a binary catalyst of Na_2WO_4-MnO_x has been widely investigated because this metal combination was identified as an active material for the OCM reaction. The modified Na_2WO_4-MnO_x catalysts reported include MO_x-Na_2WO_4-MnO_x/SiO_2 (M = Ni, Co, Fe, Li, Al, Ba, Ca, Na, and K) [9], TiO_2-Na_2WO_4/MnO_x/SiO_2 [10], and Ce_2O_3-MnO_x-Na_2WO_4/SiO_2 [7]. The C_{2+} yields and C_{2+} selectivities of those Na_2WO_4-MnO_x catalysts increased compared to the single catalysts of its component and the other metal combinations due to synergistic catalyst effects between Na_2WO_4 and MnO_x [11-14]. The additions of the promoters (e.g. TiO_2, Ce_2O_3) onto the Na_2WO_4-MnO_x catalysts resulted in improved activity of the catalysts, because the promoters could cooperate into the catalytic materials and/or the number of suitable strong basic sites increased [15, 16]. Normally, SiO_2 is used as a catalyst support because the SiO_2 support is stable under the test conditions and inert to the products [14].

Since previous results reported in the literatures showed that any catalysts containing Na_2WO_4, MnO_x, and/or SiO_2 are highly active for OCM reaction, it is of great interest and challenging to improve new catalysts that consist of any of those components and new active metal component (i.e co-active metal, promoter). In a catalyst screening for OCM reaction in our laboratory, we discovered that addition of TiO_2 onto the Na_2WO_4/SiO_2 catalyst without MnO_x can

also substantially improve the C_{2+} yield. This combination of TiO_2 and Na_2WO_4 on SiO_2 has never been reported in detail. Herein, we report on various studies on the activity of Na_2WO_4 mixed with TiO_2 on SiO_2 support. The studies include catalyst optimization, catalyst stability, operating condition for the reaction, and catalyst characterization.

II-2. Experimental section

II-2.1. Catalyst preparation

All of the catalysts were synthesized using co-impregnation of predetermined weights of SiO_2 as follows. An aqueous solution of Na_2WO_4 (sodium tungstate dihydrate, 98.0~101.0%, Daejung) andTi^{4+}(titanium (IV) isopropoxide, 97+%, Alfa Aesar) in ethanol (99.9%, QREC) were determined and pipetted into amorphous fume silica (SiO_2, surface area of 85-115 m^2/g, Alfa Aesar) to obtain a desired weight percentage of the metal components (TiO_2 and/or Na_2WO_4) on the SiO_2 support. Note that the weight percentage of TiO_2 or Na_2WO_4 on the support was determined on the basis of the mass of Ti(0) or Na_2WO_4, respectively. The mixture was continuously stirred at 120 ºC until dry. The obtained powder was then taken to calcine in an air furnace at 800 ºC for 4 h. After the calcination, a fine white powder was obtained.

II-2.2. Catalyst activity test

The activities of the prepared catalysts were evaluated for OCM reaction in a plug flow reactor at 1 atm and a reactor temperature range of 600–800 ºC. A sample (8 mg) was packed in a quartz tubular reactor that had an inner diameter of 0.5 cm. The catalyst bed length was approximately 2 mm and the catalyst was sandwiched between two layers of quartz wool. The feed gas consisted of (N_2, 99.999% purity, Praxair), methane (CH_4, 99.999% purity, Praxair), and oxygen (O_2, 99.999% purity, Praxair) at a volume ratio of (N_2:CH_4:O_2) = (0–7.5):4:1 (i.e. fixing the volume ratio of CH_4:O_2 = 4:1) with a total feed flow rate of 50 mL/min, which corresponded to a gas hourly space velocity (GHSV) of 9,500 h^{-1}. The effluent gas was analysed using a gas chromatograph (Shimadzu, GC-14A) equipped with a thermal conductivity detector (TCD; for analyzing CO, CO_2, and CH_4) and a flame ionization detector (FID; for analyzing C_2H_4, C_2H_6, C_3H_6, C_3H_8 and C_4H_8, and C_4H_{10}). The catalytic activities are expressed in terms of %CH_4 conversion, %C_{2+} selectivity, %CO_x selectivity, and %C_{2+} yield, which are shown in equations (1)–(4). The data were collected after the system had reached the set point for 2h.

$$\%\ CH_4\ \text{conversion} = \frac{\text{moles of } CH_4 \text{ input} - \text{moles of } CH_4 \text{output}}{\text{moles of } CH_4 \text{ input}} \times 100 \quad (1)$$

$$\% C_{2+} \text{ selectivity} = \frac{\text{moles of } C_{2+}}{\text{Total moles of products}} \times 100 \quad (2)$$

$$\% CO_x \text{ selectivity} = \frac{\text{moles of } CO_x}{\text{Total moles of products}} \times 100 \quad (3)$$

$$\% C_{2+} \text{ yield} = \frac{\% CH_4 \text{conversion} \times \% C_{2+} \text{selectivity}}{100} \quad (4)$$

II-2.3. Catalyst characterization

The patterns of powder X-ray diffraction (XRD) the samples were received using a powder X-ray diffractometer (PXRD; Philips X-Pert and JEOL JDX-3530, using Cu-$K\alpha$ radiation with 40 mA and 45 kV, 0.5 s step time, 0.02° step size).

The pore volumes, pore-sizes, and specific surface areas of the samples were evaluated using N_2-physisorption with a Quantachrome Autosorp-1C instrument and Brunauer-Emmett-Teller (BET) procedure at a temperature of -196 °C.

The surface morphology of the samples was imaged using a field emission scanning electron microscope (FE-SEM, JSM7600F, JEOL) with an energy dispersive X-ray spectrometer (EDS), operated at 300 kV). Each sample was coated by gold (Au) using Au sputtering technique.

The particles at the nano-scale of the catalysts were characterized using a high-resolution transmission electron microscope (HR-TEM, JEM-3100F, JEOL) performed at 300 kV.

The Fourier-transform infrared (FT-IR) patterns of the samples were acquired using an FT-IR spectrometer (Bruker TENSOR2, attenuated total reflection (ATR) mode). For the measurements, fine powder of each catalyst was mixed with potassium bromide (KBr), and then made into a KBr pellet.

The electronic states of sodium, tungsten, and titanium were analyzed using X-ray photoelectron spectroscope (XPS, Kratos Axis Ultra DLD) with Al Kα for the X-ray source.

The metal-support and metal-metal interactions were analyzed using the H_2-temperature programmed reduction (H_2-TPR) technique. The H_2-TPR profiles of the samples were attained by carrying out the measurements in a tubular reactor (Inconel tube) in a temperature range of 50–900 °C with a heating rate of 5 °C/min. A gas mixture of 9.6% H_2 in Ar at a total feed flow rate of 30 mL/min was introduced into the sample bed. A TCD-equipped gas chromatography (GC-14, Shimadzu) was used to continuously monitor the H_2 consumption.

II-3. Results and discussion

II-3.1. Activity of TiO_2/SiO_2, Na_2WO_4/SiO_2, and TiO_2-Na_2WO_4/SiO_2 catalysts

The 10wt% TiO_2/SiO_2, 10wt% Na_2WO_4/SiO_2, and (5wt% TiO_2-5wt% Na_2WO_4)/SiO_2 catalysts were prepared and tested for OCM reaction, as presented in Fig. II-1. The performance of each catalyst was described using the C_{2+} selectivity, CH_4 conversion, and C_{2+} yield. It should be noted that the C_{2+} yield is the criterion used to identify a superior catalyst when comparing the activities of catalysts. The C_{2+} yield of the Na_2WO_4-TiO_2/SiO_2 catalyst was obtained at 2.7 %, clearly greater than that of the single TiO_2/SiO_2 or Na_2WO_4/SiO_2 catalysts, approximately 1.5 or 3.8 times the C_{2+} yield of the TiO_2/SiO_2 or Na_2WO_4/SiO_2 catalysts, respectively. However, the C_{2+} selectivity for these three catalysts was similar (approximately 39–42%) but the CH_4 conversion of the TiO_2/SiO_2 and Na_2WO_4/SiO_2 catalysts was lower than that of the Na_2WO_4-TiO_2/SiO_2 catalyst. The results indicated that the combination of TiO_2 and Na_2WO_4 on the SiO_2 support reveals a synergistic catalysis effect.

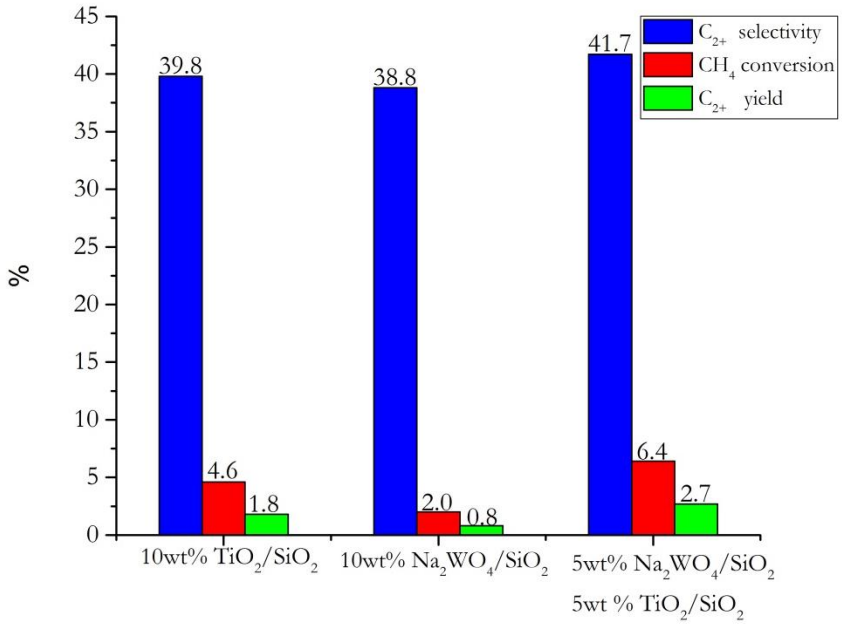

Fig. II-1. C_{2+} selectivity, CH_4 conversion, and C_{2+} yield of 10wt% TiO_2/SiO_2, 10wt% Na_2WO_4/SiO_2, and TiO_2-Na_2WO_4/SiO_2 catalysts. Testing conditions: feeding gas ratio of CH_4:O_2 = 4:1 by volume, total feed flow rate = 50 mL/min (GHSV = 9,500 h^{-1}), and reactor temperature = 700 ºC.

II-3.2. Effect of TiO_2 loading on Na_2WO_4-TiO_2/SiO_2

The Na_2WO_4-TiO_2/SiO_2 catalyst was further studied by varying the amount of TiO_2. In a previous study, 5wt% Na_2WO_4 loaded on SiO_2 using incipient-wetness impregnation was reported to produce an optimum yield for the OCM reaction [17]. However, the effect of TiO_2 loading on Na_2WO_4/SiO_2 has never been studied. In the present study, different amounts of TiO_2 on Na_2WO_4/SiO_2 were studied by varying the amounts of TiO_2 from 0 to 30% on the catalyst and keeping the amount of Na_2WO_4 on every catalyst unchanged at 5 wt%, as plotted in Fig. II-2. As increasing TiO_2 loading, the C_{2+} selectivities slowly increased from 38.0 to 44.9%, while the CH_4 conversion steadily decreased from 6.4 to 4.3%. Nevertheless, the C_{2+} yield had an optimum yield at 5 wt% loading (2.7% C_{2+} yield). This confirmed that the addition of TiO_2 into Na_2WO_4/SiO_2 enhances C_{2+} formation. However, TiO_2 loadings over 5 wt% decreased the C_{2+} yield of each catalyst. Thus, Na_2WO_4-TiO_2/SiO_2 catalyst at a total metal loading of 10 wt% and a TiO_2:Na_2WO_4 weight ratio of 1:1 (i.e. 5 wt% Na_2WO_4 + 5 wt% TiO_2) was chosen for the optimum catalyst for further studies.

II-3.3. Effect of N_2/($4CH_4$:$1O_2$) feeding gas ratio and reactor temperature

The optimal catalyst was further investigated at various N_2/($4CH_4$:$1O_2$) feeding gas ratios (N_2/($4CH_4$:$1O_2$) = 0.0–1.5) and reactor temperatures (600–800 ºC). For the previous studies in sections 3.1 and 3.2, the testing conditions were fixed at a CH_4:O_2 feeding gas ratio of 4:1 with a total feed flow rate of 50 mL/min (GHSV = 9,500 h^{-1}) without an inert gas at 700 ºC and atmospheric pressure. In this section, N_2 gas (a diluent gas) was co-fed with CH_4:O_2 by fixing the volume ratio of CH_4:O_2 = 4:1 and varying the volume ratio of N_2/CH_4:O_2 from 0.0 to 1.5, and also varying the reactor temperature from 600 to 800 ºC, while the total feed flow rate was fixed at 50 mL/min. The C_{2+} yield, C_{2+} selectivity, and CH_4 conversion under each set of condition of the optimal catalyst are presented in Figs. 3(a), 3(b) and 3(c), respectively.

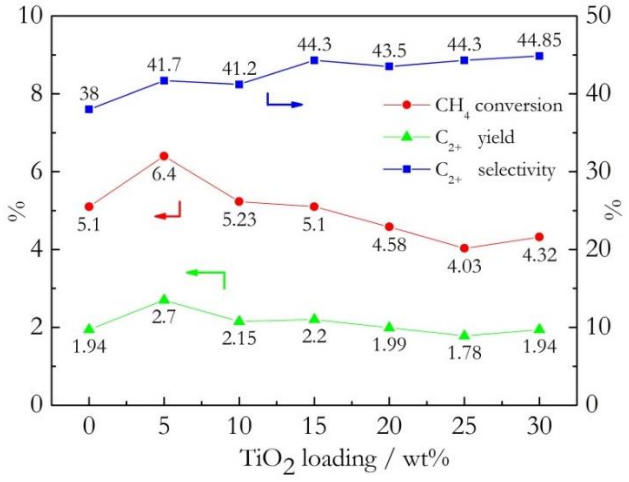

Fig. II-2. TiO_2 loadings onto Na_2WO_4/SiO_2 from 0–30 wt% by fixing the amount of Na_2WO_4 onto each catalyst at 5 wt%; Testing conditions: feeding gas ratio of CH_4:O_2 = 4:1 by volume, total feed flow rate = 50 mL/min (GHSV = 9,500 h^{-1}), and reactor temperature = 700 ºC.

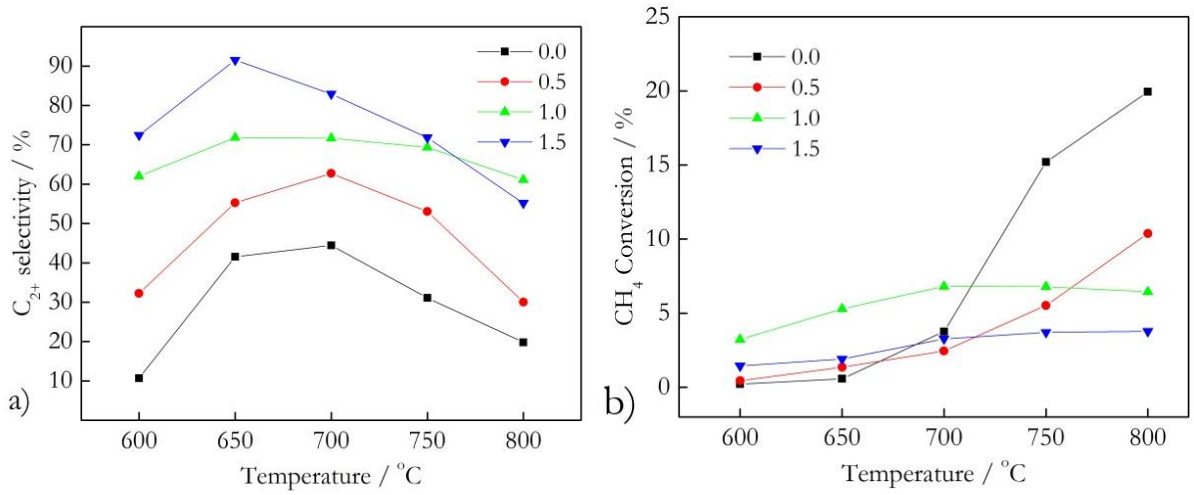

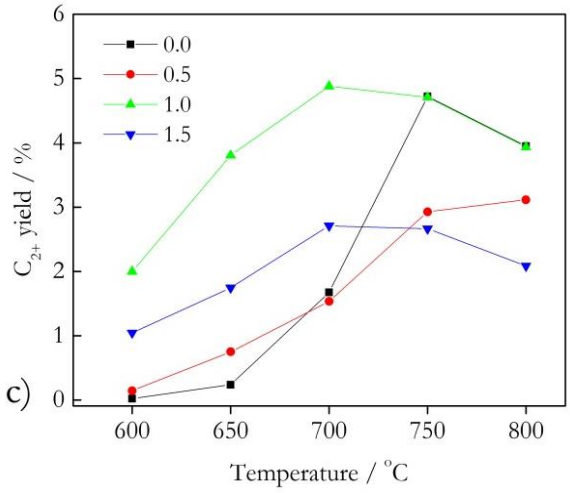

Fig. II-3. a) C_{2+} selectivity, b) CH_4 conversion, and c) C_{2+} yield of the optimum TiO_2-Na_2WO_4/SiO_2 catalyst at N_2/($4CH_4$:$1O_2$) feeding gas ratios of 0.0–1.5 by volume, reactor temperatures of 600–800 ºC, and total feed flow rate of 50 mL/min.

Comparing the C_{2+} selectivities at one reactor temperature (Fig. II-3(a)), the C_{2+} selectivity mostly increased as the N_2/($4CH_4$:$1O_2$) feeding gas ratio increased. The maximum C_{2+} selectivity obtained was 91.5% with a N_2/($4CH_4$:$1O_2$) feeding gas ratio of 1.5 by volume and a reactor temperature of 650 ºC but the CH_4 conversion and the C_{2+} yield were low at 1.9% and 1.7%, respectively. However, the C_{2+} yield at every testing temperature decreased when the N_2/($4CH_4$:$1O_2$) feeding gas ratio was over 1.0 by volume because the reactant gases (i.e. CH_4 and O_2) were too diluted. In other words, the reactants were not sufficient for the active sites of the catalyst. In contrast, the C_{2+} yield of the N_2/(4CH4:$1O_2$) feeding gas ratio of 0.0 and 0.5 was lower than that of 1.0 because the reactant gases were much more than the active sites and the heat generated by the catalytic reaction in the catalyst's bed was high, so that the products can further combust in the hotspot zone. Thus, the C_{2+} yields for these two conditions were relatively low.

Considering the catalytic activities at one N_2/($4CH_4$:$1O_2$) feeding gas ratio; the catalytic activities increased when the reactor temperatures was increased from 600 to 700 ºC. However, at reactor temperatures above 700 ºC, the C_{2+} selectivities decreased with increasing CH_4 conversion, and thus the overall C_{2+} production (i.e. C_{2+} yields) decreased because the combustion of CH_4 to CO_x products is favored at high reaction temperature [3], as well as the C_{2+} products being able to further react with some active species of the catalyst or to react with O_2 gas in the gas phase to further produce CO_x [18]. As seen in Fig. II-3(c)), the optimal C_{2+} yield was achieved at 4.9% with 71.7% C_{2+} selectivity and

6.8% CH_4 conversion when the operating conditions were an $N_2/(CH_4{:}O_2)$ feed gas ratio of 1.0 by volume and 700 ºC. These conditions were then chosen for a further study on the stability of the catalyst.

II-3.4. Catalytic stability of Na_2WO_4-TiO_2/SiO_2

The catalytic stability of the Na_2WO_4-TiO_2/SiO_2 catalyst was investigated under the optimal conditions found in section 3.3. The activities of the catalyst over 24 h are presented in Fig. II-4. Promisingly, the C_{2+} selectivities were high at approximately 69–71% during the testing period. However, the overall selectivity reduced by approximately 3% within 24 h. Moreover, the CH_4 conversions slowly decreased from 6.8 to 5.9, leading to decreased C_{2+} yield during the test period. It was also noticed that the CO_x selectivities gradually increased from 29 to 31%. The results suggested that the stability of the Na_2WO_4-TiO_2/SiO_2 catalyst was quite good for over 24 h. The slow deactivation of the catalyst requires further study, which is not the focus of this report.

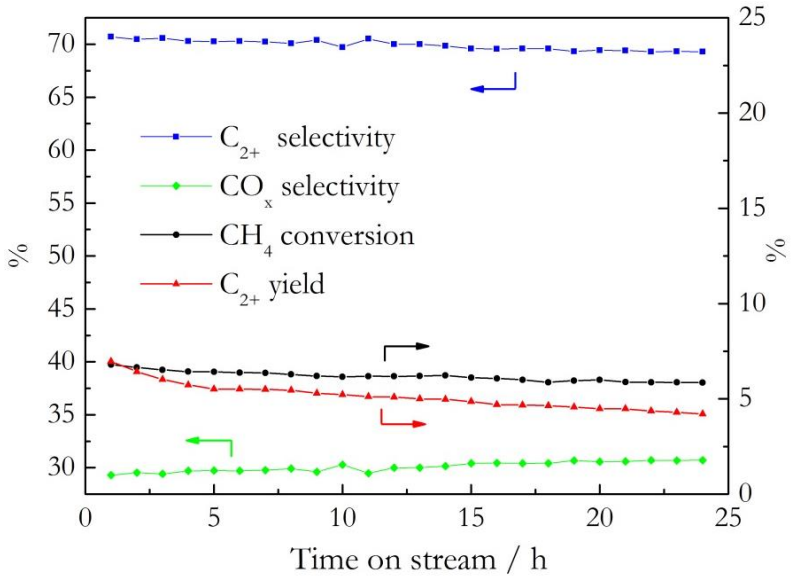

Fig. II-4. Catalytic performance of Na_2WO_4-TiO_2/SiO_2 catalyst, testing conditions: $N_2/(4CH_4{:}1O_2)$ feeding gas ratio of 1.0, reactor temperature of 700 ºC, total feed flow rate of 50 mL/min, atmospheric pressure, and 24 h of testing.

II-3.5. Characterization of TiO_2/SiO_2, Na_2WO_4/SiO_2, and Na_2WO_4-TiO_2/SiO_2 catalysts

The XRD pattern of the Na_2WO_4-TiO_2/SiO_2 catalysts compared with that of the TiO_2/SiO_2 and Na_2WO_4/SiO_2 catalysts are presented in Fig. II-5. The TiO_2/SiO_2 catalyst exhibited two small peaks at 2θ of 25.2 and 48.5, indicating the presence of crystalline TiO_2 (anatase). It was also noticed that the SiO_2 support was in the amorphous phase. For the Na_2WO_4/SiO_2 catalyst, two crystalline compounds were observed. The first one was the crystalline Na_2WO_4, showing the characteristic peaks at 2θ of 16.7, 27.5, 32.4 and 48.4. The other was the presence of α-cristobalite (one of the crystalline forms of SiO_2), exhibiting the characteristic peaks at 2θ of 21.9, 28.3, 31.3, 36.0, 47.8, and 56.9. It was surprising to observe the formation of α-cristobalite at low a calcination temperature (800 ºC) in the presence of Na_2WO_4 because this crystalline form of SiO_2 normally occurs at calcination temperatures above 1,500 ºC [19]. Similarly, the α-cristobalite phase was observed in the Na_2WO_4-TiO_2/SiO_2 catalyst as clearly indicated by the characteristic XRD pattern. It was more interesting to observe that the characteristic peaks of TiO_2 were clearly seen for the Na_2WO_4-TiO_2/SiO_2 catalyst compared to those peaks in the Na_2WO_4-TiO_2/SiO_2 catalyst. This suggested that the environment in this catalyst enhanced the crystallinity of TiO_2. Thus, the important factor that promotes the formation of C_{2+} products of the Na_2WO_4-TiO_2/SiO_2 catalyst was the formation of the crystalline components (α-cristobalite, Na_2WO_4, and TiO_2).

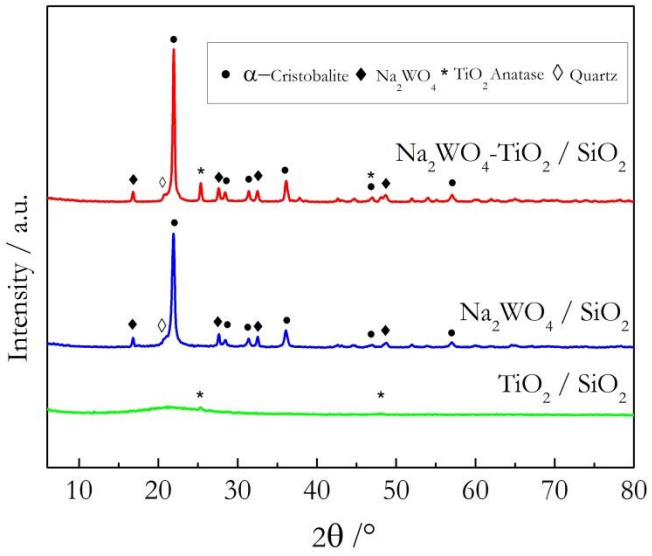

Fig. II-5. XRD patterns of TiO_2/SiO_2, Na_2WO_4 /SiO_2, and Na_2WO_4-TiO_2/SiO_2.

The surface morphologies of the three catalysts imaged using FE-SEM were compared with the pure SiO_2 support and these are illustrated in Fig. II-6(a)–Fig. II-6(f). The SiO_2 support (Fig. II-6(a)) and the TiO_2/SiO_2 catalyst (Fig. II-6(b)) are similar, in that the particles are irregular in shape with sizes ranging from 20 to 50 nm. These particles were observed mostly in the amorphous SiO_2 support. The particles of the Na_2WO_4/SiO_2 catalyst (Fig. II-6(c) and Fig. II-6(d)) were also irregular in shape. Interestingly, the typical shape of the amorphous SiO_2 was completely transformed to a new shape, which was larger in size and possessed coral-reef like structures (approximately > 0.5 μm in diameter). This new structure was the crystalline α-cristobalite as identified by the XRD pattern. The Na_2WO_4-TiO_2/SiO_2 catalyst (Fig. II-6(e) and Fig. II-6(f) had similar the size and shape to the particles of the Na_2WO_4/SiO_2 catalyst. However, some small particles (approximately 50-100 nm in diameter) were observed throughout the catalyst. These particles were identified as TiO_2 crystals.

The TEM images of the Na_2WO_4-TiO_2/SiO_2 catalyst compared with those of the TiO_2/SiO_2 and Na_2WO_4/SiO_2 catalysts are shown in Fig. II-7. The shape and size of each catalyst corresponded to the observation in the FE-SEM images (Fig. II-6). The TEM images of the Na_2WO_4/SiO_2 (Fig. II-7(c) and 7(d)) and Na_2WO_4-TiO_2/SiO_2 (Fig. II-7(e) and 7(f)) catalysts confirmed that the amorphous SiO_2 support transformed to α-cristobalite when adding Na_2WO_4, in agreement with a previous report [20]. For the Na_2WO_4-TiO_2/SiO_2 catalyst, crystalline TiO_2 particles were clearly observed with sizes ranging between 50 and 100 nm.

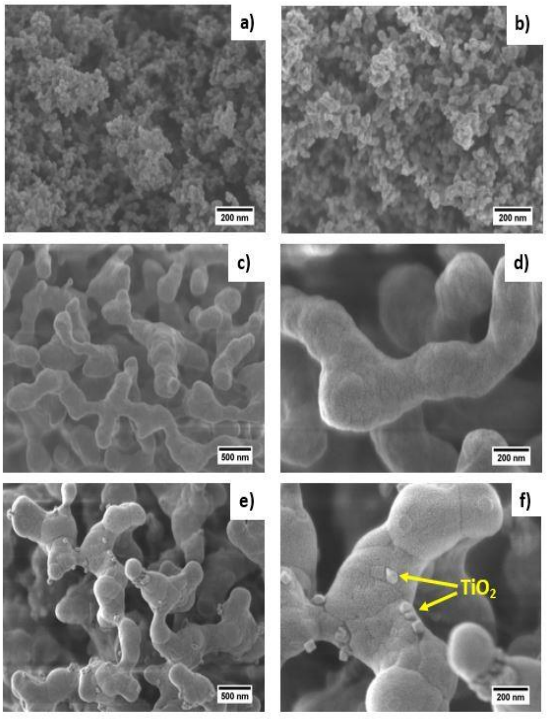

Fig. II-6. SEM images of pure SiO_2 support (a), TiO_2/SiO_2 (b), Na_2WO_4/SiO_2 (c, d), and Na_2WO_4-TiO_2/SiO_2 (e, f).

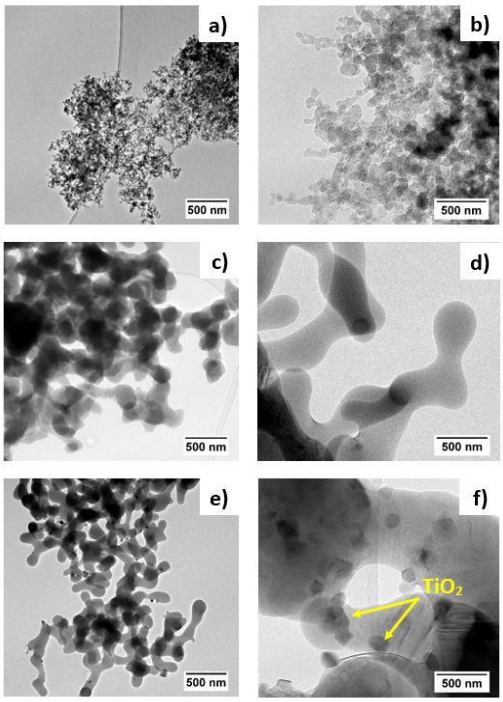

Fig. II-7. TEM images of TiO_2/SiO_2 (a, b), Na_2WO_4/SiO_2 (c, d), and Na_2WO_4-TiO_2/SiO_2 (e, f).

The BET surface areas, pore sizes, and pore volumes of the catalysts were measured using an N_2-sorption analyzer. For comparison, the commercial SiO_2 support (surface area of 85–115 m^2/g, amorphous fumed silica, Alfa Aesar) was also dried and calcined using the same method as the catalyst preparation without adding any metal precursors and conducting the BET measurement. As presented in Table II-1 and Fig. II-8, the isotherm plot of the SiO_2 support was similar to that of the TiO_2/SiO_2 catalyst, in which no hysteretic loop was observed. This indicated that the SiO_2 support and the TiO_2/SiO_2 catalyst are non-porous material, and thus their porous sizes and volumes must have been created from the inter-particles. However, the surface area of the SiO_2 support was lower than that of the TiO_2/SiO_2 catalyst, suggesting that the TiO_2 particles potentially deposited on the surface of SiO_2 and create new surfaces, and thus the surface area of the TiO_2/SiO_2 catalyst increased. The surface areas of the Na_2WO_4/SiO_2 and Na_2WO_4-TiO_2/SiO_2 catalysts were much lower than those of the SiO_2 support and the TiO_2/SiO_2 catalyst. This was consistent with the observations from using the FE-SEM (Fig. II-6.) & TEM (Fig. II-7.) images, in which the particle sizes of the catalysts containing Na_2WO_4 were larger than those of the TiO_2 catalyst. The hysteretic loops of the Na_2WO_4/SiO_2 and Na_2WO_4-TiO_2/SiO_2 catalysts were similar, in which the pore sizes and the pore volumes generated from the intra-particles and the pore sizes were classified as a meso-porous material. Although the Na_2WO_4-TiO_2/SiO_2

catalyst had a quite small specific surface area, this catalyst had the highest C_{2+} yield, indicating that the synergistic catalyst effect or the selected active components plays a significant role in the catalytic performance.

Table II-1. BET surface area (S.A.), pore size, and pore volume of TiO_2/SiO_2, Na_2WO_4/SiO_2, and Na_2WO_4-TiO_2/SiO_2 compared with pure SiO_2 support.

Material	S.A. (m^2/g)	Pore size (nm)	Pore volume (cm^3/g)
SiO_2	86.5	22.2	0.480
Na_2WO_4 / SiO_2	6.5	9.1	0.015
TiO_2 / SiO_2	106.2	17.5	0.460
Na_2WO_4-TiO_2/ SiO_2	5.4	10.0	0.013

The FT-IR patterns of the catalysts are presented in Fig. II-9. All three catalysts displayed the Si—O—Si rocking, the Si—O—Si bending, and the Si—O—Si stretching peaks appearing around 490, 800, and 1100 cm^{-1}, respectively. There was one different peak appearing at 621 cm^{-1} for Na_2WO_4-TiO_2/SiO_2 and Na_2WO_4/SiO_2, specifying the existence of α-cristobalite [19] in these two catalysts, in good agreement with the findings in Fig. II-5. As can be seen by the catalyst activities presented in Fig. II-1, the Na_2WO_4-TiO_2/SiO_2 catalyst had a C_{2+} yield greater than those of the two single catalysts. Thus, one of the important keys that can be considered to improve the C_{2+} yield is to have a catalyst consisting of α-cristobalite interacting with an active crystalline metal oxide.

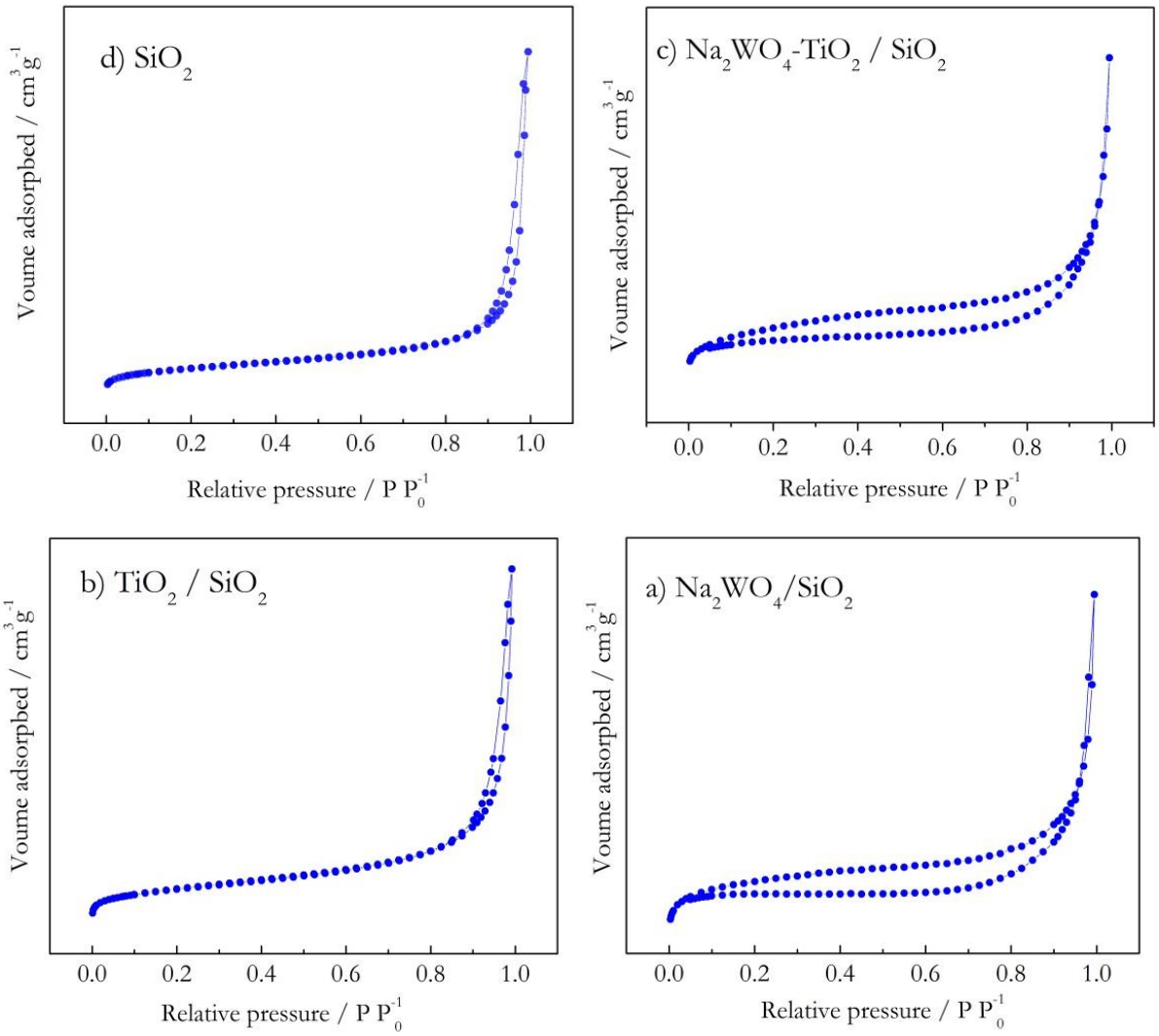

Fig. II-8. Isotherm plots of (a) Na_2WO_4/SiO_2 catalyst, (b) TiO_2/SiO_2 catalyst, (c) Na_2WO_4-TiO_2/SiO_2 catalyst, and (d) pure SiO_2 support

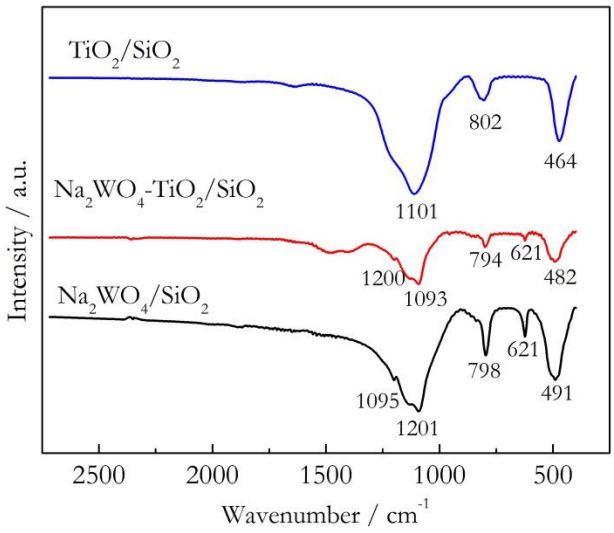

Fig. II-9. FT-IR spectra of Na_2WO_4-Ti/SiO_2, Na_2WO_4/SiO_2, and TiO_2/SiO_2 catalysts.

Fig. II-10 presents the XPS spectra of the catalysts. The XPS scans were carried out in the range of the Na, W, and Ti regions. The observed peaks corresponded to Na_2O (1s = 1071.5 eV) WO_4^{2-}($4f_{5/2}$ = 37.6 eV, $4f_{7/2}$ = 35.3 eV) for Na_2WO_4/SiO_2 and ($4f_{5/2}$ = 37.8 eV, $4f_{7/2}$ = 35.3 eV) for Na_2WO_4-TiO_2/SiO_2, and TiO_2 ($2p_{3/2}$ = 464.2 eV, $2p_{1/2}$ = 459.2 eV) for TiO_2/SiO_2 and ($2p_{3/2}$ = 464.5 eV, $2p_{1/2}$ = 458.8 eV) for Na_2WO_4-TiO_2/SiO_2. Of interest was that the peaks of $WO_4^{2-}$and TiO_2 shifted toward a higher binding energy when Na_2WO_4 and TiO_2 were present in the same catalyst. This was because the Ti or W species are more likely to attach to WO_4^{-2} or O^{2-} bonding with Ti, which is an electron withdrawing group. Thus, the oxidation state of Ti or W has a higher positive charge, and thus shifts in the binding energies can be observed.

Catalyst reducibility and the interaction between the active catalysts and the support were examined using the H_2-TPR technique (see Fig. II-11). For the TiO_2/SiO_2 catalyst, no clear H_2 reduction peak could be seen in this temperature range, consistent with previous reports [21, 22]. For Na_2WO_4/SiO_2, a broad reduction peak starting from 450 ºC to above 900 ºC with a maximum H_2 consumption at about 800 ˚C was observed, indicating the reduction of W species [22]. The reduction behavior of the Na_2WO_4-TiO_2/SiO_2 catalyst was related to that of the Na_2WO_4/SiO_2 catalyst. However, the starting reduction temperature and the maximum temperature of the Na_2WO_4-TiO_2/SiO_2 catalyst shifted toward a higher temperature (approximately 50 ºC greater than those of the Na_2WO_4/SiO_2 catalyst). This suggested that the redox properties of these metal species substantially change, probably because there is a strong interaction between the WO_4^{2-} component and the TiO_2 crystals [22].

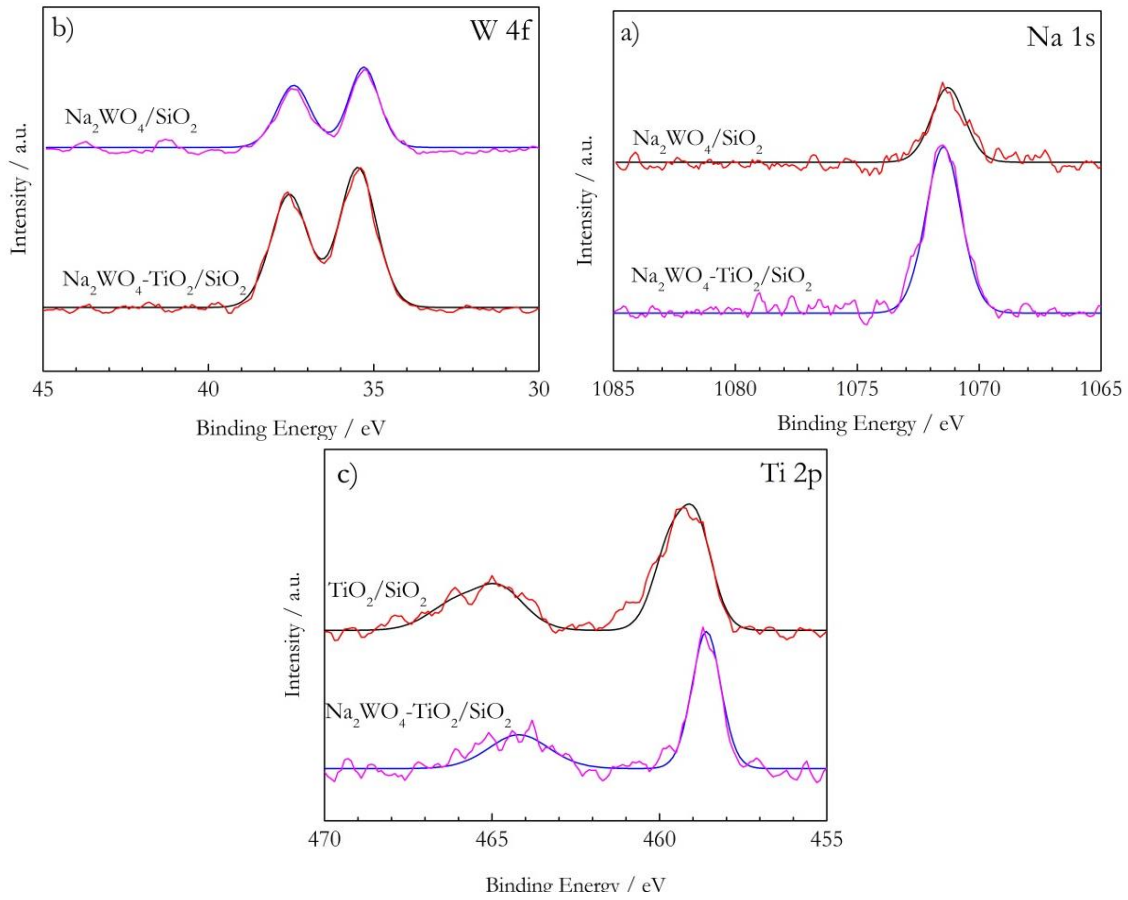

Fig. II-10. XPS spectra of Na_2WO_4-Ti/SiO_2, Na_2WO_4/SiO_2, and TiO_2/SiO_2 showing scanning in the (a) Na, (b) W, and (c) Ti ranges.

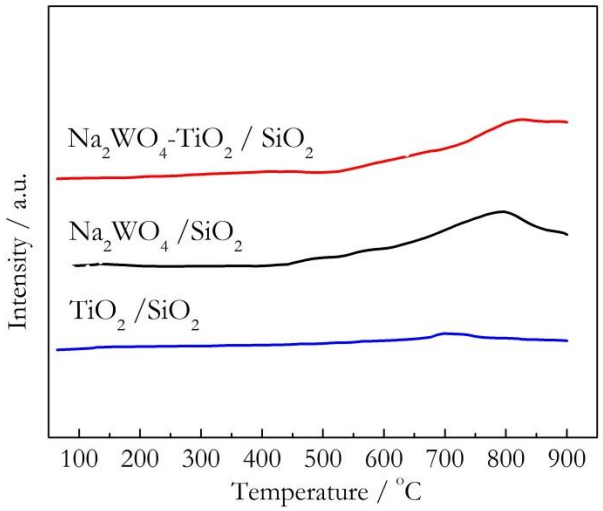

Fig. II-11. H_2-TPR patterns of Na_2WO_4-TiO_2/SiO_2, Na_2WO_4/ SiO_2, and TiO_2/SiO_2.

In previous reports on the activity of catalysts containing Na_2WO_4 and SiO_2 for OCM reaction, there have been some suggestions about the enhancement of those catalysts as follows. Ji, et al. stated that the existence of the α-cristobalite phase was a critical necessity for the C_{2+} formation of catalysts containing Na_2WO_4 and SiO_2 for OCM reaction [9]. Elkins, et al. claimed that the interaction between the α-cristobalite structure and the WO_4^{2-} tetrahedron structure was crucial in the generation of C_{2+} and the inter-phase between these two components was the active surface species. Moreover, the WO_4^{2-} tetrahedron could stabilize the Mn_2O_3 and Na_2WO_4 phases, so that the catalysts could maintain their high activity during the reaction [23]. Furthermore, Palermo, et al. suggested that Na played dual roles in promoting the activity of MnO_x-Na_2WO_4/SiO_2 catalysts by acting as both a chemical and a structural promoter [24, 25]. From these reports, it can be certainly claimed that the presence of the α-cristobalite structure, the crystalline Na_2WO_4, and the anatase-TiO_2 crystals in the Na_2WO_4-TiO_2/SiO_2 catalyst strongly enhances the activity of the catalyst and is crucial for the formation of C_{2+} in the reaction.

II-4. Conclusions

The combination of 5wt% TiO_2 and 5wt% Na_2WO_4 on SiO_2 support (i.e. Na_2WO_4-TiO_2), prepared using the co-impregnation method, was superior to the single catalysts of its component (i.e. Na_2WO_4/SiO_2, TiO_2/SiO_2). In studying the operating conditions by co-feeding N_2 gas as a diluent gas into the reactant gases at different volume ratios and different temperatures, the maximum C_{2+} yield was found at an N_2/($4CH_4$:$1O_2$) feeding gas ratio 1:1 by volume and at

700 ºC. The Na_2WO_4-TiO_2 catalyst produced the highest C_{2+} yield at 4.9% with 71.7% C_{2+} selectivity and 6.8% CH_4 conversion under these optimal operating conditions. Furthermore, the activity of the catalyst had good stability over 24 h of testing. Characterization of the Na_2WO_4-TiO_2 catalyst using XRD and FT-IR showed that α-cristobalite and crystalline anatase-TiO_2 were present. These two crystal components played a significant role in the formation of C_{2+} for the OCM reaction. The FE-SEM, TEM, and BET results were in good agreement with the findings of the XRD and FT-IR analyses. Of great interest for future study is the analysis of the kinetic mechanism of the catalyst for OCM reaction or improvement of the catalyst activity by adding promoters.

Acknowledgements

We would like to thanks the Thailand Research Fund and the Commission on Higher Education (grant numbers IRG5980004 & MRG6180232); the National Nanotechnology Center (NANOTEC), NSTDA, Ministry of Science and Technology, Thailand, through its program of Research Network NANOTEC (RNN); the Center of Excellence on Petrochemical and Materials Technology; the Kasetsart University Research and Development Institute (KURDI); and the Department of Chemical Engineering and the Faculty of Engineering at Kasetsart University for financial supports. P. Kidamorn received funding through a scholarship from the Faculty of Engineering at Kasetsart University.

References for Part II.

[1] G. J. Hutchings, M. S. Scurrell, and J. R. Woodhouse, "Oxidative coupling of methane using oxide catalyst," *Chem. Soc. Rev.*, vol. 18, pp. 251-283, 1989.

[2] M. Y. Sinev, Z. T. Fattakhova, V. I. Lomonosov, and Y. A. Fordienko, "Kinetics of oxidative coupling of methane: bridging the gap between comprehension and description," *J. Nat. Gas Chem.*, vol. 18, pp. 273-287, 2009.

[3] K. Khammona, S. Assabumrungrat, and W. Wiyarath, "Reviews on coupling of methane over catalysts for application in C_2 hydrocarbon production," *J. Eng. Appl. Sci.*, vol. 7, pp. 447-455, 2012.

[4] S. M. K. Shahri and A.N. Pour, "Ce-promoted Mn/Na_2WO_4/SiO_2 catalyst for oxidative coupling of methane at atmospheric pressure*,"J. Nat. Gas Chem*, vol. 19, pp. 47-53, 2010.

[5] R. Mariscal, M. A. Pena, and J. L. G. Fierro, "Promoter effects of dichloromethane on the oxidative coupling of methane over MnMgO catalysts," *Appl. Catal., A*, vol. 131, pp. 243-261, 1995.

[6] V. R. Choudhary, V. H. Rane, and S. T. Chaudhari, "Factors influencing activity/selectivity of La-promoted MgO catalyst prepared from La- and Mg- acetates for oxidative coupling of methane," *Fuel*, vol. 79, pp. 1487-1491, 2000.

[7] Z. Gholipour, A. Malekzadeh, R. Hatami, Y. Mortazavi, and A. Khodadadi,"Oxidative coupling of methane over (Na_2WO_4+Mn or Ce)/SiO_2 catalysts: In situ measurement of electrical conductivity," *J. Nat. Gas Chem*, vol. 19, pp. 35-42, 2010.

[8] R. T. Yunarti, M. Lee, Y. J. Hwang, D. J. Suh, J. Lee, I. W. Kim, and J. M. Ha, "Transition metal-doped TiO_2 nanowire catalysts for the oxidative coupling of methane," *Catal. Commun*, vol. 50, pp. 54-58, 2014.

[9] S. Ji, T. Xiao, S. Li, L. Chou, B. Zhang, C. Xu, R. Hou, A. P. E. York, and M. L. H Green, "Surface WO_4 tetrahedron: the essence of the oxidative coupling of methane over M-W-Mn/SiO_2 catalysts," *J. Catal.*, vol. 220, pp. 47-56, 2003.

[10] J. Y. Lee, W. Jeon, J. W. Choi, Y. W. Suh, J. M. Ha, D. J. Suh, and Y.K. Park, "Scaled-up production of C_2 hydrocarbons by the oxidative coupling of methane over pelletized Na_2WO_4/Mn/SiO_2 catalysts: Observing hot spots for the selective process," *Fuel.*, vol. 106, pp. 851-857, 2013.

[11] A. Malekzadeh, A. Khodadadi, A. K. Dalai, and M. Abedini, "Oxidative coupling of methane over Lithium doped (Mn+W)/SiO_2 catalysts," *J. Nat. Gas Chem*, vol. 16, pp. 121-129, 2007.

[12] J. Wang, L. Chou, B. Zhang, H. Song, J. Zhao, J. Yang, and S. Li, "Comparative study on oxidation of methane to ethane and ethylene over Na_2WO_4-Mn/SiO_2 catalysts prepared by different methods," *J. Mol. Catal. Chem*., vol. 245, pp. 272-277, 2006.

[13] N. Hiyoshi and T. Ikeda, "Oxidative coupling of methane over alkali chloride-Mn-Na_2WO_4/SiO_2 catalysts: Promoting effect of molten alkali chloride," *Fuel Process. Technol.,* vol. 133, pp. 29-34, 2015.

[14] T. W. Elkins and H. E. Hagelin-Weaver, "Characterization of Mn-Na_2WO_4/SiO_2 and Mn-Na_2WO_4/MgO catalysts for the oxidative coupling of methane," *Appl. Catal., A*, vol. 497, pp. 96-106, 2015.

[15] F. Papa, D. Gingasu, L. Patron, A. Miyazaki, and I. Balint, "On the nature of active sites and catalytic activity for OCM reaction of alkaline-earth oxides-neodymia catalytic systems," *Appl. Catal., A,* vol. 375, pp. 172-178, 2010.

[16] V. H. Rane, S. T. Chaudhari, and V. R. Choudhary, "Oxidative coupling of methane over La-promoted CaO catalysts: Influence of precursors and catalyst preparation method," *J. Nat. Gas Chem*., vol. 19, pp. 25-30, 2010.

[17] D. J. Wang, M. P. Rosynek, and J. H. Lunsford, "Oxidative coupling of methane over oxide-supported sodium-manganese catalysts," *J. Catal.*, vol. 155, pp. 390-402, 1995.

[18] F. Basile, G. Fornasari, F. Trifiro, and A. Vaccari, "Partial oxidation of methane: Effect of reaction parameters and catalyst composition on the thermal profile and heat distribution," *Catal. Today*, vol. 64, pp. 21-30, 2001.

[19] S. Ji, T. Xiao, S. Li, L. Chou, B. Zhang, C. Xu, R. Hou, A. P. E York, and M. L. H Green, "Surface WO_4 tetrahedron: the essence of the oxidative coupling of methane over M·W·Mn/SiO_2 catalysts," *J. Catal.*, vol. 220, pp. 47-56, 2003.

[20] A. M. Venezia, F. Raimondi, V. La Parola, and G. Deganello, " Influence of sodium on the structure and HDS activity of Co-Mo catalysts supported on silica and aluminosilicate," *J. Catal.*, vol. 194, pp. 393-400, 2000.

[21] T. Chukeaw, A. Seubsai, P. Phon-in, K. Charoen, T. Witoon, W. Donphai, P. Parpainainar, M. Chareonpanich, D. Noon, B. Zohour, and S. Senkan, " Multimetallic catalysts of RuO_2–CuO–Cs_2O–TiO_2/SiO_2 for direct gas-phase epoxidation of propylene to propylene oxide," *RSC Adv.*, vol. 6, pp. 56116-56126, 2016.

[22] J. Li, G. Lu, G. Wu, D. Mao, Y. Guo, Y. Wang, and Y.Guo, "Effect of TiO_2 crystal structure on the catalytic performance of Co_3O_4/TiO_2 catalyst for low-temperature CO oxidation," Catal. Sci. Technol., vol. 4, pp. 1268-1275, 2014.

[23] T. W. Elkins, and H. E. Hagelin-Weaver, "Characterization of Mn-Na_2WO_4/SiO_2 and Mn-Na_2WO_4/MgO catalysts for the oxidative coupling of methane," Appl. Catal., A, vol. 497, pp. 96-106, 2015.

[24] A. Palermo, J. P. H Vazquez, A. F. Lee, M. S. Tikhov, and R. M. Lambert, "Critical influence of the amorphous silica-to-cristobalite phase transition on the performance of Mn/Na_2WO_4/SiO_2 catalysts for the oxidative coupling of methane," *J. Catal.*, vol. 177, pp. 259-266, 1998.

[25] Y. T. Chua, A. R. Mohamed, and S. Bhatia, "Oxidative coupling of methane for the production of ethylene over sodium-tungsten-manganese-supported-silica catalyst (Na-W-Mn/SiO_2)," *Appl. Catal.,A*, vol. 343, pp. 142-148, 2008.

Part III : Investigation of metal oxide additives onto Na_2WO_4-Ti/SiO_2 catalysts for oxidative coupling of methane to value-added chemicals

III-1. Introduction

Methane (CH_4) is the primary component of natural gas and biogas. It is considered a greenhouse gas about 25 times stronger than CO_2 if these two gases are released to the atmosphere in the same amount [1]. Since CH_4 is abundant on Earth, it is highly attractive to worldwide researchers to explore strategies to transform it into more useful products. One of the most challenging methods is the oxidative coupling of methane (OCM), which is a type of chemical reaction using air or oxygen directly reacting with CH_4 to produce useful hydrocarbons such as ethylene, ethane, propene, propane, etc. (C_{2+}) [2-5]. In the absence or presence of a catalyst, the OCM reaction is exothermic and normally takes place in reaction temperatures of 600–1,000 °C [6]. Moreover, CO and CO_2 can be produced as byproduct. However, it is believed that if a suitable catalyst is present, the products can be controlled and the extreme reaction temperature can be reduced.

Previously, several potential catalysts have been reported for the OCM reaction to C_{2+}, especially Mn modified with a variety of co-catalysts, supports, and/or promoters, such as oxides of Mg, Na, and Ce. The activity of those catalysts was approximately <16% C_{2+} yield and 25–78% C_{2+} selectivity. Lately, a solid mixture of Na_2WO_4-Mn supported on SiO_2 has been greatly attractive to researchers worldwide, because this combination is highly active for the OCM reaction. The catalyst has also been modified with many metals (e.g. Li, Na, K, Ba, Ca, Fe, Co, Ni, Al, Ti, Ce, etc.) [7-9]. Some of these modified catalysts, especially Na_2WO_4-Mn/SiO_2 doped with TiO_2 [10, 11], exhibited an improvement on both C_{2+} yield and selectivity (i.e. 16.8% C_{2+} yield and 73% C_{2+} selectivity). The addition of a promoter into the Na_2WO_4-Mn/SiO_2 catalyst (e.g. LiCl, NaCl, KCl, or CsCl) has also been found to result in the incorporation of the promoter into the catalytic material, thus increasing the number of strong basic sites, thereby enhancing the catalyst activity [12-14].

Recently, we have found a combination of Na_2WO_4 and Ti-supported SiO_2 exhibiting high activity for the OCM reaction, giving 4.9% C_{2+} yield with 71.7% C_{2+} selectivity and 6.8% CH_4 conversion at a reactor temperature of 700 °C and atmospheric pressure [15]. The activity of the catalyst had good stability over 24 h of on-stream testing. Moreover, a crystalline structure of α-cristobalite of SiO_2 that was present along with TiO_2 crystals was found to substantially enhance the activity of the catalyst for the OCM reaction to C_{2+}. Therefore, improve the activity of this catalyst is of great interest. Herein, we modify the catalyst by adding a metal oxide additive into the Na_2WO_4-Ti/SiO_2 catalyst. The selected metal oxide additives include Co, Mn, Cu, Fe, Ce, Zn, La, Ni, Zr, Cr, and V. The most active catalyst is subsequently chosen to optimize the C_{2+} yield by varying operating conditions. Additionally, advanced instrument techniques are also used to analyze the prepared catalysts to acquire their physicochemical properties to relate with their catalytic activity.

III-2. Experimental

III-2.1. *Catalyst preparation*

All of the catalysts were prepared using co-impregnation as follows. Weights of Na_2WO_4 (Na_2WO_4•$2H_2O$, 98.0~101.0%, Daejung), Ti ($C_{12}H_{28}O_4Ti$, 97+%, Alfa Aesar), and X (X = Co, Mn, Cu, Fe, Ce, Zn, La, Ni, Zr, Cr, or V) were determined and pipetted from each stock precursor solution into amorphous fume SiO_2 (surface area of 85-115 m^2/g, Alfa Aesar) to obtain a desired weight percentage of the metal components. Note that the precursor of the 11 elements was in the form of metal nitrate hydrate, and the weight percentage of each component on the support was calculated based on the formula appearing in each catalyst's name. For example, for the Na_2WO_4-Ti-Mn/SiO_2 catalyst, the weights of Na_2WO_4, Ti(0), and Mn(0) were determined and loaded onto the SiO_2 support. After that, the mixture was stirred at room temperature for 2 h and heated to 120 °C until dried. Then, the dried powder was set to calcine in an air furnace at 800 °C for 4 h. Finally, the powder was ground until a fine powder was obtained. The weight percentage of each component for each catalyst will be elaborated in the results and discussion of that mentioned figure.

III-2.2 *Catalytic activity test*

The activity of each prepared catalyst for the OCM reaction was evaluated in a plug flow reactor at atmospheric pressure. The reactor temperature was set in the range of 600–800 °C. A catalyst (8–72 mg) was packed in a quartz tube reactor (0.5 cm inner diameter) and sandwiched between layers of quartz wool. The feed gas consisted of methane (CH_4, 99.999%, Praxair), oxygen (O_2, 99.999%, Praxair), and nitrogen (N_2, 99.999%, Praxair) at a volume ratio of CH_4:O_2:N_2 = 3:1:0, 3:1:2, or 3:1:4 with a total feed flow rate in the range of 35–95 mL/min. The effluent gas was evaluated using an online gas chromatograph (SHIMADZU, GC-14A) equipped with a flame ionization detector (FID; for analyzing C_2H_4, C_2H_6, C_3H_6, C_3H_8 and C_4H_8, and C_4H_{10}) and a thermal conductivity detector (TCD; for analyzing CO, CO_2, and CH_4). The activity of each catalyst was analyzed after the system had reached a set point of 2 h. Equations (1)–(4) show the formulas for calculating the %CH_4 conversion, %C_{2+} selectivity, %CO_x selectivity, and %C_{2+} yield.

$$\%\ \mathrm{CH_4}\ \text{conversion} = \frac{\text{moles of } \mathrm{CH_4} \text{input} - \text{moles of } \mathrm{CH_4} \text{output}}{\text{moles of } \mathrm{CH_4}\ \text{input}} \times 100 \quad (1)$$

$$\%\ \mathrm{C_{2+}}\ \text{selectivity} = \frac{\text{moles of } \mathrm{C_{2+}}}{\text{Total moles of products}} \times 100 \quad (2)$$

$$\%\ \mathrm{CO_x}\ \text{selectivity} = \frac{\text{moles of } \mathrm{CO_x}}{\text{Total moles of products}} \times 100 \quad (3)$$

$$\%\ C_{2+}\ \text{yield} = \frac{\%\ CH_4 \text{conversion} \times \%\ C_{2+} \text{selectivity}}{100} \quad (4)$$

III-2.3. *Catalyst characterization*

The X-ray diffraction (XRD) patterns of each catalyst were obtained using a powder X- ray diffractometer (PXRD; JEOL JDX-3530 and Philips X-Pert, using Cu-$K\alpha$ radiation, 45 kV and 40 mA). The electronic states of selected elements in each catalyst were examined using X-ray photoelectron spectroscopy (XPS; Kratos Axis Ultra DLD) with Al Kα for the X-ray source. The surface morphology of the samples was imaged using a scanning electron microscope (SEM, FE-SEM: JEOL JSM7600F).

III-3. Results and discussion

III-3.1. *Activity of Na_2WO_4-Ti/SiO_2 added metal oxide additives*

In catalyst screening experiments for the OCM reaction in our laboratory, we have found that 5 wt% Na_2WO_4 + 5 wt% Ti on SiO_2 (denoted as Na_2WO_4-Ti/SiO_2) showed a priming result for C_{2+} production. We also found, from an XPS measurement of the catalyst, that the form of Ti was TiO_2 (data are not shown here). In this work, the Na_2WO_4-Ti/SiO_2 catalyst was further investigated by adding 11 elements, Co, Mn, Cu, Fe, Ce, Zn, La, Ni, Zr, Cr, and V. These 11 elements were selected from the transition metals because of their availability, non-toxicity, inexpensiveness, and, more importantly, inactiveness for CH_4 combustion [16]. All of the Na_2WO_4-Ti/SiO_2 catalysts with added metal oxide additive were prepared using a metal ratio of Na_2WO_4:Ti:X = 5:5:2 (where X is an metal oxide additive and its weight is calculated on the basis of the metallic form). The total metal loading was 12 wt% for every catalyst, except Na_2WO_4-Ti/SiO_2 (i.e. 5wt% Na_2WO_4 + 5 wt% Ti). The activity test results of the catalysts are presented in Fig. III-1.

Under the same testing conditions, the catalyst without metal oxide additive exhibited 4.43% C_{2+} yield with 33.8% C_{2+} selectivity and 13.34% CH_4 conversion. The most promising catalyst was the addition of Mn into the Na_2WO_4-Ti/SiO_2 catalyst, yielding 9.97% with 35.0% C_{2+} selectivity and 29.48% CH_4 conversion. The other metal oxides, which were added into the Na_2WO_4-Ti/SiO_2 catalyst and gave a C_{2+} yield higher than that of the catalyst without metal oxide additive, were (in order) Co > Fe > Ce > Zn, giving C_{2+} yield in a range of 4.50–7.65%. The addition of Mn clearly greatly improved the activity of Na_2WO_4-Ti/SiO_2. The characterization using XRD and XPS of these catalysts will reveal how the activities of some catalysts improve, which will be presented in the next section.

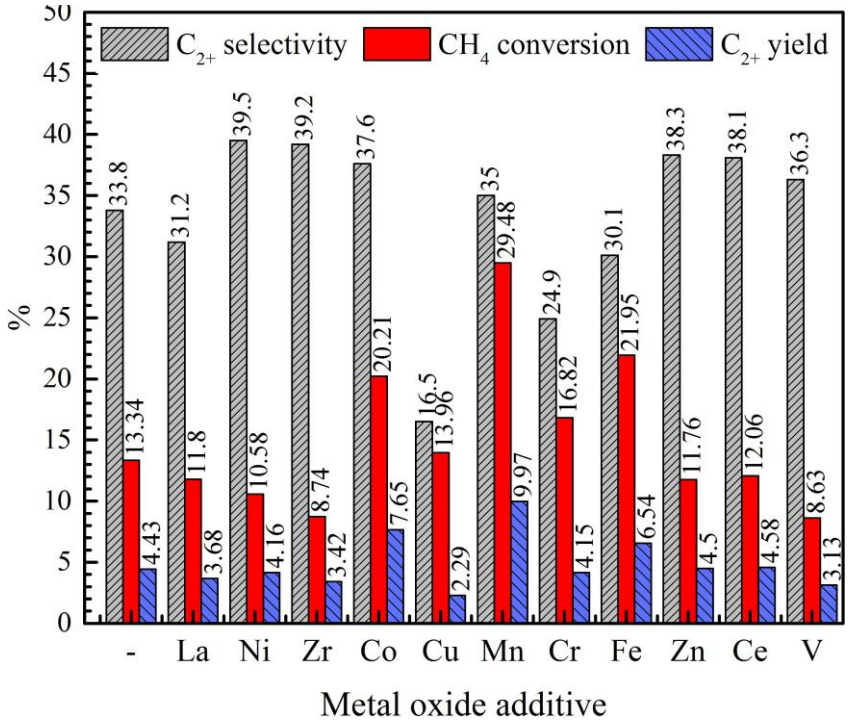

Fig. III-1. Catalyst activity of Na_2WO_4-Ti/SiO_2 added metal oxide additives. Reaction conditions: CH_4:O_2:N_2 ratio = 3:1:0, catalyst weight = 8 mg, total feed flow rate of 35 mL/min, reactor temperature = 700 °C.

III-3.2. *XRD and XPS analyses of Na_2WO_4-Ti/SiO_2 added metal oxide additives*

XRD patterns of the Na_2WO_4-Ti/SiO_2 catalysts with added metal oxide additives are presented in Fig. III-2. The characteristic peaks of α-cristobalite (2theta = 22.1, 28.6, 31.5, 36.1, 41.2, 42.9, and 44.9 (ICDD No. 00-001-0438)) appeared for all catalysts. A small XRD peak indicating the presence of α-tridymite (2theta = 21.8, 23.3, 27.3, and 30.1 (ICDD No. 00-003-0227)) was also observed. The characteristic peaks of Na_2WO_4 (16.9, 27.8, 32.4, 48.8, 52.1, and 57.1 (ICDD No. 01-074-2369)) appeared in the Na_2WO_4 catalysts with no added (-), Zn, Ni, Mn, Fe, Cu, and Co. The characteristic peaks of TiO_2 (2theta = 25.2, 37.0, 48.0, 54.1, and 55.0 (ICDD No. 01-073-1764)) were seen in the Na_2WO_4 catalysts with no added (-), Zr, Zn, V, La, and Ce. It should be noted that the most active catalyst presented in Fig. III-1 was Na_2WO_4-Ti-Mn/SiO_2. As shown in Fig. III-2, this catalyst consisted of α-cristobalite, crystalline Na_2WO_4, and crystalline Mn_2O_3 (2theta = 33.1, 38.1, and 44.8 (ICDD No. 00-002-0896)). Hence, the presence of these crystalline phases is essential for the OCM reaction. For the role of Ti, its combination with Mn has been proposed in the form of the $MnTiO_3$ phase; then, the $MnTiO_3$ phase plays an important role in remarkably improving the catalyst activity [10, 11]. However, no XRD peaks of $MnTiO_3$ can be observed in Fig. III-2, probably because a small amount of Mn was loaded and/or the crystal species is too small to be detected.

The XPS spectra of all catalysts in the range of W (4f) and Ti (2p) regions are presented in Fig. III-3 and 4, respectively. The observed peaks corresponded to $^{2-}WO_4^{2-}$ ($4f_{5/2}$ ~ 37.6 eV, $4f_{7/2}$ ~ 35.4 eV) and TiO_2 ($2p_{1/2}$ ~ 464 eV, $2p_{3/2}$ ~ 459 eV). Of interest was that the peaks of $WO_4^{2-}$and TiO_2 of each catalyst were not identical. Perhaps, the addition of metal oxides influences the interaction of WO_4^{2-} or Ti bonding with O^{2-}, thus leading to shifts of the binding energies [17-19].

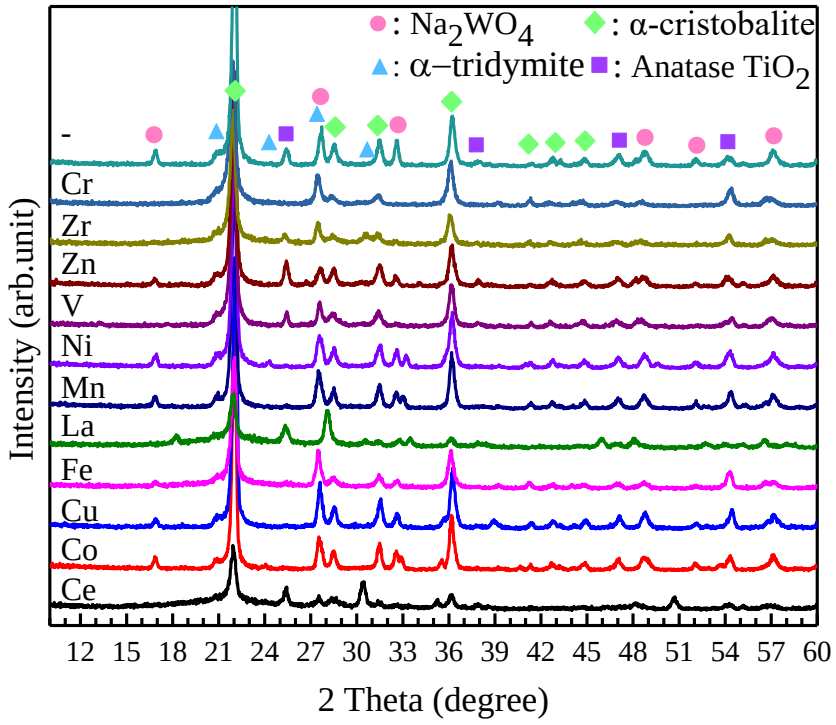

Fig. III-2. XRD patterns of Na_2WO_4-Ti/SiO_2 catalyst added metal oxide additives, fixing wt% of Na_2WO_4:Ti:X = 5:5:2 and SiO_2 balance.

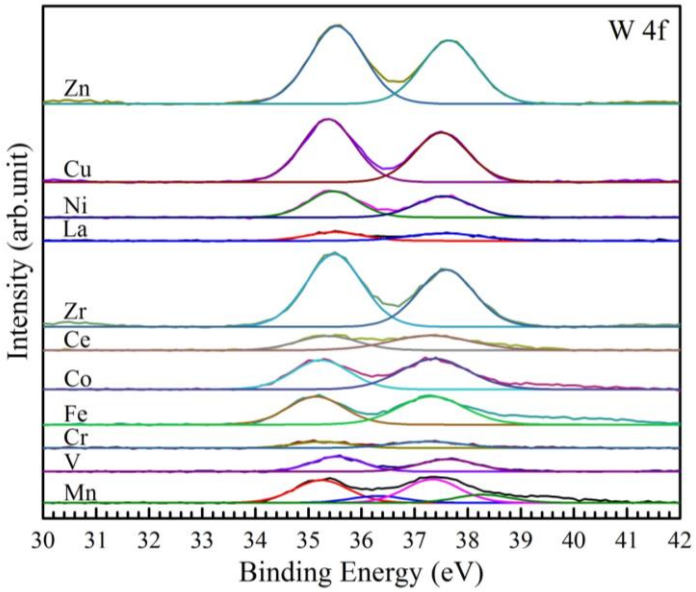

Fig. III-3. XPS spectra of Na_2WO_4-Ti/SiO_2 added different metal oxide additives showing binding energy in the range of W4f.

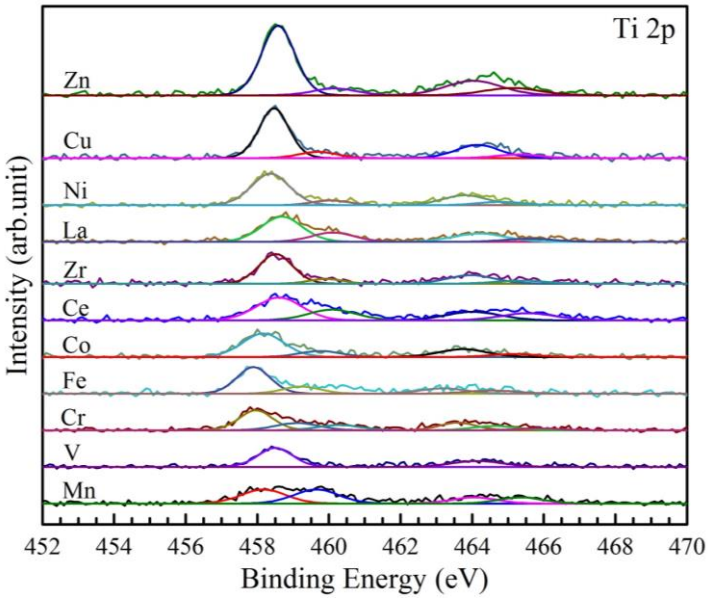

Fig. III-4. XPS spectra of Na_2WO_4-Ti/SiO_2 added different metal oxide additives showing binding energy in the range of Ti2p.

The most interesting results are presented in Fig. III-5, showing the plots of CH_4 conversion of each catalyst versus its binding energy of W $4f_{7/2}$ (Fig. III-5a) and Ti $2p_{3/2}$ (Fig. III-5b). The plots in each figure can be divided into two groups: group 1 (the catalysts containing Mn, Fe, Co, and Cr) and group 2 (the catalysts containing Cu, Zn, Ce, La, Ni, Zr, and V). The catalysts in group 1 possessed binding energies in a range of 35.12–35.24 eV for W $4f_{7/2}$ and 457.90–458.20 eV for Ti $2p_{3/2}$, while the catalysts in group 2 gave the XPS signal in a range of 35.36–35.56 eV for W $4f_{7/2}$ and 458.34–458.68 eV for Ti $2p_{3/2}$. It is interesting to see that the CH_4 conversions of the catalysts in group 1 were significantly higher than those in group 2. Moreover, the catalysts in group 1 clearly exhibited binding energies lower than the catalysts in group 2. Importantly, these findings suggest that the metal additives—that are able to shift the binding energies of W 4f and Ti 2p toward lower binding energies when added into the Na_2WO_4-Ti/SiO_2 catalyst—are highly active for the OCM reaction. It is possible that when the binding energy of W 4f or Ti 2p shifts toward a lower binding energy, the energy to remove an electron from the outer electron layer of W or Ti will become lower [18]. This reveals that it becomes easier for an oxygen atom bonding with W or Ti to dissociate or leave from the center. In other words, when an oxygen molecule adsorbs onto an active site—WO_4^{2-} associated with Ti^{2+}—it will dissociate and bond with the center of W or Ti. Due to the influence of a metal oxide additive added into the catalyst, the oxygen atom can easily detach from and leave the active metal center as H_2O [18]. This proposed behavior can significantly enhance the reaction mechanism for OCM. As a result, the catalysts in group 1 exhibit a higher CH_4 conversion relative to those in group 2. Future studies, to deeply understand the reaction mechanism, are required.

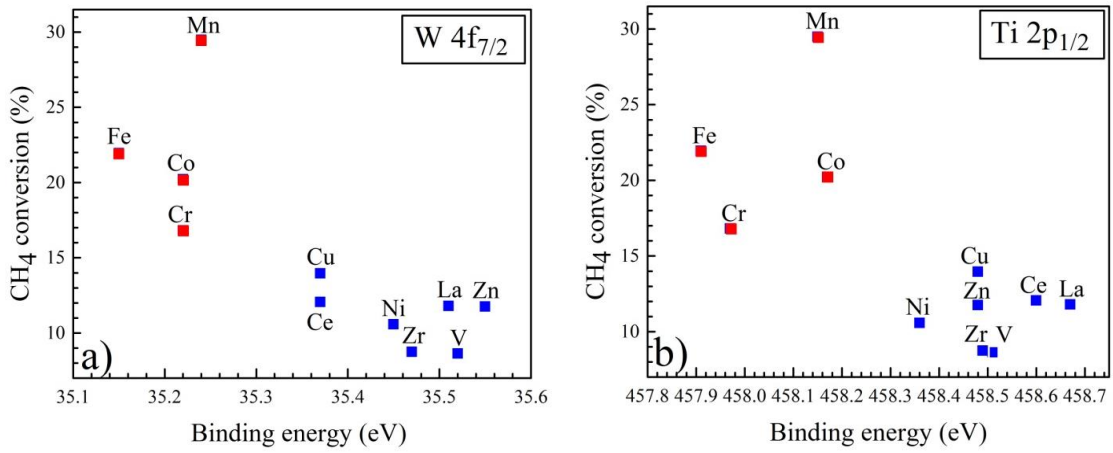

Fig. III-5. Plots of correlation between CH_4 conversions and binding energies of a) W $4f_{7/2}$ and b) Ti $2p_{1/2}$.

III-3.3. *Optimization of Na_2WO_4-Ti-Mn/SiO_2 catalyst for production of C_{2+}*

The Na_2WO_4-Ti-Mn/SiO_2 catalyst was further optimized to increase C_{2+} yield by first varying the weight percentage of Mn into Na_2WO_4-Ti/SiO_2 from 0.0 to 2.5 wt%. The results are shown in Fig. III-6. The C_{2+} yield was found to be optimized at 0.5 wt% Mn loading (12.16% C_{2+} yield with 39.7% C_{2+} selectivity and 30.62% CH_4

conversion, then the C_{2+} yields slightly decreased to approximately 9.6%). The decrease in the activity of the catalysts with Mn loading over 0.5 wt% could be due to the formation of MnO_x multilayers, which affects the generation of nucleophilic oxy species (e.g. O_2^-, O_2^{2-}, and O^-) [20]. SEM images of the catalysts shown in Fig. III-6 are illustrated in Fig. III-7. As shown, the surface morphology and particle size of all catalysts are similar. All the particles are irregularly shaped with various sizes, ranging from 50 nm to about 1 μm in diameter of coral reef-shaped particles. Nevertheless, the catalytic activity of each catalyst is different, probably due to differences in the distribution of the active Mn species (Mn_2O_3, $MnTiO_3$) in each catalyst.

The best Na_2WO_4-Ti-Mn/SiO_2 catalyst found in Fig. III-6 was further investigated by varying catalyst amounts and reactant gas feeding ratios, while the total feed flow rate was fixed at 35 mL/min for every condition. Three reactant gas feeding ratios of CH_4:O_2:N_2 were used, including CH_4:O_2:N_2 = 3:1:0, 3:1:2, and 3:1:4. The results are plotted in Fig. III-8. As expected, the activity of the catalyst increased on increasing the catalyst amount because the number of active sites increase as the catalyst amount increases. Consequently, more CH_4 can react with the active sites, thereby increasing the C_{2+} yields. The catalyst amount of each reactant gas feeding ratio that delivered the highest C_{2+} yield was 24, 48, and 64 mg, giving a C_{2+} yield of 19.19%, 19.61%, and 18.70% when the reactant gas feeding ratio of CH_4:O_2:N_2 was 3:1:0, 3:1:2, and 3:1:4, respectively. It should be noted that the optimal point of each condition is the point where the O_2 gas is completely consumed. Thus, after the optimal points, the CH_4 conversions should have been steady. However, the C_{2+} conversions minimally decreased with gradual decreases of C_{2+} yields, potentially because the C_{2+} products can further react with some special active sites to produce CO, CO_2, and even CH_4 [21-27]. Thus, the CH_4 conversion decreased as the catalyst amount increased.

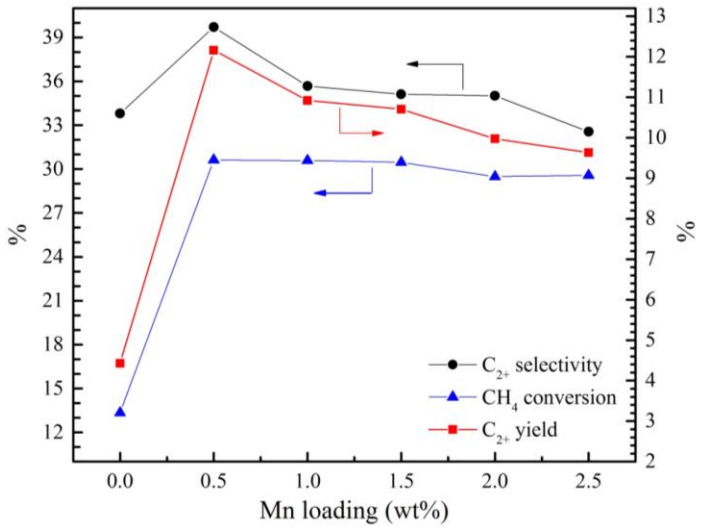

Fig. III-6. Effect of Mn loading into Na_2WO_4-Ti/SiO_2. Reaction conditions: CH_4:O_2:N_2 ratio = 3:1:0, catalyst weight = 8 mg, total feed flow rate of 35 mL/min, reactor temperature = 700 °C.

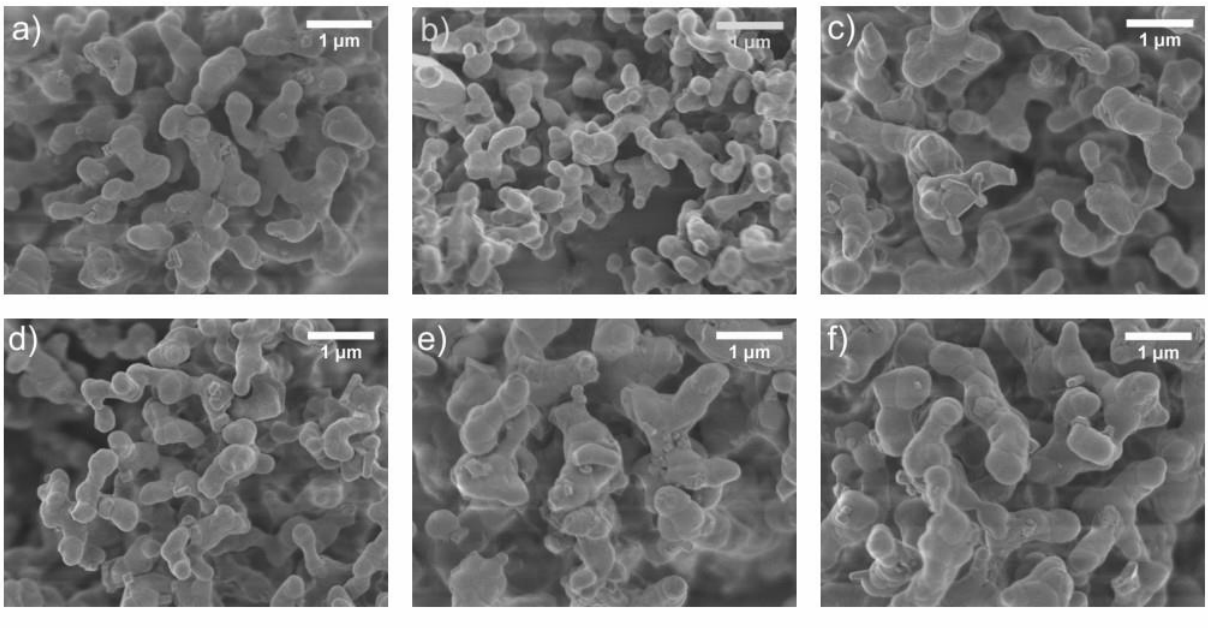

Fig. III-7. SEM images of Na_2WO_4-Ti-Mn/SiO_2 catalysts at different Mn loadings: a) 0 wt%, b) 0.5 wt%, c) 1.0 wt%, d)1.5 wt%, e) 2.0 wt%, and f) 2.5 wt%.

The optimal catalyst amount of each condition found in Fig. III-8 was selected to study the effect of reactor temperature at three different CH_4:O_2:N_2 feeding gas ratios, as shown in Fig. III-9. For every feeding gas ratio, the C_{2+} selectivities, CH_4 conversions, and C_{2+}yields increased with increase in reactor temperatures, reaching an optimal value at 700 °C. The highest C_{2+} yield was achieved at 19.61% with 60.40% C_{2+} selectivity and 32.48% CH_4 conversion when the CH_4:O_2:N_2 feeding gas ratio was 3:1:2. At reactor temperatures above 700 °C, the catalyst activity for C_{2+} formation rapidly dropped, while the CH_4 conversions slowly decreased. It is possible that the C_{2+} products quickly combust in the presence of O_2 or react further easily with active sites at high reactor temperatures. Similar to the results in Fig. III-8, the slow decreases of CH_4 conversion as reactor temperature rose were due to the additional CH_4 from the decomposition of C_{2+} [17, 28-31].

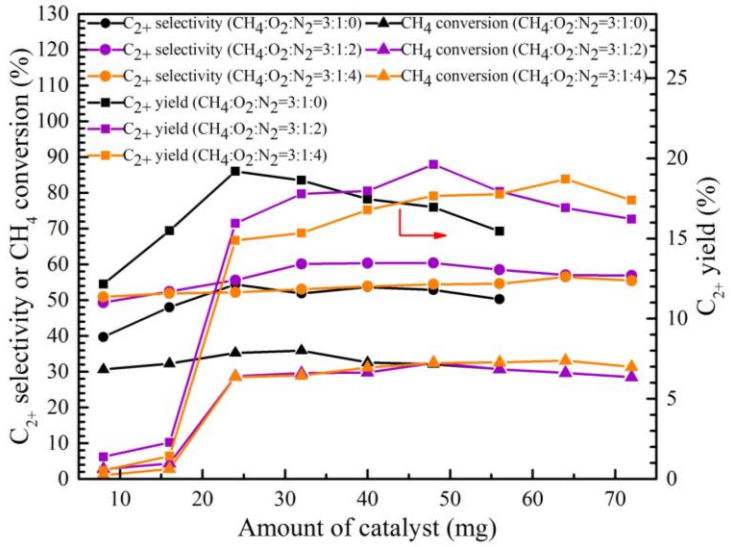

Fig. III-8. Activity of Na_2WO_4-Ti-Mn/SiO_2 catalyst at different catalyst amounts and different CH_4:O_2:N_2 feeding gas ratios.

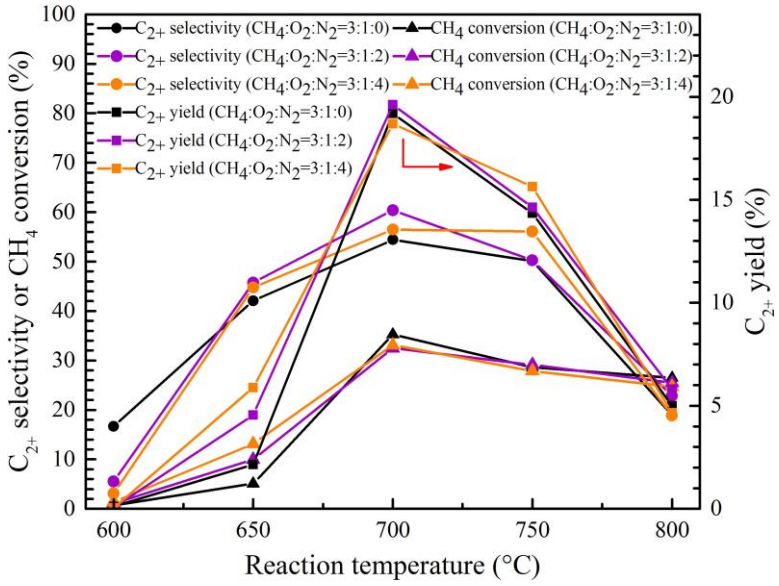

Fig. III-9. Activity of Na_2WO_4-Ti-Mn/SiO_2 catalyst at different reactor temperatures and different CH_4:O_2:N_2 feeding gas ratios. Reaction conditions: catalyst weight = 24, 48, and 64 mg for CH_4:O_2:N_2 = 3:1:0, 3:1:2, and 3:1:4, respectively, total feed flow rate = 35 mL/min.

In general, a fuel-rich condition (i.e. CH_4:O_2 ratio > 1.0) is more favorable for C_{2+} production in the OCM reaction. The complete combustion of CH_4 is strongly favorable under fuel-lean conditions. Therefore, the effect of CH_4:O_2 ratio on the activity of the optimal catalyst was studied, as shown in Fig. III-10. The CH_4:O_2 ratios were varied from 1.0 to 3.0, for which the conditions ranged from fuel-lean to fuel-rich. The results evidently showed that the C_{2+} yields slowly increased as the CH_4:O_2 ratios were lowered. In other words, O_2 increases into the feed resulted in increases of C_{2+} yields and CH_4 conversions. Nonetheless, the C_{2+} selectivities significantly decreased. The results suggest that O_2 increases into the feed enhance the formations of CO and CO_2 more than those of C_{2+} products [9, 26, 27].

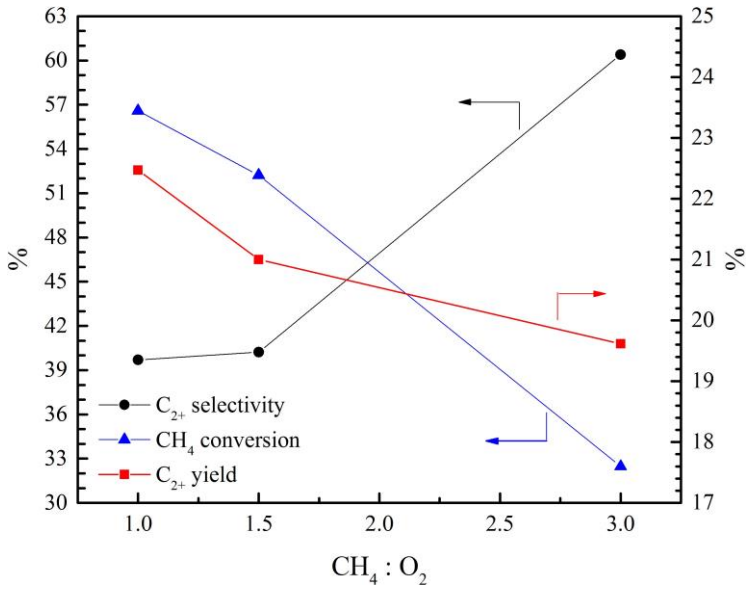

Fig. III-10. Effect of varying CH_4:O_2 ratio of Na_2WO_4-Ti-Mn/SiO_2 catalyst. Reaction conditions: (CH_4+O_2):N_2 ratio = 2:1, catalyst weight = 48 mg, total feed flow rate = 35 mL/min, reactor temperature = 700 °C.

The effect of total feed flow rate of the Na_2WO_4-Ti-Mn/SiO_2 catalyst for OCM reaction was also investigated as presented in Fig. III-11. In general, a short resident time inside a porous catalyst favors C_{2+} selectivity because it reduces chances of combustion of C_{2+} products. The results remarkably showed that the C_{2+} yields and selectivities were achieved at approximately 20–22% and 60–62%, respectively, while the CH_4 conversions were slightly changed at approximately 32–35% when the total feed flow rate was in the range of 45–75 mL/min. At above 75 mL/min, the activity of the catalyst slowly decreased, potentially because the residence time or the contact time between the reactants and the catalyst was greatly reduced.

Lastly, a time-on-stream experiment over 24 h of the Na_2WO_4-Ti-Mn/SiO_2 catalyst at the optimized operating conditions was conducted to monitor its catalyst stability. The plots are presented in Fig. III-12. It was found that the CH_4 conversions and the C_{2+} yields slightly decreased from the second to the last hour, while the C_{2+} selectivity remained virtually unchanged. The C_{2+} yield was reduced from 21 to 16% within 24 h of experiment. The catalyst used for 24 h was then observed to examine why the catalyst deactivated using SEM and XRD analyses, as shown in Fig. III-13. Apparently, the particle sizes of the used catalyst were much larger (about 50 times) than those of the fresh catalyst. This indicated that one possible cause of the gradual deactivation of the catalyst was the aggregation of the particles (i.e. catalyst sintering). Comparison of the XRD spectra of the fresh and used catalysts shows that the peaks of α-tridymite (2ϑ = 21.8, 23.3, 27.3, and 30.1 (ICDD No. 00-003-0227)) were clearer compared to those of the fresh catalyst, while the $NaWO_4$ peaks of the used catalyst were smaller relative to those of the fresh catalyst. The peaks of α-cristobalite and TiO_2, however, exhibited no substantial change. This might suggest that the crystallite size of α-tridymite could grow after many hours of testing. However, it has been reported that the change of α-cristobalite and α-tridymite does not substantially influence the activity of Na_2WO_4-MnO_x-containing catalysts for OCM reactions [32]. Thus, it is not only catalyst sintering that causes the gradual deactivation, but also the loss of Na_2WO_4.

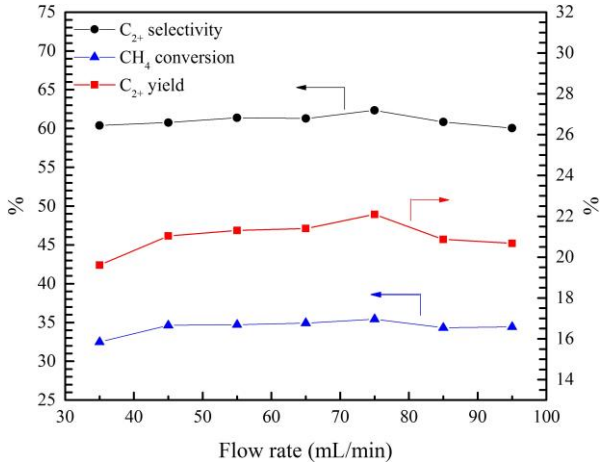

Fig. III-11. Effect of varying total feed flow rate on catalytic performance of Na_2WO_4-Ti-Mn/SiO_2. Reaction conditions: CH_4:O_2:N_2 ratio = 3:1:2, catalyst weight = 48 mg, reactor temperature = 700 °C.

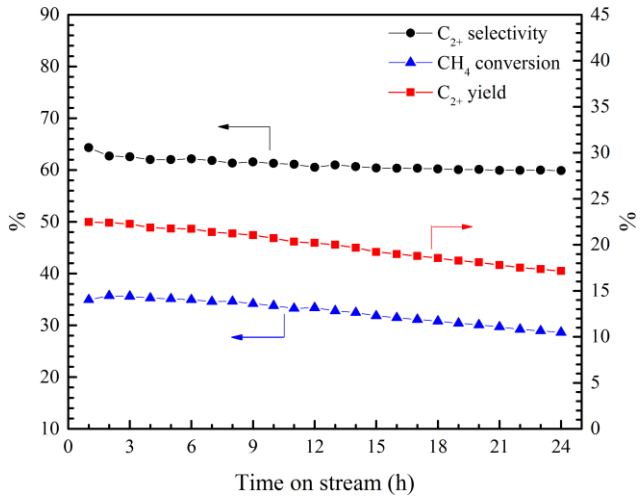

Fig. III-12. Catalyst performance of Na_2WO_4-Ti-Mn/SiO_2 of OCM reaction as a function of time on stream over 24 h. Reaction conditions: CH_4:O_2:N_2 ratio = 3:1:2, catalyst weight = 48 mg, total feed flow rate = 75 mL/min, reactor temperature = 700 °C.

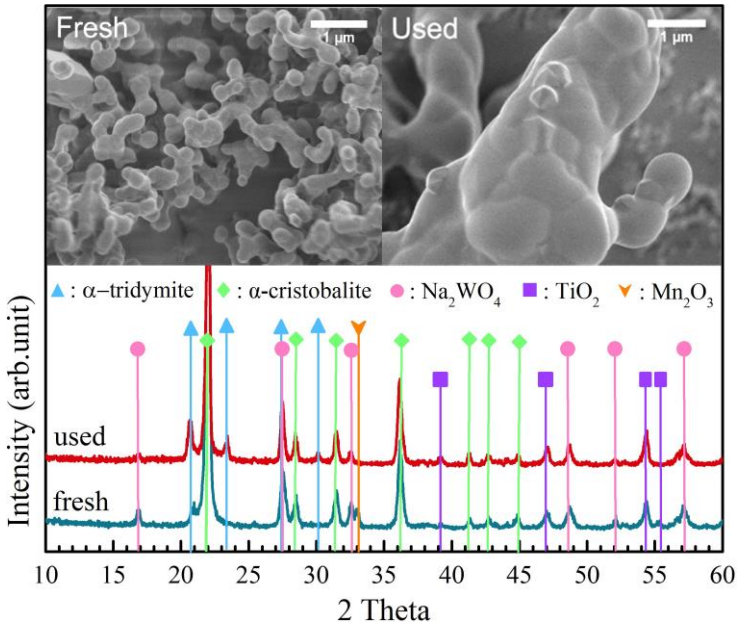

Fig. III-13. SEM images (top) and XRD spectra (bottom) of fresh and used Na_2WO_2-Ti-Mn/SiO_2 catalyst.

III-4. Conclusion

The purposes of this work were to study the effects of metal oxide additives on the performance of the TiO_2-Na_2WO_4/SiO_2 catalyst for the OCM reaction to value-added chemicals and to optimize the C_{2+} yield of the most promising catalyst. The plots between the CH_4 conversions and the binding energies of W $4f_{7/2}$ and Ti $2p_{3/2}$ of the prepared catalysts have revealed that the catalysts that exhibited lower binding energy values possessed high catalytic activity. This is because the bond strength between W or Ti with O becomes weaker, thereby promoting the OCM reaction. Moreover, the addition of Mn into the Na_2WO_4-Ti/SiO_2 catalyst was the most active catalyst. The crystalline phases of α-cristobalite, Na_2WO_4, and Mn_2O_3 were present in the most promising catalyst. In the attempts to optimize the C_{2+} yield by varying operating conditions, the maximum C_{2+} yield of the Na_2WO_4-Ti/SiO_2 catalyst added 0.5 wt% Mn was achieved at 22.09% with 62.3% C_{2+} selectivity and 35.43% CH_4 conversion. The optimal conditions were a reaction temperature of 700 °C, a CH_4:O_2:N_2 feeding gas ratio of 3:1:2, a total feed flow rate of 75 mL/min, and 48 mg of the catalyst. The stability of the catalyst was also investigated, concluding that the catalyst gradually deactivated with time on stream because of catalyst sintering and the loss of Na_2WO_4 content. How to prevent catalyst deactivation and improve the C_{2+} selectivity of the Na_2WO_4-Ti-Mn/SiO_2 catalyst will be of great interest to further studies.

Acknowledgements

This work was financially supported by the Faculty of Engineering at Kasetsart University, Bangkok, Thailand; the Kasetsart University Research and Development Institute (KURDI); the Center of Excellence on Petrochemical and Materials Technology, the National Nanotechnology Center (NANOTEC), NSTDA, Ministry of Science and Technology, Thai- land, through its program of Research Network NANOTEC (RNN); the Thailand Research Fund and the Commission on Higher Education (grant #MRG6180232).

References for Part III.

[1] C.D. Ruppel, J.D. Kessler, Rev. Geophys. 55 (2017) 126-168.

[2] G.J. Hutchings, M.S. Scurrell, J.R. Woodhouse, Chem. Soc. Rev. 18 (1989) 251-283.

[3] M.Y. Sinev, Z.T. Fattakhova, V.I. Lomonosov, Y.A. Gordienko, J. Nat. Gas Chem. 18 (2009) 273-287.

[4] M. Yildiz, Y. Aksu, U. Simon, T. Otremba, K. Kailasam, C. Göbel, F. Girgsdies, O. Görke, F. Rosowski, A. Thomas, R. Schomäcker, S. Arndt, Appl. Catal., A. 525 (2016) 168-179.

[5] H.R. Godini, A. Gili, O. Görke, S. Arndt, U. Simon, A. Thomas, R. Schomäcker, G. Wozny, Catal. Today 236 (2014) 12-22.

[6] K. Khammona, S. Assabumrungrat, W. Wiyarath, J. Eng. Appl. Sci. 7 (2012) 447-455.

[7] S. Ji, T. Xiao, S. Li, L. Chou, B. Zhang, C. Xu, R. Hou, A.P.E. York, M.L.H. Green, J. Catal. 220 (2003) 47-56.

[8] J.Y. Lee, W. Jeon, J.W. Choi, Y.W. Suh, J.M. Ha, D.J. Suh, Y.K. Park, Fuel 106 (2013) 851-857.
[9] S.M.K. Shahri, A.N. Pour, J. Nat. Gas Chem. 19 (2010) 47-53.
[10] P. Wang, X. Zhang, G. Zhao, Y. Liu, Y. Lu, Chinese J. Catal. 39 (2018) 1395-1402.
[11] P. Wang, G. Zhao, Y. Liu, Y. Lu, Appl. Catal., A. 544 (2017) 77-83.
[12] F. Papa, D. Gingasu, L. Patron, A. Miyazaki, I. Balint, Appl. Catal., A. 375 (2010) 172-178.
[13] V.H. Rane, S.T. Chaudhari, V.R. Choudhary, J. Nat. Gas Chem. 19 (2010) 25-30.
[14] N. Hiyoshi, T. Ikeda, Fuel Process. Technol. 133 (2015) 29-34.
[15] A. Seubsai, P. Tiencharoenwong, P. Kidamorn, C. Niamnuy, Eng. J. 23 (2019) 169-182.
[16] W. Kumsung, M. Chareonpanich, P. Kongkachuichay, S. Senkan, A. Seubsai, Catal. Commun. 110 (2018) 83-87.
[17] W.C. Liu, W.T. Ralston, G. Melaet, G.A. Somorjai, Appl. Catal., A. 545 (2017) 17-23.
[18] S. Gu, H.S. Oh, J.W. Choi, D.J. Suh, J. Jae, J. Choi, J.M. Ha, Appl. Catal., A. 562 (2018) 114-119.
[19] T.W. Elkins, H.E. Hagelin-Weaver, Appl. Catal., A. 497 (2015) 96-106.
[20] A. Malekzadeh, M. Abedini, A.A. Khodadadi, M. Amini, H.K. Mishra, A.K. Dalai, Catal. Lett. 84 (2002) 45-51.
[21] S.C. Oh, Y. Lei, H. Chen, D. Liu, Fuel 191 (2017) 472-485.
[22] V. Fleischer, R. Steuer, S. Parishan, R. Schomäcker, J. Catal. 341 (2016) 91-103.
[23] V. Fleischer, P. Littlewood, S. Parishan, R. Schomäcker, Chem. Eng. J. 306 (2016) 646-654.
[24] Y. Gambo, A.A. Jalil, S. Triwahyono, A.A. Abdulrasheed, J. Ind. Eng. Chem. 59 (2018) 218-229.
[25] A. Aseem, G.G. Jeba, M.T. Conato, J.D. Rimer, M.P. Harold, Chem. Eng. J. 331 (2018) 132-143.
[26] M. Ghiasi, A. Malekzadeh, S. Hoseini, Y. Mortazavi, A. Khodadadi, A. Talebizadeh, J. Nat. Gas Chem. 20 (2011) 428-434.
[27] C. Karakaya, H. Zhu, C. Loebick, J.G. Weissman, R.J. Kee, Catal. Today 312 (2018) 10-22.
[28] M. Taghizadeh, F. Raouf, Inorg. Nano-Met. Chem. 47 (2017) 1449-1456.
[29] Z. Gao, J. Zhang, R. Wang, J. Nat. Gas Chem. 17 (2008) 238-241.
[30] A. Galadima, O. Muraza, J. Ind. Eng. Chem. 37 (2016) 1-13.
[31] G. Pantaleo, V.L. Parola, F. Deganello, R.K. Singha, R. Bal, A.M. Venezia, Appl. Catal. B Environ. 189 (2016) 233-241.
[32] J. Wang, L. Chou, B. Zhang, H. Song, J. Zhao, J. Yang, S. Li, J. Mol. Catal. A Chem. 245 (2006) 272-277.

[1] D. Kahlich, U. Wiechern and J. Lindner, Propylene Oxide, Ullmann's Encyclopedia of Industrial Chemistry, John Wiley & Sons, Inc., 2000, p. 1.

[2] S.T. Oyama, Mechanisms in homogeneous and heterogeneous epoxidation catalysis, 1st ed., Elsevier, Amsterdam ; Boston, 2008.

[3] F. Cavani and J.H. Teles, ChemSusChem, 2 (2009) 508.

[4] T.A. Nijhuis, M. Makkee, J.A. Moulijn and B.M. Weckhuysen, Industrial & Engineering Chemistry Research, 45 (2006) 3447.

[5] D.L. Trent, Propylene Oxide, Kirk-Othmer Encyclopedia of Chemical Technology, Vol. 20, Wiley, New York, 2001.

[6] R.A. Vansanten and C.P.M. Degroot, Journal of Catalysis, 98 (1986) 530.

[7] T. Hayashi, K. Tanaka and M. Haruta, Journal of Catalysis, 178 (1998) 566.

[8] K. Murata and Y. Kiyozumi, Chemical Communications, (2001) 1356.

[9] T.A. Nijhuis, S. Musch, M. Makkee and J.A. Moulijn, Applied Catalysis A: General, 196 (2000) 217.

[10] W.M. Zhu, Q.H. Zhang and Y. Wang, Journal of Physical Chemistry C, 112 (2008) 7731.

[11] O.P.H. Vaughan, G. Kyriakou, N. Macleod, M. Tikhov and R.M. Lambert, Journal of Catalysis, 236 (2005) 401.

[12] H. Chu, L. Yang, Q.H. Zhang and Y. Wang, Journal of Catalysis, 241 (2006) 225.

[13] Y. Wang, H. Chu, W.M. Zhu and Q.H. Zhang, Catalysis Today, 131 (2008) 496.

[14] Z. Song, N. Mimura, J.J. Bravo-Suárez, T. Akita, S. Tsubota and S.T. Oyama, Applied Catalysis A: General, 316 (2007) 142.

[15] M. Haruta, J.H. Huang, T. Akita, J. Faye, T. Fujitani and T. Takei, Angew Chem Int Edit, 48 (2009) 7862.

[16] T. Hayasi, L.B. Han, S. Tsubota and M. Haruta, Industrial & Engineering Chemistry Research, 34 (1995) 2298.

[17] B.S. Uphade, M. Okumura, S. Tsubota and M. Haruta, Applied Catalysis a-General, 190 (2000) 43.

[18] A.K. Sinha, S. Seelan, S. Tsubota and M. Haruta, Angew Chem Int Ed Engl, 43 (2004) 1546.

[19] H. Oresek, R.P. Schulz, U. Dingerdissen and W.F. Maier, Chemical Engineering & Technology, 22 (1999) 691.

[20] M. Date, Y. Ichihashi, T. Yamashita, A. Chiorino, F. Boccuzzi and M. Haruta, Catalysis Today, 72 (2002) 89.

[21] A. Seubsai, M. Kahn and S. Senkan, Chemcatchem, 3 (2011) 174.

[22] A. Seubsai and S. Senkan, Chemcatchem, 3 (2011) 1751.

[23] A. Miller, B. Zohour, A. Seubsai, D. Noon and S. Senkan, Industrial & Engineering Chemistry Research, 52 (2013) 9551.

[24] A. Seubsai, M. Kahn, B. Zohour, D. Noon, M. Charoenpanich and S. Senkan, Industrial & Engineering Chemistry Research, 54 (2015) 2638.

[25] A. Seubsai, D. Noon, T. Chukeaw, B. Zohour, W. Donphai, M. Chareonpanich and S. Senkan, Journal of Industrial and Engineering Chemistry, 32 (2015) 292.

[26] J.L. He, Q.G. Zhai, Q.H. Zhang, W.P. Deng and Y. Wang, Journal of Catalysis, 299 (2013) 53.

[27] X. Yang, S. Kattel, K. Xiong, K. Mudiyanselage, S. Rykov, S.D. Senanayake, J.A. Rodriguez, P. Liu, D.J. Stacchiola and J.G. Chen, Angew Chem Int Ed Engl, 54 (2015) 11946.

[28] J.L. He, Q.G. Zhai, Q.H. Zhang, W.P. Deng and Y. Wang, Journal of Catalysis, 299 (2013) 53.

[29] A. Seubsai, B. Zohour, D. Noon and S. Senkan, Chemcatchem, 6 (2014) 1215.

[30] K. Zhang, C.H. Chew, G.Q. Xu, J. Wang and L.M. Gan, Langmuir, 15 (1999) 3056.

[31] K. Min, L. Tong Tao, C. Hao, Z. Sheng Mao, Z. Li Li and Z. Yu Xin, Nanotechnology, 26 (2015) 304002.

[32] S.-J. Yang and C.W. Bates, Applied Physics Letters, 36 (1980) 675.

[33] R. Sanjines, H. Tang, H. Berger, F. Gozzo, G. Margaritondo and F. Levy, Journal of Applied Physics, 75 (1994) 2945.

[34] R.M. Lambert, F.J. Williams, R.L. Cropley and A. Palermo, Journal of Molecular Catalysis a-Chemical, 228 (2005) 27.

[35] Y.J. Lei, X.H. Chen, C.Z. Xu, Z.C. Dai and K.M. Wei, Journal of Catalysis, 321 (2015) 100.

[36] W. Yao, G. Lu, Y. Guo, Y. Guo, Y. Wang and Z. Zhang, Journal of Molecular Catalysis A: Chemical, 276 (2007) 162.

[37] G. Jin, G. Lu, Y. Guo, Y. Guo, J. Wang, W. Kong and X. Liu, Journal of Molecular Catalysis A: Chemical, 232 (2005) 165.

[38] S. Kalyoncu, D. Duzenli, I. Onal, A. Seubsai, D. Noon, S. Senkan, Z. Say, E. Vovk and E. Ozensoy, Catalysis Letters, 145 (2015) 596.

[39] D. Torres, N. Lopez, F. Illas and R.M. Lambert, Angew Chem Int Ed Engl, 46 (2007) 2055.

[40] Z.L. Wang, Q.S. Liu, J.F. Yu, T.H. Wu and G.J. Wang, Applied Catalysis a-General, 239 (2003) 87.

[41] S. Galvagno, C. Crisafulli, R. Maggiore, G.R. Tauszik and A. Giannetto, J Therm Anal, 30 (1985) 611.

[42] S. Anniballi, F. Cavani, A. Guerrini, B. Panzacchi, F. Trifirò, C. Fumagalli, R. Leanza and G. Mazzoni, Catalysis Today, 78 (2003) 117.

[43] Y. Xiaojiang, Y. Fumo and D. Lin, Advances in Energy Equipment Science and Engineering, CRC Press, 2015, p. 501.

[44] E. Sheerin, G.K. Reddy and P. Smirniotis, Catalysis Today, 263 (2016) 75.

[45] S.L.C. Ferreira, R.E. Bruns, H.S. Ferreira, G.D. Matos, J.M. David, G.C. Brandão, E.G.P. da Silva, L.A. Portugal, P.S. dos Reis, A.S. Souza and W.N.L. dos Santos, Analytica Chimica Acta, 597 (2007) 179.

[46] W.G. Su, S.G. Wang, P.L. Ying, Z.C. Feng and C. Li, Journal of Catalysis, 268 (2009) 165.
[47] D. Duzenli, E. Seker, S. Senkan and I. Onal, Catalysis Letters, 142 (2012) 1234.
[48] Q. Hua, T. Cao, X.-K. Gu, J. Lu, Z. Jiang, X. Pan, L. Luo, W.-X. Li and W. Huang, Angewandte Chemie International Edition, 53 (2014) 4856.
[49] Y. Lei, X. Chen, C. Xu, Z. Dai and K. Wei, Journal of Catalysis, 321 (2015) 100.
[50] L. Cumaranatunge and W.N. Delgass, Journal of Catalysis, 232 (2005) 38.
[51] B. Taylor, J. Lauterbach and W.N. Delgass, Applied Catalysis A: General, 291 (2005) 188.
[52] B. Chowdhitry, J.J. Bravo-Suarez, M. Date, S. Tsubota and M. Haruta, Angewandte Chemie-International Edition, 45 (2006) 412.
[53] B. Taylor, J. Lauterbach and W.N. Delgass, Catalysis Today, 123 (2007) 50.
[54] J. Lu, X. Zhang, J.J. Bravo-Suárez, K.K. Bando, T. Fujitani and S.T. Oyama, Journal of Catalysis, 250 (2007) 350.
[55] S.T. Oyama, X. Zhang, J. Lu, Y. Gu and T. Fujitani, Journal of Catalysis, 257 (2008) 1.
[56] J.Q. Lu, X.M. Zhang, J.J. Bravo-Suarez, T. Fujitani and S.T. Oyama, Catalysis Today, 147 (2009) 186.
[57] T. Liu, P. Hacarlioglu, S.T. Oyama, M.-F. Luo, X.-R. Pan and J.-Q. Lu, Journal of Catalysis, 267 (2009) 202.
[58] J.H. Huang, T. Takei, T. Akita, H. Ohashi and M. Haruta, Applied Catalysis B-Environmental, 95 (2010) 430.
[59] LIU Yi-Wu, YU Huan, ZHANG Xiao-Ming and S. Ji-Shuan, Acta Physico-Chimica Sinica, 26 (2010) 1585.
[60] L.J. Yang, J.L. He, Q.H. Zhang and Y. Wang, Journal of Catalysis, 276 (2010) 76.
[61] C.-H. Liu, Y. Guan, E.J.M. Hensen, J.-F. Lee and C.-M. Yang, Journal of Catalysis, 282 (2011) 94.
[62] M. Du, G. Zhan, X. Yang, H. Wang, W. Lin, Y. Zhou, J. Zhu, L. Lin, J. Huang, D. Sun, L. Jia and Q. Li, Journal of Catalysis, 283 (2011) 192.
[63] J. Huang, E. Lima, T. Akita, A. Guzmán, C. Qi, T. Takei and M. Haruta, Journal of Catalysis, 278 (2011) 8.
[64] J. Gaudet, K.K. Bando, Z. Song, T. Fujitani, W. Zhang, D.S. Su and S.T. Oyama, Journal of Catalysis, 280 (2011) 40.
[65] G. Zhan, M. Du, J. Huang and Q. Li, Catalysis Communications, 12 (2011) 830.
[66] W.S. Lee, M.C. Akatay, E.A. Stach, F.H. Ribeiro and W.N. Delgass, Journal of Catalysis, 287 (2012) 178.
[67] J.-Q. Lu, N. Li, X.-R. Pan, C. Zhang and M.-F. Luo, Catalysis Communications, 28 (2012) 179.
[68] J.Q. Chen, S.J.A. Halin, E.A. Pidko, M.W.G.M. Verhoeven, D.M. Perez Ferrandez, E.J.M. Hensen, J.C. Schouten and T.A. Nijhuis, Chemcatchem, 5 (2013) 467.
[69] W.-S. Lee, M. Cem Akatay, E.A. Stach, F.H. Ribeiro and W. Nicholas Delgass, Journal of Catalysis, 308 (2013) 98.
[70] Y. Liu, X. Zhang and J. Suo, Chinese Journal of Catalysis, 34 (2013) 336.

[71] X. Feng, X. Duan, G. Qian, X. Zhou, D. Chen and W. Yuan, Applied Catalysis B: Environmental, 150–151 (2014) 396.

[72] W.-S. Lee, M. Cem Akatay, E.A. Stach, F.H. Ribeiro and W. Nicholas Delgass, Journal of Catalysis, 313 (2014) 104.

[73] X. Feng, X. Duan, J. Yang, G. Qian, X. Zhou, D. Chen and W. Yuan, Chemical Engineering Journal, 278 (2015) 234.

[74] M. Du, J. Huang, D. Sun and Q. Li, Applied Surface Science, 366 (2016) 292.

[75] F. Jin, Y. Wu, S. Liu, T.-H. Lin, J.-F. Lee and S. Cheng, Catalysis Today, 264 (2016) 98.

[76] V.-H. Nguyen, H.-Y. Chan, J.C.S. Wu and H. Bai, Chemical Engineering Journal, 179 (2012) 285.

[77] V.-H. NGUYEN, H.-Y. CHAN and J.C.S. WU, Journal of Chemical Sciences, 125 (2013) 859.

[78] V.-H. Nguyen, S.D. Lin, J.C.S. Wu and H. Bai, Catalysis Today, 245 (2015) 186.

[79] V.-H. Nguyen, S.D. Lin and J.C.-S. Wu, Journal of Catalysis, 331 (2015) 217.

[80] M. Kahn, A. Seubsai, I. Onal and S. Senkan, Topics in Catalysis, 53 (2010) 86.

[81] S. Kalyoncu, D. Duzenli, I. Onal, A. Seubsai, D. Noon and S. Senkan, Catalysis Communications, 61 (2015) 16.

[82] J.F. Moulder and J. Chastain, Handbook of X-ray Photoelectron Spectroscopy: A Reference Book of Standard Spectra for Identification and Interpretation of XPS Data, Physical Electronics, 1995.

[83] P. Phon-In, A. Seubsai, T. Chukeaw, K. Charoen, W. Donphai, P. Prapainainar, M. Chareonpanich, D. Noon, B. Zohour and S. Senkan, Catalysis Communications, 86 (2016) 143.

[84] S.L. Ferreira, R.E. Bruns, H.S. Ferreira, G.D. Matos, J.M. David, G.C. Brandao, E.G. da Silva, L.A. Portugal, P.S. dos Reis, A.S. Souza and W.N. dos Santos, Anal Chim Acta, 597 (2007) 179.

[85] S.J. Khatib and S.T. Oyama, Catalysis Reviews-Science and Engineering, 57 (2015) 306.

[86] K.H. Choi, D.H. Lee, H.S. Kim, Y.C. Yoon, C.S. Park and Y.H. Kim, Industrial & Engineering Chemistry Research, 55 (2016) 4443.

[87] J.Q. Lu, M.F. Luo, H. Lei and C. Li, Applied Catalysis a-General, 237 (2002) 11.

[88] T. Chukeaw, A. Seubsai, P. Phon-in, K. Charoen, T. Witoon, W. Donphai, P. Parpainainar, M. Chareonpanich, D. Noon, B. Zohour and S. Senkan, Rsc Advances, 6 (2016) 56116.

[89] J.Q. Lu, J.J. Bravo-Suarez, M. Haruta and S.T. Oyama, Applied Catalysis a-General, 302 (2006) 283.

[90] D. Sullivan, P. Hooks, M. Mier, J.W. van Hal and X.K. Zhang, Topics in Catalysis, 38 (2006) 303.

[91] J. Huang, T. Akita, J. Faye, T. Fujitani, T. Takei and M. Haruta, Angew Chem Int Ed Engl, 48 (2009) 7862.

[92] J. Chen, S.J.A. Halin, E.A. Pidko, M.W.G.M. Verhoeven, D.M.P. Ferrandez, E.J.M. Hensen, J.C. Schouten and T.A. Nijhuis, ChemCatChem, 5 (2013) 467.

[93] A. Seubsai, P. Phon-in, T. Chukeaw, C. Uppala, P. Prapainainar, M. Chareonpanich, B. Zohour, D. Noon and S. Senkan, Industrial & Engineering Chemistry Research, 56 (2017) 100.

[94] W.J. Long, Q.G. Zhai, J.L. He, Q.H. Zhang, W.P. Deng and Y. Wang, Chempluschem, 77 (2012) 27.

Outputs (Acknowledge the Thailand Research Fund)

- International Journal Publication

1) Chukeaw, T. Sringam, S., Chareonpanich, M., **Seubsai, A.*** “Screening of single and binary catalysts for oxidative coupling of methane to value-added chemicals” *Molecular Catalysis* 2019, 470: 40–47.
2) **Seubsai, A.**, Tiencharoenwong, P., Kidamorn, P., Niamnuy, C.* “Synthesis of light hydrocarbons via oxidative coupling of methane over silica-supported Na_2WO_4-TiO_2 catalyst” *Engineering Journal* 2019, 23 (5): 169–182.
3) Sringam, S., Kidamorn, P., Chukeaw, T., Chareonpanich, M., **Seubsai, A.*** “Investigation of metal oxide additives onto Na_2WO_4-Ti/SiO_2 catalysts for oxidative coupling of methane to value-added chemicals” *Catalysis Today* 2020, In press.

- Application

-

- Others e.g. national journal publication, proceeding, international conference, book chapter, patent

-

Appendices

1) Chukeaw, T. Sringam, S., Chareonpanich, M., **Seubsai, A.*** “Screening of single and binary catalysts for oxidative coupling of methane to value-added chemicals” *Molecular Catalysis* 2019, 470: 40–47.

2) **Seubsai, A.**, Tiencharoenwong, P., Kidamorn, P., Niamnuy, C.* “Synthesis of light hydrocarbons via oxidative coupling of methane over silica-supported Na_2WO_4-TiO_2 catalyst” *Engineering Journal* 2019, 23 (5): 169–182.

3) Sringam, S., Kidamorn, P., Chukeaw, T., Chareonpanich, M., **Seubsai, A.*** “Investigation of metal oxide additives onto Na_2WO_4-Ti/SiO_2 catalysts for oxidative coupling of methane to value-added chemicals” *Catalysis Today* 2020, In press.

Molecular Catalysis 470 (2019) 40–47

Contents lists available at ScienceDirect

Molecular Catalysis

journal homepage: www.elsevier.com/locate/mcat

Screening of single and binary catalysts for oxidative coupling of methane to value-added chemicals

Thanaphat Chukeaw[a,b], Sarannuch Sringam[a], Metta Chareonpanich[a,b,c], Anusorn Seubsai[a,b,c,*]

[a] Department of Chemical Engineering, Faculty of Engineering, Kasetsart University, Bangkok 10900, Thailand
[b] Center of Excellence on Petrochemical and Materials Technology, Kasetsart University, Bangkok 10900, Thailand
[c] Research Network of NANOTEC–KU on NanoCatalysts and NanoMaterials for Sustainable Energy and Environment, Kasetsart University, Bangkok 10900, Thailand

ARTICLE INFO

Keywords:
Catalyst screening
Light hydrocarbons
Metal oxide catalyst
Oxidative coupling of methane
Silica support

ABSTRACT

A combinatorial approach was applied to explore active binary catalysts for oxidative coupling of methane (OCM) to value-added hydrocarbons (C_{2+}). A screening of 25 selected single components on SiO_2 for OCM reaction identified the top-14 single active components as follows: La > Ce > Ga > Al > Ca > Cr > Ba > Na_2WO_4 > Mn > Cu > Ti > Zn > Rb > Ni. Binary catalyst screening was then performed and resulted in a combination of Na_2WO_4 and Mn producing the most active binary catalyst. X-ray powder diffraction measurement of the Na_2WO_4-Mn/SiO_2 catalyst revealed that the presence of α-cristobalite phase was essential for the activation of methane. Moreover, the X-ray photoelectron spectroscopy spectrum of the Na_2WO_4-Mn/SiO_2 catalyst showed that the binding energy of W4f and Mn 2p shifted toward a lower binding energy, thereby enhancing the catalytic activity. Optimization of C_{2+} production of the catalyst by varying Na_2WO_4:Mn weight ratios, total metal loadings, catalyst weights, and feeding gas compositions, achieved maximum C_{2+} yield of 23.54% with 60.5% selectivity and 39.67% methane conversion. Furthermore, the activity of the Na_2WO_4-Mn/SiO_2 catalyst was monitored with time-on-steam for 50 h, revealing good catalyst stability.

1. Introduction

Methane (CH_4) is the primary constituent of natural gas and biogas. Since it is abundant in natural resources, it is of great interest for conversion of CH_4 into value-added chemicals (C_{2+}) such as ethylene and ethane. Oxidative coupling of methane (OCM) using solid catalysts is one of the most attractive chemical reactions to directly convert CH_4 into value-added hydrocarbons. This catalytic reaction has been of interest to industrial and academic researchers since the 1980s. In a condition where O_2 is present without a catalyst being used, CH_4 can be directly oxidized at high temperatures (> 700 °C), known as direct gas-phase oxidation of CH_4. The input energy can break the C—H bonds of CH_4 into a methyl radical, which can further react with another methyl radical to form ethane. Additionally, ethylene, other C_{2+}, and CO_x can form under such uncontrollable pathways [1–3]. Therefore, selective solid catalysts have been researched for use in the OCM reaction.

In the past several years, many solid catalysts have been investigated for this transformation. Potential catalysts have been reported including Mn modified with various types of supports and co-catalysts [4–9], such as oxides of Mg [10,11], Na [12,13], Li [14,15], and Na_2WO_4 [16,17]. The C_{2+} yields and C_{2+}selectivities were approximately < 16.0% and 25.3–60.5%, respectively. Binary catalysts of Na_2WO_4-Mn have been widely investigated because this metal combination is highly active for OCM [18–24], providing 2.1–26.4% C_{2+} yields and 42.8–80.0% C_{2+} selectivities. Other metal oxide catalysts and mixed metal oxides have also been found active for OCM including $LaXO_3$ [25–27], Ag/$SrFeO_3$ [28], Metal or PtSn/SiO_2 [29–32], Metal–Mg [33–36], and La_2O_3/CaO [37–39]. However, a viable catalyst that meets the industrial requirements (i.e. C_{2+} selectivity plus C_{2+} yield > 110) has yet to be found. Therefore, the search for new catalysts for OCM reaction is still continuing.

For the rapid search of new active catalysts from large numbers of experiments to test via reactions, combinatorial synthesis and screening can be applied effectively [40]. Here, we present a successful attempt to rapidly search for binary catalysts for OCM by applying the combinatorial approach. First, a number of elements/components were selected from active ones that have been reported in the literature as well as taking onto account their availability. A screening test was then quickly made to attain active single components. Subsequently, a binary screening was carried out, which delivered a highly active binary

* Corresponding author at: Department of Chemical Engineering, Faculty of Engineering, Kasetsart University, Bangkok 10900, Thailand.
E-mail address: fengasn@ku.ac.th (A. Seubsai).

https://doi.org/10.1016/j.mcat.2019.03.021
Received 28 December 2018; Received in revised form 15 March 2019; Accepted 18 March 2019

catalyst. The catalyst discovered was then carefully investigated to achieve the optimal C_{2+} yield at a certain reactor temperature, and also intensively characterized to understand why it was highly active in the OCM reaction.

2. Experimental

2.1. Catalyst preparation

All catalysts were prepared using impregnation. In total, 25 single component catalysts and 91 binary catalysts were prepared on SiO_2 (amorphous fumed silica powder, surface area of 85-115 m^2/g, Alfa Aesar) at 5 and 10 wt%, respectively. The binary catalysts used a metal weight ratio of 1:1. Briefly, each metal precursor (see Table S1) was dissolved in DI water. Then, each metal ion solution was determined and pipetted into the SiO_2 support to achieve the desired weight percentages and metal weight ratio. The mixture was stirred at room temperature for 2 h, then heated to 115 °C and stirred until dried. The obtained powder was calcined at 800 °C for 4 h in an air furnace at a heating rate of 5 °C/min. After the calcination, a fine powder was obtained.

2.2. Catalyst activity test

Catalytic activity for OCM reaction of each catalyst was examined in a traditional packed bed reactor at atmospheric pressure and in a reactor temperature of 700 °C. Each prepared catalyst (2–200 mg) was packed in a quartz tube (0.5 cm in inner diameter) and sandwiched between two quartz wools. The feed gases were CH_4 (Praxair, 99.995%), O_2 (Praxair, 99.95%), and N_2 (Praxair, 99.999%) at a volume ratio of CH_4:O_2:N_2 = 3:1:0 or 3:1:4 at a total flow rate of 35 mL/min (GHSV = 210,000–2000 h^{-1}) controlled by mass flow controllers (Aalborg GFC17). The effluent gas was analyzed by gas chromatography (SHIMADZU, GC-14A) equipped with a thermal conductivity detector (TCD, for detecting CO, CO_2, and CH_4) and a flame ionization detector (FID, for detecting C_{2+} products, i.e. C_2H_4, C_2H_6, C_3H_6, C_3H_8, C_4H_8, and C_4H_{10}). The activity of the catalyst was evaluated after the system had reached the set point for 2 h. The %CH_4 conversion, %C_{2+} selectivity, %CO_x selectivity, and %C_{2+} yield were calculated using Eqs. (1)–(4).

$$\%\,CH_4\ \text{conversion} = \frac{\text{moles of } CH_4\text{in-moles of } CH_4\text{out}}{\text{moles of } CH_4\text{ in}} \times 100 \quad (1)$$

$$\%\,C_{2+}\ \text{selectivity} = \frac{\text{moles of } C_{2+}}{\text{Total moles of products}} \times 100 \quad (2)$$

$$\%\,CO_x\ \text{selectivity} = \frac{\text{moles of } CO_x}{\text{Total moles of products}} \times 100 \quad (3)$$

$$\%\,C_{2+}\ \text{yield} = \frac{\%\,CH_4\text{conversion} \times \%\,C_{2+}\text{selectivity}}{100} \quad (4)$$

2.3. Catalyst characterization

The XRD patterns of the samples were conducted using X-ray powder diffraction (X-Ray Diffractometer, XRD: Philips: X'Pert, using Cu-Kα radiation, 40 kV and 30 mA, 0.02° step size, 0.5 s step time). The surface morphology of the catalysts was imaged using a scanning electron microscope with an energy dispersive X-ray spectrometer (FE-SEM/EDS, FE-SEM: JEOL JSM7600 F). The surface area, pore volume, and pore size of the catalysts were analyzed using N_2-physisorption (BET: 3Flex Physisorption Micromeritics). The electronic states of silicon (Si 2p), tungsten (W 4f), manganese (Mn 2p), and sodium (Na 1 s) for the catalysts were characterized using X-ray photoelectron spectrometry (XPS, Kratos Axis Ultra DLD, using Al K_α for the X-ray source). Coke formation of fresh used catalysts was also analyzed using thermogravimetric analysis-derivative thermogravimetry (TGA-DTG, Perkin Elmer Pyris 1 TGA). A sample of 10 mg was loaded into an alumina crucible. Each sample was initialized by introducing air (zero gas, Lab grade purity, Thai Standard Gas Co., Ltd (TSG)) gas at a feed flow rate of 100 mL/min. The system was then heated from room temperature to 1000 °C with a heating rate of 10 °C/min.

3. Results and discussion

The catalytic activity for OCM reaction of each single component catalyst compared with a blank test (without a catalyst used) is presented in Fig. 1 (also see Table S2 & Fig. S1–S3). It should be noted that some elements/components were not chosen for the screening test because they are expensive (Ru, Rh, Pd, Ir, Pt, and Au), unstable at high temperatures (Ag), toxic, or unavailable. In addition, the elements that generally yielded a high CH_4 combustion to CO_x (Ru, Rh, Pd, Ir, and Pt [41]) were not of interest. Moreover, it is important to note that the C_{2+} yield was the criterion used to identify a superior catalyst when comparing the activities of catalysts.

From Fig. 1, La/SiO_2 had the highest C_{2+} yield at 5.56% with 52.8% C_{2+} selectivity and 10.53% CH_4 conversion under the test conditions. Surprisingly, the catalytic performance of the blank test conducted under the same test conditions was relatively high compared to these catalysts, giving 3.72% yield, 38.6% C_{2+} selectivity and 9.64% CH_4 conversion. This indicated that the gas phase reaction for the OCM reaction could take place at this reactor temperature (700 °C) [1,8,42]. The top-14 active catalysts that with a C_{2+} yield higher than that of the blank test were (in order), giving 5.56–3.83% C_{2+} yields. The other single component catalysts had a C_{2+} yield lower than that of the blank test, suggesting that those single components are inactive for the OCM reaction.

The search of binary catalysts (combinations of two main active components that exhibit a synergistic catalyst effect for the OCM reaction) was the primary purpose of this work. A number of active components must be chosen for binary screening. Practically, all of the components could be chosen for the binary catalyst screening test. However, it is believed that a combination of a relatively high active component mixed with another high active component is more likely to

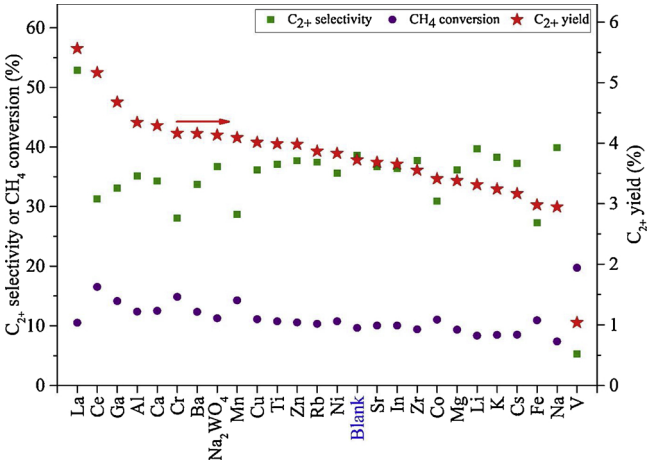

Fig. 1. C_{2+} selectivity, CH_4 conversion, and C_{2+} yield of single component catalysts (10 wt%) compared with a blank test. Testing conditions: reactor temperature = 700 °C at atmospheric pressure, CH_4:O_2:N_2 = 3:1:0, total flow rate = 35 mL/min (GHSV = 50,000 h^{-1}), catalyst amount = 8.0 mg.

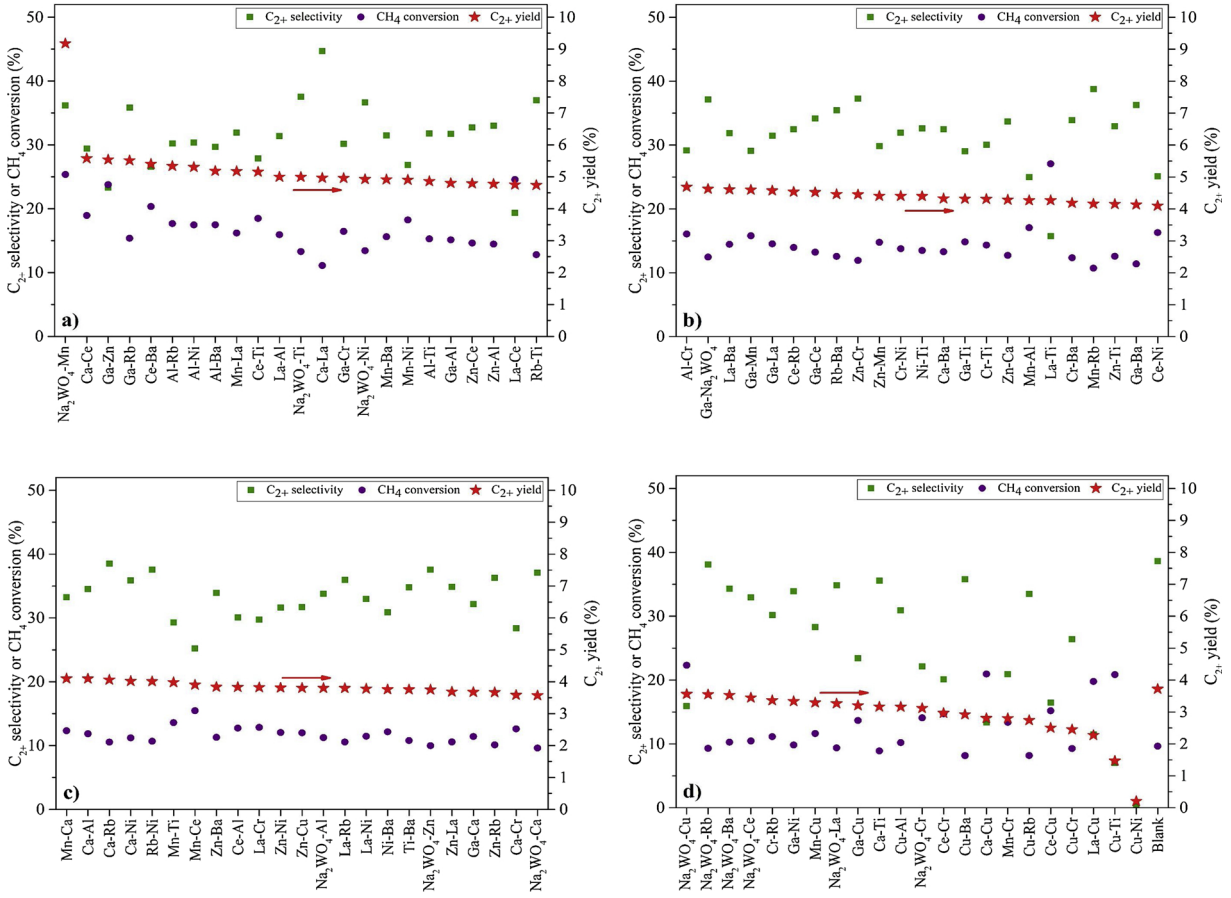

Fig. 2. a)–d) C_{2+} selectivity, CH_4 conversion, and C_{2+} yield of binary catalysts (weight ratio of 1:1 and total weight loading of 10 wt% on SiO_2) compared with a blank test. Testing conditions: reactor temperature = 700 °C at atmospheric pressure, CH_4:O_2:N_2 = 3:1:0, total flow rate = 35 mL/min (GHSV = 50,000 h^{-1}), catalyst amount = 8.0 mg.

exhibit a synergistic catalyst effect as evidenced in previous works [41,43].

In order to narrow the choices of active components and shorten the time of the screening test, the top-14 single components achieving a C_{2+} yield higher than that of the blank test shown in Fig. 1 were chosen for further binary catalyst screening. These 14 components were made into binary catalysts, which were prepared by combining each one with the other 13 in turn, providing 91 binary catalysts in total. Each catalyst was prepared using a co-impregnation method that involved an active component ratio of 1:1 and a total weight loading of the active component on SiO_2 of 10 wt%. The results of the screening test are presented in Fig. 2 a)–d) and the values of the products and the byproducts are presented in Table S3. It was found that the outstanding catalyst was the combination of Na_2WO_2 and Mn on the SiO_2 support (Na_2WO_4-Mn/SiO_2), giving the highest C_{2+} yield of 9.18% with 36.2% C_{2+} selectivity and 25.36% CH_4 conversion. Several other catalysts also provided a C_{2+} yield higher than that of the blank test. It is interesting to see that many of the binary catalysts made from Ga (including Ga-Za, Ga-Rb, Ga-Cr, Ga-Al, and Ga-Na_2WO_4) were in the top-23 active binary catalysts (Fig. 2a). Moreover, the binary catalyst that offered the highest selectivity was Ca-La, yielding 44.7% C_{2+} selectivity with 4.96% C_{2+} yield and 11.10% CH_4 conversion. These catalysts are of great interest for future study.

The Na_2WO_4-Mn/SiO_2 catalyst was further studied by varying the weight ratio of Na_2WO_4:Mn, while the total weight loading was maintained at 10 wt%. The results are plotted in Fig. 3 and the distributions

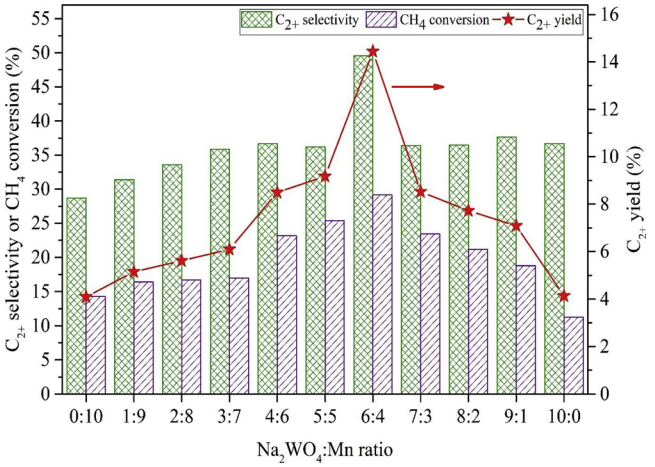

Fig. 3. C_{2+} selectivity, CH_4 conversion, and C_{2+} yield of Na_2WO_4-Mn/SiO_2 catalysts at different weight ratios of Na_2WO_4:Mn with a total weight loading of 10 wt% on SiO_2.Testing conditions: reactor temperature = 700 °C at atmospheric pressure, CH_4:O_2:N_2 = 3:1:0, total flow rate = 35 mL/min (GHSV = 50,000 h^{-1}), catalyst amount = 8.0 mg.

of the products and the byproducts are listed in Table S4. Promisingly, when the Na_2WO_4:Mn was 6:4, the values of all of the activities—C_{2+} selectivity, CH_4 conversion, and C_{2+} yield—were the highest at 49.6%,

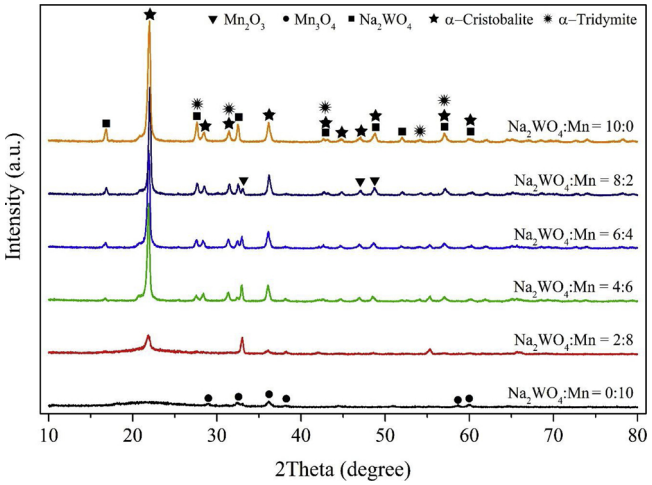

Fig. 4. XRD patterns of Na_2WO_4-Mn/SiO_2 catalysts at different weight ratios, fixing the total metal loading on SiO_2 at 10 wt%.

29.14%, and 14.44%, respectively. As seen in the XRD patterns is presented in Fig. 4 (also see Table S9), the characteristic peaks of α-cristobalite appeared for catalysts containing Na_2WO_4, while for catalysts containing Mn, the characteristic peaks of Mn_2O_3 were dominant compared to those of Mn_3O_4. Furthermore, as seen in the SEM images Fig. 5, the particle size and shape of the catalyst at the Na_2WO_4:Mn ratio of 6:4 were uniform throughout the sample. At low Na_2WO_4:Mn ratios, amorphous SiO_2 could still be observed and at high Na_2WO_4:Mn ratios, very large particles (α-cristobalite) formed. These indicated that the formation of α-cristobalite and crystalline manganese oxides and the particle size are essential for catalytic activity.

Moreover, N_2-physisorption was used to determine the surface area of the catalysts presented in Fig. 4, as shown in Table 1. The catalyst impregnated with only Mn (Na_2WO_4:Mn ratio = 0:10) had the largest BET surface area (80.01 m^2/g) among the catalysts. The BET surface area of the catalysts containing Na_2WO_4 was relatively much smaller (< 5 m^2/g) than that of the catalyst impregnated with only Mn because

Table 1
BET surface area, pore volume, and pore size of Na_2WO_4-Mn/SiO_2 catalysts at different Na_2WO_4:Mn weight ratios. The total metal loading on SiO_2 of each catalyst was fixed at 10 wt%.

Weight ratio of Na_2WO_4:Mn	BET surface area (m^2/g)	Pore volume (cm^3/g)	Pore size (Å)
0:10	80.01	0.6728	336.36
2:8	4.97	0.0166	134.43
4:6	2.65	0.0082	124.41
6:4	2.06	0.0077	150.25
8:2	0.95	0.0032	132.72
10:0	2.12	0.0071	135.20

the combinations of Na_2WO_4 and silica result in the occurrence of the α-cristobalite phase, which has large particle sizes and very small pore volumes, in good agreement with the observations in Figs. 4 and 5. In addition, the basicity of each catalyst in Fig. 4 was determined using CO_2-TPD, as shown in Figs. S7. It was found that only the catalyst impregnated with only Mn had one clear peak at 213 °C—assigned to be a weak basic site—while no clear peaks could be observed for the other catalysts. It was possible that the catalysts containing Na_2WO_4 had such a small BET surface area that a trace amount of CO_2 could be adsorbed and desorbed and/or the catalytic materials themselves possessed a low CO_2 adsorption capacity. This implies that the basicity of the catalysts containing Na_2WO_4 and Mn on SiO_2 did not play a significant role in OCM reaction due to the fact that the active site or the active component is the key to the reaction.

Furthermore, the effect of the total weight loading of Na_2WO_4 and Mn on SiO_2 was investigated, as presented in Fig. 6. The products and byproducts are also presented in Table S5. Clearly, the total weight loading of the active components strongly influenced the catalytic activity. Increasing the total weight loading from 2.5 to 10 wt% resulted in sharp increases in the C_{2+} selectivity, CH_4 conversion, and C_{2+} yield. The optimal C_{2+} yield occurred at a total weight loading of 10 wt%, yielding 14.44% C_{2+} yield with 49.6% C_{2+} selectivity and 29.14% CH_4 conversion. Above 10 wt%, the C_{2+} yield and the CH_4 conversion steadily decreased; while the C_{2+} selectivity slowly decreased until

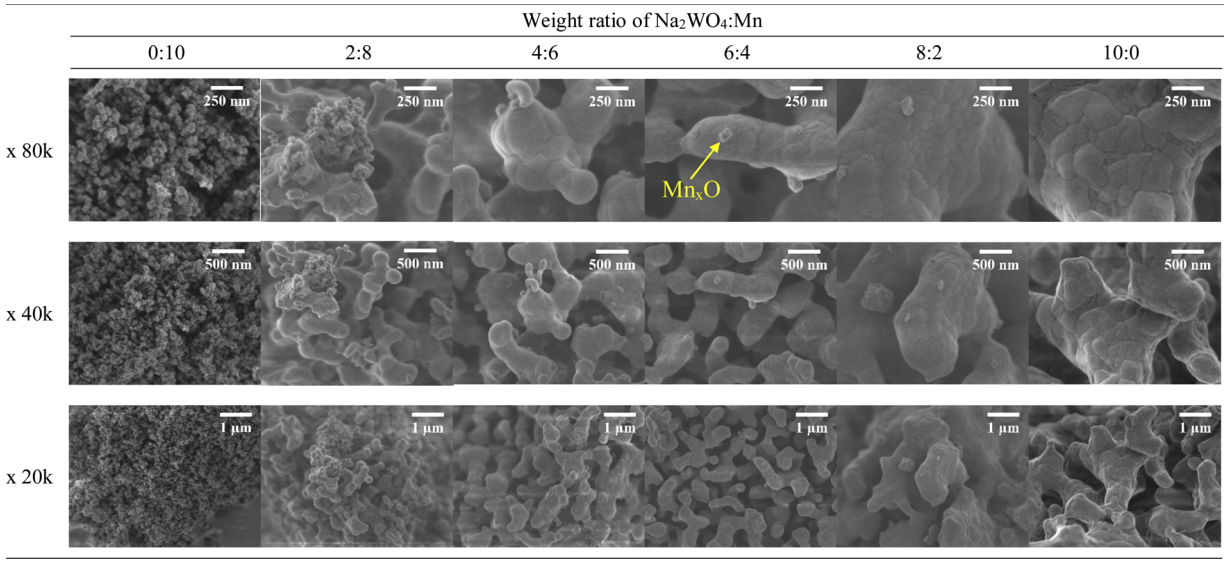

Fig. 5. FE-SEM images of Na_2WO_4:Mn catalysts at different weight ratios, fixing the total metal loading on SiO_2 at 10 wt%.

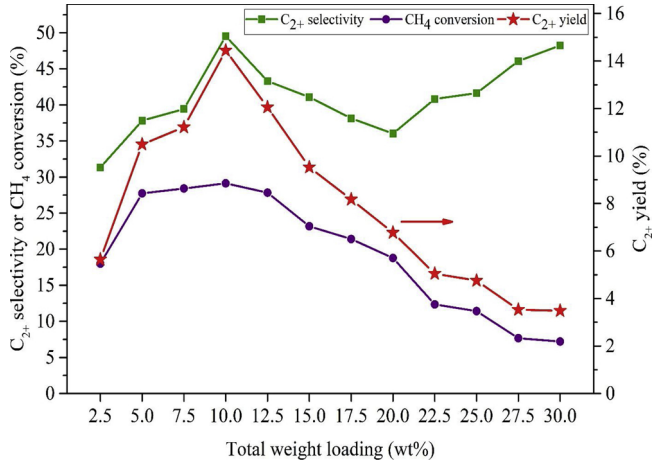

Fig. 6. C_{2+} selectivity, CH_4 conversion, and C_{2+} yield of Na_2WO_4-Mn/SiO_2 catalysts at different total weight loadings from 2.5 to 30.0 wt% on SiO_2, with the Na_2WO_4:Mn weight ratio of 6:4. Testing conditions: reactor temperature = 700 °C at atmospheric pressure, CH_4:O_2:N_2 = 3:1:0, total flow rate = 35 mL/min (GHSV = 50,000 h^{-1}), catalyst amount = 8.0 mg.

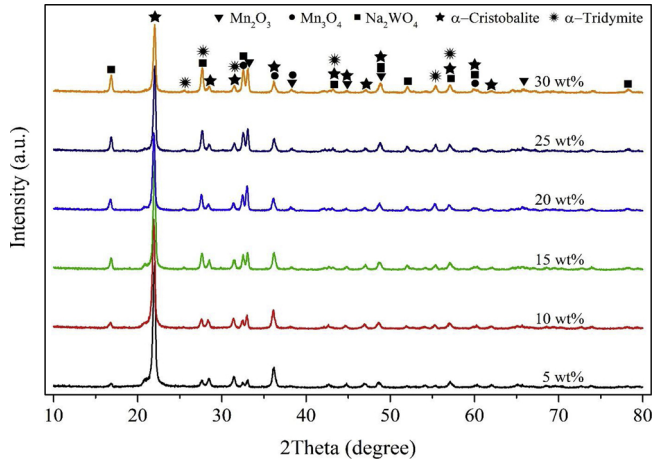

Fig. 7. XRD patterns of Na_2WO_4-Mn/SiO_2 catalysts at different total metal loadings on SiO_2, fixing the Na_2WO_4:Mn ratio at 6:4.

Table 2
BET surface area, pore volume, and pore size of Na_2WO_4-Mn/SiO_2 catalysts at different total metal loadings. The metal ratio of Na_2WO_4:Mn was fixed at 6:4.

Total metal loading of Na_2WO_4-Mn on SiO_2	BET surface area (m^2/g)	Pore volume (cm^3/g)	Pore size (Å)
5 wt%	2.38	0.0086	144.87
10 wt%	2.06	0.0077	150.25
15 wt%	0.84	0.0035	170.07
20 wt%	0.46	0.0035	303.74
25 wt%	0.35	0.0019	222.20
30 wt%	1.20	0.0046	154.32

20 wt%, and then slightly increased from 36.0% to 48.3% at 30 wt%. As observed from the XRD patterns is presented in Fig. 7 (also see Table S9) and the SEM images Fig. 8, the particle size and shape of the catalyst at 10 wt% loading were noticeably more uniform and smaller than those of the catalysts at > 10 wt%. When comparing the catalysts between 5 wt% and 10 wt%, it was more likely that there were fewer small particles (ca. 50 μm, being manganese oxides particles) of the catalyst at 5 wt% than at 10 wt%, which indicated that the catalyst at 10 wt% had the highest activity.

Furthermore, the BET surface areas, pore sizes, and pore volumes of the catalysts in Fig. 7 were determined using N_2-physisorption, as presented in Table 2. Increasing the total metal loadings from 5 to 25 wt % resulted in reductions in the BET surface areas and pore volumes, in good agreement with the observation based on the SEM images in Fig. 8. However, the BET surface area of the catalyst at 30 wt% loading increased slightly, perhaps because the amount of α-cristobalite structure was the smallest relative to the other catalysts, due to the smallest amount of SiO_2 being used, resulting in more Na_2WO_4 and MnO_x particles being present on the surface, which caused the creation of rough surfaces and thereby increased the surface area of the 30 wt% catalyst. CO_2-TPD measurements of the catalysts in Fig. 7 were also investigated, as presented in Fig. S8. Similar to Fig. S7, all the catalysts had very low basicity as described earlier.

The surface chemistries of the MnO_x/SiO_2, Na_2WO_4/SiO_2 and optimal Na_2WO_4-Mn/SiO_2 catalysts were analyzed using XPS, as presented in Fig. 9. Multiple scan spectra were conducted in the Si, Mn, Na and W regions. These spectra confirmed that the Na_2WO_4-Mn/SiO_2 catalyst comprised SiO_2 (2p = 103.5 eV), Mn_2O_3 ($2p_{3/2}$ = 641.3 eV, $2p_{1/2}$ = 653.6 eV), Na_2O (1 s = 1071.5 eV) and WO_3 ($4f_{7/2}$ = 33.2 eV, $4f_{5/2}$ = 35.3 eV) [44]. Of note was that the characteristic XPS peaks of

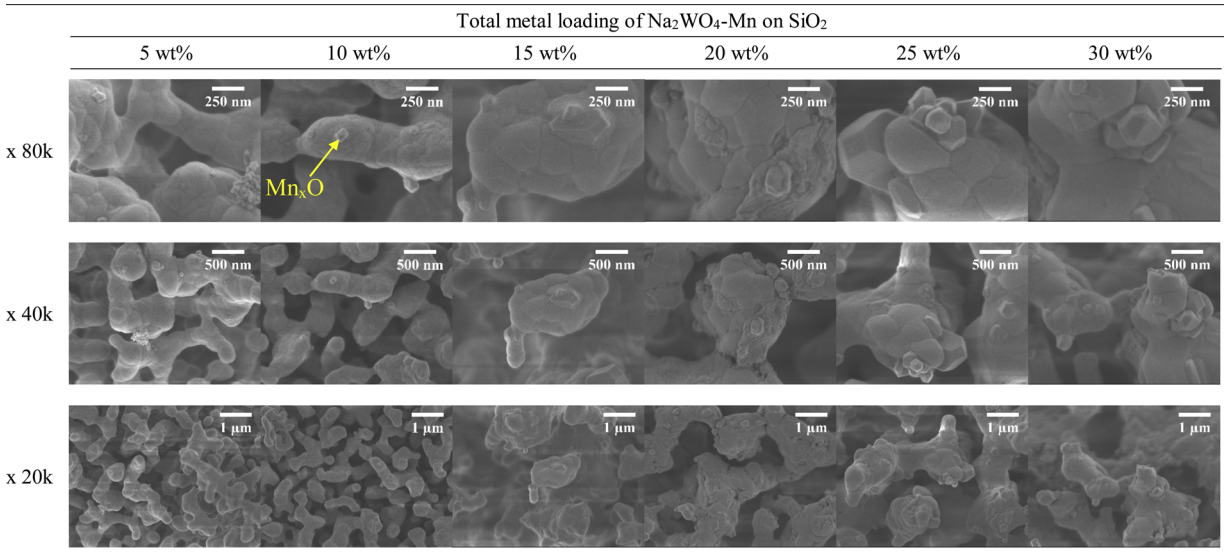

Fig. 8. FE-SEM images of Na_2WO_4-Mn/SiO_2 catalysts at different total metal loadings on SiO_2, fixing the Na_2WO_4:Mn ratio at 6:4.

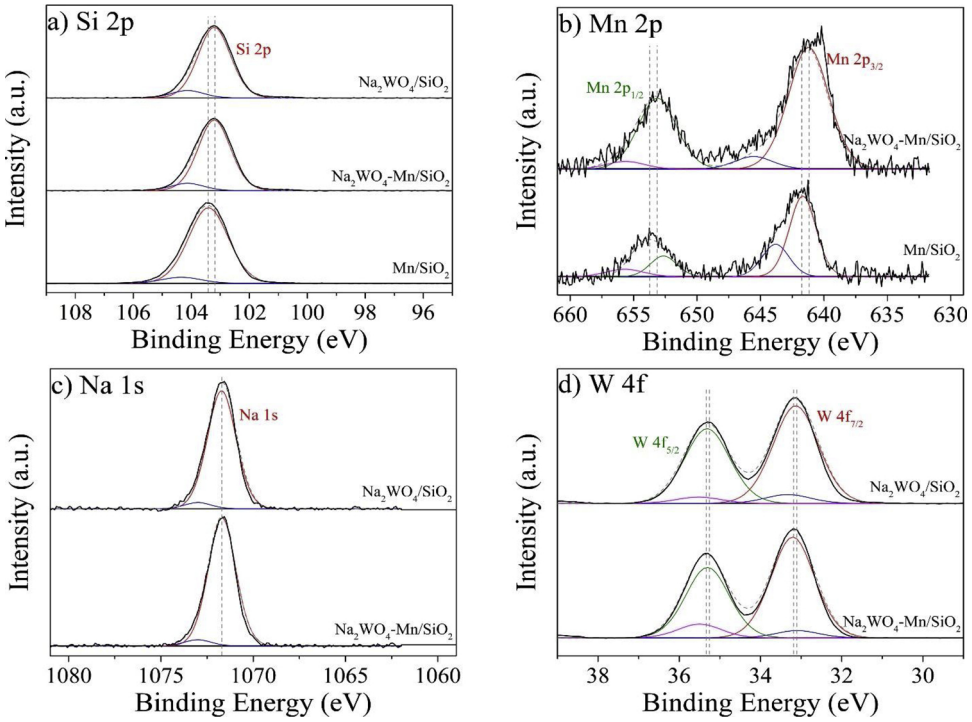

Fig. 9. XPS spectra of a) Si 2p, b) Mn 2p, c) Na 1 s and d) W 4f regions obtained from Mn/SiO_2, Na_2WO_4/SiO_2 and Na_2WO_4-Mn/SiO_2 catalysts.

Si (Fig.9a) of the Na_2WO_4/SiO_2 and Na_2WO_4-Mn/SiO_2 catalysts relative to the Mn/SiO_2 catalyst shifted from 103.5 to 103.2 eV because the SiO_2 phase in the Mn/SiO_2 catalyst is amorphous, but the SiO_2 phases in the Na_2WO_4/SiO_2 and Na_2WO_4-Mn/SiO_2 catalysts are α-cristobalite. For Na 1 s (see Fig. 9c), no substantial shift of the peaks was found. Interestingly, significant changes in binding energies were observed in Fig. 9b and d, as the binding energies of Mn 2p and W 4f of the Na_2WO_4-Mn/SiO_2 catalyst shifted toward lower binding energies compared to the binding energies of Mn and W of the single Mn/SiO_2 and Na_2WO_4/SiO_2 catalysts, respectively. This suggested that the bond strengths of W—O and Mn—O became weaker, resulting in an improvement in the oxygen mobility over the surface of the Na_2WO_4-Mn/SiO_2 catalyst, thereby enhancing the activation of CH_4 [22].

The optimal catalyst was further investigated for two feeding gas conditions—with and without N_2 gas feedings—and at different catalyst amounts in the reactor by fixing the total feed gas flow rate at 35 mL/min. The results and the details of the two conditions are shown in Fig. 10 and the values of the products and the byproducts are presented in Table S6 and S7. For the condition without N_2 feeding, the C_{2+} productivity increased rapidly with increasing catalyst amounts from 2 to 30 mg. Note that the GHSV values were lowered with increased catalyst amounts due to the increased catalyst volume. The C_{2+} yield reached an optimal point of 16.77% with 53.9% C_{2+} selectivity and 31.15% CH_4 conversion. After the optimal point, the activity of the catalyst slowly decreased. For the condition with N_2 feeding at a ratio of CH_4:O_2:N_2 = 3:1:4, the catalyst amount was in a range from 20 to 200 mg. Similarly, the C_{2+} productivity increased sharply when the catalyst amount increased from 20 to 50 mg, achieving the optimal C_{2+} yield of 18.59% with 55.0% C_{2+} selectivity and 33.82% CH_4 conversion. Above 50 mg, the C_{2+} productivity gradually decreased.

It can be noticed that when adding the inert gas to the feeding system, the optimal C_{2+} yield shifted toward a higher catalyst amount. This can be explained by considering that at the same catalyst amount (such as 20 mg), the chance for the reactant gases to interact with the active sites of the condition without N_2 feeding is lower than that of the condition with N_2 feeding, and thus more catalyst is required; consequently all of the reactant gases can interact with the active sites before

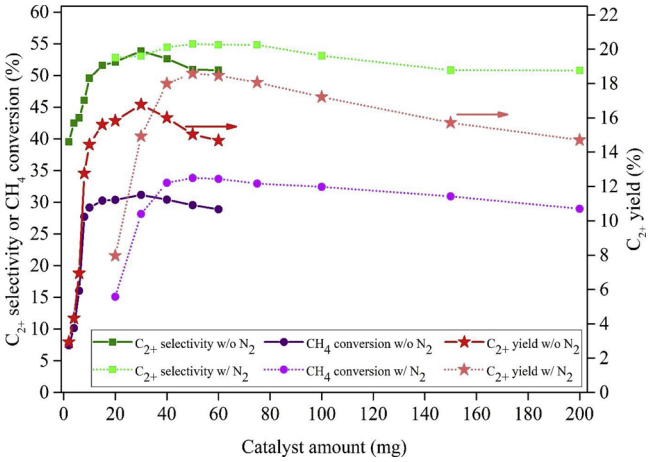

Fig. 10. C_{2+} selectivity, CH_4 conversion, and C_{2+} yield of Na_2WO_4-Mn/SiO_2 catalysts at different catalyst weights, with Na_2WO_4:Mn weight ratio of 6:4, total weight loading of 10 wt% on SiO_2. Testing conditions: reactor temperature = 700 °C at atmospheric pressure, total flow rate = 35 mL/min. For the condition w/o N_2 feeding; CH_4:O_2:N_2 = 3:1:0, catalyst weight = 2–75 mg (GHSV = 210,000–5500 h^{-1}).For the condition w/ N_2 feeding; CH_4:O_2:N_2 = 3:1:4, catalyst amount = 20–200 mg (GHSV = 17,000–2000 h^{-1}).

leaving the catalyst bed. In addition, the optimal C_{2+} yield of the condition with N_2 feed was slightly higher than that of the condition without N_2, suggesting that lowering the concentration of the reactant gases using an inert gas favored the conversion of methane. This could occur because the diffusion of the reactants and other species over the catalyst's surface in the diluted condition of the reactants is unlimited. It is also interesting to see that after the optimum catalyst amounts, the CH_4 conversion and the C_{2+} selectivity minimally reduced, resulting in a gradual decrease of the C_{2+} yield. It is possible that the C_{2+} products further reacted with other active sites of the catalyst to produce CO_x and/or a partial amount of the detected CH_4 had been generated from

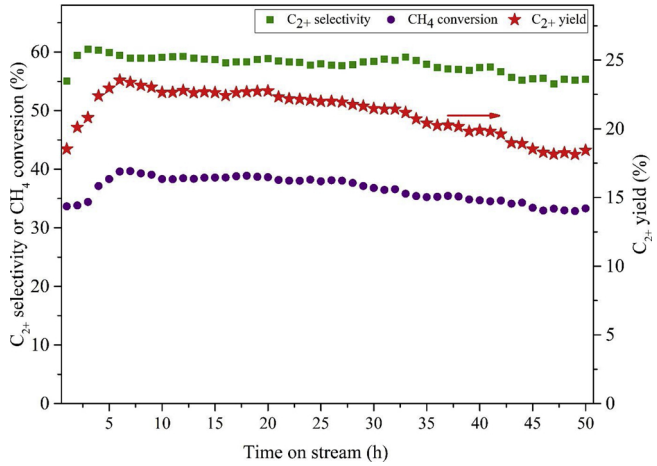

Fig. 11. Catalyst stability test of Na_2WO_4-Mn/SiO_2 catalysts, with a Na_2WO_4:Mn weight ratio of 6:4. Testing conditions: reactor temperature = 700 °C at atmospheric pressure, CH_4:O_2:N_2 = 3:1:4, total flow rate = 35 mL/min (GHSV = 14,500 h^{-1}), catalyst amount = 50.0 mg.

the C_{2+} products [2,45–47]. Thus, the C_{2+} productivity decreased with increasing CH_4 conversion.

The stability test of the Na_2WO_4-Mn/SiO_2 catalyst using the optimal conditions for 50 h is shown in Fig. 11 (see also Table S8. for the values of each product and byproduct). The performance of the catalyst constantly increased from the beginning to the maximum C_{2+} yield in the sixth hour of testing. The maximum C_{2+} yield was achieved at 23.54% with 60.5% C_{2+} selectivity and 39.67% CH_4 conversion. After that, the performance of the catalyst slightly decreased until the end of testing, resulting in a 18.44% C_{2+} yield with 55.4% C_{2+} selectivity and 33.30% CH_4 conversion, which was a C_{2+} yield reduction of approximately 21.7% from the maximum point. Hence, the catalyst was quite good during the 50 h period. The used catalyst was then taken to further analyze using SEM, XRD, and TGA-DTG, and these results were compared with those of the fresh catalyst in order to identify any causes of the slow deactivation of the catalyst, as presented in Fig. 12. The SEM images of the fresh and used catalysts (see Fig. 12a and b, respectively) revealed that the particle size of the used catalyst increased to approximately four times the fresh catalyst. The difference in the XRD patterns of the fresh and used catalysts (see Fig. 12c) was the appearance of the α-tridymite phase in the used catalyst. This implied that a phase transformation of α-cristobalite to α-tridymite slowly occurred during the reaction, considerably slowing the deactivation of the catalyst. The TGA-DTG profiles (see Fig. 12d) had no peak for coke decomposition. Generally, the peak for coke decomposition can be seen at about 500–600 °C [48]. Therefore, it was concluded that the slow deactivation of the catalyst resulted from the catalyst sintering and the phase transformation of α-cristobalite to α-tridymite without coke deposition on the catalyst's surface.

4. Conclusion

In the pursuit of binary catalysts for the OCM reaction, 25 single components were first charily selected and prepared on amorphous SiO_2. The screening of these single catalysts provided 14 single catalysts that achieved a $\%C_{2+}$ yield higher than that of the blank test. The 14 components were then chosen to prepare binary catalysts by combining each one with the other 13 in turn, giving 91 binary catalysts in total. Subsequently, binary catalyst screening was carried out, revealing several active binary catalysts. The most active binary catalyst was the combination of Na_2WO_4 and Mn. Optimization of this catalyst was further investigated carefully by varying the Na_2WO_4:Mn ratio, the total metal loading on SiO_2, the catalyst amount, and the stability test, resulting in the highest C_{2+} yield of 23.54%, with 60.5% C_{2+} selectivity and 39.67% CH_4 conversion. The measurements of the binding energies of W and Mn using XPS revealed that the bond strengths of W—O and Mn—O became weaker, thereby enhancing the catalytic activity of the Na_2WO_4-Mn/SiO_2 catalyst. Moreover, the stability of the catalyst was monitored during 50 h of testing, disclosing that the catalyst very slowly deactivated due to the catalyst sintering and the phase transformation of α-cristobalite to α-tridymite.

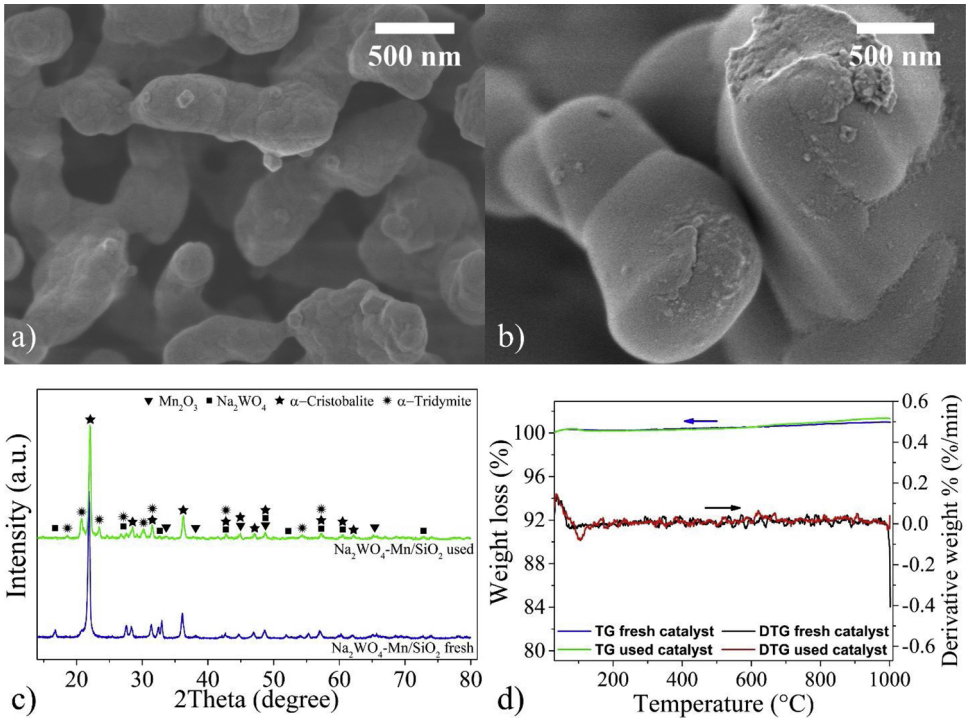

Fig. 12. The used Na_2WO_4-Mn/SiO_2 catalyst was taken to further analyze, a) FE-SEM images of fresh catalysts, b) FE-SEM images of used catalysts, c) XRD patterns of fresh and used catalyst, and d) TGA-DTG profiles of fresh and used catalyst. With Na_2WO_4:Mn weight ratio of 6:4, total weight loading of 10 wt% on SiO_2.

Notes

The authors declare no competing financial interest.

Acknowledgments

This work was financially supported by the Department of Chemical Engineering and the Faculty of Engineering at Kasetsart University, Bangkok, Thailand; the Kasetsart University Research and Development Institute (KURDI); the Center of Excellence on Petrochemical and Materials Technology; the National Nanotechnology Center (NANOTEC), NSTDA, Ministry of Science and Technology, Thailand, through its program of Research Network NANOTEC (RNN); the Thailand Research Fund and the Commission on Higher Education (grant # MRG6180232).

Appendix A. Supplementary data

Supplementary material related to this article can be found, in the online version, at doi:https://doi.org/10.1016/j.mcat.2019.03.021.

References

[1] P. Schwach, X. Pan, X. Bao, Direct conversion of methane to value-added chemicals over heterogeneous catalysts: challenges and prospects, Chem. Rev. 117 (2017) 8497–8520.
[2] J. Sun, J.W. Thybaut, G.B. Marin, Microkinetics of methane oxidative coupling, Catal. Today 137 (2008) 90–102.
[3] V.S. Arutyunov, L.N. Strekova, The interplay of catalytic and gas-phase stages at oxidative conversion of methane: a review, J. Mol. Catal. A Chem. 426 (2017) 326–342.
[4] G.E. Keller, M.M. Bhasin, Synthesis of ethylene via oxidative coupling of methane: I. Determination of active catalysts, J. Catal. 73 (1982) 9–19.
[5] D.J. Wang, M.P. Rosynek, J.H. Lunsford, Oxidative coupling of methane over oxide-supported sodium-manganese catalysts, J. Catal. 155 (1995) 390–402.
[6] S.A. Driscoll, D.K. Gardner, U.S. Ozkan, Characterization, activity, and adsorption/desorption behavior of alkali-promoted molybdate catalysts for the oxidative coupling of methane, J. Catal. 147 (1994) 379–392.
[7] M.G. Colmenares, U. Simon, M. Yildiz, S. Arndt, R. Schomaecker, A. Thomas, F. Rosowski, A. Gurlo, O. Goerke, Oxidative coupling of methane on the Na_2WO_4-Mn_xO_y catalyst: COK-12 as an inexpensive alternative to SBA-15, Catal. Commun. 85 (2016) 75–78.
[8] V.I. Vedeneev, O.V. Krylov, V.S. Arutyunov, V.Y. Basevich, M.Y. Goldenberg, M.A. Teitel boim, The role of initiation in oxidative coupling of methane, Appl. Catal. A Gen. 127 (1995) 51–63.
[9] U. Zavyalova, M. Holena, R. Schlögl, M. Baerns, Statistical analysis of past catalytic data on oxidative methane coupling for new insights into the composition of hgh-performance catalysts, ChemCatChem 3 (2011) 1935–1947.
[10] T.K. Chan, K.J. Smith, Oxidative coupling of methane over cobalt—magnesium and manganese—magnesium mixed oxide catalysts, Appl. Catal. 60 (1990) 13–31.
[11] F.P. Larkins, M.R. Nordin, The effects of transition metal oxides on the methane oxidative coupling activity of doped MgO catalysts I. Zinc and manganese, J. Catal. 130 (1991) 147–160.
[12] K. Otsuka, T. Komatsu, Active catalysts in oxidative coupling of methane, J. Chem. Soc. Chem. Commun. (1987) 388–389.
[13] S. Hou, Y. Cao, W. Xiong, H. Liu, Y. Kou, Site requirements for the oxidative coupling of methane on SiO_2-supported Mn catalysts, Ind. Eng. Chem. Res. 45 (2006) 7077–7083.
[14] Y. Amenomiya, V.I. Birss, M. Goledzinowski, J. Galuszka, A.R. Sanger, Conversion of methane by oxidative coupling, Cat. Rev. 32 (1990) 163–227.
[15] R. Burch, G.D. Squire, S.C. Tsang, Comparative study of catalysts for the oxidative coupling of methane, Appl. Catal. 43 (1988) 105–116.
[16] J.A. Sofranko, J.J. Leonard, C.A. Jones, The oxidative conversion of methane to higher hydrocarbons, J. Catal. 103 (1987) 302–310.
[17] Z.C. Jiang, C.J. Yu, X.P. Fang, S.B. Li, H.L. Wang, Oxide/support interaction and surface reconstruction in the sodium tungstate(Na_2WO_4)/silica system, J. Phys. Chem. 97 (1993) 12870–12875.
[18] A. Palermo, J.P. Holgado Vazquez, A.F. Lee, M.S. Tikhov, R.M. Lambert, Critical influence of the amorphous silica-to-cristobalite phase transition on the performance of $Mn/Na_2WO_4/SiO_2$ catalysts for the oxidative coupling of methane, J. Catal. 177 (1998) 259–266.
[19] S. Pak, P. Qiu, J.H. Lunsford, Elementary reactions in the oxidative coupling of methane over $Mn/Na_2WO_4/SiO_2$ and Mn/Na_2WO_4/MgO catalysts, J. Catal. 179 (1998) 222–230.
[20] J. Wang, L. Chou, B. Zhang, H. Song, J. Zhao, J. Yang, S. Li, Comparative study on oxidation of methane to ethane and ethylene over Na_2WO_4–Mn/SiO_2 catalysts prepared by different methods, J. Mol. Catal. A Chem. 245 (2006) 272–277.
[21] S. Gu, H.S. Oh, J.W. Choi, D.J. Suh, J. Jae, J. Choi, J.M. Ha, Effects of metal or metal oxide additives on oxidative coupling of methane using Na_2WO_4/SiO_2 catalysts: reducibility of metal additives to manipulate the catalytic activity, Appl. Catal. A Gen. 562 (2018) 114–119.
[22] T.W. Elkins, H.E. Hagelin-Weaver, Characterization of Mn–Na_2WO_4/SiO_2 and Mn–Na_2WO_4/MgO catalysts for the oxidative coupling of methane, Appl. Catal. A Gen. 497 (2015) 96–106.
[23] S. Ji, T. Xiao, S. Li, L. Chou, B. Zhang, C. Xu, R. Hou, A.P.E. York, M.L.H. Green, Surface WO_4 tetrahedron: the essence of the oxidative coupling of methane over M-W-Mn/SiO_2 catalysts, J. Catal. 220 (2003) 47–56.
[24] S. Arndt, T. Otremba, U. Simon, M. Yildiz, H. Schubert, R. Schomäcker, Mn–Na_2WO_4/SiO_2 as catalyst for the oxidative coupling of methane. What is really known? Appl. Catal. A Gen. 425–426 (2012) 53–61.
[25] N. Yamagata, Y. Abe, K. Igarashi, T. Ishikawa, M. Sahara, S. Okazaki, Importance of apparent density of $BaLa_2O_4$ catalysts in oxidative coupling of methane, Chem. Lett. 19 (1990) 1893–1896.
[26] I. Kim, G. Lee, H.B. Na, J.M. Ha, J.C. Jung, Selective oxygen species for the oxidative coupling of methane, Mol. Catal. 435 (2017) 13–23.
[27] B.M. Sollier, L.E. Gómez, A.V. Boix, E.E. Miró, Oxidative coupling of methane on Sr/La_2O_3 catalysts: improving the catalytic performance using cordierite monoliths and ceramic foams as structured substrates, Appl. Catal. A Gen. 532 (2017) 65–76.
[28] M.S.C. Chan, E. Marek, S.A. Scott, J.S. Dennis, Chemical looping epoxidation, J. Catal. 359 (2018) 1–7.
[29] R. Voyatzis, J.B. Moffat, Cation effects in the oxidative coupling of methane on slica-supported binary alkali and alkaline earths, J. Catal. 142 (1993) 45–58.
[30] R.T. Yunarti, S. Gu, J.-W. Choi, J. Jae, D.J. Suh, J.-M. Ha, Oxidative coupling of methane using Mg/Ti-doped SiO_2-supported Na_2WO_4/Mn catalysts, ACS Sustain. Chem. Eng. 5 (2017) 3667–3674.
[31] D. Gerceker, A.H. Motagamwala, K.R. Rivera-Dones, J.B. Miller, G.W. Huber, M. Mavrikakis, J.A. Dumesic, Methane conversion to ethylene and aromatics on PtSn catalysts, ACS Catal. 7 (2017) 2088–2100.
[32] X. Guo, G. Fang, G. Li, H. Ma, H. Fan, L. Yu, C. Ma, X. Wu, D. Deng, M. Wei, D. Tan, R. Si, S. Zhang, J. Li, L. Sun, Z. Tang, X. Pan, X. Bao, Direct, nonoxidative cnversion of methane to ethylene, aromatics, and hydrogen, Science 344 (2014) 616–619.
[33] A.M. Maitra, Solid-state basicity as a guide to formulation of improved catalysts for oxidative coupling of methane: I. Performance evaluation, Appl. Catal. A Gen. 114 (1994) 65–81.
[34] T.W. Elkins, S.J. Roberts, H.E. Hagelin-Weaver, Effects of alkali and alkaline-earth metal dopants on magnesium oxide supported rare-earth oxide catalysts in the oxidative coupling of methane, Appl. Catal. A Gen. 528 (2016) 175–190.
[35] K. Omata, A. Aoki, K. Fujimoto, Oxidative coupling of methane over CaO-MgO mixed oxide, Catal. Lett. 4 (1990) 241–244.
[36] L. Luo, Y. Jin, H. Pan, X. Zheng, L. Wu, R. You, W. Huang, Distribution and role of Li in Li-doped MgO catalysts for oxidative coupling of methane, J. Catal. 346 (2017) 57–61.
[37] V.R. Choudhary, S.T. Chaudhari, A.M. Rajput, V.H. Rane, Oxidative coupling of methane to C_2-hydrocarbons over La-promoted CaO catalysts, Catal. Lett. 3 (1989) 85–87.
[38] V.H. Rane, S.T. Chaudhari, V.R. Choudhary, Oxidative coupling of methane over La-promoted CaO catalysts: influence of precursors and catalyst preparation method, J. Nat. Gas Chem. 19 (2010) 25–30.
[39] L. Pirro, A. Obradović, B.D. Vandegehuchte, G.B. Marin, J.W. Thybaut, Model-based catalyst selection for the oxidative coupling of methane in an adiabatic fixed-bed reactor, Ind. Eng. Chem. Res. 57 (2018) 16295–16307.
[40] E. Danielson, J.H. Golden, E.W. McFarland, C.M. Reaves, W.H. Weinberg, X.D. Wu, A combinatorial approach to the discovery and optimization of luminescent materials, Nature 389 (1997) 944.
[41] W. Kumsung, M. Chareonpanich, P. Kongkachuichay, S. Senkan, A. Seubsai, Single and bimetallic catalyst screenings of noble metals for methane combustion, Catal. Commun. 110 (2018) 83–87.
[42] V.I. Vedeneev, V.S. Arutyunov, V.Y. Basevich, Kinetic limit of the ethane and ethylene yield in the gas phase condensation of methane, Russ. Chem. Bull. 44 (1995) 372–373.
[43] M. Kahn, A. Seubsai, I. Onal, S. Senkan, High-throughput synthesis and screening of new catalytic materials for the direct epoxidation of propylene, Comb. Chem. High Throughput Screen. 13 (2010) 67–74.
[44] J.F. Moulder, J. Chastain, Handbook of X-ray Photoelectron Spectroscopy: A Reference Book of Standard Spectra for Identification and Interpretation of XPS Data, Physical Electronics Division, Perkin-Elmer Corporation, 1992.
[45] V. Fleischer, R. Steuer, S. Parishan, R. Schomäcker, Investigation of the surface reaction network of the oxidative coupling of methane over $Na_2WO_4/Mn/SiO_2$ catalyst by temperature programmed and dynamic experiments, J. Catal. 341 (2016) 91–103.
[46] V.I. Lomfonosov, M.Y. Sinev, Oxidative coupling of methane: mechanism and kinetics, React. Kinet. Catal. Lett. 57 (2016) 647–676.
[47] C. Karakaya, H. Zhu, C. Loebick, J.G. Weissman, R.J. Kee, A detailed reaction mechanism for oxidative coupling of methane over $Mn/Na_2WO_4/SiO_2$ catalyst for non-isothermal conditions, Catal. Today 312 (2018) 10–22.
[48] Y. Sang, A. Xing, C. Wang, Z. Han, Y. Wu, Near-graphite coke deposit on nano-HZSM-5 aggregates for methanol to propylene and butylene reaction, Catalysts 7 (2017) 171.

Engineering Journal issn: 0125-8281

Article

Synthesis of Light Hydrocarbons via Oxidative Coupling of Methane over Silica-supported Na_2WO_4-TiO_2 Catalyst

Anusorn Seubsai[1,2,3], Palida Tiencharoenwong[1], Phattaradit Kidamorn[1], and Chalida Niamnuy[1,3,*]

1 Department of Chemical Engineering, Faculty of Engineering, Kasetsart University, Bangkok 10900, Thailand
2 Center of Excellence on Petrochemical and Materials Technology, Kasetsart University, Bangkok 10900, Thailand
3 Research Network of NANOTEC–KU on NanoCatalysts and NanoMaterials for Sustainable Energy and Environment, Kasetsart University, Bangkok 10900, Thailand
*E-mail: fengcdni@ku.ac.th (Corresponding author)

Abstract. Methane is of great interest for conversion into high-value hydrocarbons (C_{2+}) and olefins, via oxidative coupling of methane (OCM) using catalysts. In this work, Na_2WO_4-TiO_2/SiO_2 catalyst, along with the single catalysts of its components (Na_2WO_4/SiO_2 and TiO_2/SiO_2), was investigated for OCM reaction to C_{2+}. We found that 5 wt% Na_2WO_4+ 5 wt% TiO_2 on the SiO_2 support was a superior catalyst for OCM reaction compared to the single catalysts. The maximum C_{2+} formation of the Na_2WO_4-TiO_2/SiO_2 catalyst was found under test conditions of a N_2/($4CH_4$:$1O_2$) feed gas ratio of 1:1, a reactor temperature of 700 ºC, and gas hourly space velocity of 9,500 h^{-1}, exhibiting 71.7% C_{2+} selectivity, 6.8% CH_4 conversion, and 4.9% C_{2+} yield. Moreover, the activity of the catalyst had good stability over 24 h of on-stream testing. The characterizations of the Na_2WO_4-TiO_2/SiO_2 catalyst using XRD, FT-IR, XPS, FE-SEM, and TEM revealed that a crystalline structure of α-cristobalite of SiO_2 was present along with TiO_2 crystals, substantially enhancing the activity of the catalyst for OCM reaction to C_{2+}.

Keywords: Catalyst, light hydrocarbons, oxidative coupling of methane, sodium tungsten oxide, titanium oxide.

ENGINEERING JOURNAL Volume 23 Issue 5
Received 28 March 2019
Accepted 10 June 2019
Published 30 September 2019
Online at http://www.engj.org/
DOI:10.4186/ej.2019.23.5.169

This article is based on the presentation at The 8th International Thai Institute of Chemical Engineering and Applied Science Conference (ITIChE2018) in Chonburi, Thailand, 8th-9th November 2018.

DOI:10.4186/ej.2019.23.5.169

1. Introduction

Methane (CH_4) is the main compound of biogas and natural gas that are plentiful on Earth. It is considered a greenhouse gas with an environmental impact more than 25 times greater than CO_2 if equal amounts of these two gases are released into the atmosphere. Since methane is an abundant compound on Earth, a process that can convert methane to high value-added chemicals is a highly attractive topic for many researchers. One of the challenging topics to be considered in catalysis is oxidative coupling of methane (OCM)—a gas-phase reaction that uses O_2 or air to directly react with CH_4 to produce useful hydrocarbons (C_{2+}) such as ethylene, ethane, propane, and propylene [1, 2]. The OCM reaction is an exothermic reaction in nature and normally takes place at reaction temperatures of 600–1,000 ºC [3]. OCM can produce CO and CO_2 as byproducts. However, if a suitable catalyst is present, the reaction produces a selective product and extreme reaction temperatures can be reduced.

In the past several years, some potential catalysts have been reported, including MnO_x modified with different types of co-catalysts, supports and promotors, such as oxides of Mg, Na, and Ce. However, the C_{2+} yields and C_{2+} selectivities were quite low at approximately <16% and 25-78%, respectively [4-8]. Additionally, coke formation was found during the reaction, resulting in catalyst deactivation. Later, the coking formation was, however, prevented by introducing of chlorinated compounds with the reactant gases. Alternatively, a binary catalyst of Na_2WO_4-MnO_x has been widely investigated because this metal combination was identified as an active material for the OCM reaction. The modified Na_2WO_4-MnO_x catalysts reported include MO_x-Na_2WO_4-MnO_x/SiO_2 (M = Ni, Co, Fe, Li, Al, Ba, Ca, Na, and K) [9], TiO_2-Na_2WO_4/MnO_x/SiO_2 [10], and Ce_2O_3-MnO_x-Na_2WO_4/SiO_2 [7]. The C_{2+} yields and C_{2+} selectivities of those Na_2WO_4-MnO_x catalysts increased compared to the single catalysts of its component and the other metal combinations due to synergistic catalyst effects between Na_2WO_4 and MnO_x [11-14]. The additions of the promoters (e.g. TiO_2, Ce_2O_3) onto the Na_2WO_4-MnO_x catalysts resulted in improved activity of the catalysts, because the promoters could cooperate into the catalytic materials and/or the number of suitable strong basic sites increased [15, 16]. Normally, SiO_2 is used as a catalyst support because the SiO_2 support is stable under the test conditions and inert to the products [14].

Since previous results reported in the literatures showed that any catalysts containing Na_2WO_4, MnO_x, and/or SiO_2 are highly active for OCM reaction, it is of great interest and challenging to improve new catalysts that consist of any of those components and new active metal component (i.e co-active metal, promoter). In a catalyst screening for OCM reaction in our laboratory, we discovered that addition of TiO_2 onto the Na_2WO_4/SiO_2 catalyst without MnO_x can also substantially improve the C_{2+} yield. This combination of TiO_2 and Na_2WO_4 on SiO_2 has never been reported in detail. Herein, we report on various studies on the activity of Na_2WO_4 mixed with TiO_2 on SiO_2 support. The studies include catalyst optimization, catalyst stability, operating condition for the reaction, and catalyst characterization.

2. Experimental Section

2.1. Catalyst Preparation

All of the catalysts were synthesized using co-impregnation of predetermined weights of SiO_2 as follows. An aqueous solution of Na_2WO_4 (sodium tungstate dihydrate, 98.0~101.0%, Daejung) and Ti^{4+}(titanium (IV) isopropoxide, 97+%, Alfa Aesar) in ethanol (99.9%, QREC) were determined and pipetted into amorphous fume silica (SiO_2, surface area of 85-115 m^2/g, Alfa Aesar) to obtain a desired weight percentage of the metal components (TiO_2 and/or Na_2WO_4) on the SiO_2 support. Note that the weight percentage of TiO_2 or Na_2WO_4 on the support was determined on the basis of the mass of Ti(0) or Na_2WO_4, respectively. The mixture was continuously stirred at 120 ºC until dry. The obtained powder was then taken to calcine in an air furnace at 800 ºC for 4 h. After the calcination, a fine white powder was obtained.

2.2. Catalyst Activity Test

The activities of the prepared catalysts were evaluated for OCM reaction in a plug flow reactor at 1 atm and a reactor temperature range of 600–800 ºC. A sample (8 mg) was packed in a quartz tubular reactor that had an inner diameter of 0.5 cm. The catalyst bed length was approximately 2 mm and the catalyst was

sandwiched between two layers of quartz wool. The feed gas consisted of nitrogen (N_2, 99.999% purity, Praxair), methane (CH_4, 99.999% purity, Praxair), and oxygen (O_2, 99.999% purity, Praxair) at a volume ratio of (N_2:CH_4:O_2) = (0–7.5):4:1 (i.e. fixing the volume ratio of CH_4:O_2 = 4:1) with a total feed flow rate of 50 mL/min, which corresponded to a gas hourly space velocity (GHSV) of 9,500 h^{-1}. The effluent gas was analysed using a gas chromatograph (Shimadzu, GC-14A) equipped with a thermal conductivity detector (TCD; for analyzing CO, CO_2, and CH_4) and a flame ionization detector (FID; for analysis of C_2H_4, C_2H_6, C_3H_6, C_3H_8 and C_4H_8, and C_4H_{10}). The catalytic activities are expressed in terms of %CH_4 conversion, %C_{2+} selectivity, %CO_x selectivity, and %C_{2+} yield, which are shown in Eq. (1)–(4). The data were collected after the system had reached the set point for 2h.

$$\%\ CH_4\ \text{conversion} = \frac{\text{moles of } CH_4 \text{ input} - \text{moles of } CH_4 \text{output}}{\text{moles of } CH_4 \text{ input}} \times 100 \quad (1)$$

$$\%\ C_{2+}\ \text{selectivity} = \frac{\text{moles of } C_{2+}}{\text{Total moles of products}} \times 100 \quad (2)$$

$$\%\ CO_x\ \text{selectivity} = \frac{\text{moles of } CO_x}{\text{Total moles of products}} \times 100 \quad (3)$$

$$\%\ C_{2+}\ \text{yield} = \frac{\%\ CH_4\text{conversion} \times \%\ C_{2+}\text{selectivity}}{100} \quad (4)$$

2.3. Catalyst Characterization

The patterns of powder X-ray diffraction (XRD) the samples were received using a powder X-ray diffractometer (PXRD; X-Pert, Philips and JDX-3530, JEOL) with using Cu-K_a radiation with 40 mA and 45 kV, 0.5 s step time, 0.02° step size.

The pore volumes, pore-sizes, and specific surface areas of the samples were evaluated using N_2-physisorption with a Quantachrome Autosorp-1C instrument and Brunauer-Emmett-Teller (BET) procedure at a temperature of −196 °C.

The surface morphology of the samples was imaged using a field emission scanning electron microscope (FE-SEM, JSM7600F, JEOL) with an energy dispersive X-ray spectrometer (EDS), operated at 300 kV). Each sample was coated by gold (Au) using Au sputtering technique.

The particles at the nano-scale of the catalysts were characterized using a high-resolution transmission electron microscope (HR-TEM, JEM-3100F, JEOL) performed at 300 kV.

The Fourier-transform infrared (FT-IR) patterns of the samples were acquired using an FT-IR spectrometer (TENSOR2, Bruker, attenuated total reflection (ATR) mode). For the measurements, fine powder of each catalyst was mixed with potassium bromide (KBr), and then made into a KBr pellet.

The electronic states of sodium, tungsten, and titanium were analyzed using X-ray photoelectron spectroscope (XPS, Axis Ultra DLD, Kratos) with Al Kα for the X-ray source.

The metal-support and metal-metal interactions were analyzed using the H_2-temperature programmed reduction (H_2-TPR) technique. The H_2-TPR profiles of the samples were attained by carrying out the measurements in a tubular reactor (Inconel tube) in a temperature range of 50–900 °C with a heating rate of 5 °C/min. A gas mixture of 9.6% H_2 in Ar at a total feed flow rate of 30 mL/min was introduced into the sample bed. A TCD-equipped gas chromatography (GC-14, Shimadzu) was used to continuously monitor the H_2 consumption.

3. Results and Discussion

3.1. Activity of TiO_2/SiO_2, Na_2WO_4/SiO_2, and TiO_2-Na_2WO_4/SiO_2 Catalysts

The 10wt% TiO_2/SiO_2, 10wt% Na_2WO_4/SiO_2, and (5wt% TiO_2-5wt% Na_2WO_4)/SiO_2 catalysts were prepared and tested for OCM reaction, as presented in Fig. 1. The performance of each catalyst was described using the C_{2+} selectivity, CH_4 conversion, and C_{2+} yield. It should be noted that the C_{2+} yield is the criterion used to identify a superior catalyst when comparing the activities of catalysts. The C_{2+} yield of

the Na_2WO_4-TiO_2/SiO_2 catalyst was obtained at 2.7 %, clearly greater than that of the single TiO_2/SiO_2 or Na_2WO_4/SiO_2 catalysts, approximately 1.5 or 3.8 times the C_{2+} yield of the TiO_2/SiO_2 or Na_2WO_4/SiO_2 catalysts, respectively. However, the C_{2+} selectivity for these three catalysts was similar (approximately 39–42%) but the CH_4 conversion of the TiO_2/SiO_2 and Na_2WO_4/SiO_2 catalysts was lower than that of the Na_2WO_4-TiO_2/SiO_2 catalyst. The results indicated that the combination of TiO_2 and Na_2WO_4 on the SiO_2 support reveals a synergistic catalysis effect.

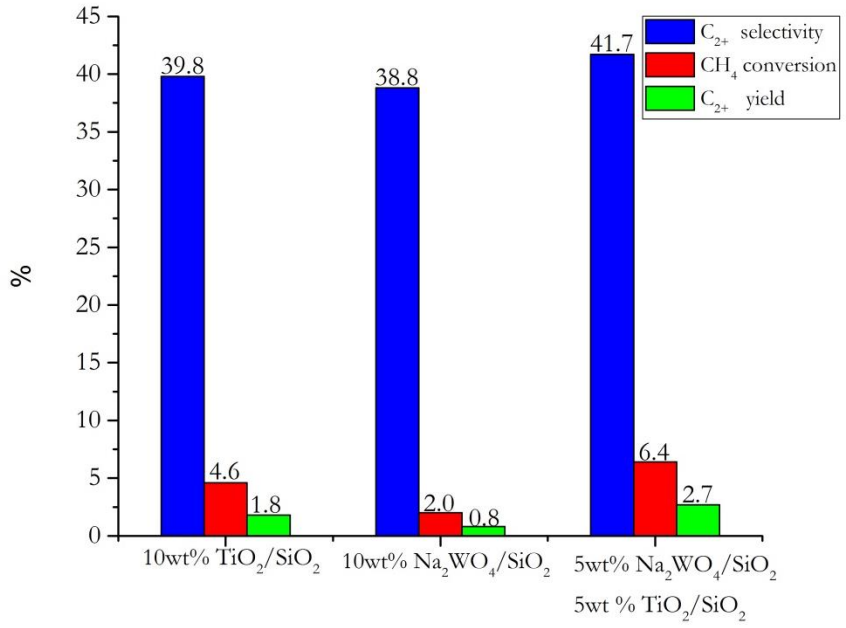

Fig. 1. C_{2+} selectivity, CH_4 conversion, and C_{2+} yield of 10wt% TiO_2/SiO_2, 10wt% Na_2WO_4/SiO_2, and TiO_2-Na_2WO_4/SiO_2 catalysts. Testing conditions: feeding gas ratio of CH_4:O_2 = 4:1 by volume, total feed flow rate = 50 mL/min (GHSV = 9,500 h^{-1}), and reactor temperature = 700 °C.

3.2. Effect of TiO_2 Loading on Na_2WO_4-TiO_2/SiO_2

The Na_2WO_4-TiO_2/SiO_2 catalyst was further studied by varying the amount of TiO_2. In a previous study, 5wt% Na_2WO_4 loaded on SiO_2 using incipient-wetness impregnation was reported to produce an optimum yield for the OCM reaction [17]. However, the effect of TiO_2 loading on Na_2WO_4/SiO_2 has never been studied. In the present study, different amounts of TiO_2 on Na_2WO_4/SiO_2 were studied by varying the amounts of TiO_2 from 0 to 30% on the catalyst and keeping the amount of Na_2WO_4 on every catalyst unchanged at 5 wt%, as plotted in Fig. 2. As increasing TiO_2 loading, the C_{2+} selectivities slowly increased from 38.0 to 44.9%, while the CH_4 conversion steadily decreased from 6.4 to 4.3%. Nevertheless, the C_{2+} yield had an optimum yield at 5 wt% loading (2.7% C_{2+} yield). This confirmed that the addition of TiO_2 into Na_2WO_4/SiO_2 enhances C_{2+} formation. However, TiO_2 loadings over 5 wt% decreased the C_{2+} yield of each catalyst. Thus, Na_2WO_4-TiO_2/SiO_2 catalyst at a total metal loading of 10 wt% and a TiO_2:Na_2WO_4 weight ratio of 1:1 (i.e. 5 wt% Na_2WO_4 + 5 wt% TiO_2) was chosen for the optimum catalyst for further studies.

3.3. Effect of $N_2/(4CH_4{:}1O_2)$ Feeding Gas Ratio and Reactor Temperature

The optimal catalyst was further investigated at various $N_2/(4CH_4{:}1O_2)$ feeding gas ratios ($N_2/(4CH_4{:}1O_2)$ = 0.0–1.5) and reactor temperatures (600–800 °C). For the previous studies in sections 3.1 and 3.2, the testing conditions were fixed at a CH_4:O_2 feeding gas ratio of 4:1 with a total feed flow rate of 50 mL/min (GHSV = 9,500 h^{-1}) without an inert gas at 700 °C and atmospheric pressure. In this section, N_2 gas (a diluent gas) was co-fed with CH_4:O_2 by fixing the volume ratio of CH_4:O_2 = 4:1 and varying the volume ratio of N_2/CH_4:O_2 from 0.0 to 1.5, and also varying the reactor temperature from 600 to 800 °C, while the

total feed flow rate was fixed at 50 mL/min. The C_{2+} yield, C_{2+} selectivity, and CH_4 conversion under each set of condition of the optimal catalyst are presented in Figs. 3(a), 3(b) and 3(c), respectively.

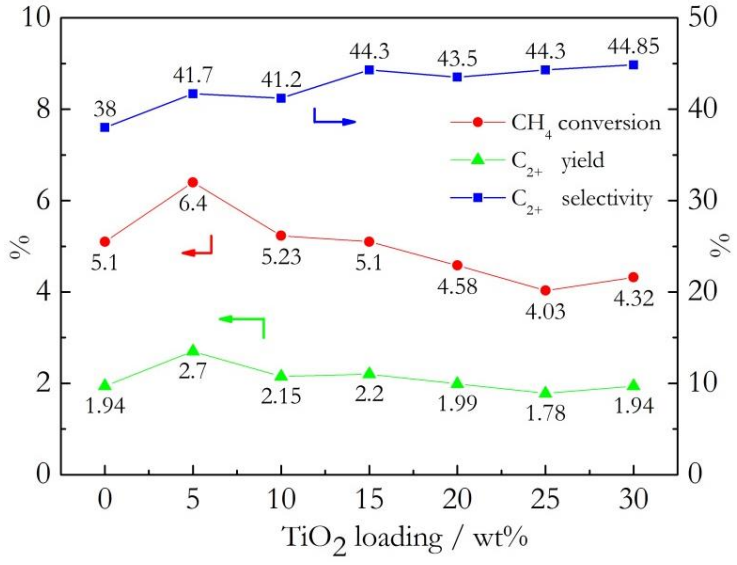

Fig. 2. TiO_2 loadings onto Na_2WO_4/SiO_2 from 0–30 wt% by fixing the amount of Na_2WO_4 onto each catalyst at 5 wt%; Testing conditions: feeding gas ratio of CH_4:O_2 = 4:1 by volume, total feed flow rate = 50 mL/min (GHSV = 9,500 h^{-1}), and reactor temperature = 700 °C.

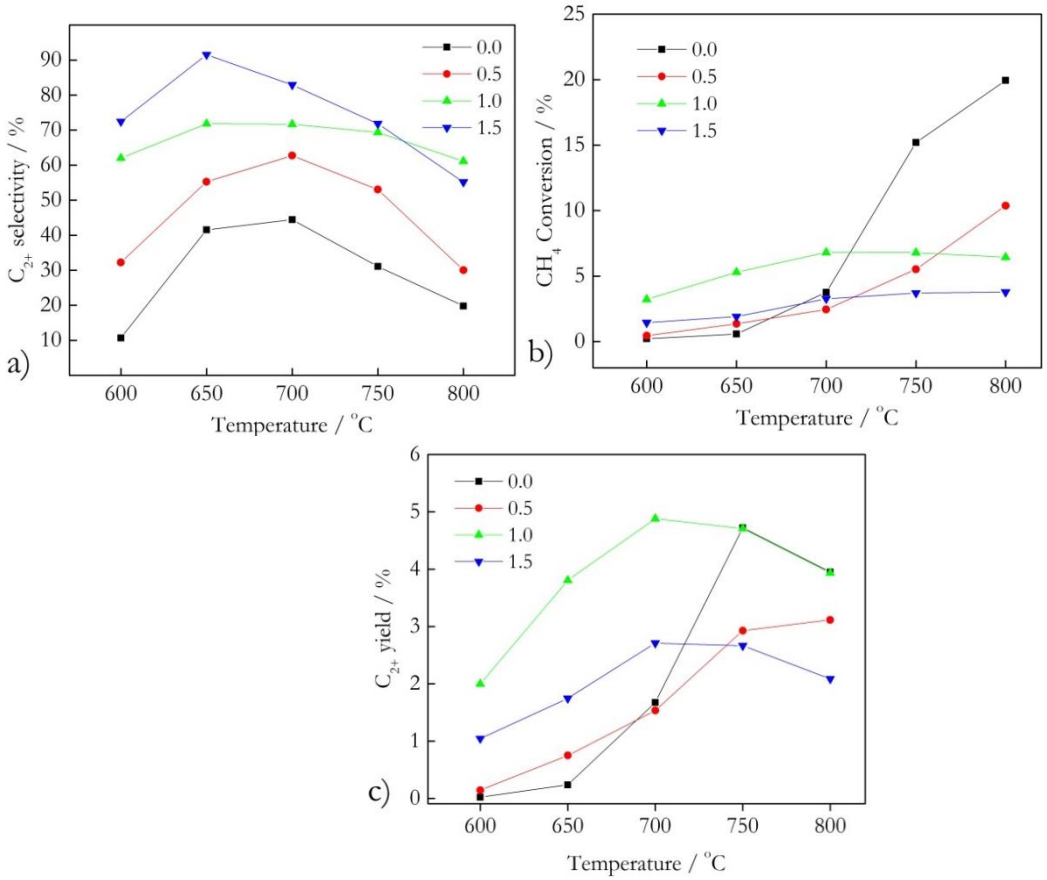

Fig. 3. a) C_{2+} selectivity, b) CH_4 conversion, and c) C_{2+} yield of the optimum TiO_2-Na_2WO_4/SiO_2 catalyst at $N_2/(4CH_4{:}1O_2)$ feeding gas ratios of 0.0–1.5 by volume, reactor temperatures of 600–800 °C, and total feed flow rate of 50 mL/min.

DOI:10.4186/ej.2019.23.5.169

Comparing the C_{2+} selectivities at one reactor temperature (Fig. 3(a)), the C_{2+} selectivity mostly increased as the $N_2/(4CH_4{:}1O_2)$ feeding gas ratio increased. The maximum C_{2+} selectivity obtained was 91.5% with a $N_2/(4CH_4{:}1O_2)$ feeding gas ratio of 1.5 by volume and a reactor temperature of 650 ºC but the CH_4 conversion and the C_{2+} yield were low at 1.9% and 1.7%, respectively. However, the C_{2+} yield at every testing temperature decreased when the $N_2/(4CH_4{:}1O_2)$ feeding gas ratio was over 1.0 by volume because the reactant gases (i.e. CH_4 and O_2) were too diluted. In other words, the reactants were not sufficient for the active sites of the catalyst. In contrast, the C_{2+} yield of the $N_2/(4CH4{:}1O_2)$ feeding gas ratio of 0.0 and 0.5 was lower than that of 1.0 because the reactant gases were much more than the active sites and the heat generated by the catalytic reaction in the catalyst's bed was high, so that the products can further combust in the hotspot zone. Thus, the C_{2+} yields for these two conditions were relatively low.

Considering the catalytic activities at one $N_2/(4CH_4{:}1O_2)$ feeding gas ratio; the catalytic activities increased when the reactor temperatures was increased from 600 to 700 ºC. However, at reactor temperatures above 700 ºC, the C_{2+} selectivities decreased with increasing CH_4 conversion, and thus the overall C_{2+} production (i.e. C_{2+} yields) decreased because the combustion of CH_4 to CO_x products is favored at high reaction temperature [3], as well as the C_{2+} products being able to further react with some active species of the catalyst or to react with O_2 gas in the gas phase to further produce CO_x [18]. As seen in Fig. 3(c), the optimal C_{2+} yield was achieved at 4.9% with 71.7% C_{2+} selectivity and 6.8% CH_4 conversion when the operating conditions were an $N_2/(CH_4{:}O_2)$ feed gas ratio of 1.0 by volume and 700 ºC. These conditions were then chosen for a further study on the stability of the catalyst.

3.4. Catalytic Stability of Na_2WO_4-TiO_2/SiO_2

The catalytic stability of the Na_2WO_4-TiO_2/SiO_2 catalyst was investigated under the optimal conditions found in section 3.3. The activities of the catalyst over 24 h are presented in Fig. 4. Promisingly, the C_{2+} selectivities were high at approximately 69–71% during the testing period. However, the overall selectivity reduced by approximately 3% within 24 h. Moreover, the CH_4 conversions slowly decreased from 6.8 to 5.9, leading to decreased C_{2+} yield during the test period. It was also noticed that the CO_x selectivities gradually increased from 29 to 31%. The results suggested that the stability of the Na_2WO_4-TiO_2/SiO_2 catalyst was quite good for over 24 h. The slow deactivation of the catalyst requires further study, which is not the focus of this report.

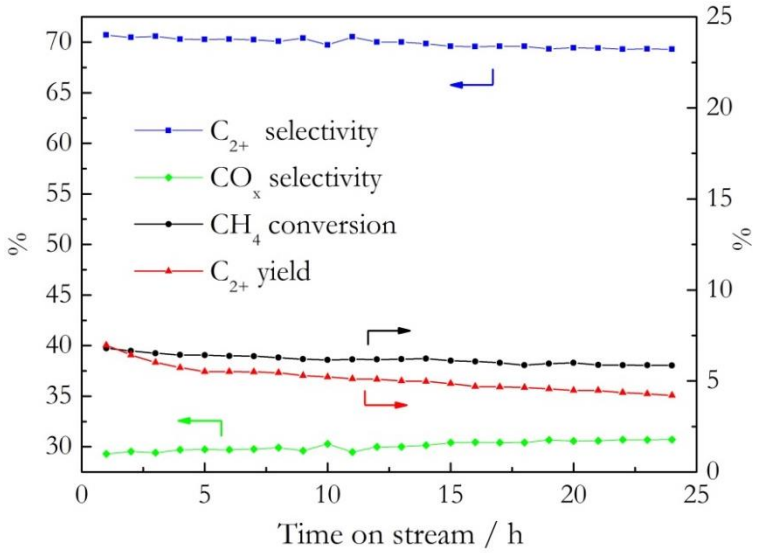

Fig. 4. Catalytic performance of Na_2WO_4-TiO_2/SiO_2 catalyst, testing conditions: $N_2/(4CH_4{:}1O_2)$ feeding gas ratio of 1.0, reactor temperature of 700 ºC, total feed flow rate of 50 mL/min, atmospheric pressure, and 24 h of testing.

3.5. Characterization of TiO_2/SiO_2, Na_2WO_4/SiO_2, and Na_2WO_4-TiO_2/SiO_2 Catalysts

The XRD pattern of the Na_2WO_4-TiO_2/SiO_2 catalysts compared with that of the TiO_2/SiO_2 and Na_2WO_4/SiO_2 catalysts are presented in Fig. 5. The TiO_2/SiO_2 catalyst exhibited two small peaks at 2θ of 25.2 and 48.5, indicating the presence of crystalline TiO_2 (anatase). It was also noticed that the SiO_2 support was in the amorphous phase. For the Na_2WO_4/SiO_2 catalyst, two crystalline compounds were observed. The first one was the crystalline Na_2WO_4, showing the characteristic peaks at 2θ of 7.16, 27.5, 32.4 and 48.4. The other was the presence of α-cristobalite (one of the crystalline forms of SiO_2), exhibiting the characteristic peaks at 2θ of 21.9, 28.3, 31.3, 36.0, 47.8, and 56.9. It was surprising to observe the formation of α-cristobalite at low a calcination temperature (800 ºC) in the presence of Na_2WO_4 because this crystalline form of SiO_2 normally occurs at calcination temperatures above 1,500 ºC [19]. Similarly, the α-cristobalite phase was observed in the Na_2WO_4-TiO_2/SiO_2 catalyst as clearly indicated by the characteristic XRD pattern. It was more interesting to observe that the characteristic peaks of TiO_2 were clearly seen for the Na_2WO_4-TiO_2/SiO_2 catalyst compared to those peaks in the Na_2WO_4-TiO_2/SiO_2 catalyst. This suggested that the environment in this catalyst enhanced the crystallinity of TiO_2. Thus, the important factor that promotes the formation of C_{2+} products of the Na_2WO_4-TiO_2/SiO_2 catalyst was the formation of the crystalline components (α-cristobalite, Na_2WO_4, and TiO_2).

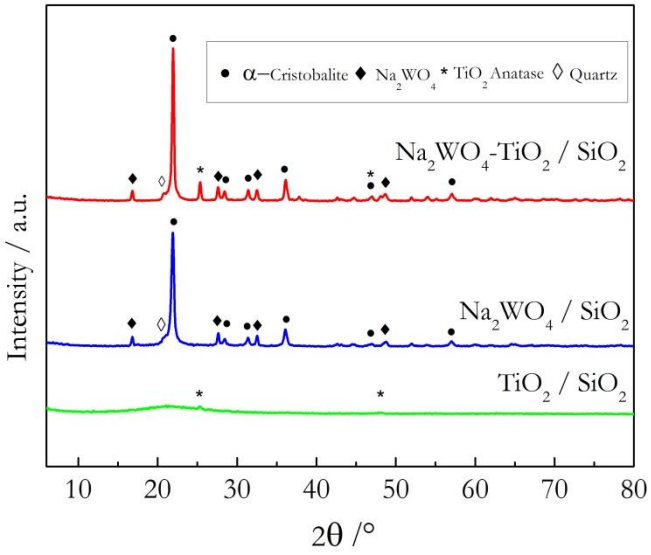

Fig. 5. XRD patterns of TiO_2/SiO_2, Na_2WO_4 /SiO_2, and Na_2WO_4-TiO_2/SiO_2.

The surface morphologies of the three catalysts imaged using FE-SEM were compared with the pure SiO_2 support and these are illustrated in Fig. 6(a)–Fig. 6(f). The SiO_2 support (Fig. 6(a)) and the TiO_2/SiO_2 catalyst (Fig. 6(b)) are similar, in that the particles are irregular in shape with sizes ranging from 20 to 50 nm. These particles were observed mostly in the amorphous SiO_2 support. The particles of the Na_2WO_4/SiO_2 catalyst (Fig. 6(c) and Fig. 6(d)) were also irregular in shape. Interestingly, the typical shape of the amorphous SiO_2 was completely transformed to a new shape, which was larger in size and possessed coral-reef like structures (approximately > 0.5 μm in diameter). This new structure was the crystalline α-cristobalite as identified by the XRD pattern. The Na_2WO_4-TiO_2/SiO_2 catalyst (Fig. 6(e) and Fig. 6(f) had similar the size and shape to the particles of the Na_2WO_4/SiO_2 catalyst. However, some small particles (approximately 50-100 nm in diameter) were observed throughout the catalyst. These particles were identified as TiO_2 crystals.

The TEM images of the Na_2WO_4-TiO_2/SiO_2 catalyst compared with those of the TiO_2/SiO_2 and Na_2WO_4/SiO_2 catalysts are shown in Fig. 7. The shape and size of each catalyst corresponded to the observation in the FE-SEM images (Fig. 6). The TEM images of the Na_2WO_4/SiO_2 (Fig. 7(c) and 7(d)) and Na_2WO_4-TiO_2/SiO_2 (Fig. 7(e) and 7(f)) catalysts confirmed that the amorphous SiO_2 support transformed to α-cristobalite when adding Na_2WO_4, in agreement with a previous report [20]. For the Na_2WO_4-

DOI:10.4186/ej.2019.23.5.169

TiO_2/SiO_2 catalyst, crystalline TiO_2 particles were clearly observed with sizes ranging between 50 and 100 nm.

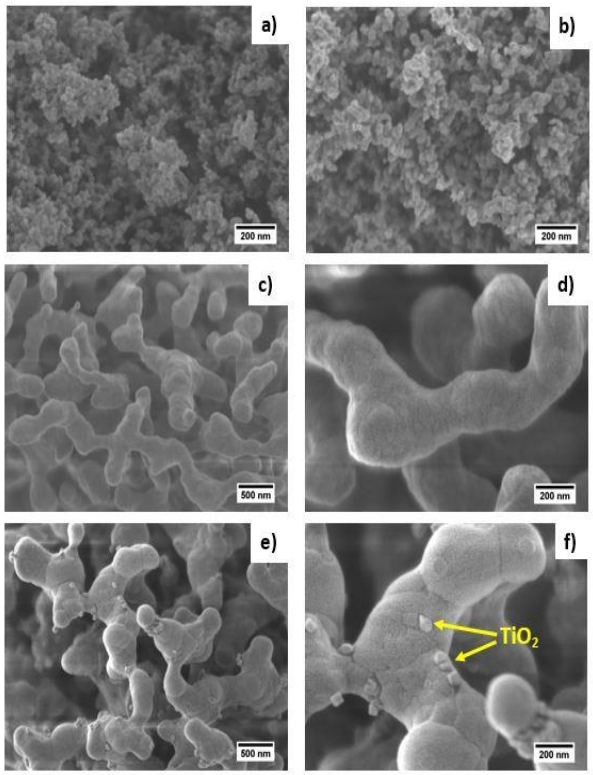

Fig. 6. SEM images of pure SiO_2 support (a), TiO_2/SiO_2 (b), Na_2WO_4/SiO_2 (c, d), and Na_2WO_4-TiO_2/SiO_2 (e, f).

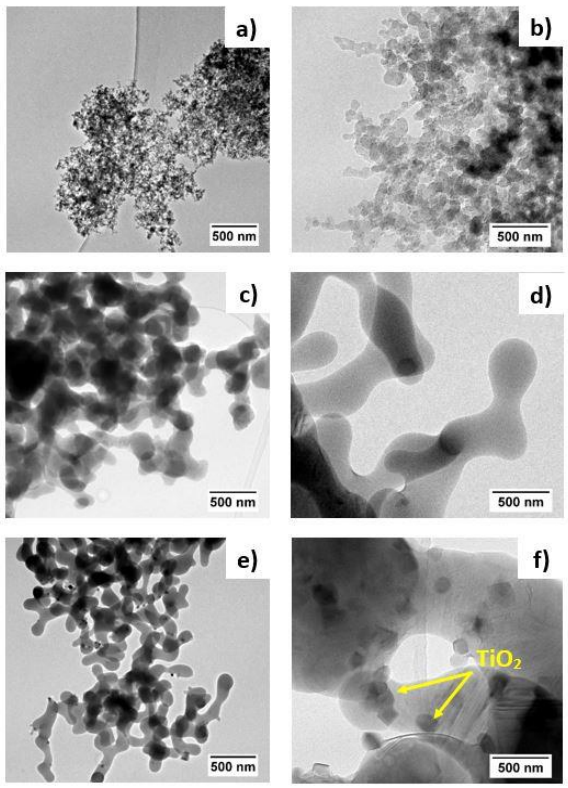

Fig. 7. TEM images of TiO_2/SiO_2 (a, b), Na_2WO_4/SiO_2 (c, d), and Na_2WO_4-TiO_2/SiO_2 (e, f).

The BET surface areas, pore sizes, and pore volumes of the catalysts were measured using an N_2-sorption analyzer. For comparison, the commercial SiO_2 support (surface area of 85–115 m^2/g, amorphous fumed silica, Alfa Aesar) was also dried and calcined using the same method as the catalyst preparation without adding any metal precursors and conducting the BET measurement. As presented in Table 1 and Fig. 8, the isotherm plot of the SiO_2 support was similar to that of the TiO_2/SiO_2 catalyst, in which no hysteretic loop was observed. This indicated that the SiO_2 support and the TiO_2/SiO_2 catalyst are non-porous material, and thus their porous sizes and volumes must have been created from the inter-particles. However, the surface area of the SiO_2 support was lower than that of the TiO_2/SiO_2 catalyst, suggesting that the TiO_2 particles potentially deposited on the surface of SiO_2 and create new surfaces, and thus the surface area of the TiO_2/SiO_2 catalyst increased. The surface areas of the Na_2WO_4/SiO_2 and Na_2WO_4-TiO_2/SiO_2 catalysts were much lower than those of the SiO_2 support and the TiO_2/SiO_2 catalyst. This was consistent with the observations from using the FE-SEM (Fig. 6.) & TEM (Fig. 7.) images, in which the particle sizes of the catalysts containing Na_2WO_4 were larger than those of the TiO_2 catalyst. The hysteretic loops of the Na_2WO_4/SiO_2 and Na_2WO_4-TiO_2/SiO_2 catalysts were similar, in which the pore sizes and the pore volumes generated from the intra-particles and the pore sizes were classified as a meso-porous material. Although the Na_2WO_4-TiO_2/SiO_2 catalyst had a quite small specific surface area, this catalyst had the highest C_{2+} yield, indicating that the synergistic catalyst effect or the selected active components plays a significant role in the catalytic performance.

Table 1. BET surface area (S.A.), pore size, and pore volume of TiO_2/SiO_2, Na_2WO_4/SiO_2, and Na_2WO_4-TiO_2/SiO_2 compared with pure SiO_2 support.

Material	S.A. (m^2/g)	Pore size (nm)	Pore volume (cm^3/g)
SiO_2	86.5	22.2	0.480
Na_2WO_4 / SiO_2	6.5	9.1	0.015
TiO_2 / SiO_2	106.2	17.5	0.460
Na_2WO_4-TiO_2/ SiO_2	5.4	10.0	0.013

The FT-IR patterns of the catalysts are presented in Fig. 9. All three catalysts displayed the Si—O—Si rocking, the Si—O—Si bending, and the Si—O—Si stretching peaks appearing around 490, 800, and 1100 cm^{-1}, respectively. There was one different peak appearing at 621 cm^{-1} for Na_2WO_4-TiO_2/SiO_2 and Na_2WO_4/SiO_2, specifying the existence of α-cristobalite [19] in these two catalysts, in good agreement with the findings in Fig. 5. As can be seen by the catalyst activities presented in Fig. 1, the Na_2WO_4-TiO_2/SiO_2 catalyst had a C_{2+} yield greater than those of the two single catalysts. Thus, one of the important keys that can be considered to improve the C_{2+} yield is to have a catalyst consisting of α-cristobalite interacting with an active crystalline metal oxide.

DOI:10.4186/ej.2019.23.5.169

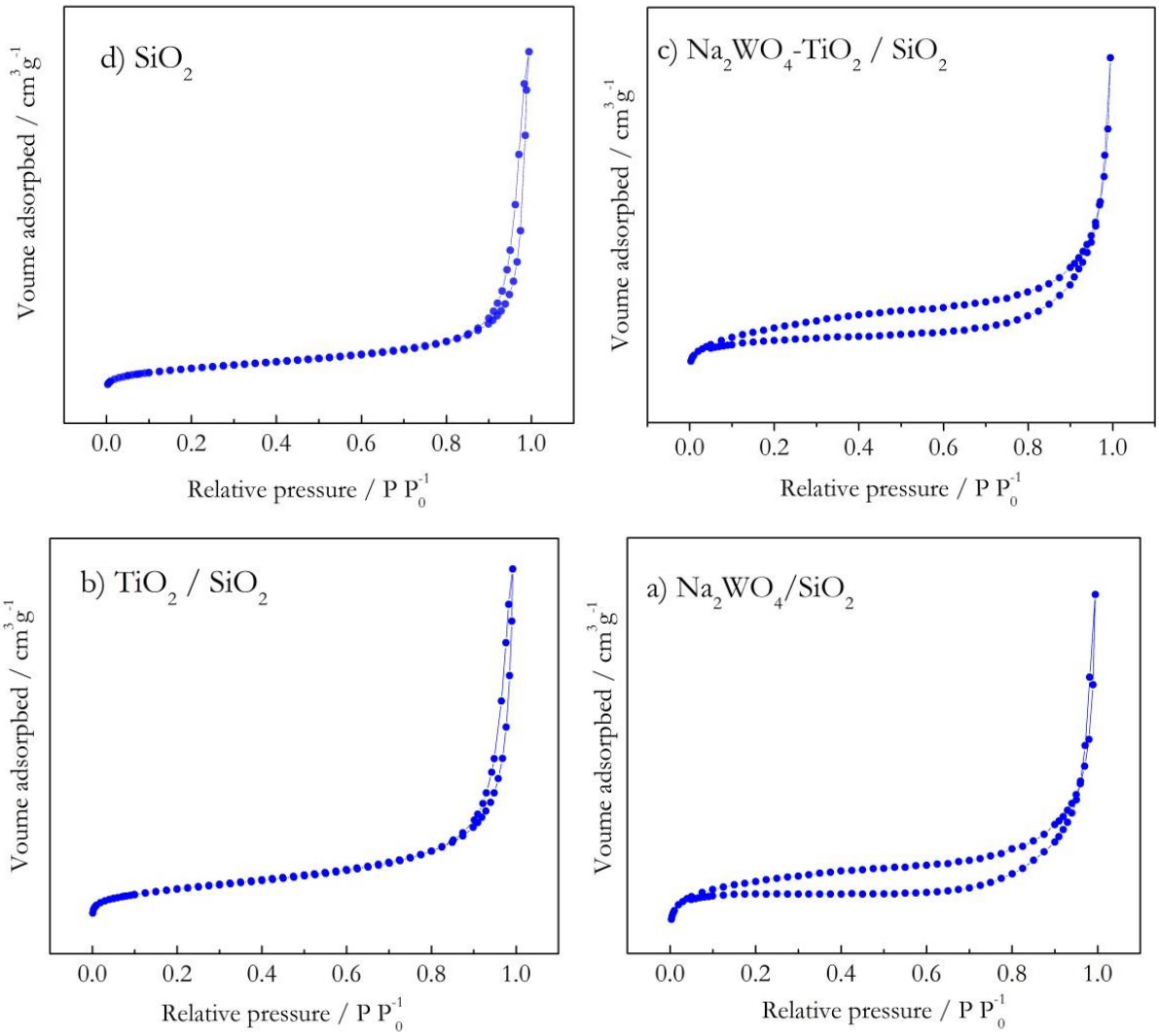

Fig. 8. Isotherm plots of (a) Na_2WO_4/SiO_2 catalyst, (b) TiO_2/SiO_2 catalyst, (c) Na_2WO_4-TiO_2/SiO_2 catalyst, and (d) pure SiO_2 support.

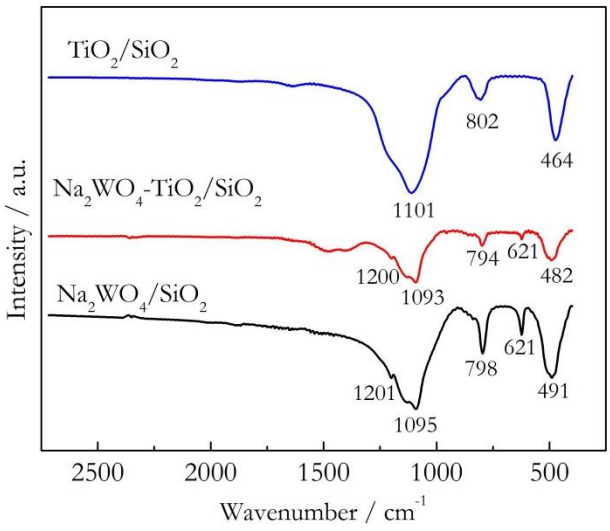

Fig. 9. FT-IR spectra of Na_2WO_4-Ti/SiO_2, Na_2WO_4/SiO_2, and TiO_2/SiO_2 catalysts.

Figure 10 presents the XPS spectra of the catalysts. The XPS scans were carried out in the range of the Na, W, and Ti regions. The observed peaks corresponded to Na_2O (1s = 1071.5 eV) WO_4^{2-}($4f_{5/2}$ = 37.6 eV, $4f_{7/2}$ = 35.3 eV) for Na_2WO_4/SiO_2 and ($4f_{5/2}$ = 37.8 eV, $4f_{7/2}$ = 35.3 eV) for Na_2WO_4-TiO_2/SiO_2, and TiO_2 ($2p_{3/2}$ = 464.2 eV, $2p_{1/2}$ = 459.2 eV) for TiO_2/SiO_2 and ($2p_{3/2}$ = 464.5 eV, $2p_{1/2}$ = 458.8 eV) for Na_2WO_4-TiO_2/SiO_2. Of interest was that the peaks of $WO_4^{2-}$and TiO_2 shifted toward a higher binding energy when Na_2WO_4 and TiO_2 were present in the same catalyst. This was because the Ti or W species are more likely to attach to WO_4^{-2} or O^{2-} bonding with Ti, which is an electron withdrawing group. Thus, the oxidation state of Ti or W has a higher positive charge, and thus shifts in the binding energies can be observed.

Catalyst reducibility and the interaction between the active catalysts and the support were examined using the H_2-TPR technique (see Fig. 11). For the TiO_2/SiO_2 catalyst, no clear H_2 reduction peak could be seen in this temperature range, consistent with previous reports [21, 22]. For Na_2WO_4/SiO_2, a broad reduction peak starting from 450 ºC to above 900 ºC with a maximum H_2 consumption at about 800 ºC was observed, indicating the reduction of W species [22]. The reduction behavior of the Na_2WO_4-TiO_2/SiO_2 catalyst was related to that of the Na_2WO_4/SiO_2 catalyst. However, the starting reduction temperature and the maximum temperature of the Na_2WO_4-TiO_2/SiO_2 catalyst shifted toward a higher temperature (approximately 50 ºC greater than those of the Na_2WO_4/SiO_2 catalyst). This suggested that the redox properties of these metal species substantially change, probably because there is a strong interaction between the WO_4^{2-} component and the TiO_2 crystals [22].

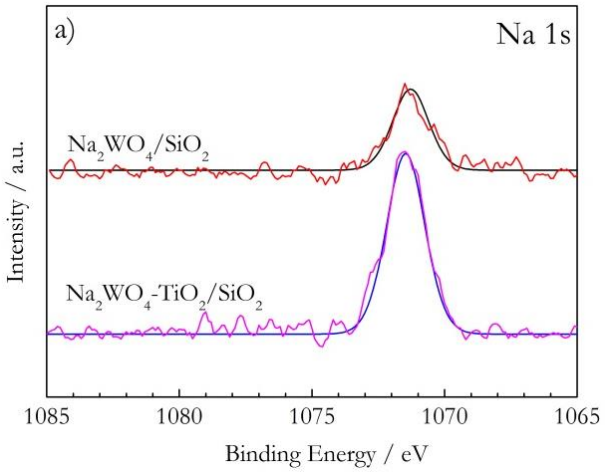

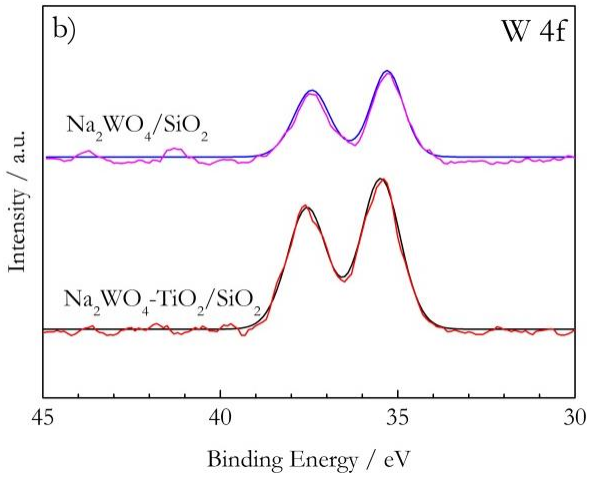

DOI:10.4186/ej.2019.23.5.169

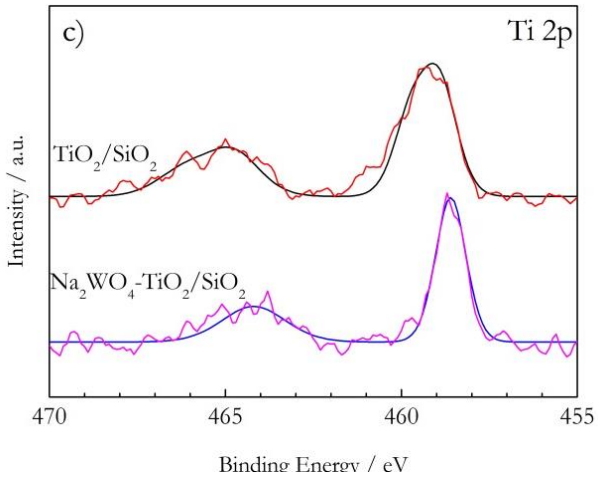

Fig. 10. XPS spectra of Na_2WO_4-Ti/SiO_2, Na_2WO_4/SiO_2, and TiO_2 /SiO_2 showing scanning in the (a) Na, (b) W, and (c) Ti ranges.

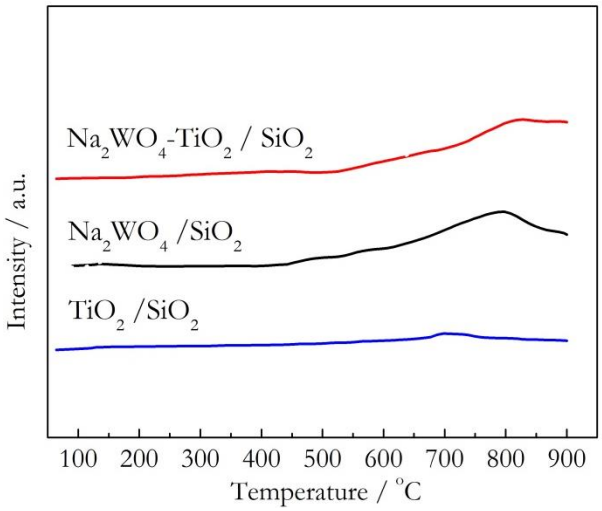

Fig. 11. H_2-TPR patterns of Na_2WO_4-TiO_2/SiO_2, Na_2WO_4/ SiO_2, and TiO_2/SiO_2.

In previous reports on the activity of catalysts containing Na_2WO_4 and SiO_2 for OCM reaction, there have been some suggestions about the enhancement of those catalysts as follows. Ji, et al. stated that the existence of the α-cristobalite phase was a critical necessity for the C_{2+} formation of catalysts containing Na_2WO_4 and SiO_2 for OCM reaction [9]. Elkins, et al. claimed that the interaction between the α-cristobalite structure and the WO_4^{2-} tetrahedron structure was crucial in the generation of C_{2+} and the inter-phase between these two components was the active surface species. Moreover, the WO_4^{2-} tetrahedron could stabilize the Mn_2O_3 and Na_2WO_4 phases, so that the catalysts could maintain their high activity during the reaction [23]. Furthermore, Palermo, et al. suggested that Na played dual roles in promoting the activity of MnO_x-Na_2WO_4/SiO_2 catalysts by acting as both a chemical and a structural promoter [24, 25]. From these reports, it can be certainly claimed that the presence of the α-cristobalite structure, the crystalline Na_2WO_4, and the anatase-TiO_2 crystals in the Na_2WO_4-TiO_2/SiO_2 catalyst strongly enhances the activity of the catalyst and is crucial for the formation of C_{2+} in the reaction.

4. Conclusions

The combination of 5wt% TiO_2 and 5wt% Na_2WO_4 on SiO_2 support (i.e. Na_2WO_4-TiO_2), prepared using the co-impregnation method, was superior to the single catalysts of its component (i.e. Na_2WO_4/SiO_2, TiO_2/SiO_2). In studying the operating conditions by co-feeding N_2 gas as a diluent gas into the reactant

gases at different volume ratios and different temperatures, the maximum C_{2+} yield was found at an $N_2/(4CH_4{:}1O_2)$ feeding gas ratio 1:1 by volume and at 700 ºC. The Na_2WO_4-TiO_2 catalyst produced the highest C_{2+} yield at 4.9% with 71.7% C_{2+} selectivity and 6.8% CH_4 conversion under these optimal operating conditions. Furthermore, the activity of the catalyst had good stability over 24 h of testing. Characterization of the Na_2WO_4-TiO_2 catalyst using XRD and FT-IR showed that α-cristobalite and crystalline anatase-TiO_2 were present. These two crystal components played a significant role in the formation of C_{2+} for the OCM reaction. The FE-SEM, TEM, and BET results were in good agreement with the findings of the XRD and FT-IR analyses. Of great interest for future study is the analysis of the kinetic mechanism of the catalyst for OCM reaction or improvement of the catalyst activity by adding promoters.

Acknowledgements

We would like to thanks the Thailand Research Fund and the Commission on Higher Education (grant numbers IRG5980004 & MRG6180232); the National Nanotechnology Center (NANOTEC), NSTDA, Ministry of Science and Technology, Thailand, through its program of Research Network NANOTEC (RNN); the Center of Excellence on Petrochemical and Materials Technology; the Kasetsart University Research and Development Institute (KURDI); and the Department of Chemical Engineering and the Faculty of Engineering at Kasetsart University for financial supports. P. Kidamorn received funding through a scholarship from the Faculty of Engineering at Kasetsart University.

References

[1] G. J. Hutchings, M. S. Scurrell, and J. R. Woodhouse, "Oxidative coupling of methane using oxide catalyst," *Chem. Soc. Rev.*, vol. 18, pp. 251-283, 1989.

[2] M. Y. Sinev, Z. T. Fattakhova, V. I. Lomonosov, and Y. A. Fordienko, "Kinetics of oxidative coupling of methane: bridging the gap between comprehension and description," *J. Nat. Gas Chem.*, vol. 18, pp. 273-287, 2009.

[3] K. Khammona, S. Assabumrungrat, and W. Wiyarath, "Reviews on coupling of methane over catalysts for application in C_2 hydrocarbon production," *J. Eng. Appl. Sci.*, vol. 7, pp. 447-455, 2012.

[4] S. M. K. Shahri and A. N. Pour, "Ce-promoted Mn/Na_2WO_4/SiO_2 catalyst for oxidative coupling of methane at atmospheric pressure," *J. Nat. Gas Chem*, vol. 19, pp. 47-53, 2010.

[5] R. Mariscal, M. A. Pena, and J. L. G. Fierro, "Promoter effects of dichloromethane on the oxidative coupling of methane over MnMgO catalysts," *Appl. Catal., A*, vol. 131, pp. 243-261, 1995.

[6] V. R. Choudhary, V. H. Rane, and S. T. Chaudhari, "Factors influencing activity/selectivity of La-promoted MgO catalyst prepared from La- and Mg- acetates for oxidative coupling of methane," *Fuel*, vol. 79, pp. 1487-1491, 2000.

[7] Z. Gholipour, A. Malekzadeh, R. Hatami, Y. Mortazavi, and A. Khodadadi,"Oxidative coupling of methane over (Na_2WO_4+Mn or Ce)/SiO_2 catalysts: In situ measurement of electrical conductivity," *J. Nat. Gas Chem*, vol. 19, pp. 35-42, 2010.

[8] R. T. Yunarti, M. Lee, Y. J. Hwang, D. J. Suh, J. Lee, I. W. Kim, and J. M. Ha, "Transition metal-doped TiO_2 nanowire catalysts for the oxidative coupling of methane," *Catal. Commun*, vol. 50, pp. 54-58, 2014.

[9] S. Ji, T. Xiao, S. Li, L. Chou, B. Zhang, C. Xu, R. Hou, A. P. E. York, and M. L. H Green, "Surface WO_4 tetrahedron: The essence of the oxidative coupling of methane over M-W-Mn/SiO_2 catalysts," *J. Catal.*, vol. 220, pp. 47-56, 2003.

[10] J. Y. Lee, W. Jeon, J. W. Choi, Y. W. Suh, J. M. Ha, D. J. Suh, and Y. K. Park, "Scaled-up production of C_2 hydrocarbons by the oxidative coupling of methane over pelletized Na_2WO_4/Mn/SiO_2 catalysts: Observing hot spots for the selective process," *Fuel.*, vol. 106, pp. 851-857, 2013.

[11] A. Malekzadeh, A. Khodadadi, A. K. Dalai, and M. Abedini, "Oxidative coupling of methane over Lithium doped (Mn+W)/SiO_2 catalysts," *J. Nat. Gas Chem*, vol. 16, pp. 121-129, 2007.

[12] J. Wang, L. Chou, B. Zhang, H. Song, J. Zhao, J. Yang, and S. Li, "Comparative study on oxidation of methane to ethane and ethylene over Na_2WO_4-Mn/SiO_2 catalysts prepared by different methods," *J. Mol. Catal. Chem.*, vol. 245, pp. 272-277, 2006.

[13] N. Hiyoshi and T. Ikeda, "Oxidative coupling of methane over alkali chloride-Mn-Na_2WO_4/SiO_2 catalysts: Promoting effect of molten alkali chloride," *Fuel Process. Technol.,* vol. 133, pp. 29-34, 2015.
[14] T. W. Elkins and H. E. Hagelin-Weaver, "Characterization of Mn-Na_2WO_4/SiO_2 and Mn-Na_2WO_4/MgO catalysts for the oxidative coupling of methane," *Appl. Catal., A*, vol. 497, pp. 96-106, 2015.
[15] F. Papa, D. Gingasu, L. Patron, A. Miyazaki, and I. Balint, "On the nature of active sites and catalytic activity for OCM reaction of alkaline-earth oxides-neodymia catalytic systems," *Appl. Catal., A,* vol. 375, pp. 172-178, 2010.
[16] V. H. Rane, S. T. Chaudhari, and V. R. Choudhary, "Oxidative coupling of methane over La-promoted CaO catalysts: Influence of precursors and catalyst preparation method," *J. Nat. Gas Chem.*, vol. 19, pp. 25-30, 2010.
[17] D. J. Wang, M. P. Rosynek, and J. H. Lunsford, "Oxidative coupling of methane over oxide-supported sodium-manganese catalysts," *J. Catal.*, vol. 155, pp. 390-402, 1995.
[18] F. Basile, G. Fornasari, F. Trifiro, and A. Vaccari, "Partial oxidation of methane: Effect of reaction parameters and catalyst composition on the thermal profile and heat distribution," *Catal. Today*, vol. 64, pp. 21-30, 2001.
[19] S. Ji, T. Xiao, S. Li, L. Chou, B. Zhang, C. Xu, R. Hou, A. P. E York, and M. L. H Green, "Surface WO_4 tetrahedron: the essence of the oxidative coupling of methane over M·W·Mn/SiO_2 catalysts," *J. Catal.*, vol. 220, pp. 47-56, 2003.
[20] A. M. Venezia, F. Raimondi, V. La Parola, and G. Deganello, "Influence of sodium on the structure and HDS activity of Co-Mo catalysts supported on silica and aluminosilicate," *J. Catal.*, vol. 194, pp. 393-400, 2000.
[21] T. Chukeaw, A. Seubsai, P. Phon-in, K. Charoen, T. Witoon, W. Donphai, P. Parpainainar, M. Chareonpanich, D. Noon, B. Zohour, and S. Senkan, "Multimetallic catalysts of RuO_2–CuO–Cs_2O–TiO_2/SiO_2 for direct gas-phase epoxidation of propylene to propylene oxide," *RSC Adv.*, vol. 6, pp. 56116-56126, 2016.
[22] J. Li, G. Lu, G. Wu, D. Mao, Y. Guo, Y. Wang, and Y.Guo, "Effect of TiO_2 crystal structure on the catalytic performance of Co_3O_4/TiO_2 catalyst for low-temperature CO oxidation," *Catal. Sci. Technol.*, vol. 4, pp. 1268-1275, 2014.
[23] T. W. Elkins, and H. E. Hagelin-Weaver, "Characterization of Mn-Na_2WO_4/SiO_2 and Mn-Na_2WO_4/MgO catalysts for the oxidative coupling of methane," *Appl. Catal., A*, vol. 497, pp. 96-106, 2015.
[24] A. Palermo, J. P. H Vazquez, A. F. Lee, M. S. Tikhov, and R. M. Lambert, "Critical influence of the amorphous silica-to-cristobalite phase transition on the performance of Mn/Na_2WO_4/SiO_2 catalysts for the oxidative coupling of methane," *J. Catal.*, vol. 177, pp. 259-266, 1998.
[25] Y. T. Chua, A. R. Mohamed, and S. Bhatia, "Oxidative coupling of methane for the production of ethylene over sodium-tungsten-manganese-supported-silica catalyst (Na-W-Mn/SiO_2)," *Appl. Catal., A*, vol. 343, pp. 142-148, 2008.

Catalysis Today xxx (xxxx) xxx–xxx

Contents lists available at ScienceDirect

Catalysis Today

journal homepage: www.elsevier.com/locate/cattod

Investigation of metal oxide additives onto Na_2WO_4-Ti/SiO_2 catalysts for oxidative coupling of methane to value-added chemicals

Sarannuch Sringam[a], Phattaradit Kidamorn[a], Thanaphat Chukeaw[a,b], Metta Chareonpanich[a,b,c], Anusorn Seubsai[a,b,c,*]

[a] Department of Chemical Engineering, Faculty of Engineering, Kasetsart University, Bangkok, 10900, Thailand
[b] Center of Excellence on Petrochemical and Materials Technology, Kasetsart University, Bangkok, 10900, Thailand
[c] Research Network of NANOTEC–KU on NanoCatalysts and NanoMaterials for Sustainable Energy and Environment, Kasetsart University, Bangkok, 10900, Thailand

ARTICLE INFO

Keywords:
Catalyst
Manganese oxide
Oxidative coupling of methane
Sodium tungstate
Titanium dioxide

ABSTRACT

The oxidative coupling of methane (OCM) is a closely related reaction process involving the transformation of methane (CH_4) and O_2 mixtures into value-added chemicals such as ethylene and ethane (i.e. C_{2+}). This work presents the effects of metal oxide additives into the Na_2WO_4-Ti/SiO_2 catalyst on the performance of the OCM reaction. Several metal oxide additives—including oxides of Co, Mn, Cu, Fe, Ce, Zn, La, Ni, Zr, Cr, and V—were investigated with the Na_2WO_4-Ti/SiO_2 catalyst. All of the catalysts were prepared using co-impregnation and the catalyst activity test was performed in a plug flow reactor at a reactor temperature range of 600–800 °C and atmospheric pressure. The physicochemical properties of the prepared catalysts relating to their catalytic activity were discussed by using the information of X-ray diffraction (XRD), X-ray photoelectron spectroscopy (XPS), and scanning electron microscopy (SEM) measurements. Na_2WO_4-Ti/SiO_2 added Mn was found to be the most active catalyst, involving shifts of binding energies of W 4f and Ti 2p toward lower binding energies. Moreover, a variety of operating conditions—including reactant- to-nitrogen gas ratio, catalyst mass, reactor temperature, and total feed flow rate—were intensively examined for the OCM reaction using the Na_2WO_4-Ti-Mn/SiO_2 catalyst. The maximum C_{2+} yield was subsequently discovered at 22.09% with 62.3% C_{2+} selectivity and 35.43% CH_4 conversion. Additionally, the stability of the Na_2WO_4-Ti-Mn/SiO_2 catalyst was also monitored with time on stream for 24 h.

1. Introduction

Methane (CH_4) is the primary component of natural gas and biogas. It is considered a greenhouse gas about 25 times stronger than CO_2 if these two gases are released to the atmosphere in the same amount [1]. Since CH_4 is abundant on Earth, it is highly attractive to worldwide researchers to explore strategies to transform it into more useful products. One of the most challenging methods is the oxidative coupling of methane (OCM), which is a type of chemical reaction using air or oxygen directly reacting with CH_4 to produce useful hydrocarbons such as ethylene, ethane, propene, propane, etc. (C_{2+}) [2–5]. In the absence or presence of a catalyst, the OCM reaction is exothermic and normally takes place in reaction temperatures of 600–1,000 °C [6]. Moreover, CO and CO_2 can be produced as byproducts. However, it is believed that if a suitable catalyst is present, the products can be controlled and the extreme reaction temperature can be reduced.

Previously, several potential catalysts have been reported for the OCM reaction to C_{2+}, especially Mn modified with a variety of co-catalysts, supports, and/or promoters, such as oxides of Mg, Na, and Ce. The activity of those catalysts was approximately < 16% C_{2+} yield and 25–78% C_{2+} selectivity. Lately, a solid mixture of Na_2WO_4-Mn supported on SiO_2 has been greatly attractive to researchers worldwide, because this combination is highly active for the OCM reaction. The catalyst has also been modified with many metals (e.g. Li, Na, K, Ba, Ca, Fe, Co, Ni, Al, Ti, Ce, etc.) [7–9]. Some of these modified catalysts, especially Na_2WO_4-Mn/SiO_2 doped with TiO_2 [10,11], exhibited an improvement on both C_{2+} yield and selectivity (i.e. 16.8% C_{2+} yield and 73% C_{2+} selectivity). The addition of a promoter into the Na_2WO_4-Mn/SiO_2 catalyst (e.g. LiCl, NaCl, KCl, or CsCl) has also been found to result in the incorporation of the promoter into the catalytic material, thus increasing the number of strong basic sites, thereby enhancing the catalyst activity [12–14].

Recently, we have found a combination of Na_2WO_4 and Ti-supported SiO_2 exhibiting high activity for the OCM reaction, giving 4.9%

* Corresponding author at: Department of Chemical Engineering, Faculty of Engineering, Kasetsart University, Bangkok, 10900, Thailand.
E-mail address: fengasn@ku.ac.th (A. Seubsai).

https://doi.org/10.1016/j.cattod.2020.03.048
Received 2 March 2019; Received in revised form 19 February 2020; Accepted 25 March 2020

C_{2+} yield with 71.7% C_{2+} selectivity and 6.8% CH_4 conversion at a reactor temperature of 700 °C and atmospheric pressure [15]. The activity of the catalyst had good stability over 24 h of on-stream testing. Moreover, a crystalline structure of α-cristobalite of SiO_2 that was present along with TiO_2 crystals was found to substantially enhance the activity of the catalyst for the OCM reaction to C_{2+}. Therefore, improve the activity of this catalyst is of great interest. Herein, we modify the catalyst by adding a metal oxide additive into the Na_2WO_4-Ti/SiO_2 catalyst. The selected metal oxide additives include Co, Mn, Cu, Fe, Ce, Zn, La, Ni, Zr, Cr, and V. The most active catalyst is subsequently chosen to optimize the C_{2+} yield by varying operating conditions. Additionally, advanced instrument techniques are also used to analyze the prepared catalysts to acquire their physicochemical properties to relate with their catalytic activity.

2. Experimental

2.1. Catalyst preparation

All of the catalysts were prepared using co-impregnation as follows. Weights of Na_2WO_4 (Na_2WO_4•$2H_2O$, 98.0 ~ 101.0%, Daejung), Ti ($C_{12}H_{28}O_4Ti$, 97 + %, Alfa Aesar), and X (X = Co, Mn, Cu, Fe, Ce, Zn, La, Ni, Zr, Cr, or V) were determined and pipetted from each stock precursor solution into amorphous fume SiO_2 (surface area of 85-115 m^2/g, Alfa Aesar) to obtain a desired weight percentage of the metal components. Note that the precursor of the 11 elements was in the form of metal nitrate hydrate, and the weight percentage of each component on the support was calculated based on the formula appearing in each catalyst's name. For example, for the Na_2WO_4-Ti-Mn/SiO_2 catalyst, the weights of Na_2WO_4, Ti(0), and Mn(0) were determined and loaded onto the SiO_2 support. After that, the mixture was stirred at room temperature for 2 h and heated to 120 °C until dried. Then, the dried powder was set to calcine in an air furnace at 800 °C for 4 h. Finally, the powder was ground until a fine powder was obtained. The weight percentage of each component for each catalyst will be elaborated in the results and discussion of that mentioned figure.

2.2. Catalytic activity test

The activity of each prepared catalyst for the OCM reaction was evaluated in a plug flow reactor at atmospheric pressure. The reactor temperature was set in the range of 600–800 °C. A catalyst (8–72 mg) was packed in a quartz tube reactor (0.5 cm inner diameter) and sandwiched between layers of quartz wool. The feed gas consisted of methane (CH_4, 99.999%, Praxair), oxygen (O_2, 99.999%, Praxair), and nitrogen (N_2, 99.999%, Praxair) at a volume ratio of CH_4:O_2:N_2 = 3:1:0, 3:1:2, or 3:1:4 with a total feed flow rate in the range of 35–95 mL/min. The effluent gas was evaluated using an online gas chromatograph (SHIMADZU, GC-14A) equipped with a flame ionization detector (FID; for analyzing C_2H_4, C_2H_6, C_3H_6, C_3H_8 and C_4H_8, and C_4H_{10}) and a thermal conductivity detector (TCD; for analyzing CO, CO_2, and CH_4). The activity of each catalyst was analyzed after the system had reached a set point of 2 h. Equations (1)–(4) show the formulas for calculating the %CH_4 conversion, %C_{2+} selectivity, %CO_x selectivity, and %C_{2+} yield.

$$\%\,CH_4\ \text{conversion} = \frac{\text{moles of } CH_4 \text{ input} - \text{moles of } CH_4 \text{output}}{\text{moles of } CH_4 \text{ input}} \times 100 \quad (1)$$

$$\%\,C_{2+}\ \text{selectivity} = \frac{\text{moles of } C_{2+}}{\text{Total moles of products}} \times 100 \quad (2)$$

$$\%\,CO_x\ \text{selectivity} = \frac{\text{moles of } CO_x}{\text{Total moles of products}} \times 100 \quad (3)$$

$$\%\,C_{2+}\ \text{yield} = \frac{\%\,CH_4\ \text{conversion} \times \%\,C_{2+}\text{selectivity}}{100} \quad (4)$$

2.3. Catalyst characterization

The X-ray diffraction (XRD) patterns of each catalyst were obtained using a powder X- ray diffractometer (PXRD; JEOL JDX-3530 and Philips X-Pert, using Cu-K_α radiation, 45 kV and 40 mA). The electronic states of selected elements in each catalyst were examined using X-ray photoelectron spectroscopy (XPS; Kratos Axis Ultra DLD) with Al Kα for the X-ray source. The surface morphology of the samples was imaged using a scanning electron microscope (SEM, FE-SEM: JEOL JSM7600 F).

3. Results and discussion

3.1. Activity of Na_2WO_4-Ti/SiO_2 added metal oxide additives

In catalyst screening experiments for the OCM reaction in our laboratory, we have found that 5 wt% Na_2WO_4 + 5 wt% Ti on SiO_2 (denoted as Na_2WO_4-Ti/SiO_2) showed a priming result for C_{2+} production. We also found, from an XPS measurement of the catalyst, that the form of Ti was TiO_2 (data are not shown here). In this work, the Na_2WO_4-Ti/SiO_2 catalyst was further investigated by adding 11 elements, Co, Mn, Cu, Fe, Ce, Zn, La, Ni, Zr, Cr, and V. These 11 elements were selected from the transition metals because of their availability, non-toxicity, inexpensiveness, and, more importantly, inactiveness for CH_4 combustion [16]. All of the Na_2WO_4-Ti/SiO_2 catalysts with added metal oxide additive were prepared using a metal ratio of Na_2WO_4:Ti:X = 5:5:2 (where X is an metal oxide additive and its weight is calculated on the basis of the metallic form). The total metal loading was 12 wt% for every catalyst, except Na_2WO_4-Ti/SiO_2 (i.e. 5 wt% Na_2WO_4 + 5 wt % Ti). The activity test results of the catalysts are presented in Fig. 1.

Under the same testing conditions, the catalyst without metal oxide additive exhibited 4.43% C_{2+} yield with 33.8% C_{2+} selectivity and 13.34% CH_4 conversion. The most promising catalyst was the addition of Mn into the Na_2WO_4-Ti/SiO_2 catalyst, yielding 9.97% with 35.0% C_{2+} selectivity and 29.48% CH_4 conversion. The other metal oxides, which were added into the Na_2WO_4-Ti/SiO_2 catalyst and gave a C_{2+} yield higher than that of the catalyst without metal oxide additive, were (in order) Co > Fe > Ce > Zn, giving C_{2+} yield in a range of 4.50–7.65%. The addition of Mn clearly greatly improved the activity of

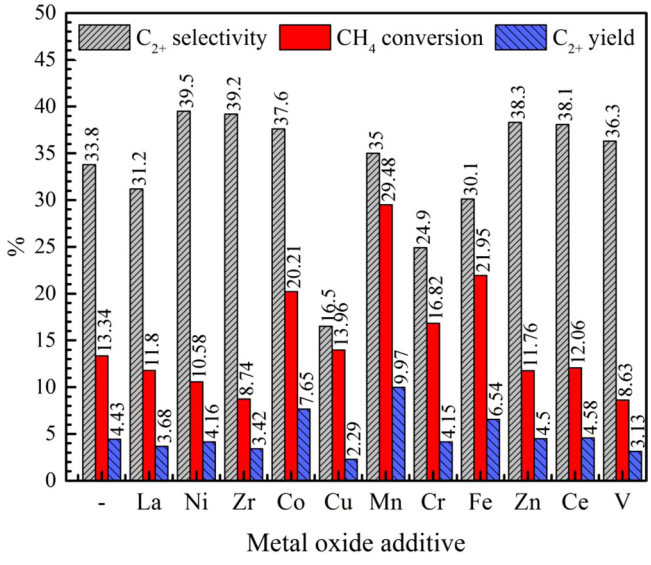

Fig. 1. Catalyst activity of Na_2WO_4-Ti/SiO_2 added metal oxide additives. Reaction conditions: CH_4:O_2:N_2 ratio = 3:1:0, catalyst weight = 8 mg, total feed flow rate of 35 mL/min, reactor temperature = 700 °C.

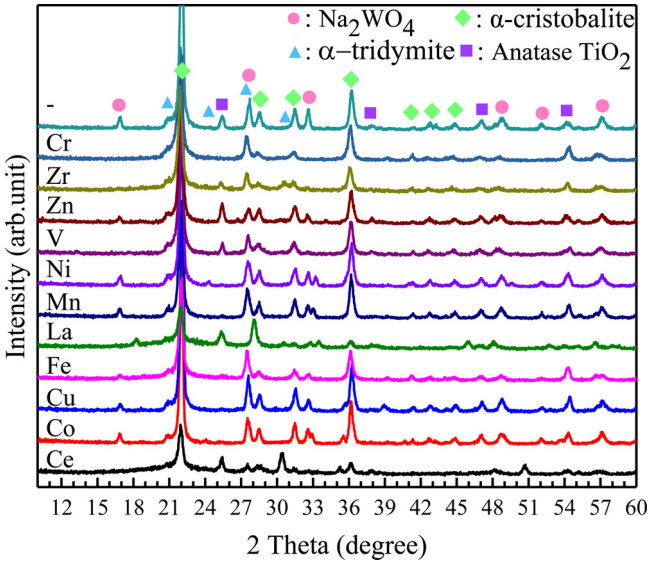

Fig. 2. XRD patterns of Na_2WO_4-Ti/SiO_2 catalyst added metal oxide additives, fixing wt% of Na_2WO_4:Ti:X = 5:5:2 and SiO_2 balance.

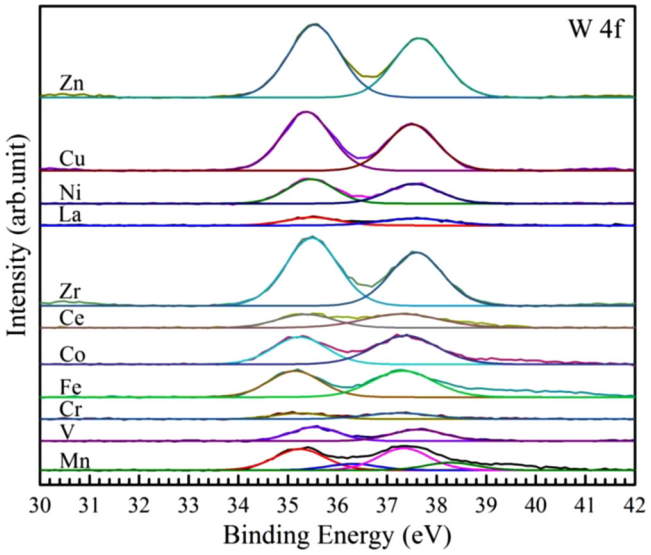

Fig. 3. XPS spectra of Na_2WO_4-Ti/SiO_2 added different metal oxide additives showing binding energy in the range of W4f.

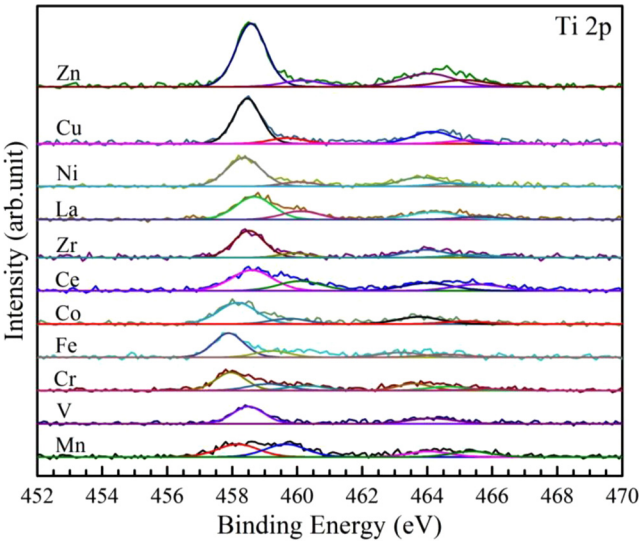

Fig. 4. XPS spectra of Na_2WO_4-Ti/SiO_2 added different metal oxide additives showing binding energy in the range of Ti2p.

Na_2WO_4-Ti/SiO_2. The characterization using XRD and XPS of these catalysts will reveal how the activities of some catalysts improve, which will be presented in the next section.

3.2. XRD and XPS analyses of Na_2WO_4-Ti/SiO_2 added metal oxide additives

XRD patterns of the Na_2WO_4-Ti/SiO_2 catalysts with added metal oxide additives are presented in Fig. 2. The characteristic peaks of *α*-cristobalite (2θ = 22.1, 28.6, 31.5, 36.1, 41.2, 42.9, and 44.9 (ICDD No. 00-001-0438)) appeared for all catalysts. A small XRD peak indicating the presence of *α*-tridymite (2θ = 21.8, 23.3, 27.3, and 30.1 (ICDD No. 00-003-0227)) was also observed. The characteristic peaks of Na_2WO_4 (16.9, 27.8, 32.4, 48.8, 52.1, and 57.1 (ICDD No. 01-074-2369)) appeared in the Na_2WO_4 catalysts with no added (-), Zn, Ni, Mn, Fe, Cu, and Co. The characteristic peaks of TiO_2 (2θ = 25.2, 37.0, 48.0, 54.1, and 55.0 (ICDD No. 01-073-1764)) were seen in the Na_2WO_4 catalysts with no added (-), Zr, Zn, V, La, and Ce. It should be noted that the most active catalyst presented in Fig. 1 was Na_2WO_4-Ti-Mn/SiO_2. As shown in Fig. 2, this catalyst consisted of *α*-cristobalite, crystalline Na_2WO_4, and crystalline Mn_2O_3 (2θ = 33.1, 38.1, and 44.8 (ICDD No. 00-002-0896)). Hence, the presence of these crystalline phases is essential for the OCM reaction. For the role of Ti, its combination with Mn has been proposed in the form of the $MnTiO_3$ phase; then, the $MnTiO_3$ phase plays an important role in remarkably improving the catalyst activity [10,11]. However, no XRD peaks of $MnTiO_3$ can be observed in Fig. 2, probably because a small amount of Mn was loaded and/or the crystal species is too small to be detected.

The XPS spectra of all catalysts in the range of W (4f) and Ti (2p) regions are presented in Figs. 3 and 4, respectively. The observed peaks corresponded to WO_42-($4f_{5/2}$ ~ 37.6 eV, $4f_{7/2}$ ~ 35.4 eV) and TiO_2 ($2p_{1/2}$ ~ 464 eV, $2p_{3/2}$ ~ 459 eV). Of interest was that the peaks of $WO_42-$and TiO_2 of each catalyst were not identical. Perhaps, the addition of metal oxides influences the interaction of WO_4-2 or Ti bonding with O2−, thus leading to shifts of the binding energies [17–19].

The most interesting results are presented in Fig. 5, showing the plots of CH_4 conversion of each catalyst versus its binding energy of W $4f_{7/2}$ (Fig. 5a) and Ti $2p_{3/2}$ (Fig. 5b). The plots in each figure can be divided into two groups: group 1 (the catalysts containing Mn, Fe, Co, and Cr) and group 2 (the catalysts containing Cu, Zn, Ce, La, Ni, Zr, and V). The catalysts in group 1 possessed binding energies in a range of 35.12–35.24 eV for W $4f_{7/2}$ and 457.90–458.20 eV for Ti $2p_{3/2}$, while the catalysts in group 2 gave the XPS signal in a range of 35.36–35.56 eV for W $4f_{7/2}$ and 458.34–458.68 eV for Ti $2p_{3/2}$. It is interesting to see that the CH_4 conversions of the catalysts in group 1 were significantly higher than those in group 2. Moreover, the catalysts in group 1 clearly exhibited binding energies lower than the catalysts in group 2. Importantly, these findings suggest that the metal additives—that are able to shift the binding energies of W 4f and Ti 2p toward lower binding energies when added into the Na_2WO_4-Ti/SiO_2 catalyst—are highly active for the OCM reaction.

It is possible that when the binding energy of W 4f or Ti 2p shifts toward a lower binding energy, the energy to remove an electron from the outer electron layer of W or Ti will become lower [18]. This reveals that it becomes easier for an oxygen atom bonding with W or Ti to dissociate or leave from the center. In other words, when an oxygen molecule adsorbs onto an active site—WO_4^{2-} associated with Ti^{2+}—it will dissociate and bond with the center of W or Ti. Due to the influence of a metal oxide additive added into the catalyst, the oxygen atom can easily detach from and leave the active metal center as H_2O [18]. This

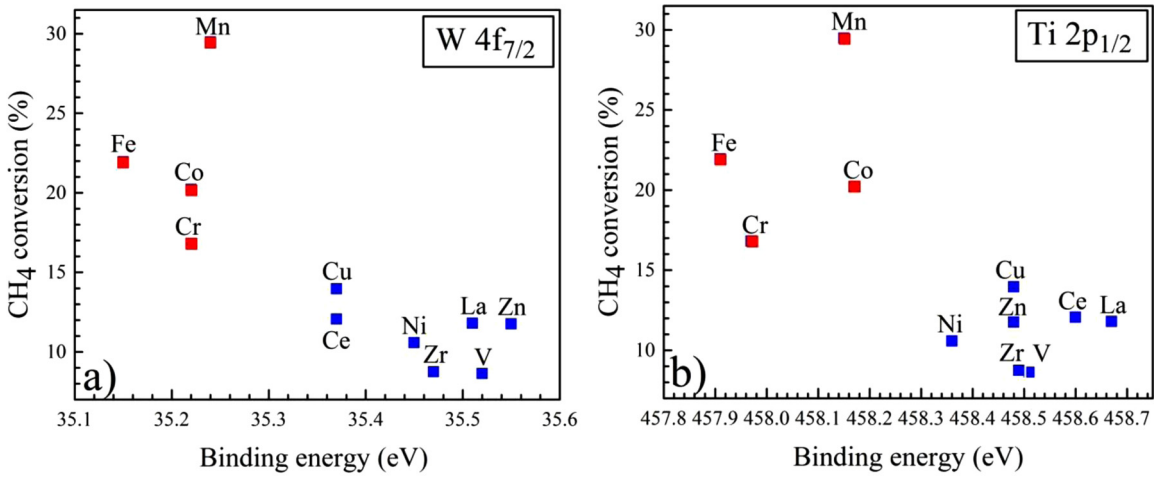

Fig. 5. Plots of correlation between CH_4 conversions and binding energies of a) W $4f_{7/2}$ and b) Ti $2p_{1/2}$.

proposed behavior can significantly enhance the reaction mechanism for OCM. As a result, the catalysts in group 1 exhibit a higher CH_4 conversion relative to those in group 2. Future studies, to deeply understand the reaction mechanism, are required.

3.3. Optimization of Na_2WO_4-Ti-Mn/SiO_2 catalyst for production of C_{2+}

The Na_2WO_4-Ti-Mn/SiO_2 catalyst was further optimized to increase C_{2+} yield by first varying the weight percentage of Mn into Na_2WO_4-Ti/SiO_2 from 0.0 to 2.5 wt%. The results are shown in Fig. 6. The C_{2+} yield was found to be optimized at 0.5 wt% Mn loading (12.16% C_{2+} yield with 39.7% C_{2+} selectivity and 30.62% CH_4 conversion, then the C_{2+} yields slightly decreased to approximately 9.6%). The decrease in the activity of the catalysts with Mn loading over 0.5 wt% could be due to the formation of MnO_x multilayers, which affects the generation of nucleophilic oxy species (e.g. O_2–, O_2^{2-}, and O–) [20]. SEM images of the catalysts shown in Fig. 6 are illustrated in Fig. 7. As shown, the surface morphology and particle size of all catalysts are similar. All the particles are irregularly shaped with various sizes, ranging from 50 nm to about 1 μm in diameter of coral reef-shaped particles. Nevertheless, the catalytic activity of each catalyst is different, probably due to differences in the distribution of the active Mn species (Mn_2O_3, $MnTiO_3$) in each catalyst.

The best Na_2WO_4-Ti-Mn/SiO_2 catalyst found in Fig. 6 was further

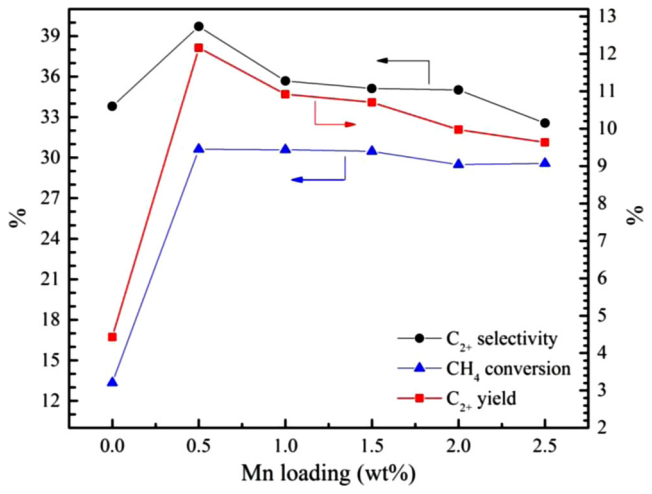

Fig. 6. Effect of Mn loading into Na_2WO_4-Ti/SiO_2. Reaction conditions: CH_4:O_2:N_2 ratio = 3:1:0, catalyst weight = 8 mg, total feed flow rate of 35 mL/min, reactor temperature = 700 °C.

investigated by varying catalyst amounts and reactant gas feeding ratios, while the total feed flow rate was fixed at 35 mL/min for every condition. Three reactant gas feeding ratios of CH_4:O_2:N_2 were used, including CH_4:O_2:N_2 = 3:1:0, 3:1:2, and 3:1:4. The results are plotted in Fig. 8. As expected, the activity of the catalyst increased on increasing the catalyst amount because the number of active sites increase as the catalyst amount increases. Consequently, more CH_4 can react with the active sites, thereby increasing the C_{2+} yields. The catalyst amount of each reactant gas feeding ratio that delivered the highest C_{2+} yield was 24, 48, and 64 mg, giving a C_{2+} yield of 19.19%, 19.61%, and 18.70% when the reactant gas feeding ratio of CH_4:O_2:N_2 was 3:1:0, 3:1:2, and 3:1:4, respectively. It should be noted that the optimal point of each condition is the point where the O_2 gas is completely consumed. Thus, after the optimal points, the CH_4 conversions should have been steady. However, the C_{2+} conversions minimally decreased with gradual decreases of C_{2+} yields, potentially because the C_{2+} products can further react with some special active sites to produce CO, CO_2, and even CH_4 [21–27]. Thus, the CH_4 conversion decreased as the catalyst amount increased.

The optimal catalyst amount of each condition found in Fig. 8 was selected to study the effect of reactor temperature at three different CH_4:O_2:N_2 feeding gas ratios, as shown in Fig. 9. For every feeding gas ratio, the C_{2+} selectivities, CH_4 conversions, and C_{2+}yields increased with increase in reactor temperatures, reaching an optimal value at 700 °C. The highest C_{2+} yield was achieved at 19.61% with 60.40% C_{2+} selectivity and 32.48% CH_4 conversion when the CH_4:O_2:N_2 feeding gas ratio was 3:1:2. At reactor temperatures above 700 °C, the catalyst activity for C_{2+} formation rapidly dropped, while the CH_4 conversions slowly decreased. It is possible that the C_{2+} products quickly combust in the presence of O_2 or react further easily with active sites at high reactor temperatures. Similar to the results in Fig. 8, the slow decreases of CH_4 conversion as reactor temperature rose were due to the additional CH_4 from the decomposition of C_{2+} [17,28–31].

In general, a fuel-rich condition (i.e. CH_4:O_2 ratio > 1.0) is more favorable for C_{2+} production in the OCM reaction. The complete combustion of CH_4 is strongly favorable under fuel-lean conditions. Therefore, the effect of CH_4:O_2 ratio on the activity of the optimal catalyst was studied, as shown in Fig. 10. The CH_4:O_2 ratios were varied from 1.0 to 3.0, for which the conditions ranged from fuel-lean to fuel-rich. The results evidently showed that the C_{2+} yields slowly increased as the CH_4:O_2 ratios were lowered. In other words, O_2 increases into the feed resulted in increases of C_{2+} yields and CH_4 conversions. Nonetheless, the C_{2+} selectivities significantly decreased. The results suggest that O_2 increases into the feed enhance the formations of CO and CO_2 more than those of C_{2+} products [9,26,27].

The effect of total feed flow rate of the Na_2WO_4-Ti-Mn/SiO_2 catalyst

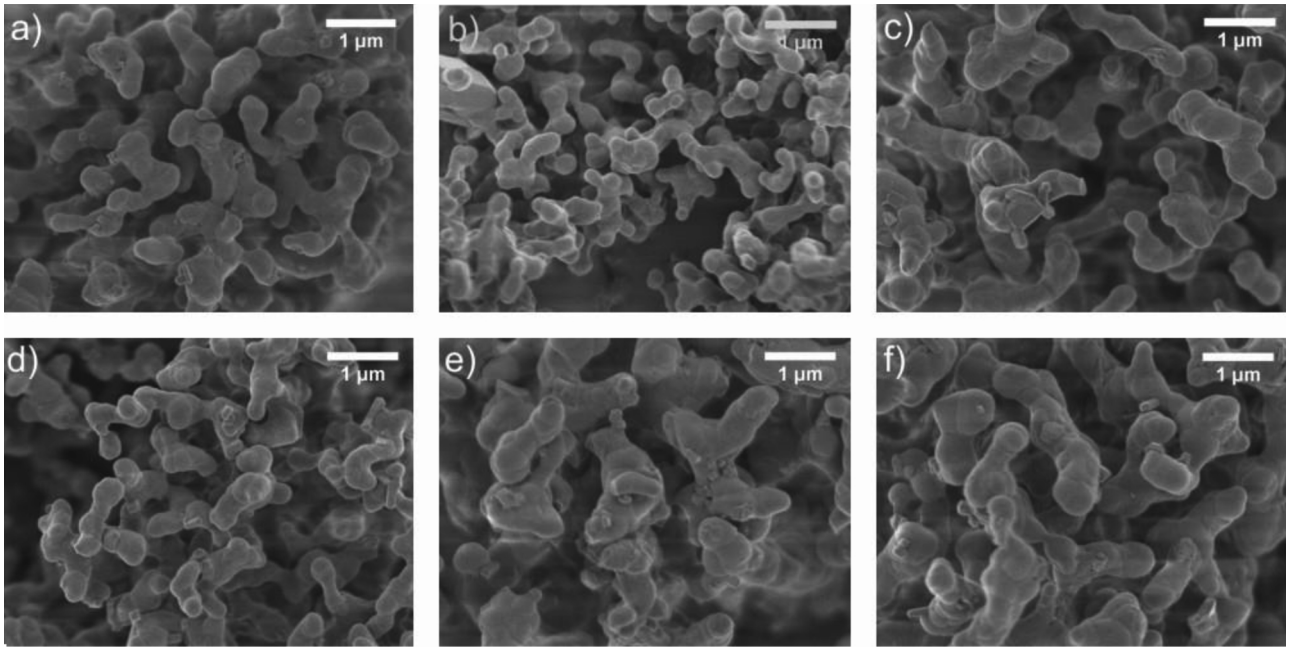

Fig. 7. SEM images of Na_2WO_4-Ti-Mn/SiO_2 catalysts at different Mn loadings: a) 0 wt%, b) 0.5 wt%, c) 1.0 wt%, d)1.5 wt%, e) 2.0 wt%, and f) 2.5 wt%.

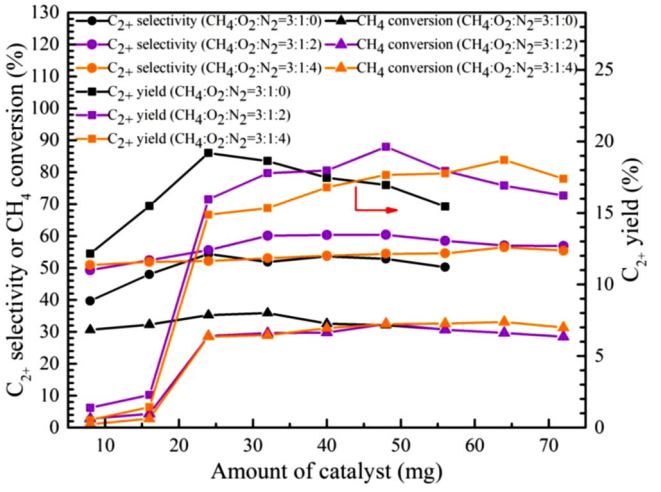

Fig. 8. Activity of Na_2WO_4-Ti-Mn/SiO_2 catalyst at different catalyst amounts and different CH_4:O_2:N_2 feeding gas ratios.

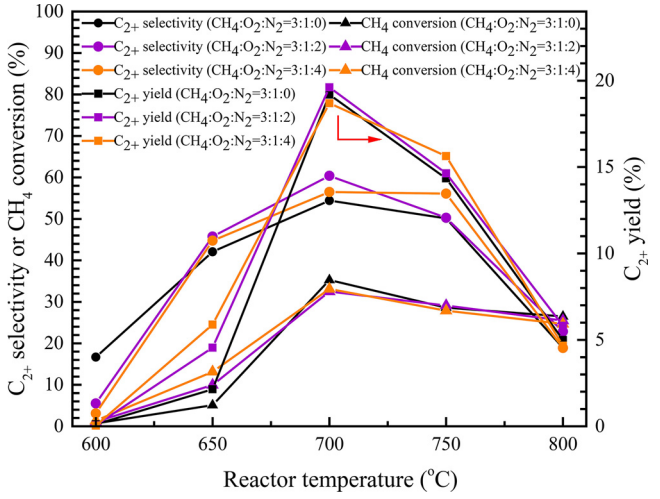

Fig. 9. Activity of Na_2WO_4-Ti-Mn/SiO_2 catalyst at different reactor temperatures and different CH_4:O_2:N_2 feeding gas ratios. Reaction conditions: catalyst weight = 24, 48, and 64 mg for CH_4:O_2:N_2 = 3:1:0, 3:1:2, and 3:1:4, respectively, total feed flow rate =35 mL/min.

for OCM reaction was also investigated as presented in Fig. 11. In general, a short resident time inside a porous catalyst favors C_{2+} selectivity because it reduces chances of combustion of C_{2+} products. The results remarkably showed that the C_{2+} yields and selectivities were achieved at approximately 20–22% and 60–62%, respectively, while the CH_4 conversions were slightly changed at approximately 32–35% when the total feed flow rate was in the range of 45–75 mL/min. At above 75 mL/min, the activity of the catalyst slowly decreased, potentially because the residence time or the contact time between the reactants and the catalyst was greatly reduced.

Lastly, a time-on-stream experiment over 24 h of the Na_2WO_4-Ti-Mn/SiO_2 catalyst at the optimized operating conditions was conducted to monitor its catalyst stability. The plots are presented in Fig. 12. It was found that the CH_4 conversions and the C_{2+} yields slightly decreased from the second to the last hour, while the C_{2+} selectivity remained virtually unchanged. The C_{2+} yield was reduced from 21 to 16% within 24 h of experiment. The catalyst used for 24 h was then observed to examine why the catalyst deactivated using SEM and XRD analyses, as shown in Fig. 13. Apparently, the particle sizes of the used catalyst were much larger (about 50 times) than those of the fresh catalyst. This indicated that one possible cause of the gradual deactivation of the catalyst was the aggregation of the particles (i.e. catalyst sintering). Comparison of the XRD spectra of the fresh and used catalysts shows that the peaks of α-tridymite (2θ = 21.8, 23.3, 27.3, and 30.1 (ICDD No. 00-003-0227)) were clearer compared to those of the fresh catalyst, while the $NaWO_4$ peaks of the used catalyst were smaller relative to those of the fresh catalyst. The peaks of α-cristobalite and TiO_2, however, exhibited no substantial change. This might suggest that the crystallite size of α-tridymite could grow after many hours of testing. However, it has been reported that the change of α-cristobalite and α-tridymite does not substantially influence the activity of Na_2WO_4-MnO_x-containing catalysts for OCM reactions [32]. Thus, it is not only catalyst sintering that causes the gradual deactivation, but also the loss of Na_2WO_4.

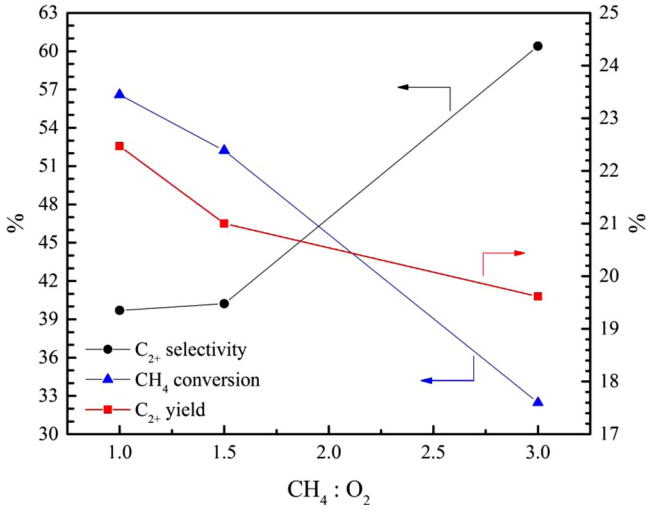

Fig. 10. Effect of varying CH_4:O_2 ratio of Na_2WO_4-Ti-Mn/SiO_2 catalyst. Reaction conditions: ($CH_4 + O_2$):N_2 ratio = 2:1, catalyst weight = 48 mg, total feed flow rate = 35 mL/min, reactor temperature = 700 °C.

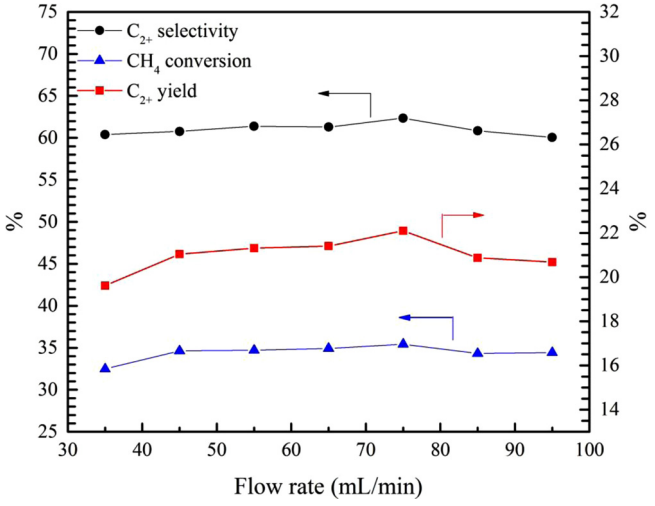

Fig. 11. Effect of varying total feed flow rate on catalytic performance of Na_2WO_4-Ti-Mn/SiO_2. Reaction conditions: CH_4:O_2:N_2 ratio = 3:1:2, catalyst weight = 48 mg, reactor temperature = 700 °C.

4. Conclusion

The purposes of this work were to study the effects of metal oxide additives on the performance of the TiO_2-Na_2WO_4/SiO_2 catalyst for the OCM reaction to value-added chemicals and to optimize the C_{2+} yield of the most promising catalyst. The plots between the CH_4 conversions and the binding energies of W $4f_{7/2}$ and Ti $2p_{3/2}$ of the prepared catalysts have revealed that the catalysts that exhibited lower binding energy values possessed high catalytic activity. This is because the bond strength between W or Ti with O becomes weaker, thereby promoting the OCM reaction. Moreover, the addition of Mn into the Na_2WO_4- Ti/SiO_2 catalyst was the most active catalyst. The crystalline phases of α-cristobalite, Na_2WO_4, and Mn_2O_3 were present in the most promising catalyst. In the attempts to optimize the C_{2+} yield by varying operating conditions, the maximum C_{2+} yield of the Na_2WO_4-Ti/SiO_2 catalyst added 0.5 wt% Mn was achieved at 22.09% with 62.3% C_{2+} selectivity and 35.43% CH_4 conversion. The optimal conditions were a reactor temperature of 700 °C, a CH_4:O_2:N_2 feeding gas ratio of 3:1:2, a total feed flow rate of 75 mL/min, and 48 mg of the catalyst. The stability of the catalyst was also investigated, concluding that the catalyst

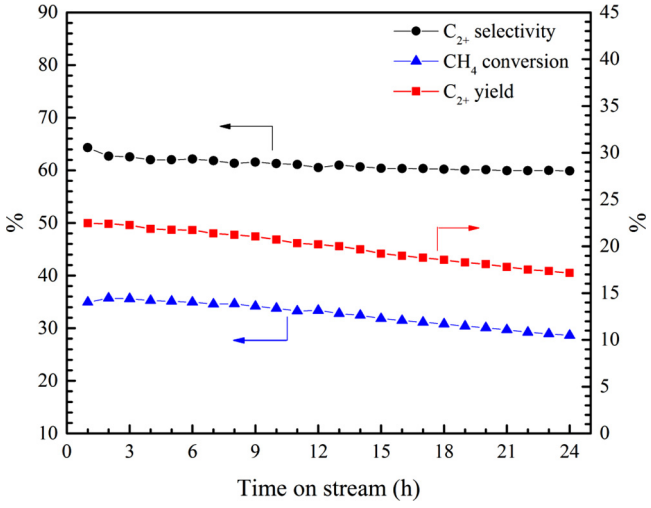

Fig. 12. Catalyst performance of Na_2WO_4-Ti-Mn/SiO_2 of OCM reaction as a function of time on stream over 24 h. Reaction conditions: CH_4:O_2:N_2 ratio = 3:1:2, catalyst weight = 48 mg, total feed flow rate = 75 mL/min, reactor temperature = 700 °C.

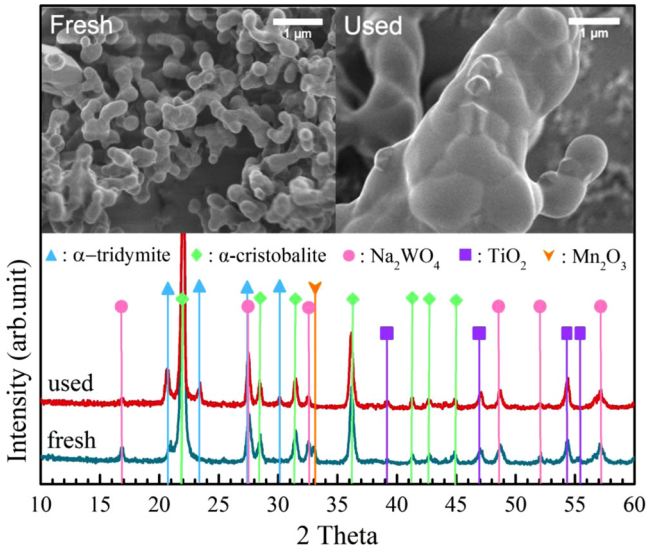

Fig. 13. SEM images (top) and XRD spectra (bottom) of fresh and used Na_2WO_2-Ti-Mn/SiO_2 catalyst.

gradually deactivated with time on stream because of catalyst sintering and the loss of Na_2WO_4 content. How to prevent catalyst deactivation and improve the C_{2+} selectivity of the Na_2WO_4-Ti-Mn/SiO_2 catalyst will be of great interest to further studies.

Acknowledgements

This work was financially supported by the Faculty of Engineering at Kasetsart University, Bangkok, Thailand; the Kasetsart University Research and Development Institute (KURDI); the Center of Excellence on Petrochemical and Materials Technology, the National Nanotechnology Center (NANOTEC), NSTDA, Ministry of Science and Technology, Thai- land, through its program of Research Network NANOTEC (RNN); the Thailand Research Fund and the Commission on Higher Education (grant #MRG6180232).

References

[1] C.D. Ruppel, J.D. Kessler, Rev. Geophys. 55 (2017) 126–168.

[2] G.J. Hutchings, M.S. Scurrell, J.R. Woodhouse, Chem. Soc. Rev. 18 (1989) 251–283.
[3] M.Y. Sinev, Z.T. Fattakhova, V.I. Lomonosov, Y.A. Gordienko, J. Nat. Gas Chem. 18 (2009) 273–287.
[4] M. Yildiz, Y. Aksu, U. Simon, T. Otremba, K. Kailasam, C. Göbel, F. Girgsdies, O. Görke, F. Rosowski, A. Thomas, R. Schomäcker, S. Arndt, Appl. Catal. A 525 (2016) 168–179.
[5] H.R. Godini, A. Gili, O. Görke, S. Arndt, U. Simon, A. Thomas, R. Schomäcker, G. Wozny, Catal. Today 236 (2014) 12–22.
[6] K. Khammona, S. Assabumrungrat, W. Wiyarath, J. Eng. Appl. Sci. 7 (2012) 447–455.
[7] S. Ji, T. Xiao, S. Li, L. Chou, B. Zhang, C. Xu, R. Hou, A.P.E. York, M.L.H. Green, J. Catal. 220 (2003) 47–56.
[8] J.Y. Lee, W. Jeon, J.W. Choi, Y.W. Suh, J.M. Ha, D.J. Suh, Y.K. Park, Fuel 106 (2013) 851–857.
[9] S.M.K. Shahri, A.N. Pour, J. Nat. Gas Chem. 19 (2010) 47–53.
[10] P. Wang, X. Zhang, G. Zhao, Y. Liu, Y. Lu, Chinese J. Catal. 39 (2018) 1395–1402.
[11] P. Wang, G. Zhao, Y. Liu, Y. Lu, Appl. Catal. A 544 (2017) 77–83.
[12] F. Papa, D. Gingasu, L. Patron, A. Miyazaki, I. Balint, Appl. Catal. A. 375 (2010) 172–178.
[13] V.H. Rane, S.T. Chaudhari, V.R. Choudhary, J. Nat. Gas Chem. 19 (2010) 25–30.
[14] N. Hiyoshi, T. Ikeda, Fuel Process. Technol. 133 (2015) 29–34.
[15] A. Seubsai, P. Tiencharoenwong, P. Kidamorn, C. Niamnuy, Eng. J. 23 (2019) 169–182.
[16] W. Kumsung, M. Chareonpanich, P. Kongkachuichay, S. Senkan, A. Seubsai, Catal. Commun. 110 (2018) 83–87.
[17] W.C. Liu, W.T. Ralston, G. Melaet, G.A. Somorjai, Appl. Catal. A 545 (2017) 17–23.
[18] S. Gu, H.S. Oh, J.W. Choi, D.J. Suh, J. Jae, J. Choi, J.M. Ha, Appl. Catal. A. 562 (2018) 114–119.
[19] T.W. Elkins, H.E. Hagelin-Weaver, Appl. Catal. A 497 (2015) 96–106.
[20] A. Malekzadeh, M. Abedini, A.A. Khodadadi, M. Amini, H.K. Mishra, A.K. Dalai, Catal. Lett. 84 (2002) 45–51.
[21] S.C. Oh, Y. Lei, H. Chen, D. Liu, Fuel 191 (2017) 472–485.
[22] V. Fleischer, R. Steuer, S. Parishan, R. Schomäcker, J. Catal. 341 (2016) 91–103.
[23] V. Fleischer, P. Littlewood, S. Parishan, R. Schomäcker, Chem. Eng. J. 306 (2016) 646–654.
[24] Y. Gambo, A.A. Jalil, S. Triwahyono, A.A. Abdulrasheed, J. Ind. Eng. Chem. 59 (2018) 218–229.
[25] A. Aseem, G.G. Jeba, M.T. Conato, J.D. Rimer, M.P. Harold, Chem. Eng. J. 331 (2018) 132–143.
[26] M. Ghiasi, A. Malekzadeh, S. Hoseini, Y. Mortazavi, A. Khodadadi, A. Talebizadeh, J. Nat, Gas Chem. 20 (2011) 428–434.
[27] C. Karakaya, H. Zhu, C. Loebick, J.G. Weissman, R.J. Kee, Catal. Today 312 (2018) 10–22.
[28] M. Taghizadeh, F. Raouf, Inorg. Nano-Met. Chem. 47 (2017) 1449–1456.
[29] Z. Gao, J. Zhang, R. Wang, J. Nat. Gas Chem. 17 (2008) 238–241.
[30] A. Galadima, O. Muraza, J. Ind. Eng. Chem. 37 (2016) 1–13.
[31] G. Pantaleo, V.L. Parola, F. Deganello, R.K. Singha, R. Bal, A.M. Venezia, Appl. Catal. B Environ. 189 (2016) 233–241.
[32] J. Wang, L. Chou, B. Zhang, H. Song, J. Zhao, J. Yang, S. Li, J. Mol. Catal. A Chem. 245 (2006) 272–277.